RADIATION DOSE AND IMAGE QUALITY FROM PELVIC LOCALISATION COMPUTED TOMOGRAPHY IN ONCOLOGY

by

Verreynne, VC

Dissertation submitted in fulfilment of the requirements for a Master's degree in Radiography (Therapy)

At

Faculty of Health and Environmental Sciences

Department of Clinical Sciences (Programme Radiography)

Central University of Technology (Free State) Bloemfontein

2020

STUDY LEADERS

Prof. H. Friedrich-Nel

Dr. D. Long

Dedication

This research is dedicated to the memory of

Steam punk Princess
My Angel Horse

(2010 – 2017)

Whose passing inspired me to conduct the research in the first place.

Acknowledgements

First, I would like to acknowledge my study leaders for their continuous patience reading and guiding my work. This research would certainly not be anything if it wasn't for your many hours that you both put into it. I thank you so much. Prof. Friedrich-Nel and Dr Long. Thank you both for your encouragement and pep talks when I needed it.

Dr Long my appreciation of your assistance in working hours and when possible allowing time for me to work on this research, it reduced the time frame by months.

Prof Sherriff thank you not only for allowing the research to take place in your department, but also for the encouragement to stay with the topic, for which I have such a passion, even when others did not see the relevance of it.

I would also like to thank Ms O'Reilly, head medical physicist for the CT, for reading my proposal and confirming the calculations in it. As well as assisting in showing me how to set-up the phantoms for my research. Also, to the medical interns who when needed assisted with the phantom set-ups (the anthropomorphic phantom is not a one-man job).

A note of thanks to Mr Roux who assisted with the automatic calculations utilised in the Microsoft Excel spreadsheets. As well as the automatic look-up to tables and BMI colour assistance.

To Ms Lebotho for her guidance in the translation of the Se-Sotho consent form and information leaflet. Thank you, Ms Lebotho, for your diligent work to ensure the translation was readable and easily understood by most African language patients.

To the porters who assisted in the consent for the patients who required SeSotho forms. Thank you for explaining and ensuring all questions were answered.

A special word of thanks to the Head of the CT scanner, Mrs Du Plessis for assisting with all the patient CT scans and as well as to everyone who worked there for the duration of the research. Most notably but not limited to, Mrs Fouché, Mrs Stroebel and Ms Wainwright, thank you.

To all staff members at the oncology department, thank you, for having patience with my many talks about my masters and for the encouragement when I faltered in my research. A huge thank you to each and every one of you!

To my colleague Mr Loots, who joined me in this master's journey. Thank you for your encouragement and understanding when I was struggling. As well as rejoicing when all was going well.

A deep gratitude toward Ms Viljoen for her statistical contribution to my work and the explanation of the data. As well as to Omnilingua and Ms Smit for the language editing of my final document. Thank you both for enhancing my research with your expertise.

Thank you to my parents for their patience and encouragement, with the many hours spent with my research.

Lastly, but not least, thank you to the patients who agreed to participate in this research. The research is intended first and foremost for future patients benefit. Without your participation this would not be possible, so thank you.

Abbreviations

2D	Two dimensional
3D	Three dimensional
4D	Four dimensional
Abdo-Pelvis	Abdomen pelvis region
ALARA Principles	As Low As Reasonably Achievable
AP	Anterior posterior
BMI	Body mass index
CNR	Contrast-to-noise ratio
CNRD	Dose weighted CNR
CT	Computed tomography
CTDI	Computed tomography dose index
$CTDI_{vol}$	Volume CTDI
$CTDI_{w}$	Weighted CTDI
CUT	Central University of Technology
DLP	Dose length product
DRL	Diagnostic reference levels
f	Conversion factor for SSDE measurement
FOV	Field-of-view
FSDOH	Free State Department of Health
HOD	Head of department
HU	Hounsfield unit or CT number
ICRP	International Commission of Radiation Protection
IMRT	Intensity modulated radiotherapy
kV	Kilo-voltage or tube potential
Lat	Lateral directional measurement of patient
mA	Milliampere or Tube Current
mAs	Effective tube current and time
MRI	Magnetic resonance imaging
mSv	Millisievert, measure of effective dose
PMMA	Polymethyl-methacrylate cylindrical phantoms
ROI	Region of Interest
RT No.	Radiotherapy number of a patient
S	Seconds
SD	Standard deviation
SNR	Signal-to-Noise Ratio
SSDE	Size-specific dose estimate

Table of Contents

List of tables

List of Figures

Abstract

Introduction: Computed tomography (CT) in radiation therapy plays an important role in the accurate identification of the position of the tumour and organs at risk, through high geometric fidelity of the CT image. It has been determined that the radiation dose from CT is amongst the highest from all medical imaging. There is concern over the increased radiation dose from pelvic CT localisation scans, due to the increased scan length and the necessity for high image quality used in radiation therapy planning. The necessity for high image quality, while lowering the CT dose and honouring the ALARA principles, is essential.

Four article-style studies, which evaluate the CT dose and image quality produced for pelvic localisation scans and that are ultimately aimed at publication, are presented in this research paper.

Purpose: The purpose of this research was to determine the CT dose and image quality produced for pelvic localisation scans in a department of oncology, Free State. The aim was to measure the dose received by patients during pelvic CT localisation scans and to determine whether the dose is justified in terms of imaging requirements for radiation therapy planning. The objectives of the research were to (i) determine baseline dose level for pelvic CT scan utilising an anthropomorphic phantom, (ii) measure patients' CT pelvic localisation dose by using size-specific dose estimates, (iii) to verify whether the field of view (FOV) modified image quality for patients of different sizes, utilising water phantoms and (iv) objectively examine image quality using the contrast-to-noise ratio (CNR) for patients' CT localisation scans. The significance of this research is reflected in filling the gap in existing literature, as most published studies were conducted on diagnostic CT dose and image quality.

Methodology: The research was conducted as a prospective research study, performed between January and June 2019, after ethical approval was obtained. All CT scans were produced on a TSX-201A (Toshiba Aquilion © Large Bore) CT scanner. The CT baseline dose level was established utilising an anthropomorphic phantom. The patient dose for pelvic CT localisation was calculated by the size-specific dose estimate (SSDE) that determines the dose, based on individual patient dimensions. The participants were divided into three body mass index (BMI) categories; these were underweight, normal weight and overweight. The CT image quality was examined based on scans of different sized water phantoms utilising CT quality assurance tests. The patients' CT image quality was derived from the contrast-to-noise ratio (CNR).

Results: A total of 131 participants met the inclusion criteria of the research study and were grouped according to their BMI into categories, these being categorised as: overweight-, normal- and underweight BMI category. For the baseline dose level, the best kV and FOV combination was determined for the 120 kV setting with a large (L), large-large (LL) or extra-large (XL) FOV, which calculated at 14.0 cGy using SSDE. In terms of the BMI patient category the median dose was determined as: 12.3 cGy for an overweight BMI; 14.8 cGy for a normal BMI, which is in line with the baseline CT dose and 17.1 cGy for the underweight BMI category.

The image quality determined as per phantom indicated that the 135 kV demonstrated the highest quality as well as the highest dose. In terms of FOV the small and medium sized phantom could be scanned with any size FOV. However, the large phantom excelled with the L, LL and XL FOV. The results for the patients in terms of image quality, based on CNR illustrated that the normal BMI category patients had the highest quality. It was furthermore concluded that the overweight BMI patient category reflected the lowest image quality.

Conclusion: The research questions were addressed and the objectives of this research were indeed met. In addition, this research addressed the gap in relevant literature, by determining results based on oncological CT scans and protocols in terms of dose and image quality. The fact that only one anthropomorphic phantom was available for dose calculations and that no tissue types were present in the phantom to utilise for the image quality, limited the research. The researcher recommends that protocols for patients in different BMI categories be established for CT pelvic localisation scans whilst simultaneously adhering to the ALARA principles. Research demonstrates that there is an industrial drive to decrease dose while maintaining image quality. Numerous techniques have been introduced to assist with the reduction of dose. One of these techniques was illustrated by Irish researchers who established national diagnostic reference levels (DRL's) for breast CT protocols in oncology. It is believed that by utilising knowledge from both diagnostic and oncology CT scan techniques, the reduction of CT dose - while maintaining image quality - is an achievable goal.

Keywords: CT radiation dose, CT image quality, Size-specific dose estimate, Contrast-to-noise ratio, Pelvic localisation, Radiation therapy.

Chapter 1

Computed Tomography Localisation Scans for Pelvic Oncology

"I am one of those who think, like Nobel, that humanity will draw more good than evil from new discoveries."

"I was taught that the way of progress is neither swift nor easy."

Marie Currie née Skłodowska (1867 – 1934)

1.1. Introduction

Through anecdotal observation within radiation therapy departments, Sanderud *et al.* (2016) noted that high radiation doses from radiation therapy computed tomography (CT) scans are of little concern. Technological advancement in radiation therapy has led to an increased demand for high quality CT images for radiation therapy planning purposes (Sanderud *et al.*, 2016). More recently, CT localisation scans are considered as the standard of care for treatment planning purposes in radiation therapy and relatively high radiation doses have been associated with the CT modality (O'Connor *et al.* 2016). The ability of the CT scans to allow the visualisation of structures with low contrast is primarily limited by the image noise, which is closely associated with radiation dose (Goldman, 2007). The image quality improves in terms of decreased image noise and the ability to perceive low contrast structures with an increase in the CT dose (Goldman, 2007). Due to the necessity for a high image quality for CT localisation scans, as well as the extended CT examination area required, a higher radiation potential exists (Sanderud *et al.*, 2016).

This research examines the CT dose and image quality in a department of oncology in the Free State province of South Africa (from hereon it will be referred to as the oncology department). The current research was approached from the perspective of a radiation therapist. Various articles relevant to the subject of the research were consulted in order to gain a thorough understanding and knowledge of the available literature before embarking on the research. The section following hereafter provides an overview of the fundamental principles of the CT as well as the principles of radiation dose and image quality. This chapter will thus give background to the research to follow.

1.2. Overview of Computed Tomography in Oncology

Oncological treatment consists of three main modalities, namely surgery, chemotherapy (referred to as medicines in ancient times) and radiation therapy (Pereira *et al.* 2014). The oldest modality is surgical cancer treatment, with records circa 1600 BC and discovered by an American Egyptologist Edwin Smith. In the early 1900s a German chemist Paul Ehrlich, first used chemotherapy to treat cancer patients. In 1895 Wilhelm Röntgen, discovered a type of ionising radiation called x-rays and within months of the discovery x-rays were being used to treat tumours (Pereira *et al.*, 2014). Within 8 years of the discovery of x-rays in 1903 Dr C.L. Leonard stated that the Röntgen rays (x-rays) appeared to alter the malignant cells' character, which frequently cured patients or restored patients' health for months or years (Halperin *et al.*, 2013).

The clinical modality of radiation therapy deals with the treatment of patients that have malignant neoplasia though the use of ionising radiation (Halperin *et al.* 2008). The aim of radiation therapy is to eradicate the tumour. This results in high life quality and prolonged survival. By precisely measured irradiation dose to the defined tumour volume, with the healthy surrounding tissue obtaining minimal damage (Halperin *et al.*; 2008). The evolution of radiation therapy was noted by the method of treatment delivery and treatment planning changes. Initially during the late 1800s skin erythema was used to quantify the dose delivery. In the mid-1900s single point calculations inside the patient and in the late 1960s computer-based dose calculation was used. With the invention of CT, three dimensional (3D) based dose planning became possible (Pereira *et al.*, 2014).

The word tomography is derived from the Greek word "*tomos*" which means slice or section. Since the 1920s medical imaging has demonstrated layers or 'slices' in the human body by utilising the mechanical movement of an x-ray source and imaging media. CT has been used clinically for radiological diagnosis since 1972 (Bridge & Tipper, 2011). The CT creates cross sectional images of a person's body in many different directions, measuring x-ray attenuation properties (McCollough *et al.,* 2009).

1.2.1. Fundamental Principles of Computed Tomography

The CT consists of a number of detector elements arranged in an arc and an x-ray tube source, which rotate simultaneously around the isocenter of the gantry (Bridge & Tipper, 2011). Figure 1.1 illustrates the detector array (D) and the x-ray tube source

(S), as well as their simultaneous movement around the patient. The size of each single detector determines the resolution of the entire CT system (Bridge & Tipper, 2001).

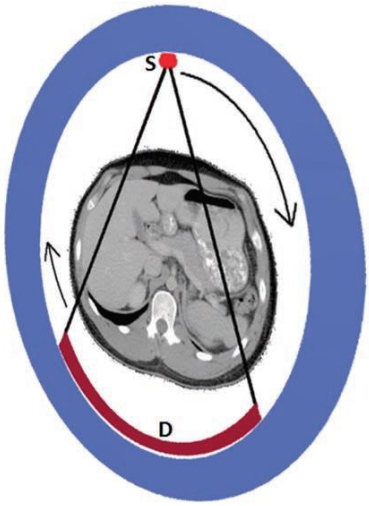

Figure 1.1: CT scanner, x-ray tube and detector array arrangement.
Courtesy of Bridge & Tipper, 2011.

The images produced for radiation therapy are spiral or “helical” (see Figure 1.2) and produced by simultaneously moving the table and the patient during image acquisition through the scanner (Bridge & Tipper, 2011). Tiny gaps between the spirals are produced and later interpolated by reconstruction algorithm software. Patient dose and scan times may be reduced by moving the scan table faster. However, this produces wider gaps and impacts negatively on image detail (Bridge & Tipper, 2011). The term “pitch” is the ratio between the tube rotation and the amount of table movement. This affects both image quality as well as patient dose. A low pitch creates the highest image quality by slow table movement through the gantry, however it increases patient x-ray dose.

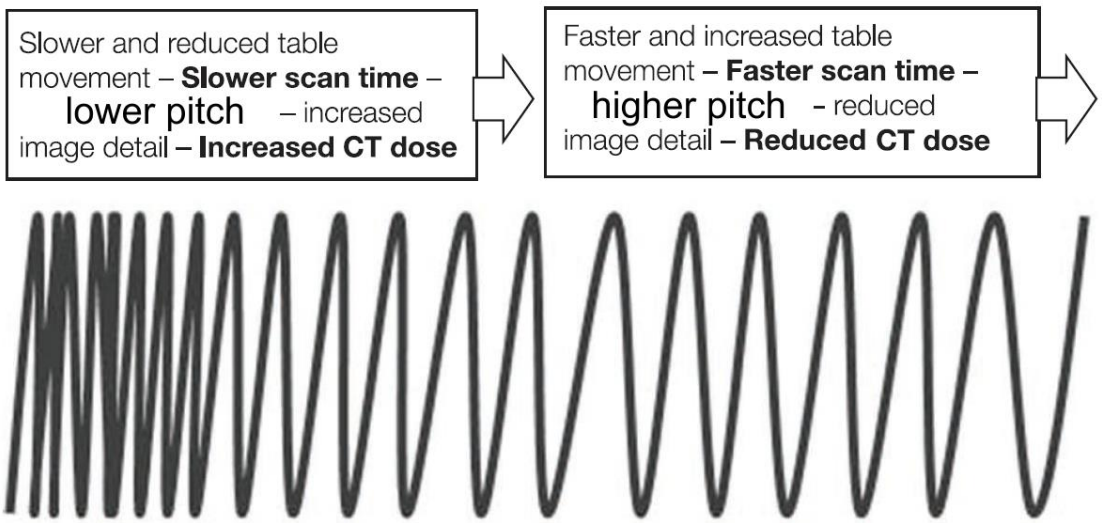

Figure 1.2: Lower pitch to higher pitch.
Courtesy of Bridge & Tipper, 2011: 5, modified by researcher.

CT images are most often viewed from the axial viewpoint; where each slice of the CT image is a two-dimensional (2D) image, which can also be measured in depth (Bridge & Tipper, 2011). The depth is manipulated at the time of CT acquisition (Bridge & Tipper, 2011). The CT image can be divided into an x and y-axis while the z-axis denotes the depth of the image (Bridge & Tipper, 2011), as illustrated in Figure 1.3. The CT image consists of pixel and voxel elements. The two-dimensional pixel is short for “picture element” of a CT image and each pixel represents 4096 possible shades of grey (Bushberg *et al*., 2002). A pixel is formed on the x and y axis of the CT image. The three-dimensional “volume element” of the CT image is referred to as a voxel. The voxel’s two dimensions are equal to that of the pixel. However, the third dimension is created from the CT scan’s slice thickness (Bushberg *et al.*, 2002).

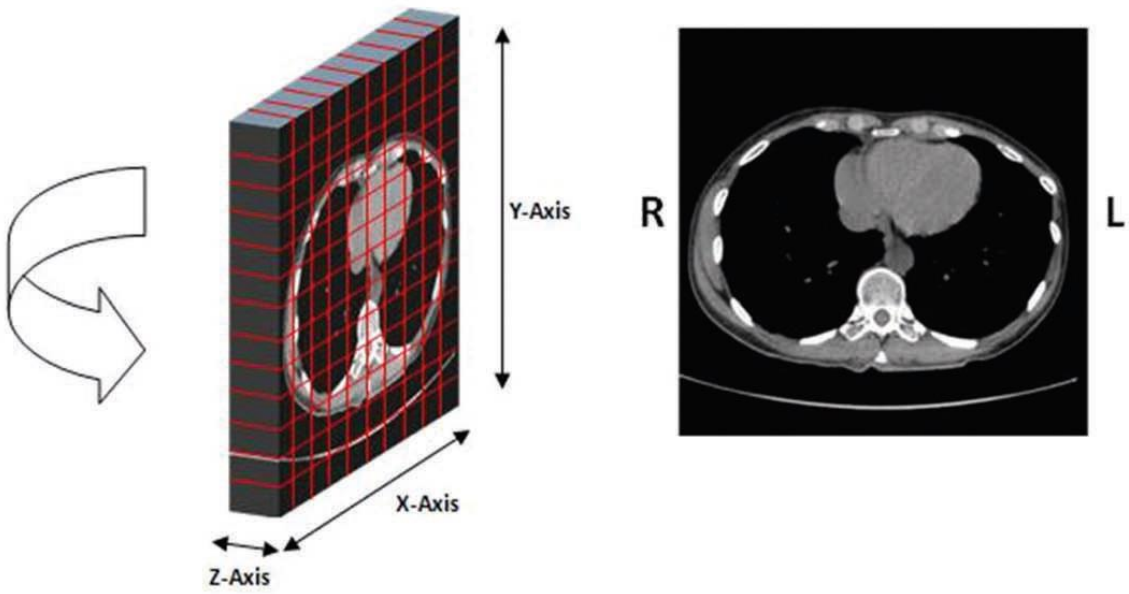

Figure 1.3: A CT slice showing the axis and how an image is viewed on screen.
Courtesy of Bridge & Tipper, 2011.

Image quality is improved with the use of bowtie filters and in comparison, to flat filters; a 50% reduction in surface dose is found (Zacharias *et al*., 2013). The bowtie filters harden the x-ray beam by removing low energy x-rays that would not reach the detectors, but be absorbed by the patient (Zacharias *et al.*; 2013). In order for bowtie filters to function accurately the patient should be positioned correctly in the gantry isocenter (Zacharias *et al.*; 2013).

Through research conducted during the 1980s and early 1990s, a diagnostic CT scanner was integrated into 3D treatment planning systems; this led to the concept of a virtual simulator, later referred to as the CT simulator (Halperin *et al.*, 2013). With the advent of the CT simulator greater precision in dose optimisation, dose distribution as well as patient positioning was achieved. Three-dimensional dose calculation was an important advancement as it allowed treatment to be delivered to the tumour and reduce radiation to normal tissue as well as organs at risk which surround the tumour (Pereira *et al.*, 2014).

1.2.2. Computed Tomography in Radiation Therapy

Radiation therapy CT scanners differ from their diagnostic counterparts. The radiation therapy scanner, in order to aid patient position for treatment, should have the largest possible aperture (Barret *et al.*, 2009). While a standard diagnostic CT has an aperture of 70 cm, a radiation therapy CT usually has an 85 cm wide-bore to assist with large

patients and positioning for example, breast cancer patients who are positioned at a 15-degree inclined plane (Barret *et al.*, 2009). The CT couch in radiation therapy must have 1 mm couch registration accuracy and a flat top. Various patient immobilisation devices and supporting aids are used Tattoos are made on the patient's skin which ensure correct patient setup from simulation through to radiation treatment (Barret *et al.*, 2009). Pins which are radio-opaque are stuck on the tattoos to make them visible in the treatment planning process. Patients are positioned and immobilised as they will be during their radiation therapy treatment (Halperin *et al.*, 2008). Accuracy at this stage is vital to ensure correct planning and treatment delivery. To ensure patient alignment and correct positioning, CT tomograms are evaluated before the CT scan (Halperin *et al.*, 2008).

The typical range of 2 mm to 8 mm slice thickness and 50 to 200 slices are used for planning CT scan protocols, which are tumour site-dependent (Halperin *et al.*, 2013). In radiation therapy the ideal is to scan the patient with the smallest slice thickness possible to ensure maximum image resolution. However, the smaller slices increase the number of images produced (Bridge & Tipper, 2011). A higher dose is required with a thin slice to reduce image noise to an acceptable level (Bridge & Tipper, 2011). CT images acquired for radiation therapy planning purposes are used to interpret tumour volumes and critical structures and herein rests uncertainty (Bellon *et al.*; 2014). In radiation therapy there is an ever increase in complexity of treatment techniques, in particular stereotactic radiosurgery which involves delivering a high dose of radiation on a precise target (Bellon *et al.*, 2014). This dependence on tumour delineation for accurate treatment delivery is reliant on correct tumour delineation and patient setup. This in turn is dependent on CT slice thickness (Bellon *et al.*, 2014). For radiosurgery a reduction of slice thickness of the CT from 3 mm to 1.5 mm improved precision by a factor of two (Bellon *et al.*, 2014). For 3D conformal radiation therapy plans of the brain CT slice thickness of 2.5 mm is recommended, if the tumour is less than 25 cc. However, a 5 mm slice thickness would be sufficient for a tumour which is larger than 25 cc (Bellon *et al.*, 2014).

1.2.3. Radiation Dose and Image Quality

The capabilities of CT have improved with scanning technology and computer calculation speed. Thus, there is an increase in CT usage in both diagnostic and radiation therapy (Chang *et al.*, 2017). The effects from exposure to ionising radiation were noticed shortly after the discovery of x-rays (Suliman *et al.*, 2018). In the past

decades there have been many vital steps taken in order to mitigate the risks and maximise the benefit of ionising radiation (Suliman *et al.*; 2018). In radiological terms the CT has the highest source of radiation exposure (Bharkhada *et al.*, 2009). The CT is estimated to account for 40% of the delivered radiation dose, although thought to constitute only 4% of all radiological procedures (Bharkhada *et al.*, 2009). It is estimated that between 1.5% to 2% of all cancers are due to exposure to CT and therefore the risk associated with CT dose received by the patient is of growing concern (Bharkhada *et al.*, 2009). Therefore, medical justification is vital with regard to patient dose. The risk from radiation exposure must be far outweighed by the benefits of the radiological investigation (Suliman *et al.*, 2018).

In radiation therapy, one of the main purposes of CT imaging is to accurately identify the position of the tumour and surrounding tissue as well as the organs at risk, through high geometric fidelity of the CT image (Davis *et al.*; 2017). Improved image quality in terms of CT imaging is associated with a higher CT dose, due to the use of higher voltage (kV) and/or higher electrical current (mA) (Chang *et al.*, 2017). Therefore, in order to produce acceptable image quality, while ensuring limited radiation exposure to the patient is an issue for researchers (Chang *et al.*, 2017). The relationship between image quality and CT dose is crucial in CT radiation protection (Chang *et al.*, 2017). In this research the CT dose is examined, followed by the CT image quality to determine if the dose is justified by the image quality.

1.3. Literature which Inspired the Research

Research conducted by Karim *et al.* (2016) determined the radiation dose from CT practices in Malaysia and examined the radiation dose delivered to the patients in four centres that conducted CT procedures. The authors utilised a form that had to be completed by the CT staff which listed the case ID, examination type, as well as patient's characteristics such as age, weight, height and body mass index (BMI) (Karim *et al.*, 2016). For this specific research a CT form was created for the patient scans, using these concepts (refer to Chapter 3 and 5). The following CT parameters were used: tube potential or kilovolt (kV), tube current or milliampere (mA), time in seconds (s), effective tube current, which is milliampere seconds (mAs), nominal collimation beam width, table feed, slice thickness and scan range. These parameters are displayed on the console of the CT scanner and also include the radiation output in terms of $CTDI_{vol}$, DLP and total mAs. The research was conducted over a two-month period. Similar research was conducted by Suliman *et al.* (2018) during which they

examined the effective doses for CT examinations in Saudi Arabia. The parameters collected for their research included patient age, gender, tube potential (kVp), tube current time produce (mAs), scan rotation time, slice width and number of slices, scan length, table increments and start and end positions for the scan, the $CTDI_{vol}$ as well as the dose length product from the CT console's display (Suliman *et al.*, 2018). These concepts were utilised to determine the CT dose for the phantom scans (refer to Chapter 2) as well as the patients CT scans (refer to Chapter 3). The data utilised in the research was inspired by the details obtained from the above research and the same data was obtained for the current research.

Qurashi *et al.* (2017) in their research determined an optimal CT protocol for obese patients. Their data capture included patient demographics, height and weight of the patient as well as their anteroposterior diameter (Qurashi *et al.*, 2017). Similarly, Sanderud *et al.* (2016) used the patients' BMI which is determined by their height and weight. The research considered each scan protocol and the impact the BMI had on the $CTDI_{vol}$. The study population was divided into a low and high BMI group (overweight and obese group) (Sanderud *et al.*, 2016). The use of BMI is used in the current research in determining the CT dose to the patient (refer to Chapter 3) as well as the patient image quality (refer to Chapter 5).

Phantom data was also obtained in research conducted by Chen *et al.* (2017) during which they used a CatPhan 500 phantom to find a balance between dose and image quality. In order to calculate the contrast-to-noise ratio a 15 mm region of interest was created inside the CatPhan phantom and another next to the target, but without overlapping another target volume inside the CatPhan. The analysis of the phantom data created optimal parameters (Chen *et al.*, 2017). The image quality was determined with the use of phantoms (refer to Chapter 4).

Bearing in mind the importance of CT dose and image quality, the next section outlines the statistical data obtained from the oncology department prior to the onset of the research.

1.4. Statistical Data to Support the Research

The research was conducted in the oncology department. The CT simulator for localisation scans was integrated into the oncology department during 2009 for the purpose of radiation therapy planning. Annually, over 1000 localisation CT scans are

performed at the oncology department. A five-year overview (2013 to 2017) of the number of scans and rescans performed at the oncology department is illustrated in Figure 1.4.

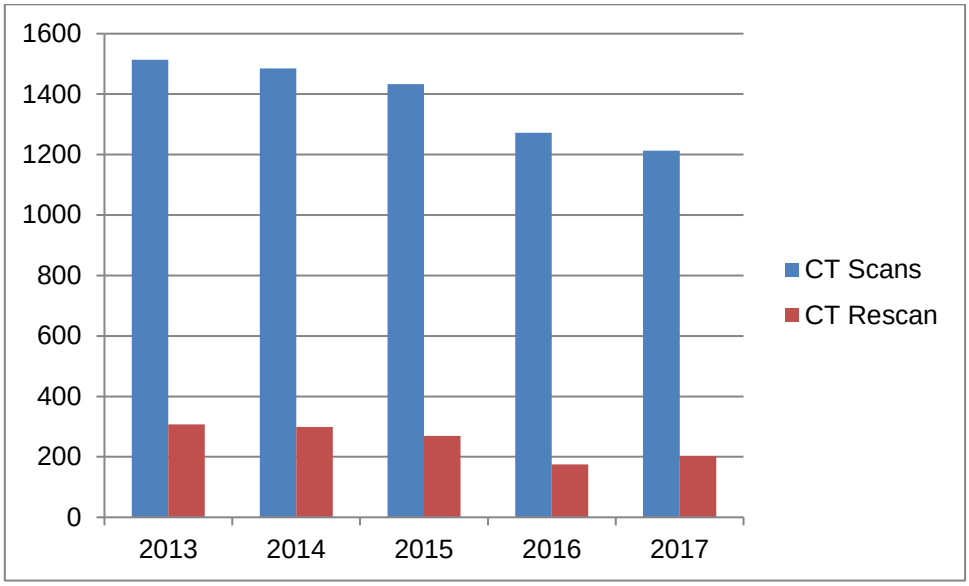

Figure 1.4: Localisation scans and rescan, performed at the oncology department from 2013 to 2017.
Statistical data courtesy of the oncology department, 2017.

The division of the annual scans as per anatomical site is demonstrated in Figure 1.5. Utilising the figure, it can be determined that with an annual average of 567 scans, pelvic scans are the most prevalent, followed by 390 thorax scans and 357 head and neck (H&N) CT scans. A limited number of children are scanned annually with an average of 27 at the oncology department. Rescans often occur due to patient movement during a scan, the necessity for increased scan length or due to patients necessitating a full bladder or empty bowel.

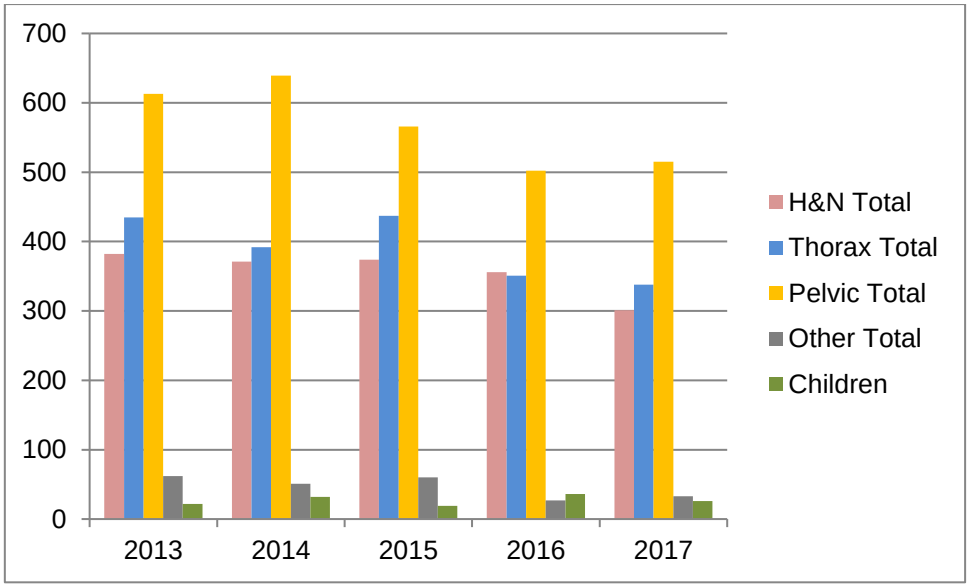

Figure 1.5: Division of the annual CT scans into anatomical sites.
Statistical data courtesy of the oncology department, 2017.

As stated, the pelvic CT localisation scans were the most prevalent annual scans conducted at the oncology department. Utilising the statistical data, the research was aimed at determining the CT dose and image quality derived from CT localisation scans of the pelvis.

1.5. Research Problem

The researcher was concerned regarding the increased radiation dose of the pelvic CT localisation scan, due to the increased scan length and necessity for high quality images for planning purposes. The dilemma that became evident is that an increase in CT radiation dose to the patient is associated with high quality CT images as well as the necessity for increasing the length of the scanned area.

1.6. Research Question

What was the radiation dose received by the patient during pelvic CT localisation in the oncology environment?

Was this dose justified due to the high image quality requirements from CT localisation in the oncology environment?

1.7. Aim and Objectives of the Study

The aim of the research was to (a) measure the dose that the oncology patient receives during a pelvic CT localisation scan and (b) to determine if this dose is justified due to imaging requirements for oncology treatment planning.

The objectives of the study were:

- To utilise an anthropomorphic phantom to determine the ***baseline dose levels*** for a pelvic CT scan (refer to Chapter 2: Baseline dose levels for computed tomography scans of the pelvis in oncology.),
- To measure ***patients' radiation dose*** determined by the use of size-specific dose estimate (SSDE) as resulting from pelvic CT localisation scan (refer to Chapter 3: Patient Radiation Dose from Pelvic Computed Tomography Localisation),
- To verify through the use of ***water phantoms*** if the field of view (FOV) modifies the ***image quality*** for patients of different sizes (refer to Chapter 4: Computed Tomography Image Quality Derived from Water Phantom Scans in an Oncology Environment),
- To objectively examine the ***image quality*** by determining the contrast-to-noise ratio (CNR) which states the difference in contrast between two structures in the **patient's** CT scan (refer to Chapter 5: Image Quality Derived from Patient CT Localisation Scans).

1.8. Ethical Approval

Ethical approval was sought and obtained prior to the onset of the research. The letters pertaining to ethical approval are found in appendix E. Approval for the study was granted firstly from the Head of the Department (HOD) of Oncology, Universitas Annex, Free State. Ethical approval was granted from both the Free State Department of Health (FSDOH) and the Health Sciences Research Ethics committee at the University of the Free State (UFS). The ethical clearance number is: *UFS-HSD2018/1159/2711*. No approval was required from the Radiation Control Committee due to the fact that the patients did not receive additional radiation, only the routine CT localisation scans which were necessary for the oncological treatment planning and delivery.

1.9. Significance of the Research

After a thorough investigation of the relevant literature, it was determined that most of the literature on which CT dose is based relates to diagnostic imaging. Very little information could be gleaned from the literature for oncology patients receiving CT localisation scans. This specific research is specifically aimed at answering the research question pertaining to the dose and image quality obtained from pelvic CT localisation scans in the oncology department.

Utilising the ALARA principle, a baseline CT dose was obtained through the use of an anthropomorphic phantom. Phantoms of different sizes also assisted in the process of determining how the CT dose was influenced by different diameters. The patients' CT dose from CT localisation scans was examined. Patients were divided into BMI categories to see the effect different body habitus has on the CT dose and whether this dose aligned with the baseline dose determined from the anthropomorphic phantom scan.

The researcher also examined the image quality of the pelvic CT localisation scans by utilising phantoms of different sizes as well as different FOV and kV settings to establish the influence of the FOV for different diameters. In addition, the researcher examined the patients' CT scan images to determine the image quality for different BMI patients.

The results of the research study enabled the researcher to make recommendations for future use in the oncology department. Data on CT dose for pelvic localisation scans based in oncology could not be gleaned from literature. The current research compares the dose obtained at the oncology department with international diagnostic CT doses. This research thus aims to address the gap in the literature regarding the CT dose for localisation scans of the pelvis.

1.10. Layout of Dissertation

Chapter 1 introduces the fundamental CT concepts in an oncology environment, provides statistical data, states the research study's aim and objectives, defines the ethical considerations and the significance of the research. The second chapter demonstrates the CT dose as measured by phantoms and determines the baseline CT dose. The third chapter examines the CT dose for patients who received CT localisation scans of the pelvis. The fourth chapter determines the quality of the CT

images based on phantoms and different FOV settings. The fifth chapter demonstrates the image quality obtained by patient who received a CT scan for pelvic localisation. The sixth chapter concludes the research.

Since Chapters 2 through Chapter 5 are presented in the style of an article. The repetition of information is purposeful to ensure completeness of an article style. A literature section is found at the beginning of each chapter. The reference list pertaining to each chapter is presented at the end of each chapter.

An overview of the research was discussed in this chapter. The chapter that follows determines the baseline dose for pelvic localisation scans as determined by phantoms.

Chapter 2

Baseline Dose Levels for Computed Tomography Scans of the Pelvis in Oncology

2.1. Introduction

This chapter is based on the first objective of the research study, which is to utilise the anthropomorphic phantom scans to determine the baseline dose levels for pelvic Computed Tomography (CT) scans in the oncology department. In addition to the afore mentioned, the research includes the use of water phantoms to illustrate the effect of the size-specific dose estimate (SSDE) on phantoms of different sizes.

To determine the baseline dose levels for the pelvic CT scans in the oncology department, the researcher utilised an anthropomorphic phantom. An anthropomorphic phantom is constructed from tissue equivalent materials. These phantoms are historically used for radiation dosimetry studies to represent the attenuation characteristics of the physical body's anatomy (Winslow *et al.*; 2009). For the purpose of this research study, it is necessary to explore the following concepts: (i) the ALARA principle, (ii) the CT dose in terms of this research, which relates to the effective dose and size-specific dose estimate, (iii) field of view parameters and (iv) diagnostic reference levels.

CT was introduced as an imaging modality in 1972 and used primarily for diagnostic purposes (Karim *et al.*, 2016). Research in the 1980s and early 1990s led to the use of a CT simulator for three-dimensional (3D) planning purposes (Halperin *et al.*, 2013). Since the onset of the use of CT as a diagnostic tool, the CT scan dose received by a patient has remained a focus of interest; which is due to the concern over the continuous radiation output during scanning in the z-axis (Karim *et al.*, 2016). The continuous radiation output causes dose values greater than other x- and gamma-ray imaging modalities (Karim *et al.*, 2016).

In a radiation therapy planning environment, the necessity for increased length CT scans, as well as an extended CT area in order to include the positioning apparatus has caused an increase in CT dose for oncology patients (Sanderud *et al.*, 2016). Sanderud *et al.* (2016) examined thoracic CT of adults in both diagnostic and radiation therapy scans. The authors have found that the $CTDI_{vol}$ was almost four times higher in radiation therapy scans compared to diagnostic CT scans. The radiation therapy CT

scans also had an increase of nearly four times in length of the DLP, in comparison to diagnostic CT scans. The mean $CTDI_{vol}$ was found to be 38.1 mGy and DLP was 1472 mGy.cm for radiation therapy, while in diagnostic imaging the mean values were 9,6 mGy and 376.5 mGy.cm respectively (Sanderud *et al.*, 2016). The radiation therapy scans were found to have an effective dose of 30 mSv while their diagnostic counterparts received 7.7 mSv (Sanderud *et al.*, 2016). The typical range of 2 mm to 8 mm slice thickness and 50 to 200 slices is used for planning CT scan protocols, which are tumour site-dependent (Halperin *et al.*, 2013).

With the aforementioned information in mind, the researcher investigated the dose received during CT localisation pelvic scans in an oncology environment. This justified medical examination in an oncology department must be optimised in order to obtain the required image quality for treatment planning purposes.

2.1.1. ALARA Principle

The ALARA principle is an acronym for “As Low As Reasonably Achievable”, which applies to all medical exposure (Miller & Schauer, 2015). The ALARA concept was first contemplated of at the time of the Manhattan Project (Auxier & Dickenson, 1983), with refinement made to express the new uses of radiation. Later the ALARA principle in medical imaging was defined as the dose needed for a justified medical examination with the dose being the optimal dose to obtain the desired image (Miller & Schauer, 2015).

The CT examination is in itself non-invasive. However, as CT utilises radiation to create the images, the cumulative effect of CT dose is of clinical concern (Halperin *et al.*; 2013). An increase in the use of CT has been noted in the past decade. The addition of multiple CT scans increases the potential for cancer induced biological damage to patients over time (Lumbreras *et al.*; 2019). The effective dose of 100 mSv is seen to increase the risk of fatal cancer of 1 in 200 adults. In Japan the Effect Research Foundation reported that the radiation dose follows a linear-no-threshold risk model (Lumbreras *et al.*, 2019). The research conducted by Lumbreras *et al.* (2019), involved a 12-year study of cumulative exposure of patients to radiation dose. The study found that 3.1% of the research participants received cumulative doses between 50 and 100 mSv. Doses that exceeded 100 mSv were found in 1.5% of the study sample. If only the CT dose is considered, 2.5% of the participants who were in the 0 to 20-year age group received doses above 50 mSv (Lumbreras *et al.*, 2019). The cumulative effect of

the CT dose can thus be illustrated by the 12-year research conducted by Lumbreras *et al.* (2019).

The baseline dose as determined by this research is also the dose delivered that upheld the ALARA principle. The phantoms will therefore demonstrate the effect of the kV and FOV on the dose, without fear of harm from the radiation dose to an individual patient. Thus, a baseline patient dose can be established for a patient of average build. The water phantoms of different sizes have also been scanned to determine the effect of different sized diameters on dose, when all other variables remain constant.

2.1.2. Fundamental Concepts of CT Dose

In the broader terms of radiation there are two concepts of dose, firstly radiation exposure and secondly radiation dose. Radiation exposure concerns the production of x-ray photons and the number of ionizing events that occur in the air as a result of this production (Kanal *et al.*, 2017). The radiation dose or absorbed radiation dose indicates the result of the exposure to radiation and the amount of radiation energy deposited in the patient's body from said exposure (Kanal *et al.*, 2017). The absorbed radiation energy is what is used to determine the effect of the CT dose, in terms of the effective dose (2.1.2.1) and the actual dose based on SSDE (2.1.2.2).

In 1981 the CT dose index (CTDI) was introduced by Shope *et al.* (1981) in research titled "*A method for describing the doses delivered by transmission of x-ray computed tomography*", as the standard measure of radiation output of the CT system (McCollough *et al.*, 2011). The term CTDI uses the word index to differentiate it from the radiation dose that is absorbed by the patient (McCollough *et al.*, 2011). In the modern CT scanner setup, the volume CTDI ($CTDI_{vol}$) is displayed on the CT, which is the weighted CTDI ($CTDI_w$) divided by the pitch. Thus, the $CTDI_{vol}$ is the standardised measurement and it is measured by utilising CT phantoms. The measurement is based on the radiation output of the CT system, which allows users to determine the amount of emitted radiation. This measurement thus makes a comparison between the different CT protocols or CT scanners (McCollough *et al.*, 2011).

The dose length product (DLP) is the product of the $CTDI_{vol}$ and the irradiated scan length (McCollough *et al.*, 2011). The $CTDI_{vol}$ and DLP are independent of the size of the patient, but change with the scan parameters, the tube voltage, tube current, the time the gantry rotates, the pitch and the bowtie filter (American Association of Physicists in Medicine (AAPM), 2011).

The two fundamental CT dose related radiation parameters are the $CTDI_{vol}$ and DLP. Both these parameters are used to calculate the dose received by the patient during a CT examination. In the following section these parameters and the related dose calculations that occur will be examined.

2.1.2.1. Effective Dose

The effective dose (E) is a concept that reflects the stochastic risk from exposure to ionising radiation, rather than a measure of dose (McCollough *et al.*, 2009). The International Commission on Radiological Protection (ICRP) first defined the effective dose in ICRP 60 (1990) and then revised it in ICRP 103 (2007). The ICRP 60 tissue weighting factors as defined in 1990 (ICRP 60, 1990) and the ICRP 103 defined in 2007 (ICRP 103), indicated in Table 2.1.

Table 2.1: Tissue weighting factors from ICRP 60 and 103 (Adapted by the researcher from ICRP 60 & 103).

Recommendation of ICRP 60 - 1990	
Tissue or Organ	***Tissue Weighting Factor***
Gonads	0.20
Bone marrow (red)	0.12
Colon	0.12
Lung	0.12
Stomach	0.12
Bladder	0.05
Breast	0.05
Liver	0.05
Oesophagus	0.05
Thyroid	0.05
Skin	0.01
Bone surface	0.01
Remainder	0.05

Recommendation of ICRP 103 - 2007	
Tissue or Organ	***Tissue Weighting Factor***
Gonads	0.08
Bone-marrow (red)	0.12
Colon	0.12
Lung	0.12
Stomach	0.12
Bladder	0.04
Liver	0.04
Oesophagus	0.04
Thyroid	0.04
Skin	0.01
Bone surface	0.01
Salivary glands	0.01
Brain	0.01

The important change to the effective dose was that a computational phantom based on medical tomographic images of a human body was to replace the mathematical models previously used for the external and internal doses (ICRP 103, 2007). The effective dose is calculated from age and sex-averaged tissue weighting factors which are based on the updated risk data (ICRP 103, 2007).

$$E \approx k \, x \, DLP$$

Equation 2.1: Effective dose calculation.

E is measured in mSv and *k* is the coefficient that is obtained from the ICRP 103 (Karim *et al.*, 2016). Effective dose is influenced by the CT scans' kVp, mAs and total scan length (Schawkat *et al.*, 2017).

The ICRP 103 document (2007) states that the effective dose is intended to be used for radiation protection quantity. The prospective dose assessment for the planning and optimisation in radiation protection is the main purpose of the effective dose (ICRP 103, 2007). The effective dose is also utilised for comparison between technologies and patient groups, but not for individual patient measurement (Kalender, 2014). The patient's CT dose is dependent on the scanner radiation output as well as the size of the patient (AAPM, 2011).

2.1.2.2. Size-Specific Dose Estimate

When calculating the effective dose, the DLP is used to determine dose and therefore only the length of the CT scan and not the patient's size is taken into account. Report 204 was written in 2011 by the American Association of Physicist in Medicine (AAPM). The report was based on a joint task group consisting of the International Commission on Radiation Units and Measurements (ICRU) and the Image Gently Campaign of the Alliance for Radiation Safety in Paediatric Imaging (AAPM, 2011). This task group authored the report on size-specific dose estimate (SSDE) in paediatric and adult body CT examinations. Thus, a new estimate of patient dose was determined, which uses $CTDI_{vol}$ and a size related parameter.

The lateral (Lat) dimension of the patient is measured from the left to right dimension of the patient. The anterior posterior (AP) dimension is the thickness of the body part being scanned (AAPM, 2011). The sum of the Lat and AP dimension is then calculated, as it is linearly related to the effective diameter (AAPM, 2011). The effective diameter can be thought of as the diameter being equal to the diameter of the circle of which the area is the same as the patient's cross section (AAPM, 2011).

The equation for the effective diameter is:

$$Effective\ diameter = \sqrt{AP\ x\ Lat}$$

Equation 2.2: Effective diameter calculation.

Thus, an estimate of the patient dose is made and called the size-specific dose estimate (SSDE) (AAPM, 2011).

To calculate the SSDE (*in mGy*):

$$SSDE = CTDI_{vol}\ x\ f$$

Equation 2.3: SSDE calculation.

The conversion factor (*f*), which is necessary in order to estimate the patient dose can be found in the AAPM Report 204 (See appendix A).

The SSDE was shown to provide a direct comparison with radiation dose between various parameter settings and between different CT scanners (Schawkat *et al.*, 2017). Schawkat *et al.* (2017) found that SSDE correlates with the effective diameter of the patient as well as the, kV and mAs used.

2.1.3. Field-of-View Parameter

The field-of-view (FOV) parameter is linked to the bowtie filters. In order for the bowtie filters to work optimally, there is a presumption that the patient is centred correctly within the CT scanners FOV (Philips, 2016). Improper patient positioning has been shown to increase the average surface dose by 23% and the image noise by 7%, when scanning a phantom (Habibzadeh *et al.*, 2012). Research conducted by Kaasalainen *et al.*, (2014) utilised child sized phantoms and found that incorrect positioning in both the horizontal and vertical axis led to an increase in surface dose of 16% and an increase of 24% for the thyroid gland. This increase can have a significant impact on paediatric patients as well as patients with smaller body habitus, as small positioning errors are more likely to occur (Raman *et al.*, 2013).

To ensure the CT scan encompasses the patient's body as well as any immobilisation device, a large FOV is needed (Wu *et al.*, 2020). A CT scanner in an oncology department is used to simulate the patient position for treatment purposes, which include the immobilisation devices and radiopaque markers, which are placed on the patient for planning purposes (Halperin *et al.*, 2013), all of which must be visible in the FOV of the CT image. Of large patients, 28% are often found to have bodies which extend beyond the conventional CT FOV. This causes truncation of the image and potentially simulation errors. It is for this reason that dedicated oncology CT's have a larger bore of 70 cm or greater (Wu *et al.*, 2020).

2.1.4. Diagnostic Reference Levels

Diagnostic reference levels (DRL) were first mentioned by the ICRP in 1990, and in 1996 DRLs were further clarified (Kanal *et al.*, 2017). In 2007 the ICRP stated that "*Diagnostic reference levels apply to radiation exposure of patients resulting from procedures performed for medical imaging purposes. They do not apply to radiation therapy*" (ICRP, 2007). In addition, the ICRP stated that optimisation in radiation therapy involves delivery of the prescribed dose to the tumour and protecting healthy tissues falling outside the target volume. The ICRP also published guidelines regarding radiation protection in the 1985 publication 44 entitled "*Protection of the patient in radiation therapy*" (2007). At the time of publication (1985), the necessity to use the CT for planning purposes was not consistent. In the 1985 publication 44, the authors made mention of the CT as an ancillary piece of equipment in radiation therapy (ICRP, 1985).

Research conducted by Sanderud *et al.* (2016) examined the radiation dose differences between thoracic diagnostic CT scans and thoracic radiation therapy planning CT. This Norwegian research was conducted between April 2013 and May 2014. There were 110 patient scans that were identified for the research. The radiation therapy treatment CT scans constituted 55 (50%) of the patients and the remaining 50% were for diagnostic purposes (Sanderud *et al.*, 2016). The research revealed that the radiation dose for the radiation therapy planning CT was on average four times higher than the diagnostic CT scan for the thorax. These authors concluded that patients with a low BMI had the greatest difference in radiation dose. The researchers stated that not using modified CT protocols based on patient size was the main cause of the higher dose detected (Sanderud *et al.*, 2016).

The DRL is an optimisation tool (Kanal *et al.*, 2017). DRLs determine if dose levels are unnecessarily high and, if without decreasing image quality, the dose may possibly be decreased (McCollough, 2010). In order to identify situations where the dose level to the patient is unusually high, a DRL phantom scan can be used (Kanal *et al.*, 2017). The phantoms used are a 16 cm or 32 cm diameter, polymethyl-methacrylate cylinder phantom. The doses that are measured using these phantoms represent the average patient (Kanal *et al.*, 2017). The scanned phantom represents only patients of the same size as the phantom (Kanal *et al.*, 2017). DRLs are used to determine whether departmental CT scan doses are high in comparison to national and international standards (Kanal *et al.*, 2017). The facility can then optimise their dose and lower it (Kanal *et al.*, 2017). A cross-sectional average dose is approximated by the $CTDI_{vol}$ for

the phantom. The dose in terms of scan length is based on the $CTDI_{vol}$ and the DLP (Kanal *et al.*, 2017). The $CTDI_{vol}$ and DLP are displayed on the CT console and represent the dose to the standard phantoms (Kanal *et al.*, 2017). The European Commission (2018) on radiation protection recommend that in order to set DRLs, both the $CTDI_{vol}$ and DLP be used. The patient dose is relevant from the $CTDI_{vol}$, while the patient dose in terms of scan length is indicated by the DLP (European Commission, 2018). Table 2.2 demonstrates suggested DRLs from European countries (McCollough, 2010). These DRLs can be utilised by a department to ensure their CT scans are optimised.

Table 2.2: Adult DRLs for abdomen to pelvis (abdo-pelvis) CT scans.

Adult DRLs for Abdo-pelvis		
Country	***$CTDI_{vol}$***	***DLP***
United Kingdom 2003	14	560
Netherlands 2008	15	700
European Commission 2004	15	700

Data from McCollough, 2010.

The medical physicist, radiologist and radiographer have to work together to determine if image quality can be obtained at lowered dose levels and what these levels are (McCollough, 2010). To maintain image quality Kanal *et al.* (2017) stated that the dose must increase with patient size. There is currently no guidance, such as DRLs, available for adults of small and large sizes (Kanal *et al.*, 2017). The DRLs currently do not relay information based on patient size, they are a representation of an average patient based on phantom dose (Kanal *et al.*, 2017).

The information about the use of DRLs convinced the researcher that DRLs should be applied to the oncology department, to ensure that the dose from the CT is justified by the image quality necessary for the radiation treatment planning purposes. The CT dose should be optimised, thereby ensuring that it is as low as possible for each procedure. The first step in doing this, is to ensure that the dose is optimised in terms of kV and FOV for the oncology department. This research therefore aimed to establish baseline dose levels for CT scans of the pelvis by utilising an anthropomorphic phantom and water phantoms of different sizes, representing different sized patients.

This section outlines parameters used to calculate the dose received by the patient during a CT examination as it will be applied in the present study, as described in the methodology.

2.2. Methodology

The anthropomorphic phantom (refer to Figure 2.3) scans data were collected to determine how the different FOV's influenced the radiation dose delivered and to establish baseline dose levels for pelvic CT scans, as per the objective of the study. In addition, the data from the water phantom scans were collected to determine the effect the phantoms of different sizes had on the CT dose. The water phantoms are all equal in width, with the exception of the small water phantom, which has an extension (refer to Figure 2.4). Therefore, the dose that was calculated was based on the same factors, these being equal DLP and $CTDI_{vol}$, with the exception of the effective diameter (for the extra-large, large and medium water phantoms). The $CTDI_{vol}$ and DLP were used as part of the CT dose calculation. The dose levels were calculated using the SSDE. The effective diameter (Equation 2.2) was calculated by measuring the thickest part of the anthropomorphic phantom in the scan range in both the AP and LAT dimensions. This value was then used to determine the conversion factor *f*, used in Equation 2.3 with the $CTDI_{vol}$. The effective dose (*E*) was calculated by using the *k* value and DLP (Equation 2.1) for the pelvis and abdomen related to the kV chosen for the CT scan.

2.2.1. Research Tools

The research tools that were used during the research process are listed as follows:

1. A TSX-201A (Toshiba Aquilion © Large Bore (LB)) CT scanner, which was compliant at the time with the annual quality assurance tests as well as the daily checks that were carried out by the onsite medical physicists of the department. The Toshiba Aquilion © LB CT scanner is used exclusively for CT localisation scans at the oncology department. The Toshiba Aquilion LB CT scanner utilised does not use automatic exposure control (AEC) and the kV is not manually selected.
2. The pelvic examination setting was chosen on the CT console and used for the purpose of the research. The different examination selections on the Toshiba Aquilion © LB CT scanner is illustrated in Figure 2.1. At that time of the research, the only variable that was being modified by the radiation therapist during the patients' CT scans was the FOV's.

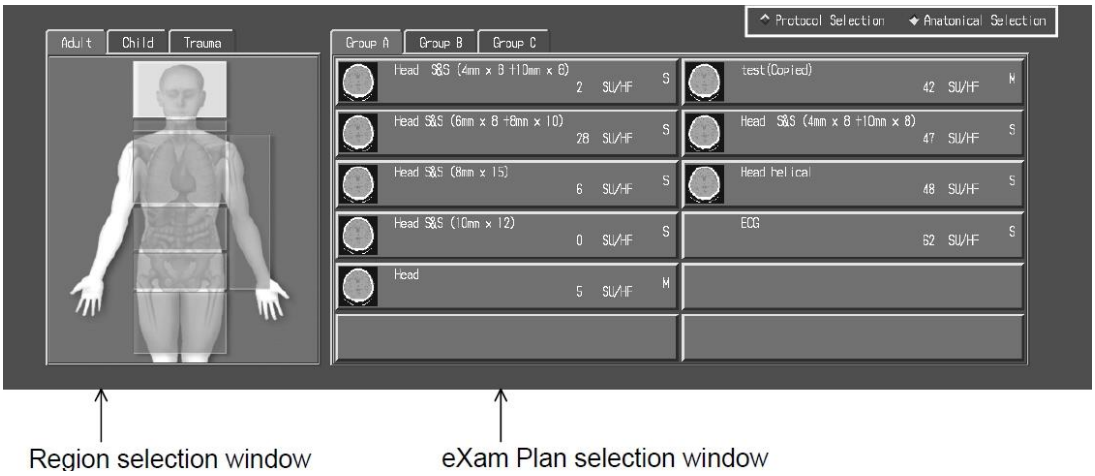

Figure 2.1: Protocol selection on Toshiba Aquilion © LB CT scanner.
(Courtesy of Toshiba © Medical Systems Corporation 2004.)

- The kV settings used for the research were the 135 kV, 120 kV and 80 kV.
- The FOVs used were the extra-large (XL) =70 cm in diameter, large-large (LL) =55 cm in diameter, large (L) =40 cm in diameter and medium (M) =32 cm in diameter for the 135 kV and 120 kV respectively.
  The small (S) = 24 cm in diameter FOV was used with the 80 kV.

3. The pelvic CT scan protocol for the oncology department, states that the scan must include from T10 to below the symphysis pubis (Department protocol: 2019).

4. An anthropomorphic phantom from the medical physics department was scanned to measure the dose for different FOVs using the pelvic CT examination setting.

5. Water phantoms of various sizes from the medical physics department, were scanned to determine dose differences with different FOVs and kV settings for phantoms of varying size.

6. The calculations used in the research were as follows:
   - The effective dose was calculated using the DLP measured in mSv and the *k* coefficient that is obtained from the ICRP 103 (Appendix A):

     $$E \approx k \, x \, DLP$$ (Equation 2.1).

   - The effective diameter was calculated by measuring the widest part of the phantom in the AP dimension:

     $$Effective\ diameter = \sqrt{AP \, x \, Lat}.$$ (Equation 2.2).

   - SSDE was calculated using the effective diameter, then obtaining the conversion factor *f* used to estimate patient dose. The calculation (measured in mGy) is then:

     $$SSDE = CTDI_{vol} \, x \, f$$ (Equation 2.3).

2.2.2. Research Process

The research process to determine the baseline dose level followed the steps depicted in figure 2.2.

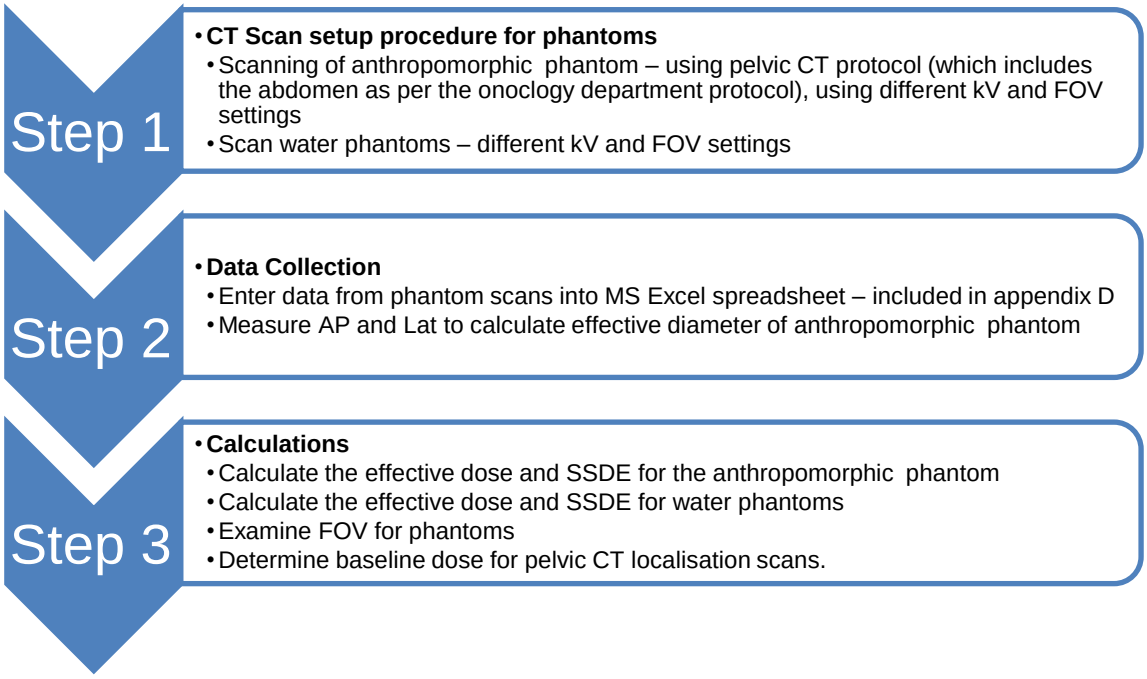

Figure 2.2: The research process to determine the baseline dose.

2.2.2.1. CT Scan Set-up Procedure for Phantoms

The next section describes the procedure to scan both the anthropomorphic and water phantoms (see section 2.2.1). The setup procedure as described is used by the medical physicists in the oncology department. As stated in the methodology, the medical physicist assisted the researcher by demonstrating the correct setup for the phantoms.

Anthropomorphic Phantom

The anthropomorphic phantom (Figure 2.3a) consists of slices, which contain human bone. The slices are held together in a frame which allows the correct number of slices to be added or subtracted. The slices are numbered to ensure correct installation of the phantom.

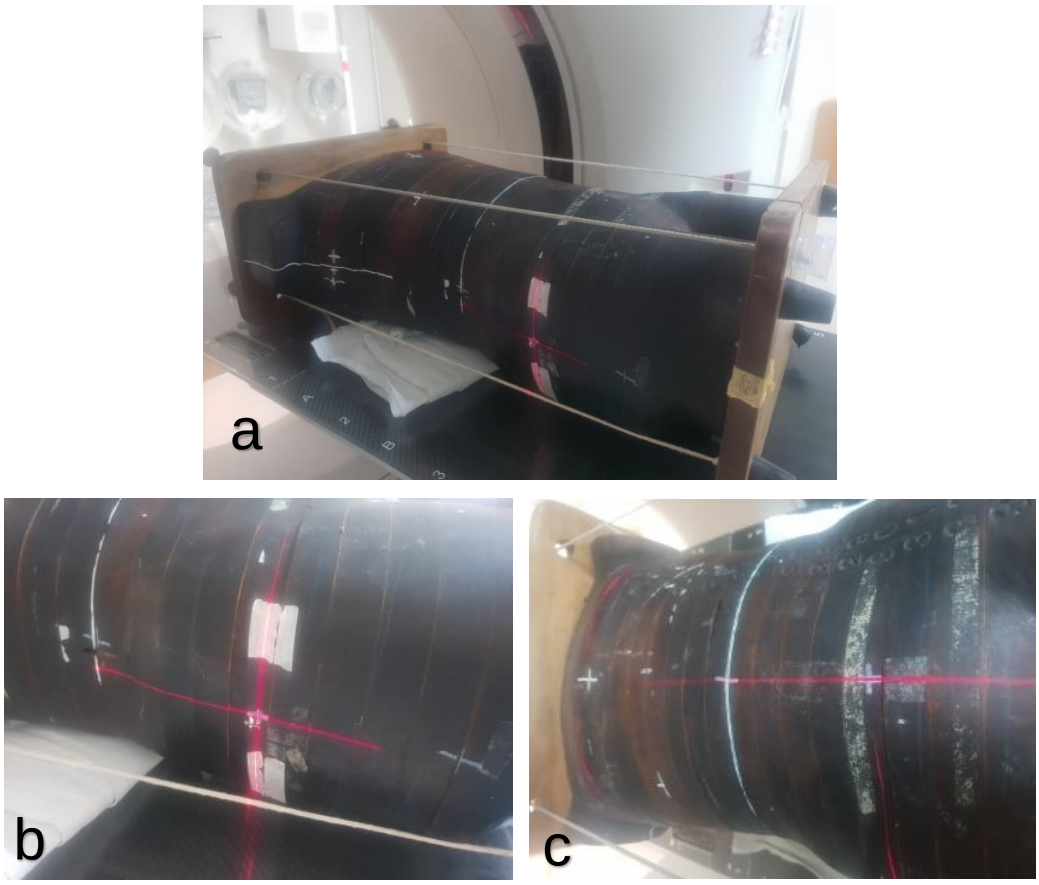

Figure 2.3: Anthropomorphic phantom.
(Courtesy of researcher photos taken during research process).

The researcher placed the phantom flat on the CT couch and selected the pelvic examination setting for the supine pelvis on the CT console. The zero slice was chosen by using lateral markers indicated on the phantom with a white marker (Figure 2.3b), that ensured the exact same point was used for all the scans. The midline position of the phantom was guaranteed by using the midline and, white marker, on the phantom (Figure 2.3c). The CT laser light was used in conjunction with these markings to ensure that the phantom was in the correct position to be scanned.

The phantom was scanned by modifying the kV setting and the field of view (FOV) as described in the aforementioned. To ensure consistency, the phantom was zeroed at the same point and the scan start and end length were maintained throughout the scans. The scan range was set as starting at 220 mm and scan end point of -160 mm from the zero point (as described previously). The scan range was chosen as it fitted the oncology department's protocol, which states that pelvic scans must include from thoracic vertebra number 10 (T10) to below the symphysis pubis. The CT bed was moved in for 23 cm after zeroing the bed for each scan. Consistency was thus ensured

by having each scan on the same point for the zero slice and having the same number of images per scan.

Water Phantoms

The water phantoms in the department are of different sizes and range from small to extra-large, as illustrated in figure 2.4. These water phantoms of the Toshiba CT scanner are employed as part of the quality assurance programme performed by the medical physicists in the oncology department.

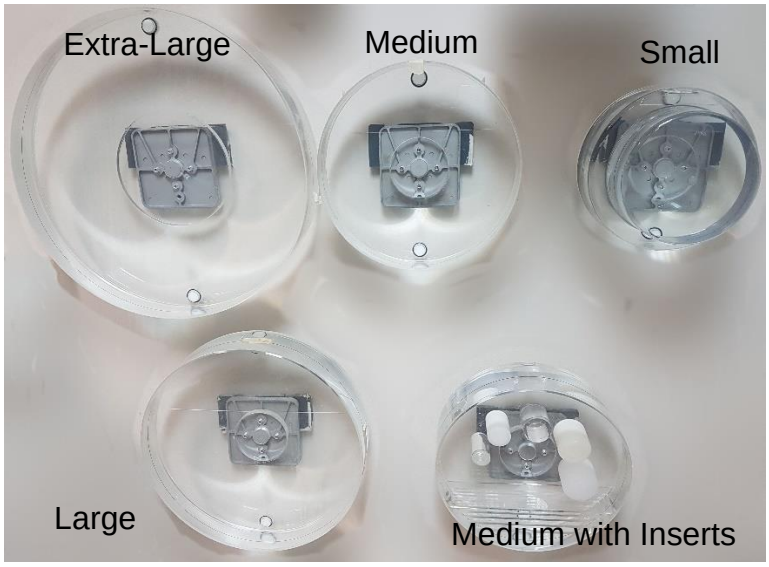

Figure 2.4: Water phantoms found at the oncology department.
(Courtesy of the oncology department)

The water phantoms are of varying sizes and their diameters are measured as follows: the extra-large = 50 cm, the large = 40 cm, medium = 30 cm and the small water phantom = 25 cm. The phantoms were scanned by selecting the pelvic examination setting for the supine pelvis on the CT console. The scan range was from scan start at 50 mm and scan end at -46 mm. The small water phantom had a larger scan range due to the smaller extension (this is specifically used for head and neck scans). The scan range for the small phantom was scan start 50 mm and scan end -120 mm. This was determined from the zero slice as indicated by the black line along the circumference of the water phantom. The phantoms were set up as show in Figure 2.5. The CT bed was moved in after zero for 6 cm, therefore from the zero, the researcher ensured that the 6 cm was fed in. This resulted in an exact position for the start of the scan range. This also ensure consistency between all the scan ranges.

Figure 2.5: Water phantom set-up with red laser, lateral and anterior view.
(Courtesy of the researcher, photos taken during research).

2.2.2.2. Data Collection

The data was captured directly after the CT scan was performed by means of a Microsoft (MS) Excel spreadsheet (Table 2.3). The spreadsheet was created based on a variety of research articles about CT dose (refer to: 1.4). Before the onset of the pilot study the Excel spreadsheet was tested to determine if the calculations were correct. This was further confirmed at the onset of the pilot study.

Table 2.3: Phantom dose data capture sheet.

	Measure		CT information									
Scan No.	AP	Lat	kV	mA	FOV	mAs	Scan Time	Total Number of Images	Scan Start	Scan End	$CTDI_{vol}$	DLP

The Scan No is the scan name allocated in order to identify the method of the scan. The AP and Lat measurements for the anthropomorphic phantom scans were measured and used to calculate the effective diameter. The water phantoms' AP and Lat dimensions were the dimensions of the phantoms themselves.

The CT information was captured from the information seen on the CT console (figure 2.6.)

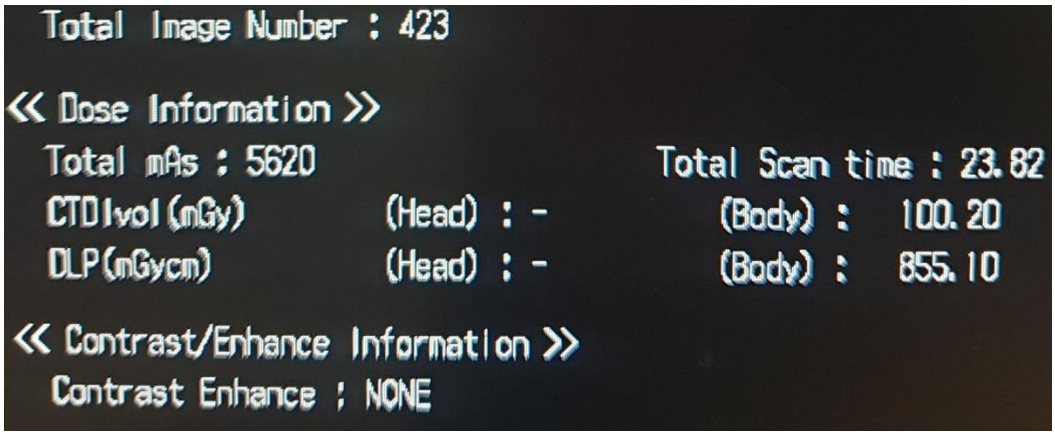

Figure 2.6: CT information for phantom scans.
(Courtesy of the Researcher, photo taken from CT screen during research)

The information captured from Figure 2.6 was the mAs, scan time, total number of images, $CTDI_{vol}$ and DLP. The kV, mA and scan start-and-end were determined from the scan data on the CT. The $CTDI_{vol}$ and DLP were used to calculate the SSDE and effective dose respectively.

2.2.2.3. Analysis of Captured Data

The CT data, once entered into the MS Excel spreadsheet, automatically calculated the results. The calculations that were produced are illustrated in Table 2.4. The CT data was verified upon completion of entry by the use of photographs of the CT information to ensure the data was correctly entered.

Radiation absorbed dose's SI unit is in gray (Gy): 100 centigray (cGy) is equivalent to 1 Gy and 10 milligray (mGy) is equivalent to 1 cGy. The $CTDI_{vol}$ is in mGy and all calculations are based on mGy. In oncology the dose given per fraction of radiation is given in cGy, therefore all doses calculated during the research are presented in either mGy or converted to cGy.

Table 2.4: Phantom dose calculations sheet.

Calculations						
Effective Diameter	**SSDE**	**cGy**	**Effective Dose-Pelvis**	**cGy**	**Effective Dose -Abdomen**	**cGy**

cGy is the converted (either SSDE, or effective dose for pelvis or abdomen) from mGy.

The calculations occur as previously described (refer to: 2.2.1.) The effective diameter was calculated from the CT data of the phantoms' AP and Lat dimensions. The dose for the SSDE is in mGy and converted to cGy. The effective dose is in mSv and converted to cGy. The radiation weighting factor for x-rays is 1, therefore, to convert Sv

to Gy it is determined that 1 Gy is equal to 1 Sv. Thus, 1 mSv is equal to 1 mGy and it is known that 1 mGy is equal to 0.1 cGy (Bluemke & Liu: 2012).

2.2.3. Validity and Reliability

Validity of research is described by Kumar (2011) as ensuring the correct application of procedures to determine the answer to the proposed question. While the quality of the measurement procedure that ensures the repeatability and accuracy is defined as the study's reliability (Kumar, 2011). The phantom scans were part of the pilot study for the research project.

The following points ensured the validly and reliability of the research:

- For all CT scans included in the research, both phantom and patient data, only one CT scanner was used. Therefore, the information of the dose output remained consistent.
- The CT scanner used had passed all quality assurance test performed by the medical physicists; these are daily, weekly and monthly tests.
- The resident medical physicist in charge of the CT scanner assisted the researcher by demonstrating the correct setup of the phantoms, which were scanned for the research.
- The medical physicist also verified the mathematical formulas.
- The MS Excel spreadsheet utilised for calculations was tested for accuracy prior to the commencement of the research and then again upon commencement of the research. No modifications were made after the pilot study.
- The research demonstrated dose as defined by SSDE, which is frequently used in research papers. The AAPM state that SSDE should be used to determine dose to patients, especially children.
- All CT data were collected by the researcher only.
- The researcher validated the information captured on the MS Excel spreadsheet. Incorrect entries were revalidated and corrected or excluded from the research. The validation was first a check from the written data of the research, whereafter a further validation was done to confirm the data by means of a photograph taken of the CT information for each CT scan.

- The researcher photographed each dose information page on the CT to ensure that the correct information was maintained. These photographs were used to verify every phantom and patient's dose information used in the research.

2.3. Results

The anthropomorphic phantom and water phantom analysed data for the radiation dose for pelvic localisation CT in the oncology department are presented here. The calculated CT dose using the effective dose and SSDE are given. The FOV parameters for the anthropomorphic phantom are shown. The baseline CT dose for pelvic localisation was created based on the phantom information obtained.

2.3.1. CT Scan Dose

The anthropomorphic phantom was scanned and the dose assessed for both the effective dose and SSDE. The water phantoms of different sizes were scanned and the calculated dose used to determine the effect of different sized phantoms on CT dose.

2.3.1.1. Anthropomorphic Phantom CT Scan Dose

The information of the CT scans for the anthropomorphic phantom are presented in Table 2.5.

Table 2.5: CT Information using different kV and FOV settings for anthropomorphic phantom with AP and Lat measurements 22.7 cm and 30.3 cm respectively.

	CT information									
Scan No.	***kV***	***mA***	***FOV***	***mAs***	***Scan Time (seconds)***	***Total Number of Images***	***Scan Start***	***Scan End***	***$CTDI_{vol}$ (mGy)***	***DLP (mGy.cm)***
135XL	135	300	Extra Large	5620	23.82	423	260	-160	130.40	1113.10
135LL	135	300	Large Large	5620	23.82	423	260	-160	130.40	1113.10
135L	135	300	Large	5620	23.82	423	260	-160	130.40	1113.10
135M	135	300	Medium	5620	23.82	423	260	-160	87.40	745.50
120XL	120	300	Extra Large	5620	23.82	423	260	-160	100.20	855.10
120LL	120	300	Large Large	5620	23.82	423	260	-160	100.20	855.10
120L	120	300	Large	5620	23.82	423	260	-160	100.20	855.10
120M	120	300	Medium	5620	23.82	423	260	-160	65.40	558.60
80S	80	300	Small	5620	23.82	423	260	-160	53.10	453.30

Scan no = Name for scan, using kV and FOV as indicator. kV=kV chosen for each scan. mA = mA used for each scan. FOV = FOV chosen for each scan. mAs = mA and time that was used for each scan. Scan Time (seconds) = the time it takes for each scan as indicated in seconds. Total number of images = the number of images that were created by the CT scan. Scan start = the CT position for the start of the CT scan. Scan end = the CT position at the end of the CT scan. $CTDI_{vol}$ = $CTDI_{vol}$ that is determined by CT scan. DLP= the DLP that is determined by the CT scan.

The different kV settings are shown; the lowest 80 kV is demonstrated as dark green, the 120 kV in light green and the 135 kV in white. The mA is constant at 300. There are a few constants with the CT information, these are the mAs, scan time, total number of images and the position of the scan start and where the scan ends. The information that remains constant, indicate which data is not influencing the calculated CT dose. The $CTDI_{vol}$ is the same for the XL, LL and L FOV for each kV. The $CTDI_{vol}$ decreases with kV and is lowest for the 80 kV. The DLP follows the same trend as the $CTDI_{vol}$.

...

The dose calculation (Table 2.6), demonstrates the calculations performed, based on the CT information obtained. The effective diameter was calculated from the AP and Lat measurements of the anthropomorphic phantom. The SSDE was calculated: the effective diameter was utilised to obtain the conversion factor *f*. The $CTDI_{vol}$ was then multiplied by the *f* factor and the calculated SSDE is indicated in mGy. The cGy column converted the SSDE from mGy to cGy. Finally, the effective dose for the pelvis and abdomen were calculated in mSv, using the conversion factor (*k*), based on the kV that was used for the scan as well as the DLP.

Table 2.6: Anthropomorphic phantom CT dose calculations.

Scan No.	*Effective Diameter*	*SSDE (mGy)*	*SSDE (cGy)*	*f*	*Effective Dose-Pelvis (mSv)*	*k Pelvis*	*Effective Dose –Abdomen (mSv)*	*k Abdomen*
135XL	26.23	186.47	19	1.43	14.58	0.0131	17.25	0.0155
135LL	26.23	186.47	19	1.43	14.58	0.0131	17.25	0.0155
135L	26.23	186.47	19	1.43	14.58	0.0131	17.25	0.0155
135M	26.23	124.98	12	1.43	9.77	0.0131	11.56	0.0155
120XL	26.23	143.29	14	1.43	11.03	0.0129	13.08	0.0153
120LL	26.23	143.29	14	1.43	11.03	0.0129	13.08	0.0153
120L	26.23	143.29	14	1.43	11.03	0.0129	13.08	0.0153
120M	26.23	93.52	9	1.43	7.21	0.0129	8.55	0.0153
80S	26.23	75.93	8	1.43	5.80	0.0128	6.84	0.0151

Scan no= name of the scan using the kV and FOV. Effective diameter = converted effective diameter from AP and Lat calculation. SSDE (mGy)= calculated SSDE in mGy. SSDE (cGy) = converted SSDE into cGy. Effective dose-pelvis/abdomen (mSv)= the calculated effective dose for the pelvis/abdomen in mSv.

The effective dose for both the pelvis and abdomen was calculated. Although only one CT is used, the effective dose for the abdomen- and pelvis were calculated separately as there are different *k* coefficients for each. The 135 kV XL, LL and L FOV had an effective dose for the pelvis of 14.6 mSv and the abdomen 17.3 mSv. The 120 kV XL, LL and L FOV had an effective dose for the pelvis as 11.0 mSv and 13.1 mSv. The M FOV effective dose for the pelvis was 9.9 mSv for the 135 kV and 7.2 mSv for the 120 kV. The abdominal effective dose was 11.6 mSv for the 135 kV and 8.6 mSv for the 120 kV M FOV. The 80 kV S FOV is 5.8 mSv for the pelvic effective dose and 6.8 mSv for the abdominal effective dose.

The effective diameter was determined to be 26.2 cm, using an electronic calliper. The SSDE was calculated and converted to cGy dose, as shown in the cGy column of Table 2.5. The SSDE for the 135 kV and 120 kV, XL, LL and L FOV calculated to 19 cGy and 14 cGy, respectively. The SSDE for the M FOV is 12 cGy for the 135 kV and 9 cGy for the 120 kV. The 80 kV S FOV had an 8 cGy SSDE.

Figure 2.7 demonstrates the CT dose values for the different kV energies and different FOVs used. The effective dose has been converted to cGy to compare to the SSDE (see Table 2.6.). In comparison to the table 2.6 which indicates the effective dose in mSv, by converting to cGy an extensive difference between the SSDE and effective dose is visualised in Figure 2.7.

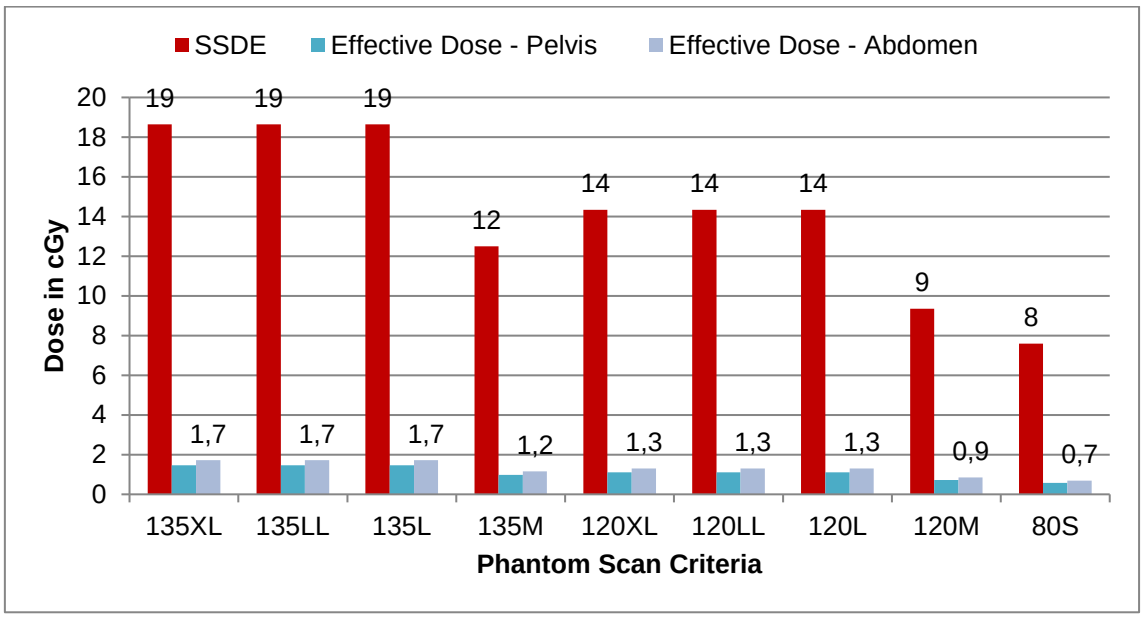

Figure 2.7: Dose values based on anthropomorphic phantom scan data.

Figure 2.7 illustrates that SSDE has an impact on the patient dose. The SSDE of the anthropomorphic phantom indicated that the 80 kV has the lowest dose however, it is limited to the S FOV, which was found to exclude adult patient tissue from the FOV. Therefore, the S FOV can only be used for paediatric patients (not part of this specific research study). The 120 kV produced a lower dose than the 135 kV. The FOV dose for the XL, LL and L remains constant. The trends can be observed in Figure 2.8.

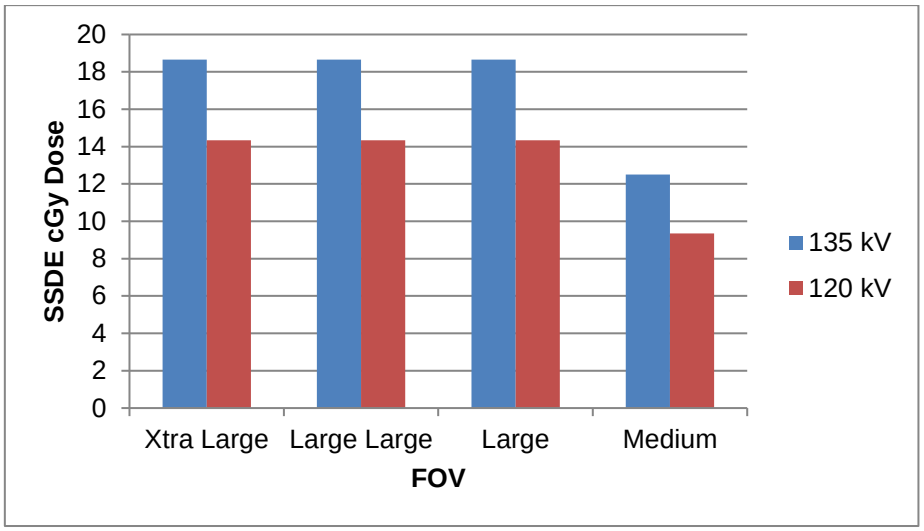

Figure 2.8: Anthropomorphic phantom scans indicating the relationship between kV and FOV.

Figure 2.8 demonstrates the relationship between the 135 kV (blue bar) and 120 kV (red bar) SSDE dose for the anthropomorphic phantom and the four different FOVs used. The SSDE dose remains constant for the XL, LL and L FOV for the 135 and 120 kV, respectively. The decrease in the CT from the 135 kV to 120 kV can also be distinguished. The M FOV is shown to have the lowest dose. The dose reduction occurs in the M FOV and S FOV due to a decrease in the $CTDI_{vol}$. A decrease is also noted from the 135 kV to 120 kV (refer to Table 2.5).

2.3.1.2. Water Phantom CT Scan Dose

The four water phantoms were scanned and the SSDE was calculated in order to determine the effect that the size of a phantom has on the dose (SSDE). The doses for the small, medium, large and extra-large water phantoms data are demonstrated. The CT dose calculations included the effective dose and the SSDE. The small water phantom has an extension in the front section; this caused an increase in the mAs, scan time and number of images. The scan start position and end positions were also increased for the small water phantom. For a full examination of the dose results the Tables A.2.1 to A.2.4 found on the accompanying Compact Disc (CD) may be examined.

The $CTDI_{vol}$ and DLP followed the same trend as seen with the anthropomorphic phantom, for all the water phantoms. A trend can be observed, that is that the $CTDI_{vol}$ shows an increase with an increase in kV. The XL, LL and L FOV had an equal $CTDI_{vol}$ for the 135 kV and 120 kV, respectively. The DLP followed the same trend. Both the

$CTDI_{vol}$ and DLP are lower for the M FOV for both the 135 kV and 120 kV. The 80 kV with the S FOV has the lowest $CTDI_{vol}$.

The effective doses for the medium, large and extra-large water phantoms are all the same (see Table A.2.2 to A.2.4). This is due to the same scan length being used. However, the small phantom dose is higher, due to the increased scan length. Table 2.7 provides the effective dose data for the all the water phantoms, including the small, which as stated already, has an extra scan length.

Table 2.7: Summary of effective dose for extra-large, large medium and small water phantom scans of the pelvis and abdomen.

		Extra-large, large and medium water phantom		Small water phantom			
Scan Setting		Effective Dose (mSv)				*k* Factor	
kV	*FOVs*	*Pelvis*	*Abdomen*	*Pelvis*	*Abdomen*	*k Pelvis*	*K Abdomen*
135	XL, LL, L	4.3	5.1	6.7	7.9	0.0131	0.0155
120	XL, LL, L	3.3	3.9	5	6	0.0129	0.0153
135	M	2.9	3.4	4.5	5.3	0.0131	0.0155
120	M	2.1	2.5	3.3	3.9	0.0129	0.0153
80	S	1.7	2	2.7	3.1	0.0128	0.0151

Scan setting are the kV and FOV used for the scan. The effective dose in mSv for the pelvis and abdomen for the extra-large, large and medium, followed by the small water phantoms data.

Table 2.7 demonstrates the calculated doses for the effective dose for the 135 kV, 120 kV and 80 kV. The dose is constant for the Extra-large, large and medium water phantom, the difference with the small phantom si the increased scan length due to the additional section found on the phantom (refer to 2.2.2.1). The green highlighted area illustrates the M FOV. The lowest effective dose is found with the 80 kV as the dose increases with an increase in kV. The small water phantom shows an increase in dose for all the effective doses when compared to the other water phantoms. Therefore, the impact of the increased scan length can be noted.

Table 2.8 illustrates the SSDE for all the water phantoms. Note that the small phantom has an increased length scan.

Table 2.8: Summary SSDE for the extra-large, large, medium and small water phantoms.

Scan Setting		Phantom Size – SSDE (cGy)							
kV	*FOVs*	*Extra-large*	*f*	*Large*	*f*	*Medium*	*f*	*Small*	*f*
135	XL, LL, L	9	0.71	11	0.85	16	1.23	19	1.48
120	XL, LL, L	7	0.71	9	0.85	12	1.23	15	1.48
135	M	6	0.71	7	0.85	11	1.23	13	1.48
120	M	5	0.71	6	0.85	8	1.23	10	1.48
80	S	4	0.71	5	0.85	7	1.23	8	1.48

Scan setting kV and FOV used in the scan. The calculated SSDE in cGy for the different phantom sizes. f = conversion factor determined from the effective diameter of the phantom.

The SSDE can be seen to decrease with a decrease in kV as for the effective dose. However, the SSDE increases with a decrease in phantom size.

Figure 2.9 shows the SSDE for the water phantoms and illustrates the effect that the different phantoms' diameters have on the dose of the phantom whilst all other aspects remain constant.

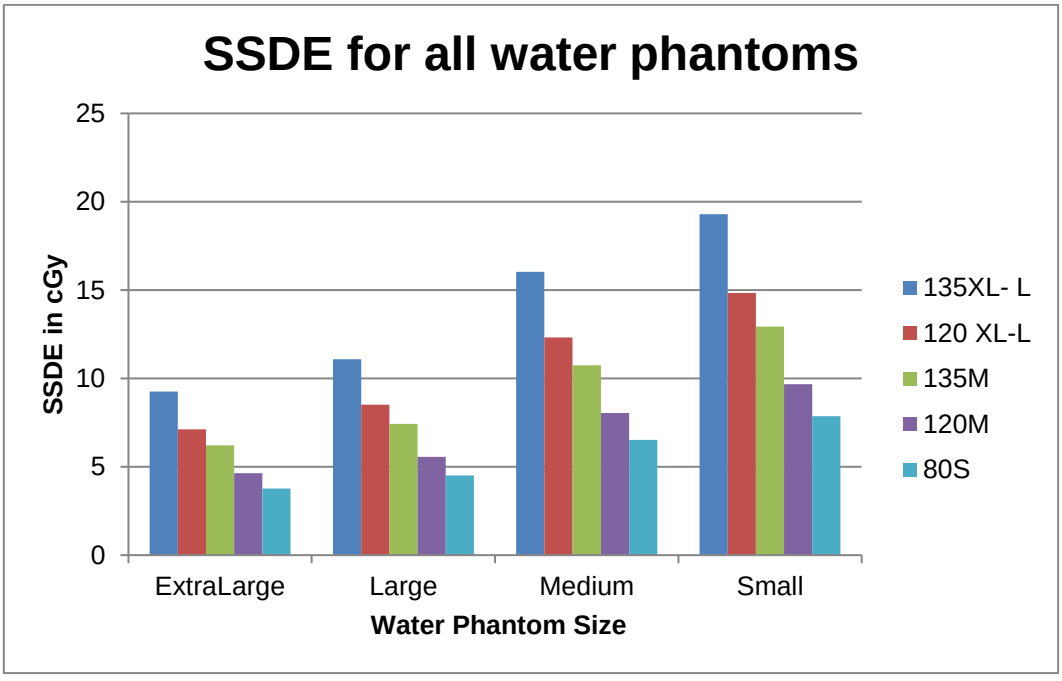

Figure 2.9: SSDE for water phantoms.

The SSDE is decreased with an increased phantom size. The SSDE demonstrates the difference that the patients' size makes to the dose. The water phantoms decrease in size by 10 cm, except for the small water phantom. The sizes for the water phantoms are as follows: extra-large = 50 cm, large = 40 cm, medium = 30 cm and the small water phantom = 25 cm. Thus, the SSDE for the first three water phantoms shows the increase of dose for every 10 cm decrease in effective diameter.

2.3.2. *Field of View of the Anthropomorphic Phantom*

The FOV of the anthropomorphic phantom was examined to ensure that the entire phantom had been included in the FOV. Table 2.9 demonstrates the different FOV's and whether they are deemed appropriate, too wide or too narrow for the anthropomorphic phantom CT scan. Using the zero-slice, a measurement from the phantom circumference that is closest to the edge of the FOV is measured. The last column illustrates the measurement that occurs when the CT couch is excluded and the measurement is taken from the posterior of the patient's contours. The couch may be excluded for 3D conformal planning. However, certain radiation therapy plans must include the table as well as the patient setup equipment as this is part of the oncology department protocol (Sherriff, 2019). These inclusions are used with intensity modulated radiation therapy (IMRT) planning. Which require the equipment's density, to ensure correct dose distribution to the tumour and surrounding tissue, as calculated by the planning programme.

Table 2.9: Anthropomorphic phantom FOV information (XL, LL, L & M).

Field of View				Measurement (cm)				
FOV size	*Phantom in relation to*	*Size Lat dimension*	*Size Ant Post direction*	*L Lat*	*R Lat*	*Ant*	*Post*	*Post excl. table*
XL	Centre of FOV	Too Wide	Too Wide	19.1	18.8	22.8	23.9	18.8
LL	Centre of FOV	Too Wide	Too Wide	11.3	12.4	15.4	16.4	11.4
L	Centre of FOV	Appropriate	Appropriate	4.2	5.3	7.8	9.2	3.6
M	Centre of FOV	Too Narrow	Too Narrow	0.0	1.3	3.8	5.3	0.0

Field of View = size of the FOV, where the patient is positioned in relation to the FOV, this could be in the centre, left or right. The size of the lateral or anterior or posterior dimension in terms of the FOV: this could be too wide or narrow or appropriate. The measurements in cm = the measurement from the phantom to the edge of the FOV in terms of the left, right and anterior or posterior of the phantom. The Post excl. table is the posterior measurement with the CT couch excluded, i.e., from the posterior of the patient.

The guidelines to determine if the FOV was too narrow or correct, was deemed as below 5 cm being too narrow, between 5 cm and 10 cm being appropriate and above 10 cm as too wide. The anthropomorphic phantom was scanned to represent a patient. As contours of patients often vary in areas, i.e. from abdominal to pelvic area. The 5 cm should thus include these variations, especially in the pelvic and abdominal area. Thus, the FOV should include the entire contour of the patient.

As illustrated in Table 2.9, the M FOV was too narrow for the patients' scans. The L FOV was appropriate and the LL and XL were too wide for the anthropomorphic phantom. The difference between the left and right lateral demonstrates that the phantom was about 1 cm towards the right side. From Table 2.9 it can also be noted from the Ant and Post columns, which indicate the measurement from the posterior and anterior aspect of the phantom to the FOV edge, that the phantom was 1 cm too posterior for all the setups. For radiation therapy planning purposes the patient is aligned with lasers and tattoos are made, thus the patient is often not perfectly aligned in the centre of the FOV. The anthropomorphic phantom is positioned as a patient would be, thus the phantom is aligned at the midline of the phantom as well as in the lateral aspect of the phantom. Therefore, with the slight differences from posterior and anterior the phantom is deemed to be in the centre. The phantom is therefore well centred in the FOV, as described previously in section 2.1.3.

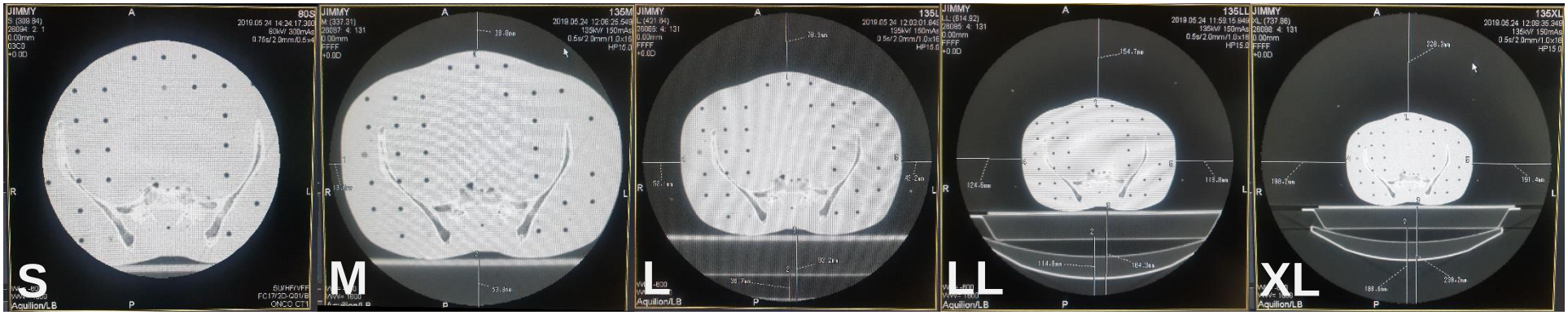

Figure 2.10: Anthropomorphic positioning from S to XL FOV.

Figure 2.10 demonstrates the different FOV's and how the phantom contour fits into the FOV's. As stated previously, the FOV must include the entire patient for correct dose calculation in CT planning software. From Figure 2.10, it can be gleaned that the S FOV is inappropriate, as no gap is visible between the FOV and the phantom. The M FOV is also too narrow, when the patient's diameter increases within the CT scan range which would result in the patient's body contour being excluded from the CT scan imaging. Therefore, the L, LL and XL FOV can only be used for the phantom's diameter.

2.3.3. Baseline CT Dose Data

The baseline dose for the CT localisation of the pelvis was determined based on the concept of a DRL (refer to Section: 2.1.4). In terms of DRLs, the anthropomorphic phantom was scanned to determine the effect of the FOV and kV on the dose. Thus, the lowest possible dose was determined based on the FOV and kV setting that could be used. It is advised that the CT dose with the lowest dose possible is recommended. In terms of dose this would be the 80 kV however, only a S FOV is available in this range. Most patients would not fit into the small FOV. The next lowest dose is the 120 kV. Thus, the baseline CT dose would be 120 kV, as the dose is consistent for all FOVs, except the medium FOV. However, the M FOV is not able to be used for most adult patients as it is too small for the anthropomorphic phantoms' body contour.

2.4. Discussion

The objective of this research was to determine baseline dose levels for pelvic CT localisation scans in the oncology department, by scanning an anthropomorphic phantom. The results of this research have demonstrated how the CT dose for both SSDE and effective dose were respectively affected by the different kV and FOV settings. An anthropomorphic phantom was utilised to determine the effect of the FOV and kV settings on the CT dose. The dose in terms of the effective dose and SSDE as well as the FOV and kV settings and their effect on the dose will be discussed. Four water phantoms of different sizes were scanned to determine the effect of the CT dose (SSDE) on different sized phantoms. As the FOV was the only variable modified during the CT scans, the resultant scans were examined to ensure that the entire anthropomorphic phantom contour was visible in the FOV. Finally, a baseline dose was determined for the pelvic CT localisation scans based on the anthropomorphic phantom scan data, determining the lowest dose possible at the appropriate FOV.

2.4.1. Effective Dose

The effective dose is based on the DLP that was measured during the CT scan. The changes in the effective dose are reflected in the DLP (Table 2.5 and Table 2.6). Effective dose does not indicate actual risk to a specific patient however, it reflects the average risk to an average sized patient in the world population (Kalra *et al.*, 2015). The resultant scans of this specific research demonstrated that the effective dose remained constant for XL, LL and L FOV. Therefore, a patient can be scanned with

either one of these FOVs and no changes in the effective dose will occur. As the kV decreased (i.e., from 135 kV to 120 kV), the effective dose decreased as well. The lowest effective dose was found with the 80 kV S FOV. However, this FOV did not allow for the full contour of the anthropomorphic phantom to be visible (refer to Figure 2.10). The S FOV selection on the CT scanner is therefore only suitable for very small paediatric patients.

The effective dose for the anthropomorphic phantom for the 120 kV and L, LL and XL FOV was calculated as 11 mSv for the pelvis and 13 mSV for the abdomen respectively (Table 2.6). Research conducted by Karim *et al.* (2016) in four different CT departments measured the mean pelvic and abdominal effective dose as 7.1 mSv and 11.2 mSv, respectively. Their research makes no mention of the chosen FOV as it focused on the CT radiation doses. The research of Karim *et al.* (2016) was conducted mostly in diagnostic departments. Sanderud *et al.* (2016) stated that oncology CT scans have an increased scan length, which in turn increases the dose measured. Therefore, the increase in CT dose is due to the increased length of the oncology scans, which is justified in the oncological setting for treatment planning purposes where nodal involvement must be assessed for patients' treatment planning.

The effective dose for the extra-large, large and medium water phantoms remained constant for the 120 kV, XL, LL and L FOV, as the DLP remained constant. The pelvis measured 3 mSv and the abdomen 4 mSv effective dose, respectively (Table 2.7). As for the small water phantom, which has an extension on it and thus an increase in DLP, the effective dose measured 5 mSv for the pelvis and 6 mSv for the abdomen (120 kV), respectively (Table 2.7). Therefore, with an increased scan length of 7.4 cm, the effective dose increased. The DLP has less impact from the patient's characteristics, that is the patients' body habitus however, it is more a measure of the amount of incidental radiation to the patient (Karim *et al.*, 2016). The effective dose does not take patient size into consideration for its calculations, as only the length of the scan is used with the calculation.

2.4.2. SSDE

$CTDI_{vol}$, which is the other measurement used for dose information, is the amount of radiation delivered per unit length of the patient and is a measure of radiation intensity (Karim *et al.*, 2016). The $CTDI_{vol}$ is also independent on patient characteristics. Thus, a conversion factor that considers the patient's diameter was created. The SSDE is determined by the size of the patient and demonstrates the dose adaption that occurs

with different sizes of patients. The XL, LL and L FOV gave consistent results for the SSDE and effective dose. The anthropomorphic phantom scan demonstrated an increase in the $CTDI_{vol}$ that correlates with an increase in kV. The XL, LL and L FOV had an equal $CTDI_{vol}$ for the 135 kV and 120 kV, respectively (Table 2.6). Both the $CTDI_{vol}$ and DLP are lower for the M FOV for both the 135 kV and 120 kV (Figure 2.6). The 80 kV with the S FOV had the lowest $CTDI_{vol}$ and DLP. The SSDE for the same FOVs at 120 kV is 14 cGy (Figure 2.7). Kaasalainen *et al.* (2014) stated that anthropomorphic phantoms may be used to approximate the gross attenuation properties found in patients. These researchers used different anthropomorphic phantoms to compare the dose between them. For the purpose of this specific research, access was available to one anthropomorphic phantom only. Therefore, four water phantoms of varying sizes were also scanned to determine the dose difference that occurred with the modification in size. The 120 kV XL, LL and L FOV results were as follows for the water phantoms: extra-large = 7 cGy, large = 9 cGy, medium = 12 cGy and small = 15 cGy (Figure 2.9). There is an increase in dose with a decrease in phantom size (Figure 2.9). Therefore, the smaller the patient's effective diameter the higher the SSDE the patient will receive.

2.4.3. FOV

The FOV is also an important indicator for correct scan procedure in an oncology setting. As determination of therapeutic dose is based on the patient's tissue, the CT scan must include the entire circumference of the patient. The different FOVs and the calculation from the edge of the CT field are illustrated in Table 2.9. The corresponding imagery is demonstrated in Figure 2.6. The XL FOV shows the position of the anthropomorphic phantom in relation to the centre of the FOV. The results of the FOV measurement points out that the anterior measurement (refer to Table 2.9) is 23 cm from the anterior aspect of the phantom to the anterior border of the FOV. The posterior measurement is 24 cm from the posterior aspect of the phantom to the posterior aspect of the FOV. The phantom is well centred in the FOV for patient dose. By examining the Table 2.9 it can be noted that all FOVs are well centred with a 1 cm difference from anterior to posterior. When incorrectly positioning a child-sized phantom in the horizontal and vertical axis, Kaasalainen *et al.* (2014) found that a 24% increase occurred for the thyroid gland and a 16% increase in the surface dose. Raman *et al.* (2013) stated that this could have a significant impact on paediatric and patients with smaller body habitus, as positioning errors are more likely to occur. Thus, the smaller the FOV, the lesser chances of incorrect axial positioning occurring.

The CT localisation scanner can perform scans at XL, LL, L and M FOV for 135 kV and 120 kV. With 80 kV, only a S FOV is available. It was determined that the CT dose for the XL, LL and L are all equal. The M FOV had a decrease in dose and S FOV (only possible with 80 kV) the lowest dose. The S FOV revealed shown to be too small for the anthropomorphic phantom. The conclusion was that the S FOV would not work with most adult patients. Therefore, the next size, being the M FOV, would be a preferred choice. However, the M FOV appeared to not show the entire anthropomorphic phantom. Therefore, the most used FOV would be the XL, LL or L FOV. The dose results for these three FOVs are the same.

As the baseline of the patient is dependent on the FOV that is used, a determination of this FOV is provided as part of baseline CT dose scan. The anthropomorphic phantom is deemed an average adult patient. The ideal patient FOV for a 3D conformal plan is determined to be a L FOV, as can be seen in Figure 2.10., where the entire CT couch is not visible but the entire patient body contour is. However, certain radiation therapy plans, including pelvic, must have the entire CT couch visible in the CT scanned image, as part of the protocol at the oncology department. The research conducted by Munjal *et al.* (2006) found that attenuation due to carbon fibre (the material used for treatment couch construction) was between 3.8% and 8%. This attenuation could cause under-dosing of the tumour volume when planning radiation therapy. Therefore, with certain CT scans that are for specific types of plans, for example prostate patients who receive more complex planning, the FOV will need to be increase to either LL or XL FOV. The XL FOV will be necessary, in particular with immobilisation equipment of the patient, which may go beyond the CT couch borders.

2.4.4. Baseline Dose

A baseline dose was determined during this research. This dose gives an indication of the dose that could be received by a patient for a CT localisation scan in the oncology department. In the research the $CTDI_{vol}$ for the anthropomorphic phantom was 100.2 mGy for the 120 kV and the DLP was 855 mGy.cm (Table 2.5). DRLs are used internationally for diagnostic scans, of which the results indicate a value for a scan. These are not dose limits but are used to determine if any decrease in dose can be obtained in a department. The DRLs indicate the recommended $CTDI_{vol}$ and DLP that could be or should be obtained. In Table 2.2 a suggestion of DRLs from various European countries is shown. From the table it can be gleaned that the highest suggestion for the $CTDI_{vol}$ is 15 mGy and for DLP it is 700 mGy.cm. In 2013 the ACR

determined that the DRL for abdominal CT examinations was 25 mGy (Kalara *et al.*, 2015). The DLP for the anthropomorphic phantom at 120 kV XL, LL or L FOV is 855 mGy.cm, which is close to the suggested DLP. However, the $CTDI_{vol}$ found for the 120 kV, XL, LL or L FOV is 100.2, which is much more than the recommend $CTDI_{vol}$.

2.4.5. Decreasing Dose

Radiation protection is an important concept in any department that deals with radiation. As part of the radiation protection for the patient, decreasing the CT radiation dose is included and is in keeping with the ALARA principles. The need for a reduction in dose is important for small adults as well as paediatric patients (excluded from the current research). The risk for exposure to radiation is thought to be greater in younger patients as they have an increased division of cells and generally have an increased life expectancy (Kalra *et al.*, 2015). Also due to breast, ovarian and uterine cancer, female patients are also at higher risk from radiation exposure. There is also an increased risk for thyroid and lung cancer (Kalra *et al.*, 215). An effective method of decreasing dose to the patient is to reduce the kV. The reduction of kV from 120 kV to 100 kV reduces the radiation dose by 33%. Further reduction to 80 kV can reduce the dose by 65% (Raman *et al.*, 2013). Research conducted by Qurashi *et al.* (2017) whereby they concluded that the use of lower kV (100 kV) for obese patients undergoing a low contrast abdominal CT scan was possible, which decreased their radiation dose by 60%. There was an increase in the mAs however, with the lower kV the dose was reduced due to the exponential relationship with the dose (Qurashi *et al.*, 2017).

It is commonly known in the field of oncology that CT scans for radiation therapy planning may have an increased scan length. The $CTDI_{vol}$ and DLP are much higher than what are recommended by DRLs. Research by Sanderud *et al.* (2016) indicated that radiation therapy scans were four times longer than diagnostic scans, which increases dose. Therefore, further research into dose reduction for CT localisation scan for the pelvis in the oncology department is suggested.

2.4.6. Limitations of the Research

- The oncology department had only one anthropomorphic phantom available. Therefore, a comparison of different dose to different types of anthropomorphic phantoms was not achievable.

2.4.7. Recommendations

- The medical physicist, radiation therapist and oncologist need to collaborate and determine DRL for the oncology department, for all types of oncological localisation scans.
- In line with the image gently campaign, a protocol created for paediatric patients' CT scans should be created with either 80 kV or 100 kV as a lower kV decreases CT dose.

2.5. Conclusion

This phase of the research was conducted to create a baseline CT dose for pelvic localisation scans in the oncology department. The dose recommendation for an average patient in terms of the anthropomorphic phantom was to use 120 kV and XL, LL or L FOV. The dose delivered in terms of SSDE was 14 cGy, which will be used as the baseline CT dose for this research study.

This research by utilising the anthropomorphic phantom, demonstrated the relationship between the increase in kV and the increase in CT dose (for both the effective dose and SSDE). The effective dose and SSDE was consistent for the XL, LL and L FOV for both the 135 kV and 120 kV. The lowest dose was observed with the 80 kV and a S FOV, followed by the 120 kV and M FOV setting.

The water phantoms illustrated the effect of the decreasing phantom diameter on the SSDE. The smaller the diameter, the higher the dose for the different FOVs. However, there was an increase in scan length. The medium, large and extra-large water phantoms had the same scanning criteria. The M FOV had the highest dose of the three and the dose decreased as the phantom diameter increased. This was due to the decrease in the *f* factor based on the increased phantom effective diameter. This indicated that patients should be scanned with the lowest kV and smallest FOV as possibly achievable.

A baseline dose for the CT localisation scan of the pelvis was established, with the use of the data from the anthropomorphic phantom scans, which represents an average person. By having a baseline for the radiation dose received by the oncology patient for pelvic localisation scans as well as the influence of the FOV and kV settings, the radiation therapist can ensure that the optimised dose is received by the patient during their oncological CT localisation scan.

Further research into optimising the dose is encouraged to ensure that the ALARA principles are being upheld during the patients CT scans. The chapter that follows examined the effect the FOV and kV settings had on the image quality of the water phantoms.

References

American Association of Physicists in Medicine (AAPM). 2011. Size-Specific Dose Estimates (SSDE) in Paediatric and Adult Body CT Examinations. *AAPM Report No. 204*. Report of AAPM Task Group 204, developed in collaboration with the International Commission on Radiation Units and Measurements (ICRU) and the Image Gently Campaign of the Alliance for Radiation Safety in Paediatric Imaging. Date of Access: 25 November 2017. <https://www.aapm.org/pubs/reports/RPT_204.pdf>

Auxier, J.A. and Dickenson, H.W. 1983. Guest editorial: concern over recent use of the ALARA philosophy. *Health Physics*. 44 (6) 595-600

Bluemke, D.A. and Liu, S. 2012. *Principles and Practice of Clinical Research. 3rd edition*. Elsiveir. Chapter 41 – *Imaging in Clinical Trials* (pages 597-617)

European Commission. 2018. Radiation Protection: European Guidelines on Diagnostic Reference Levels for Paediatric Imaging. *Radiation Protection N° 185*

Habibzadeh, M.A., Ay, M.R., Kamali Asl, A.R., Ghadiri, H. and Zaidi, H. 2012. Impact of miscentering on patient dose and image noise in x-ray CT imaging: phantom and clinical studies. *Physica Medica*. (28) 191-9.

Halperin, E.C., Wazer, D.E., Perez, C.A. and Brady, L.W. 2013. *Perez and Brady's Principles and Practice of Radiation Oncology*. 5th edition. Lippincott Williams & Wilkins: Philadelphia.

International Commission on Radiological Protection (ICRP). 1985. Annuals of ICRP: ICRP Publication 44. *Protection of the Patient in Radiation Therapy.* Volume 15 No 2

International Commission on Radiological Protection (ICRP). 1990. Annuals of ICRP: ICRP Publication 60. The 1990 Recommendation of the International Commission on Radiological Protection. Volume 21 No 1-3.

International Commission on Radiological Protection (ICRP) 2007. Annuals of the IRCP. IRCP Publication 103. *The 2007 Recommendation of the International Commission on Radiological Protection*. Volume 37. Nos 2-4.

Kaasalainen, T., Palmu, K., Reijonen, V. and Kortesniemi, M. 2014. Effect of Patient Centering on Patient Dose and Image Noise in Chest CT. *American Journal of Roentgenology*. 203: 123-130.

Kalender, W.A. 2014. Dose in X-Ray Computed Tomography. *Physics in Medicine and Biology*. 59 (R129-R150.).

Kalra, M.K., Sodickson, A.D. and Mayo-Smith, W.W. 2015. CT Radiation: Key Concepts for Gentle and Wise Use. *Radiographics*. 35: 1706-1721.

Kanal, K.M., Butler, P.F., Sengupta, D., Bhargavan-Chatfield, M., Coombs, L.P. and Morin, R.L. 2017. U.S. Diagnostic Reference Levels and Achievable Doses for 10 Adult CT Examinations. *Radiology*. (248: 1): 120 – 133.

Karim, M.K.A., Hashim, S, Bradley, D. A., Bakar, K. A.; Haron, M. R. and Kayun, Z. 2016. Radiation doses from computed tomography practice in Johor Bahru Malaysia. *Radiation Physics and Chemistry*. 121 (69-74).

Kumar, R. 2011. *Research Methodology: A Step-by-Step Guide for Beginners*. 3rd Edition. SAGE Publications Ltd: London.

Lumbreras, B., Salinas, J.M. and Gonzalez-Alvarez, I. 2019. Cumulative Exposure to Ionising Radiation from Diagnostic Imaging Tests: a 12 Year Follow-up Population-Based Analysis in Spain. *BMJ Open*. 9:e030905. doi:10.1136/ bmjopen-2019-030905.

McCollough, C.H. 2010. *Diagnostic Reference Levels*. American College of Radiology. Date of Access: 10 December 2017: <http://www.imagewisely.org/~/media/ImageWisely-Files/Medical-Physicist-Articles/IW-McCullough-Diagnostic-Reference-Levels.pdf>

McCollough, C.H., Leng, S., Yu, L., Cody, D.D., Boone, J.M. and McNitt-Gray, M.F. 2011. CT Dose Index and Patient Dose: They Are Not The Same Thing. *Radiology*. Volume 259: (311-316).

Miller, D.L. and Schauer, D. 2015. The ALARA principles in Medical Imaging. AAPM Newsletter. Vol 40 No 1.

Munjal, R.K., Negi, P.S., Babu, A.G., Sinha, S.N., Anand, A.K. and Kataria, T. 2006. Impact of 6MV photon Beam Attenuation by Carbon Fiber Couch and Immobilization Devices in IMRT Planning and Dose Delivery. *Journal of Medical Physics.* 31: (2) (67-71).

Philips. 2016. *The Importance of Patient Centering on CT Radiation Dose Optimization*. Online. Date of Access: 2.2.2018 <http://incenter.medical.philips.com/doclib/enc/13037837/The_Importance_of_Patient_Centering_on_CT_radiation_dose_optimization.pdf%3Ffunc%3Ddoc.Fetch%26nodeid%3D13037837>

Qurashi, A., Rainford, L., Ajlan, A., Khashoggi, K., Ashkar, L., Al-Raddadi, M., Al-Ghamdi, M., Al-Thobaiti, M. and Foley, S. 2017. Optimal Abdominal CT Protocol for Obese Patients. *Radiography*.1-12.

Raman, S.P., Mahadeveppa, M., Blasko, R.V., and Fishman, E.K. 2013. CT Scan Parameters and Radiation Dose: Practical Advice for Radiologists. *Journal of American College of Radiology*. 10: 840-846.

Sanderud, A., England, A., Hogg, P., Fossa, K., Svensson, S.F. and Johansen, S. 2016. Radiation Dose Differences between Thoracic Radiotherapy Planning CT and Thoracic Diagnostic CT Scans. *Radiography*. (22) 107-111.

Schawkat, K., Fischer, R.M., Heverhagen, J.T. and Christe, A. 2017. The Impact of Integrated Circuit Detector Technology in Routine MDCT: Improved Image Quality Compared to Conventional Detector Design for Constant SSDE. *Hellenic Journal of Radiology*. 2 (1): 23 – 29.

Shope, T.B., Gagne, R.M. and Johnson, G.C. 1981. A method for describing the doses delivered by transmission x-ray computed tomography. *Medical Physics.* 8(4):488–495.

Toshiba Medical Systems Corporation. 2004. Operation Manual for Whole-Body x-ray CT scanner.

Winslow, J.F., Hyer, D.E., Fisher, R.F., Tien, C.J. and Hintenlang, D.E. 2009. Construction of Anthropomorphic Phantoms for use in Dosimetry Studies. *Journal of Applied Clinical Medical Physics*. 10 (3): 195 – 203.

Wu, R.Y., Williamson, T.D., Sahoo, N., Nguyen, T., Ikner, S.M., Liu, A.Y., Wisdom, P.G., Lii MF., Hunter, R.A., Alvarez, P.E. Gunn, G.B., Frank, S.J., Hojo, Y., Zhu, X.R. and Gillin, M.T. 2020. Evaluation of the high definition field of view option of a large-bore computed tomography scanner for radiation therapy simulation. *Physics and Imagining in Radiation Oncology.* 13 (44-49).

Chapter 3

Patient Radiation Dose from Pelvic Computed Tomography Localisation

3.1. Introduction

The previous Chapter 2 discussed the radiation dose as measured by the phantom's scans. This chapter is centred on the second objective of the research, which was to measure the patients' estimated radiation dose for pelvic CT localisation scan through the use of size-specific dose estimate (SSDE). In addition, the effective dose is examined as well as the dose for a rescan.

Statistically, as stated in Chapter 1 (refer to 1.5) the most common CT scan performed at the oncology department is the pelvic localisation scan. For the purpose of this research, it is necessary to explore the following concepts. These include previously discussed and expanded upon concepts such as the CT dose in terms of this research, which relates to the (i) effective dose and (ii) size-specific dose estimate, (iii) field of view parameters and in addition, (iv) the body mass index.

The use of CT for radiotherapy treatment planning has been on the increase in the last decade (Sanderud *et al.*, 2016). The CT examination is in itself non-invasive, however, as CT utilises radiation to create the images, the cumulative effect of the CT doses is of clinical concern (Halperin *et al.*; 2013). The United States (US) Food and Drug Administration has created a Code of Federal Regulations (2017), in which they specify the length, diameter, and composition of two polymethyl-methacrylate cylindrical phantoms (PMMA). The first is a 16 cm phantom designed to test the head scanning mode of a CT scanner. The second is a 32 cm diameter phantom designed for testing the any CT body modes of a CT scanner (Code of Federal Regulations, 2017). In the modern CT scanner setup, the volume CTDI ($CTDI_{vol}$) is shown on the CT, which is the weighted CTDI ($CTDI_w$) divided by the pitch. Thus, the $CTDI_{vol}$ is the standardised measurement, of the radiation output of the CT system, which allows users to determine the amount of emitted radiation and make a comparison between the different CT protocols or CT scanners (McCollough *et al.*, 2011).

The CT dose is calculated utilising the DLP for effective dose (refer to: 2.1.2.1) and the $CTDI_{vol}$ for SSDE (refer to: 2.1.2.2). Both concepts were already described in Chapter 2, but an overview of these and other concepts will now be examined.

3.1.1. Effective Dose

The effective dose (*E*) is a concept that is described in Chapter 2 (refer to: 2.1.2.1.) This dose calculation is based on radiobiological considerations (Karim *et al.*, 2016). In 1980 the effective dose annually from medical procedures was 0.5 millisievert (mSv) and by 2006 the dose had increased six-fold to 3 mSv (Schawkat *et al.* 2017). The *E* calculation can be used to compare imaging modalities by examining the radiation risk involved. The calculation is based on the DLP:

$$E \approx k\ x\ DLP$$

Equation 2.4: Effective dose calculation

A limitation of effective dose is that the choice of body region is not always simple and explicit (Kalender, 2014). The estimates are also based not on the patient specifically but on phantom data. Patient size is not taken into account and organ dose values are not provided.

3.1.2. Size Specific Dose Estimate

The SSDE is discussed in detail in Chapter 2 (refer to 2.1.2.2.). To calculate the SSDE the patient's effective dose is first determined. Electronic callipers are utilised to measure the patient's Lat and AP dimensions. These measurements can be taken before or after the completion of the CT scan. Before completion of the CT scan, the measurement can be made for the Lat dimension in the anterior scout view, conversely the AP dimension can be measured in the lateral scout view. The Lat dimension is from the left to the right of the patient. The AP dimension is the thickness of the body part being scanned; it is measured for example from the patient's surface of their stomach to the surface of their back (AAPM, 2011). Upon completion of the CT scan, the measurements can also be made on the scanned CT image (AAPM, 2011). The effective diameter is then calculated using equation 2.2.

$$Effective\ diameter = \sqrt{AP\ x\ Lat}$$

Equation 2.2: Effective diameter calculation.

Using the effective diameter, the SSDE can be calculated from the conversion factor (*f*) (AAPM, 2011). To calculate the SSDE (*in mGy*) equation 2.3 is used:

$$SSDE = CTDI_{vol}\, x\, f$$

Equation 2.3: SSDE calculation.

There are four different methods to obtain *f*. They are, by measuring either the AP + Lat, the AP, the Lat or by using the calculated effective diameter (Kalender, 2014). All the different conversion factors, based on the 32 cm diameter PMMA phantom for $CTDI_{vol}$, are to be found in Appendix A. Kalender (2014) states that consistency can be compromised when measuring, as patient diameter varies with anatomical levels over the examination range. Paediatric patients have a very small effective diameter. CT dose is of great concern when it comes to paediatric CT examinations, as children are especially more susceptible to radiation effects than adults, therefore minimising radiation dose is critical for paediatric patients (Masuda *et al.,* 2016).

3.1.3. Field-of-View Parameter

The influence of the FOV on CT dose is discussed in Chapter 2 (refer to 2.1.3). Habibzadeh *et al.* (2012) in their research examined the effect of miscentering for both phantom and patient studies. The researchers concluded that miscentering increased the surface dose delivered to a patient (Habibzadeh *et al.*, 2012). The researchers examined a total of 450 patients' AP and Lat scout views from seven different imaging centres for the purpose of their research (Habibzadeh *et al.*, 2012). The researchers determined that a 7.2% increase in dose was found with a miscentering average of 1.6 cm when comparing imaging centres two and one (Habibzadeh *et al.*, 2012). Likewise, comparing imaging centres six and four, a 0.9 cm positioning error caused an increase of 6.8% in dose. From a 64 slice CT scanner, the centring errors ranged in the isocentre from 6 cm below to 4.4cm above (Habibzadeh *et al.*, 2012). Habibzadeh *et al.* (2012) observed in their research that 85% of patients were positioned below the isocentre and the other 15% above the isocentre.

The researchers Habibzadeh *et al.* (2012) concluded that due to an increase in CT dose, more attention should be given to ensure that patients are correctly centred for CT scans. A suggestion of examining the AP scout view to determine if the patient is centred was recommended (Habibzadeh *et al.*, 2012).

3.1.4. Body Mass Index

During the 1930s the Belgian astronomer, statistician, sociologist and mathematician Lambert Adolphe Jacques Quetelet under the premise that "*the transverse growth of*

man is less than the vertical" (Brazier, 2017) established the formula known as Quetelet's Index (World Health Organisation (WHO), 2020). Quetelet determined that the relative body weight could be characterised by the ratio of the weight in kilogrammes (kg) over the height in meters (m) squared (Brazier, 2017). In 1972 the formula received its modern name of body mass index (BMI) from Ancel Keys (Brazier, 2017). During the 1970s the Seven Countries study was conducted and based on the data and report from this study, the researchers determined that the adiposity and problems related to being overweight, the BMI appeared to be a good proxy (WHO, 2020). The formula for BMI is illustrated in equation 3.1. (WHO, 2020):

$$BMI = \frac{Weight}{(Height)^2}$$

Equation 3.1: Body mass index.

In the research by Qurashi *et al.* (2017) the authors measured the patients' BMI as their research centred around obese patients. The research stated that BMI is often used to characterise the obese population. The BMI is used as a diagnostic tool and a way to measure body fat indirectly (Qurashi *et al.*, 2017). However, BMI cannot determine the distribution of body fat or differentiate between fat and lean body mass (Qurashi *et al.*, 2017). The researchers further stated that the use of the patient's diameter is recommended as a method to determine approximate CT dose and for optimising CT protocols (Qurashi *et al.*, 2017).

Sanderud *et al.* (2016) assessed the impact of BMI on the $CTDI_{vol}$ for different CT scan protocols that they employed in their research. The researchers divided their study population into two groups; these being low BMI less than 25 and the other overweight and obese with a BMI above 25 (Sanderud *et al.*, 2016). The World Health Organisation (WHO: 2020) defines the different BMI groups as illustrated in Table 3.1.

Table 3.1: BMI index table.

BMI	Nutritional status
Below 18.5	Underweight
18.5–24.9	Normal weight
25.0–29.9	Pre-obesity
30.0–34.9	Obesity class I
35.0–39.9	Obesity class II
Above 40	Obesity class III

The researcher used these concepts and based the methodology for the current research on them. In the following section the methodology is discussed.

3.2. Methodology

This section will present the methodology used to determine patient dose for CT localisation scans. In addition, the research determined the dose received by the patient when a rescan was necessary.

The research was a prospective study, as the researcher obtained the CT information weekly after the patients had received their CT localisation scans. The research involved quantitative data collection of the radiation dose received by patients during their pelvic CT localisation scan.

The research for this quantitative study fell under the pre-experimental design. Utilising the description by De Vos *et al.* (2011), the study did not include a control group. The design can further be broken down into ex post facto design. Ex post facto design literally means *"after the fact*". This study design is used to determine how a specific independent variable (such as the patients' BMI in this research) can influence the dependent variables, such as the dose and image contrast in the research (De Vos *et al.*, 2011). Hence, the research collected data with conditions as they exist currently and investigates the possible relationship between these factors and the consequential characteristics that occur.

To determine which patients would partake in the research, a stratified systematic sampling method was implemented whereby every second patient meeting the inclusion and exclusion criteria was included in the research. Stratified sampling indicates the data is broken down into strata, which is relevant to the study (Bowers, 2008), in the case of this specific research, being the patient BMI category. Systemic

sampling was also applied, whereby the sampling frame is accumulated until the required amount is reached by a fixed fraction of the sampling size; in this research it is every second patient (Bowers, 2008).

The following section provides the study sample for the research, the criteria used for inclusion and exclusion of a patient as well as the research tools used.

3.2.1. Study Sample

Statistical data from the oncology department has shown that an average of 567 pelvic scans are performed annually (refer to: 1.5.). The pelvic localisation scan constitutes 40% of the scanned localisation at the oncology department, thus making it the most common anatomical site scanned.

Patients scanned at the oncology department between January 2019 and June 2019 for pelvic CT localisation, were considered to take part in the research. The patients were divided into three categories, (a) underweight, (b) normal and (c) overweight, which included obese patients. This information was determined from the patients' BMI. A total of 131 patients were included systematically.

3.2.1.1. Inclusion and Exclusion Criteria

To determine which patients would be included or excluded from the research study, the following Table 3.2 was used as a guideline.

Table 3.2: Inclusion and exclusion criteria for the research sample.

Inclusion Criteria	Exclusion Criteria
Patients receiving pelvic CT localisation scan at department of oncology	Patients who receive thorax, head and neck or other CT localisation scans
Patients 18 years and older	Infants and children (younger than 18)
Pelvic localisation scans that are in the scan range T10 to symphysis pubis	Pelvic localisation scans that do not include T10 or the symphysis pubis
Patients who are mobile, in order to stand for weight and height measurements	Patients who are immobile
	Patients who weigh more than 150 kg

3.2.1.2. Research Tools

Following here are the research tools that were used during the research process. The research tools 1 through 3 are a duplicate of Chapter 2.

1. A TSX-201A (Toshiba Aquilion © Large Bore (LB)) CT scanner, as used and discussed in Chapter 2 for the phantom studies.
2. The pelvic examination setting was chosen on the CT console and utilised for the research. The only variable that is modified during the time of the patients' scans is the FOV.
3. The pelvic CT scan protocol for the oncology department states that the scan must include from T10 to below the symphysis pubis (Department protocol: 2019).
4. The participating patients were weighed using a digital scale. The participating patient height was measured against a wall with height measurements affixed; this was set up by the researcher at the CT scanner.
5. The equations used in the research were as follows:
    - BMI: The participating patient's body mass index (BMI) was calculated from their weight and height measurements determined at the time of the CT scan. The BMI determines if the patient is considered as being overweight, of ideal weight or underweight, as demonstrated in Table 3.1. The Microsoft Excel programme calculated the patient BMI.

$$BMI = \frac{Weight}{(Height)^2} \quad \text{(Equation 3.1)}$$

The patients' effective dose was determined. The effective dose is calculated using the DLP. Measured in mSv and the k coefficient that is obtained from the ICRP 103:

$$E \approx k\ x\ DLP \quad \text{(Equation 2.1)}$$

- The effective diameter of the patient was calculated by measuring the widest part of the patient in the anterior and posterior dimension, then using the calculation:

$$Effective\ diameter = \sqrt{AP\ x\ Lat.} \quad \text{(Equation 2.2)}$$

- SSDE was calculated using the effective diameter, then obtaining the conversion factor f used to estimate patient dose. The calculation (measured in mGy) is then:

$$SSDE = CTDI_{vol}\ x\ f \quad \text{(Equation 2.3)}$$

3.2.2. Research Process

The research process to determine the baseline dose process followed the steps that follow in Figure 3.1.

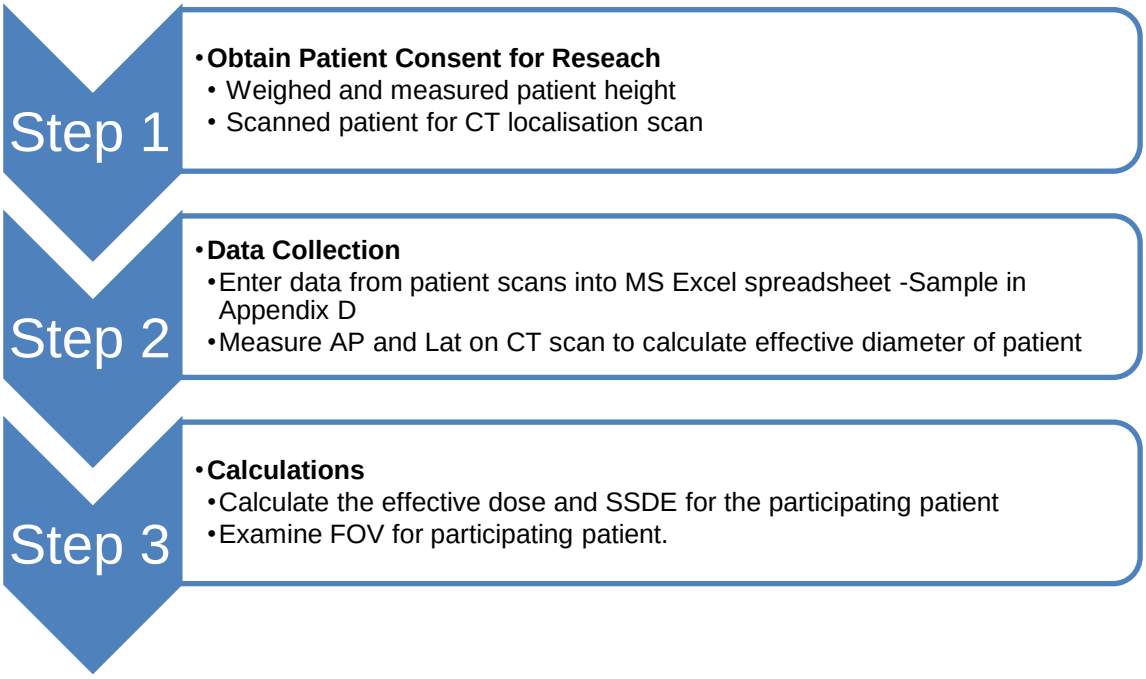

Figure 3.1: The research process to obtain patient dose for CT localisation scans.

3.2.2.1. Step 1: Participating Patient's Scan

When a patient requiring pelvic radiation therapy was sent for a CT localisation scan, the patient was asked if they were willing to take part in the research. If the patient was willing a consent form was signed by the patient. The forms were available in English, Afrikaans and Sesotho, depending on the patient's preference. The patients also received an information leaflet regarding the research. A representation of the forms and information leaflet are presented in Appendix B. Consent was obtained in the patients' language of choice. The researcher trained co-workers who speak Afrikaans and Sesotho to assist with consent when those languages were required.

The participating patient was then taken to have their weight and height measured. A digital scale was used for measuring the patient's weight, in order to ensure consistency. The height was measured with a height tool affixed to the wall at the CT; this to ensure consistency. The data was written on a CT form (Appendix C). Other data collected included the patient's radiotherapy number (RT no.), an individual number used for each patient. In addition to the RT, weight and height, the patient's age and diagnosis were filled in. The radiographer also indicated whether the patient

was having a rescan and the reason for said rescan. As part of patient demographics, the patient's gender was also noted.

The patient was then scanned on the Toshiba Aquilion © Large Bore CT scanner. The pelvic examination setting was chosen from the CT console. The patient's scan was performed from T10 to below the symphysis pubis.

3.2.2.2. Step 2: Data Collection

The research data were obtained on a weekly basis from the participating patients' CT scans. The researcher also obtained demographic data from the participating patients. Table 3.3 illustrates the demographic data that was collected for the scanned patients.

Table 3.3: Patient demographic information.

Patient Information			
Patient RT	***Gender***	***Age***	***Diagnosis***

Patient RT=An individual number dedicated to each patient in the oncology department. Gender=Male or female, Age=Age of the patient at time of the CT scan. Diagnosis=The patient's cancer diagnosis.

Additional patient information obtained from the individual patient is set out in Table 3.4. This includes the individual patient's weight and height measured at the time of their CT localisation scan, the type of radiation therapy treatment that will be administered to the patient and lastly, the electronic calliper measurement of the patients' AP and Lat dimensions measured on the CT scanner images.

Table 3.4: Patient measured information.

Patient Information					
Weight (Kg)	***Height (cm)***	***Height (m)***	***3D/IMRT***	***AP (cm)***	***Lat (cm)***

Weight = The patient's weight in kg. Height= The patients measured height in meters. 3D/IMRT= This is a choice of radiation therapy plans, i.e. 3D conformal or Intensity Modulated Radiation Therapy. AP= Anterior to posterior measurement of patient at thickest junction in centimetre. Lat=Left to right measurement of patient at widest junction in centimetres.

On the CT scanner itself CT information is obtained, refer to Table 3.5. The information is captured from the CT's scanned pelvic localisation for each individual patient.

Table 3.5: CT information for scanned patients.

CT information									
kV	***mA***	***FOV***	***mAs***	***Scan Time***	***TNI***	***Scan Start***	***Scan End***	***$CTDI_{vol}$***	***DLP***

kV=The potential energy of the x-ray beam, it will be either 80 kV, 120 kV or 135 kV. mA=The milliamperage of the x-ray beam, usually 300 mA. Scan time=The time it takes to conduct the scan in seconds. TNI=The total number of images that were produced from the CT scan. Scan Start=The start position of the CT scanner. Scan end=The end position of the CT scanner. $CTDI_{vol}$=The $CTDI_{vol}$ as stated by the CT scanner. DLP=The dose length product as calculated by the CT scanner.

The researcher also recorded if the patient was scanned twice in one session and if rescans were performed. The dose was recorded for the rescans and even though this was not the focus of the research, the information was still noted.

The researcher completed a patient check list, found on the Microsoft Excel spreadsheet on a separate sheet, in order to determine if the patient was scanned in the centre of the CT, as this can influence surface dose and image quality. A check list for the scout view was created to determine if the FOV for the scout was adequate to ensure patient coverage or if the coverage was too large. Focussing on the largest part of the patient, the researcher noted in writing whether the coverage in the lateral dimension was adequate, too narrow (a section is cut off from the patient) or too wide (more than 10 cm in the lateral dimension). If required the same information can be gleaned for the anterior posterior width of the patient. An example can be seen in Appendix D, Table A.9.

Information from the CT scan itself was captured onto the Microsoft Excel spreadsheet on the CT Data sheet (Appendix D: Table A.9). The researcher captured the patient RT number and how the patient was positioned, i.e., in the centre of the FOV, to the left of the FOV (this will be chosen if the patient centre is 5 cm to the left of the CT centre) and lastly to the right of the FOV (chosen if the patient is 5 cm to the right of the CT centre). Analysis of the CT scan itself will also determine if the FOV was appropriate for the body habitus of the patient. A note on the determination of the FOV criteria: for radiation planning purposes the CT must extend at least 5 cm below the planned area, this criterion was utilised. In addition, miscentreing increased surface dose from 33.3 % for 4 cm to 51.1% for 6 cm (Habibzadeh *et al*. 2012), thus exceeding 5 cm results in an increased dose.

3.2.2.3. Step 3: CT Data Calculations

Calculations were performed on the data that was obtained by means of a MS Excel spreadsheet (Appendix D: Table A.8). This data included the patients' BMI as

determined from their weight and height measurements (Equation 3.1.). The system then determined within which category the patient falls and colour coded the cell for easy visualisation. The BMI categories were colour coded in the following way: underweight BMI category patients are yellow, normal weight BMI category patients are green and overweight BMI category patients are red.

Calculations based on CT data obtained are the effective dose, the effective diameter and the SSDE. A description of these calculations follows. The effective dose was calculated using Equation 2.1. This uses the DLP and the *k* coefficient (Appendix A, Table A.2) based on kV chosen and anatomical region. The conversion factor for different tube voltage on the abdomen and pelvis for an adult is indicated, as well as for children and infants. Both the abdomen and pelvis calculations were performed, since the scans are abdo-pelvic examinations (as per the oncology department protocol). The effective diameter of the patient was also calculated (Equation 2.2). The SSDE could thus be calculated from the effective diameter results. The SSDE was calculated by the use of a conversion factor based on the patient's effective diameter that was calculated (Appendix A: Table A.1.). The determined conversion factor and $CTDI_{vol}$ were used in Equation 2.3.

3.2.3. Ethical Considerations

All patient data were kept confidential. Before the patient arrived at the CT scanner, the oncologist had already obtained informed consent from the patient for all the related imaging and radiation treatment procedures. Therefore, on the consent form for the research study the patient only consented to participate in the study. The patients were ensured that they may refuse to take part in the researcher study. However, this would not prevent them from receiving the CT scan, as the scan procedure was part of their prescribed treatment protocol for their specific cancer. The CT information was gleaned from the CT scan data.

Patient information leaflet and consent forms for the study, available in English, Afrikaans and Se-Sotho are included as Appendix B. The forms were signed by the patients, if they were eligible and were willing to take part in the research. No compensation was given to the patients who were included in the research.

3.2.4. Validity and Reliability

Validity of research is described by Kumar (2011) as ensuring the correct application of procedures to determine the answer to the proposed question. While the measurement procedure's quality that ensures the repeatability and accuracy is defined as the studies' reliability (Kumar, 2011). As part of the pilot study, six patients were scanned for the research. These patients were divided into two for each BMI category. If the patients met the inclusion and exclusion criteria the data was kept as part of the research.

The following points ensured the validly and reliability of the research. (Note: some duplication from Chapter 2).

- For all the CT scans included in the research, only one CT scanner was used, therefore the information of the dose output remained consistent.
- The CT scanner used, had passed all quality assurance test performed by the medical physicists; these are daily, weekly and monthly.
- The medical physicist also verified all the mathematical formulas (refer to: 3.2.1.2.).
- The MS Excel spreadsheet used for calculations was tested for accuracy prior to the commencement of the research and then again upon commencement of the research. No modifications were made after the pilot study.
- The research demonstrated dose as defined by SSDE, which is frequently used in research papers. The AAPM (2011: Report No. 204) state that SSDE should be used to determine dose to patients, especially children.
- All CT data were collected by the researcher only. All CT scans were performed by the radiation therapist assigned to the CT scanner; this ensured no bias or skewed data on the part of the researcher.
- The researcher validated the information captured on the MS Excel spreadsheet. Incorrect entries were revalidated and corrected or excluded from the research.
- As the CT scans could not be stored for more than a week and the CT information is only displayed on the CT scanner itself, the researcher photographed each dose information page on the CT to ensure correct information was maintained. These photographs were used to verify every patient's dose information used in the research.

3.2.5. Statistical Information

The data that were obtained was entered into the spreadsheets as indicated, the calculations were performed and the data were validated by the researcher. The researcher sorted the data based on patient BMI category. All patient data were sent to the bio-statistician for analysis. The data analysis consisted of all patients' data; which were subsequently sorted into the different BMI categories. The p-value was determined using the Shapiro-Wilk test. The Shapiro-Wilk test is used to determine whether a normal distribution of the data occurs (Petrie & Sabin, 2000). If the p-value is less than 0.05, then the data is skewed. In the case of skewed data, the median and interquartile ranges (IQR) are reported on. However, if the p-value is greater than or equal to 0.05, a normal distribution is found. The mean and standard deviations are reported in the case of normal data (Statistician, 2019).

The median value is the value in the middle of the data, as opposed to the mean or average. The IQR assists with problems with data that present an extreme outlier, by discarding a quarter (25%) of the data from both ends of the distribution. This method removes outliers that could be causing skewed data, allowing the remaining values to have ranges that can be measured. The one issue with this method is that not all data are used in the statistics as the bottom and top values are excluded (Bowers, 2008).

This section described the methodology used to calculate the CT dose delivered by CT localisation of the pelvis. The next section indicates the derived results.

3.3. Results

The analysed results of the patients scanned for pelvic CT localisation in the oncology department, are presented in this section. The objective of this part of the research was to determine the patients' radiation dose received during pelvic CT localisation scans, by means of the SSDE. Other aspects such as the patient demographics, the dose in relation to patients, as well as the dose received from re-scans will be reflected in this section.

3.3.1. Patient Demographics

All patients who were included in the results met the inclusion criteria as stipulated in 3.2.1.1. In the time period between January 2019 to June 2019, 530 patients were scanned for CT localisation at the oncology department. Of these 279 were pelvic

patients, which constituted 53% of scans performed during the specified time frame. Of the 279 scanned patients, 158 agreed to participate in the research, of which only 131 patients met the scanned CT inclusion criteria for the research. Twenty-seven patients were excluded from the research due to the following reasons: (a) the patients were scanned too low and the scanned data did not include T10 at the start of the scan range (b) some patients' CT data were not complete as it was partially deleted accidently, thus not all information could be gleaned for those scans (c) the patient was not scanned for pelvic CT localisation, (e) the patient weighed in excess of 150 kg and (d) patients were scanned on the brachytherapy CT (used mainly for brachytherapy, but used as backup when the CT simulator has maintenance performed on it. However, it must be noted that the second CT was not part of the research). The 131 patients scanned were divided into the three BMI categories: 50 overweight patients (38.17%), 50 normal weight patients (38.17%) and 31 underweight patients (23.66%).

Table 3.6: Patients divided by cancer type.

Cancer Types												
	Cervix	***Prostate***	***Anus***	***Rectum***	***Vulva***	***Metastatic***	***Ovarian Ablation***	***Uterus***	***Vagina***	***Penis***	***Bladder***	***TOTAL***
Number of participants	78	22	10	9	7	2	1	1	1			131
All pelvic CT scans	161	55	14	16	14	2	1	12	1	2	1	279

Table 3.6 illustrates the cancer type of the participating patients as well as all the pelvic CT localisation scans that were performed at the time of the research. The cancer diagnosis for the participating patients ranged from 78 with cervix cancer, 22 patients with prostate cancer, 10 anus cancer patients, 9 patients with rectum cancer, 7 patients with vulva cancer and 2 patients with metastatic disease to the pelvis. Lastly only 1 patient for each of the following cancer types: an ovarian ablation, uterus cancer and vaginal cancer.

Table 3.7: Participating patient demographics.

Demographics of Patients													
Gender		***Age***		***Weight***		***Height***		***Treatment Type***		***Dimension***			
Male	*Female*	*Youngest*	*Oldest*	*Lowest*	*Highest*	*Shortest*	*Tallest*	*3DCRT*	*IMRT*	*Anterior ↓**	*Anterior ↑***	*Lateral ↓**	*Lateral ↑***
30	101	28	85	30 kg	128 kg	147	190	112	19	15.1 cm	40.6 cm	21.7 cm	49.2 cm

Gender is between male and female. Age is from youngest to oldest. Weight is from lowest to highest. Height is from shortest to tallest measurement. Treatment type is either 3D-conformal (3DCRT) or Intensity Modulated Radiation Therapy (IMRT). The patient's dimensions are from anterior and lateral showing the * (↓) lowest and ** (↑) highest measurement.

Of the 131 participating patients scanned, there were 101 females and 30 males (Table 3.7). The patients' ages varied between 28 and 85. The different age groups are reflected in Figure 3.2. The lowest weight was 30 kg and the shortest height was 147 cm. The highest weight was 128 kg and the tallest patient was 190 cm. Of the total patients 112 required 3DCRT versus the 19 patients who were scanned for IMRT radiation. The patient's dimensions varied from 15.1 cm to 40.6 cm in the anterior dimension and 21.7 cm to 49.2 cm in the lateral dimension (Table 3.7).

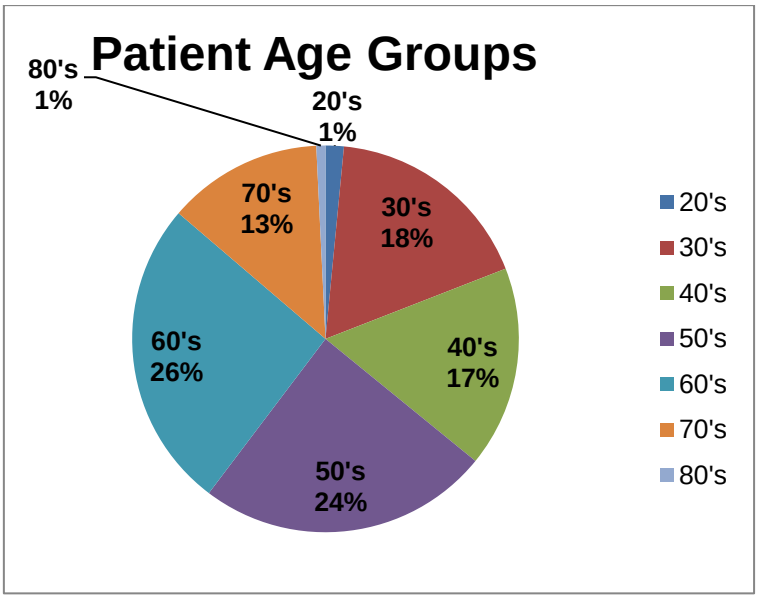

Figure 3.2: Patients divided into age groups.

From Figure 3.2 it can be determined that the majority of patients were in their 60's (26%) and 50's (24%), while the very youngest and oldest (20's and 80's) both contributed only 1% towards the total number of patients.

Refer to Table Annex, Table TA.3.1 on the accompanying compact disc (CD) to see the full details of the patient demographics. The data contain all the scanned patients' demographics, including their gender, age and diagnosis as well as the height and weight of the patients, their AP and Lat dimension as measured from their scan data, at the time of their CT scans. Each patient's intended treatment plan is also indicated, therefore if either IMRT or 3D conformal radiation therapy (3DCRT) was to be delivered.

3.3.2. Overview of Patient Scan Data

All the patients' scans utilised 120 kV for the research. With the exception of one patient with 350 mA, all patients were scanned with 300 mA. The CT scan time ranged from 24.8 seconds to 42.4 seconds. The total number of images varied from 453 to 657, with the start of the scan range beginning at 200 mm to 400 mm and ending between -400 to -150 mm. The $CTDI_{vol}$ remained consistent at 100.2 mGy with the exception of 350 mA, which resulted in 138.7 mGy. The mAs varied from a minimum of 5920 to a maximum of 8560 utilising the 300 mA. For the 350 mA the result was 11860. The median mAs was 6920, with the IQR value in the lower quartile 6720 and upper quartile of 7020. The DLP ranged from 910.8 mGy.cm to 1400.8 mGy.cm and the 350

mA with the highest at 1943.8 mGy.cm. The median value was 1077.8 mGy.cm. The scan data that were collected from the patients are presented in Table Annex TA.3.2 and the calculated data are presented in Table Annex TA.3.3. which are stored on the accompanying CD.

Calculations that were derived from the patient data include the patients' BMI, which ranged from 12.5 to 49.3. The median BMI value was 22.3, with IQR from 18.7 to 27.2. The patients' effective diameter ranged from 18.3 cm to 40.8 cm. The median value was 26.3 cm with the IQR from 23 to 29.1 cm. The resultant SSDE was calculated to be in the range of 85.2 mGy to 191.3 mGy, which was then modified further into cGy dose resulting in dose ranging from 8.5 cGy to 19.1 cGy. The median was 14.3 cGy with IQR from 12.8 cGy to 16.5 cGy. The effective dose was 13.9 mSv to 21.4 mSv for the abdominal dose and 11.7 mSv to 18 mSv for the pelvic dose with 300 mA. With the 350 mA, the results increased to 29.7 mSv for the abdomen and 25 mSv for the pelvis dose. The median value for the abdominal effective dose was 16.5 mSv with the IQR between 18.7 mSv and 27.2 mSv. The pelvic effective dose had a median value of 13.9 mSv and the IQR between 12.8 mSv and 16.5 mSv. All statistical data, as indicated in the aforementioned are reflected in Table 3.8.

Table 3.8: All patients scan data related to CT dose.

Patient Type	Variable	Shapiro-Wilk p Value	SD	Median	IQR		Mean	Min	Max
					Lower Quartile	Upper Quartile			
All	**MAs**	0.0001	542.79	6920.00	6720.00	7020.00	6933.44	5920.00	11860.00
	DLP	0.0001	95.89	1077.80	1059.30	1114.90	1090.41	910.80	1943.80
	Effective Diameter	0.0002	4.76	26.25	22.96	29.10	26.64	18.34	40.82
	BMI	0.0001	6.83	22.34	18.73	27.21	23.73	12.49	49.27
	Effective Dose abdomen	0.0001	1.47	16.49	16.21	17.06	16.68	13.94	29.74
	Effective Dose pelvis	0.0001	1.24	13.90	13.66	14.38	14.07	11.75	25.08
	SSDE cGy	0.0415	2.32	14.33	12.83	16.53	14.44	8.52	19.14

The Shapiro-Wilk p-value: < 0.05 the data is skewed, ≥ 0.05 data has normal distribution. SD = standard deviation. IQR = Interquartile range.

An overview of all participating patients' settings and dose has been indicated in the section. The following section examines the CT dose per BMI category.

3.3.3. Patient CT Dose According to BMI Category

All BMI category patient data are reflected in Table 3.8, which demonstrates the Shapiro-Wilk test with the p-values that were calculated. The Table demonstrates by means of colour coding the different variables in the overweight, normal and underweight category. The statistical results were mostly skewed, that is that a normal distribution was not found, as demonstrated by the Shapiro-Wilk p-value test. Table 3.9 demonstrates the normal distribution by the colour green in the p-value column, while the skewed distribution is represented by a blue coloured cell.

Table 3.9: Shapiro-Wilk test based on 3 categories of BMI.

Overweight Variable	Shapiro-Wilk p Value	Normal Variable	Shapiro-Wilk p Value	Underweight Variable	Shapiro-Wilk p Value
mAs	0.0001	***mAs***	0.0001	***mAs***	0.0457
DLP	0.0001	***DLP***	0.0001	***DLP***	0.0314
Effective Diameter	0.0057	***Effective Diameter***	0.4848	***Effective Diameter***	0.0187
BMI	0.0001	***BMI***	0.0054	***BMI***	0.013
Effective Dose Abdomen	0.0001	***Effective Dose Abdomen***	0.0001	***Effective Dose Abdomen***	0.0314
Effective Dose Pelvis	0.0001	***Effective Dose Pelvis***	0.0001	***Effective Dose Pelvis***	0.0314
SSDE cGy	0.0311	***SSDE cGy***	0.2704	***SSDE cGy***	0.0183

The overweight variables are shown in orange, the normal weight variables are shown in green, the underweight variables are shown in yellow. The variables are the mAs, the Dose Length Product (DLP), the effective diameter as calculated from the patient. The calculated BMI of the patients. The effective dose in terms of the pelvis and abdomen, as well as the Size-specific dose estimate (SSDE).

Only the normal BMI category patients' effective diameter and SSDE were found to be normal data and not skewed data. These results could be due to the varied size of the patients in the underweight and overweight category.

The dose to the patients is divided by the patients' BMI categories (i.e., either the underweight, normal weight and overweight category). The division of the patients with their highest and lowest dose is demonstrated in Table 3.10.

Table 3.10: CT dose divided by BMI category.

BMI Category	Overweight BMI			Normal BMI		Underweight BMI	
	Lowest	Highest	350 mA	Lowest	Highest	Lowest	Highest
mAs	6420	7440	11860	6420	8560	5920	7740
DLP	1003.6	1192.9	1943.8	1003.6	1400.8	910.8	1248.6
Effective Diameter	25.1	40.8		20.8	30.7	18.3	27.8
Effective Dose Abdomen	15.3	29.7		15.4	21.4	13.9	19.1
Effective Dose Pelvis	12.9	25		12.9	18	11.7	16.1
SSDE in cGy	8.5	14.8		12.3	17.8	13.7	19.1

The lowest **mAs** (5920) was found in the underweight BMI, with the normal and overweight patients having the same lowest mAs of 6420. The highest mAs, where 300 mA was utilised, is found in the normal BMI patients (8560), with the overweight and underweight patients sharing the same high mAs of 7740. The one patient who was scanned with a 350 mA, was in the overweight BMI patient category and the resultant mAs measured 11860, the highest in the research study. As standard practice the CT is set to use 300 mA, in the instance where 350 mA was utilised, the oncology radiographer modified the setting due to the patient's diameter. The statistical data for the mAs are illustrated in Table 3.11. All BMI patient categories presented skewed data. The median value was the same (6920 mAs), for the overweight and normal patients, whilst all patients within the underweight BMI category having a median value of 6720 mAs. The IQR for the lower quartile was the lowest for the underweight patients at 6620 mAs and the highest for the overweight patients at 6820 mAs. The lower quartile was the same for the normal and underweight patients with 7020 mAs and the highest for the overweight patients with 7120 mAs.

Table 3.11: mAs per BMI category.

mAs								
Patient Type	Shapiro-Wilk p Value	SD	Median	Lower Quartile	Upper Quartile	Mean	Min	Max
All	0.0001	542.79	6920.00	6720.00	7020.00	6933.44	5920.00	11860.00
Overweight	0.0001	729.89	6920.00	6820.00	7120.00	7056.80	6420.00	11860.00
Normal	0.0001	390.73	6920.00	6720.00	7020.00	6909.20	6420.00	8560.00
Underweight	0.0457	323.17	6720.00	6620.00	7020.00	6773.55	5920.00	7740.00

The Shapiro-Wilk p-value: < 0.05 the data is skewed, ≥ 0.05 data has normal distribution. SD = standard deviation..

The **DLP** was the lowest minimum for the underweight BMI patients' category (910.8 mGy.cm) with the overweight and normal BMI patients sharing the minimum DLP of 1003.6 mGy.cm. The highest DLP is found in the overweight BMI patient category, at 1943.8 mGy.cm, followed by the normal BMI patient category at 1400.8 mGy.cm and lastly the underweight BMI category patients with a value of1248.6 mGy.cm. Skewed statistical data occurred for all BMI categories as illustrated in Table 3.12. The median and IQR can be determined from this table.

Table 3.12: DLP per BMI category.

DLP								
Patient Type	Shapiro-Wilk p Value	SD	Median	Lower Quartile	Upper Quartile	Mean	Min	Max
All	0.0001	95.89	1077.80	1059.30	1114.90	1090.41	910.80	1943.80
Overweight	0.0001	126.77	1096.40	1059.30	1114.90	1112.95	1003.60	1943.80
Normal	0.0001	71.46	1077.80	1040.70	1114.90	1086.21	1003.60	1400.80
Underweight	0.0314	58.96	1059.30	1040.70	1096.40	1060.83	910.80	1248.60

The **effective diameter** increased as the patient BMI category increase. Therefore, the smallest effective diameter was seen in the underweight BMI patient category with 18.3 cm. The largest effective diameter was found in the overweight BMI category at 40.8 cm. As demonstrated in Table 3.13, only the normal BMI patients presented data that was not skewed. The normal patient BMI category minimum diameter is 20.8 cm which is a 2.5 cm difference when compared to the underweight BMI patient category effective diameter minimum. The minimum overweight BMI patient category is calculated at 4.3 cm difference compared to the normal BMI patient category. Therefore, the minimum effective diameters do not differ very extensively in the different BMI patient categories.

Table 3.13 Effective diameter per BMI Category.

Effective Diameter								
Patient Type	**Shapiro-Wilk p Value**	**SD**	**Median**	**Lower Quartile**	**Upper Quartile**	**Mean**	**Min**	**Max**
All	0.0002	4.76	26.25	22.96	29.10	26.64	18.34	40.82
Overweight	0.0057	3.76	30.41	28.46	33.31	31.24	25.11	40.82
Normal	0.4848	2.23	25.04	23.30	26.76	25.02	20.82	30.77
Underweight	0.0187	1.87	21.56	20.96	22.77	21.82	18.34	27.79

The Shapiro-Wilk p-value: < 0.05 the data is skewed, ≥ 0.05 data has normal distribution. SD = standard deviation.

The median **effective dose** for both the abdomen and pelvis was determined to be the lowest for the underweight BMI category patients (16.2 mSv and 13.7 mSv for the abdomen and pelvis respectively), the normal and overweight BMI category patients had similar effective dose of 16.5 mSv and 16.8 mSv respectively for the abdomen and 13.9 and 14.1 mSv for the pelvis respectively. The highest effective dose was found in the overweight BMI patient category (Abdomen = 29.7 mSv; Pelvis = 25 mSv); and the effective dose decreased as there was a decrease in BMI category. Thus, the maximum effective dose decreased from 21.4 mSv to 19.1 mSv and from 18.1 to 16.1 mSv in the normal to underweight BMI patient category for the abdomen and pelvis respectively. The analysis of the effective dose for both the abdomen and pelvis is presented in Table 3.14.

Table 3.14: Effective dose for abdomen and pelvis per BMI patient category.

Effective Dose – Abdomen								
Patient Type	Shapiro-Wilk p Value	SD	Median	Lower Quartile	Upper Quartile	Mean	Min	Max
All	0.0001	1.47	16.49	16.21	17.06	16.68	13.94	29.74
Overweight	0.0001	1.94	16.77	16.21	17.06	17.03	15.36	29.74
Normal	0.0001	1.09	16.49	15.92	17.06	16.62	15.36	21.43
Underweight	0.0314	0.90	16.21	15.92	16.77	16.23	13.94	19.10
Effective Dose – Pelvis								
Patient Type	Shapiro-Wilk p Value	SD	Median	Lower Quartile	Upper Quartile	Mean	Min	Max
All	0.0001	1.24	13.90	13.66	14.38	14.07	11.75	25.08
Overweight	0.0001	1.64	14.14	13.66	14.38	14.36	12.95	25.08
Normal	0.0001	0.92	13.90	13.43	14.38	14.01	12.95	18.07
Underweight	0.0314	0.76	13.66	13.43	14.14	13.68	11.75	16.11

The Shapiro-Wilk p-value: < 0.05 the data is skewed, ≥ 0.05 data has normal distribution. SD = standard deviation.

An illustration of the effective dose for the abdomen and pelvis per BMI patient category is seen in Figure 3.3.

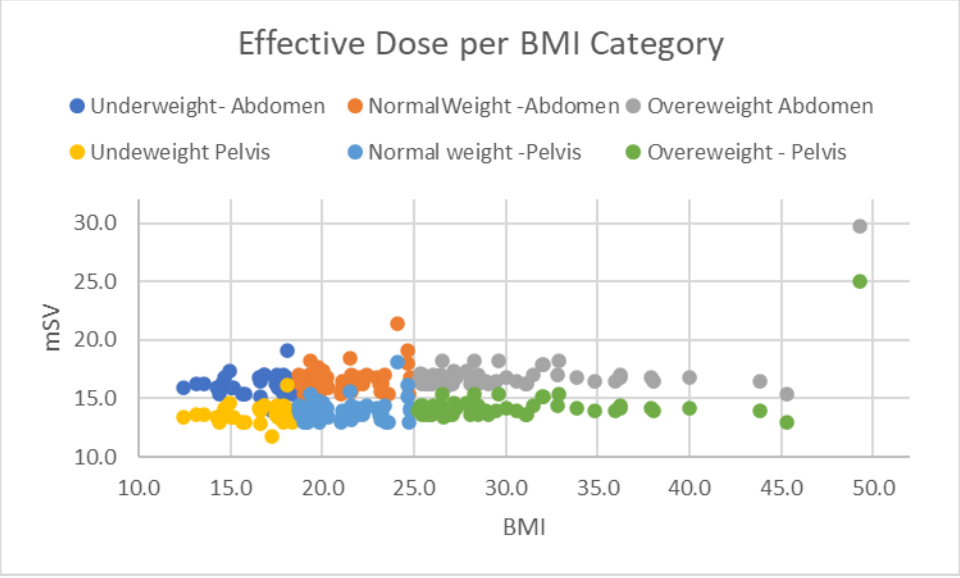

Figure 3.3: Effective dose.

From Figure 3.3 it can be noted that the pelvic effective dose is parallel to the abdominal effective dose for the different BMI patient categories. However, the pelvic effective dose measured lower, due to the lower *k* factor.

The highest dose in terms of **SSDE** was calculated for the underweight BMI patient category at 19.1 cGy dose. The lowest dose (SSDE) was calculated for the overweight BMI patient category at 8.5 cGy dose. Therefore, the SSDE decreases as there was an increase in patient BMI. These results occur due to the increase in the conversion factor *f*, as the effective diameter decreases. Thus, as the BMI increases the SSDE decreases. The decrease can be noted in Table 3.15. In terms of median value, the SSDE for the underweight BMI patient category calculated to 17.1 cGy. There was a decrease in dose for the normal BMI patient category to 14.8 cGy and finally the lowest SSDE was calculated for the overweight BMI patient category at 12.3 cGy.

Table 3.15: SSDE in cGy as per BMI patient category.

SSDE in cGy								
Patient Type	**Shapiro-Wilk p Value**	**SD**	**Median**	**Lower Quartile**	**Upper Quartile**	**Mean**	**Min**	**Max**
All	0.0415	2.32	14.33	12.83	16.53	14.44	8.52	19.14
Overweight	0.0311	1.46	12.32	11.02	13.23	12.16	8.52	14.83
Normal	0.2704	1.23	14.83	14.33	15.93	15.13	12.32	17.84
Underweight	0.0183	1.16	17.13	16.53	17.84	16.99	13.73	19.14

The Shapiro-Wilk p-value: < 0.05 the data is skewed, ≥ 0.05 data has normal distribution. SD = standard deviation.

The SSDE increased as the BMI patient category decreased, as demonstrated in Figure 3.4. The underweight BMI category patients are visualised by blue, the normal BMI patient category by red and the overweight BMI patient category by green. It should be noted that the blue has the highest values and there is a decrease as it moves towards the green (i.e. from the underweight, normal and finally the overweight BMI patient category).

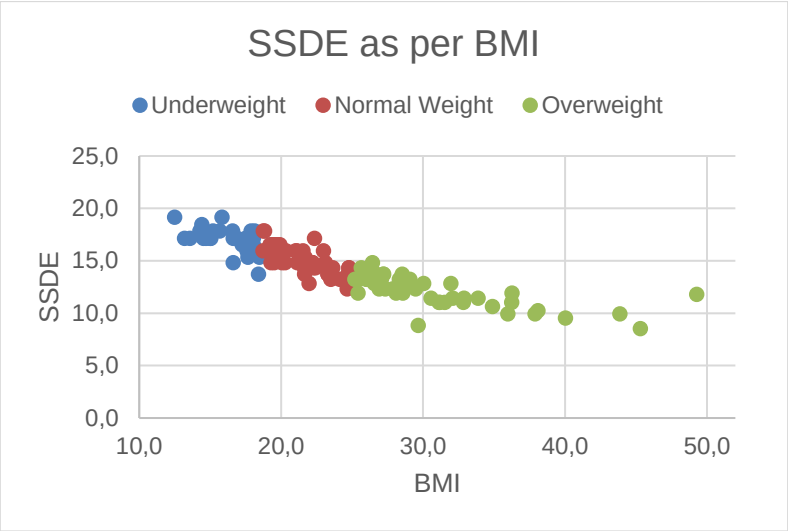

Figure 3.4: SSDE as per BMI.

The CT dose in terms of both equivalent dose and SSDE has been established in this section, for the participating patients, as well as the patients' demographics. Rescans were performed for some of the participating patients. The following section determines the effect the rescans had on the overall CT dose to the patient.

3.3.4. Rescan Dose

From the 131 participating patients scanned, it was determined that 20 of these patients had had rescans performed, thus 15% of patients. Of these 20 patients who had had a rescan, 8 had additional rescans. The resultant rescans' dose was examined to determine the cumulative dose effect that occurs due to the rescans. Table 3.16 demonstrates the resultant rescan dose and includes the reason for the rescan. The main reason for the rescan was to modify the position from supine to prone as well as the patient needing a full bladder for the scan. The reason for both is that by the patient lying prone and in addition, having a full bladder, assist in moving the small bowl (an organ at risk) out of the radiation field. Another reason often cited for a rescan is due to the patient's bowels being very full of faecal matter, which modifies the placement of the area of tumour bed (most often the prostate).

From the patient rescan data, 3 patients had a CT scout view or a brief one slice scan before a rescan was performed (to check the bowels emptying or bladder filling). The resultant data included a "0 slice" scanned only, which indicates that the scout views were imaged as well as one slice of the CT. The information gleaned indicated that

1100 mA was given in 8.8 seconds. The $CTDI_{vol}$ was 81.6 mGy and the DLP 16.3 mGy.cm, the resultant SSDE in cGy for each scan was 2.4, 11.6 and 13.4 cGy dose respectively. Where only the scout views were imaged, the resultant data was 400 mA and 800 mA, with 4 and 8 second scans.

In terms of completed rescans, the SSDE calculated to a minimum of 9.2 cGy and a maximum of 17.8 cGy. To calculate the dose received by the patient for the CT localisation, this additional dose would need to be added to the final scan dose. Table 3.16 indicates this by highlighting the patient ID in orange if more than one rescan was performed.

Table 3.16: Patient rescan dose information.

	Patient Information	CT information				Calculations				
ID	Reason for Rescan	mAs	Scan Time	CTDIvol	DLP	Effective Diameter	SSDE	Effective Dose - Abdomen	Effective Dose - Pelvis	SSDE cGy
106a	full bladder	7020	28.48	100.2	1114.9	25.4	148.3	17.1	14.4	14.8
106b	full bladder	7020	28.48	100.2	1114.9	24.8	153.3	17.1	14.4	15.3
111b	prostate	6620	27.15	100.2	1040.7	24.1	153.3	15.9	13.4	15.3
112a	rescan	6820	27.82	100.2	1077.8	26.9	143.3	16.5	13.9	14.3
112pre	bladder check	3620	17.15	100.2	484	26.9	143.3	7.4	6.2	14.3
114a	Bowel Prep	5920	24.82	100.2	910.8	22.2	165.3	13.9	11.7	16.5
118a	full bladder	6620	27.15	100.2	1040.7	20.4	178.4	15.9	13.4	17.8
118b	rescan	6620	27.15	100.2	1040.7	20.4	178.4	15.9	13.4	17.8
17a	Bowel Prep	7120	31.48	100.2	1059.3	25.5	148.3	16.2	13.7	14.8
26a	Bowel Prep	7020	28.48	100.2	1114.9	30.3	123.2	17.1	14.4	12.3
26b	full bladder	7020	28.48	100.2	1114.9	29.5	128.3	17.1	14.4	12.8
26c	Bowel Prep	7020	28.48	100.2	1114.9	29.5	128.3	17.1	14.4	12.8
28a	Bowel Prep	7740	30.88	100.2	1248.6	24.1	153.3	19.1	16.1	15.3
28b	Bowel Prep	6620	27.15	100.2	1040.7	24.1	153.3	15.9	13.4	15.3
32a	Small Plan	6720	27.48	100.2	1059.3	27.7	137.3	16.2	13.7	13.7
32b	full bladder	7020	28.48	100.2	1114.9	27.3	137.3	17.1	14.4	13.7
53a	full bladder	6720	27.48	100.2	1059.3	24.8	153.3	16.2	13.7	15.3
54a	full bladder	7520	32.82	100.2	1133.5	37.8	95.2	17.3	14.6	9.5
66a	table top skew	7640	30.55	100.2	1230	34.4	106.2	18.8	15.9	10.6
68a	Bowel Prep	7420	29.82	100.2	1189.2	38.5	92.2	18.2	15.3	9.2
69a	Bowel Prep	6920	28.15	100.2	1096.4	33.5	110.2	16.8	14.1	11.0
71a	After DUT	7020	28.48	100.2	1114.9	25.2	148.3	17.1	14.4	14.8
77a	colostomy	7020	28.48	100.2	1114.9	23.2	159.3	17.1	14.4	15.9
79a	full bladder	7420	29.82	100.2	1189.2	22.6	165.3	18.2	15.3	16.5

79b	Bowel Prep	7420	29.82	100.2	1189.2	22.6	165.3	18.2	15.3	16.5
8a	Enema	7120	28.82	100.2	1133.5	27.2	137.3	17.3	14.6	13.7
97a	Prone full bladder	7020	28.48	100.2	1114.9	23.4	159.3	17.1	14.4	15.9
98a	Prone full bladder	7020	28.48	100.2	1114.9	23.1	159.3	17.1	14.4	15.9

3.3.5. FOV Parameter

To determine if a smaller FOV could be utilised the researcher examined the 0 slice of the CT scan. As seen in Chapter 2 (refer to: 2.3.1-2) the phantom scans indicated that, if a M FOV could be used there would be a decrease in CT dose. Thus, if it is possible to decrease the FOV for patients of smaller body habitus or indeed paediatric patients, this would lead to a decrease in the dose received by the patient for CT localisation scans. For the overweight patients in the lateral dimension only 4 patients measured less than 10 cm and only 3 in the anterior/posterior dimension. There is also a decrease in surface dose if the patient is scanned in the centre of the FOV in both the horizontal and vertical dimensions, as stated by Kaasalainen *et al.* (2014) (refer to: 2.1.3). In this current research the majority of the patients were scanned in the centre of the vertical FOV (78%), with 14% to the right and 8% to the left of the FOV.

In the overweight BMI category, all but one patient (LL FOV) were scanned with XL FOV. The majority of overweight BMI category patients (39 patients or 78%) were scanned in the centre of the FOV. While only 7 patients out of 50 to the right of the FOV.

The patients who fall within the Normal weight BMI category, were mainly scanned in the centre of the FOV (42 patients or 84%) and an equal amount scanned to the left or right (4 patients in each direction or 8%). In the lateral dimension 1 patient (2%) was too narrow in the lateral dimension, with only 10 patients or 20% having an appropriate lateral dimension scan. In addition, only 9 patients (18%) were deemed appropriate in the anterior/posterior dimension.

Of the underweight BMI category patients, 80% were scanned in the centre of the FOV. While 2 patients were scanned to the left and 4 scanned to the right of the FOV. In the lateral dimension 48% of the patients were scanned correctly while 45% were appropriate in the anterior posterior dimension. A summary of the results is illustrated in Table 3.17. The majority of the patients were scanned in the centre of the FOV, with the overweight patients at the lowest of 78%.

Table 3.17: Summary scout view for different BMI patient categories.

Scout view	Scanned in relation to:			Scanned less than 10 cm	
	Centre of the FOV	Left of FOV	Right of FOV	Lateral Dimension	Ant/Post Dimension
Overweight	78%	8%	14%	8%	6%
Normal	84%	8%	8%	20%	18%
Underweight	80%	7%	13%	48%	45%

The FOV most frequently used for the patients was the XL FOV, with 88 patients being scanned with this setting. The second most frequent is the LL FOV with 27 patients scanned. Lastly, 16 patients were scanned with a L FOV.

From Table 3.18 the FOV that is predominantly used for the overweight and normal patients is the XL FOV with only 2% of patients that were overweight being scanned with a LL FOV. Of the normal BMI patients 28% were scanned with a LL FOV and 8% had a L FOV. Of the underweight patients only 23% were scanned with an XL FOV and an equal number scanned with a LL or L FOV.

Table 3.18: FOV usage for the patients.

FOV	Extra-large	Large-Large	Large
Overweight	49	1	
Normal	32	14	4
Underweight	7	12	12

The visual effect of the FOV on the patient, BMI category will now be examined. The underweight patients had the highest percentage of less than 10 cm in the lateral and anterior/posterior dimensions. Figure 3.5 demonstrates that this results from a L FOV, therefore the higher percentage for the lateral dimension comes from the 39% of patients with a L or LL FOV.

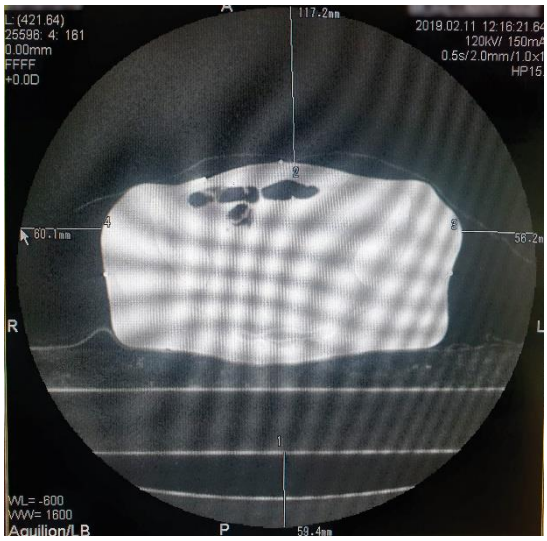

Figure 3.5: Underweight patient with appropriate FOV (L).

The normal BMI category patients were scanned mainly with an XL FOV. Figure 3.6 demonstrates that for some normal BMI category patients the L FOV is appropriate. It also demonstrates that the LL FOV is appropriate for some of normal BMI category patients who receive a CT localisation scan for IMRT treatment. As the CT couch is visible with this FOV, which is a necessity to determine correct IMRT dose. Only 28% of patients were scanned with the LL FOV and only 20% were correct in their lateral dimensions for the normal BMI patient category.

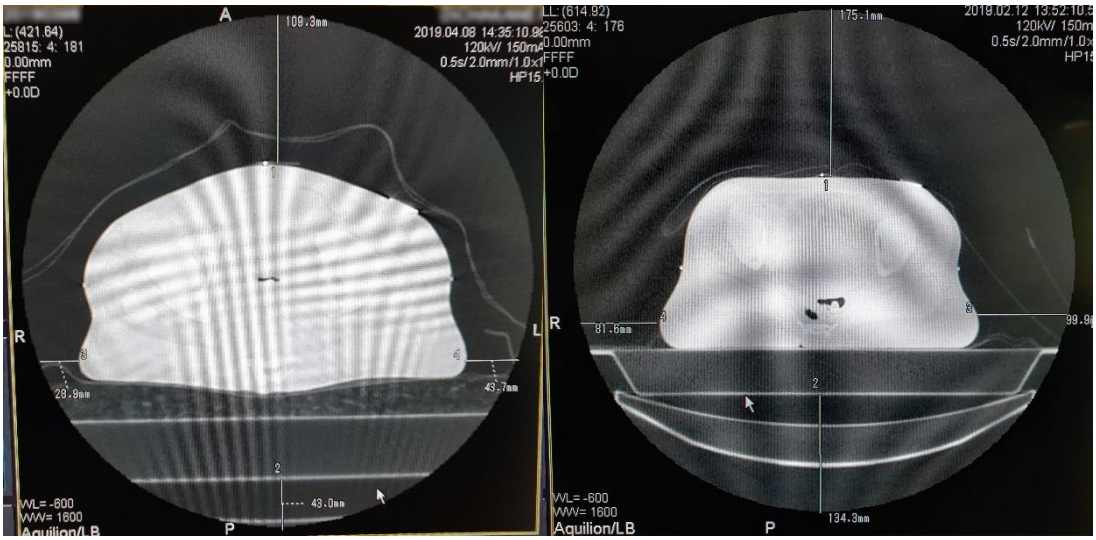

Figure 3.6: Normal patient with appropriate FOV (L FOV on left and LL FOV on right).

The overweight BMI category patients are indicated in Figure 3.7, both visuals exhibiting scans performed with an XL FOV. On the left the patient just fits into the view and on the right the patient is lying prone in a vacuum bag (vac-bag). The vac-bag is a

pillow-like bag used to stabilise a patient's position for radiation therapy. The vac-bag is moulded around the patient and then has the air vacuumed out to maintain the shape of the patient's position. For the planning purposes the vac-bag and table top need to be entirely visible in the CT scan. Therefore, both examples in Figure 3.7 are deemed appropriate. Very few patients were found to have less than 10 cm in the lateral dimension (only 8%). Furthermore, only one patient in this category was scanned with a LL FOV, all others were scanned with an XL FOV. The weight difference in this category ranged from 70 kg to 107 kg.

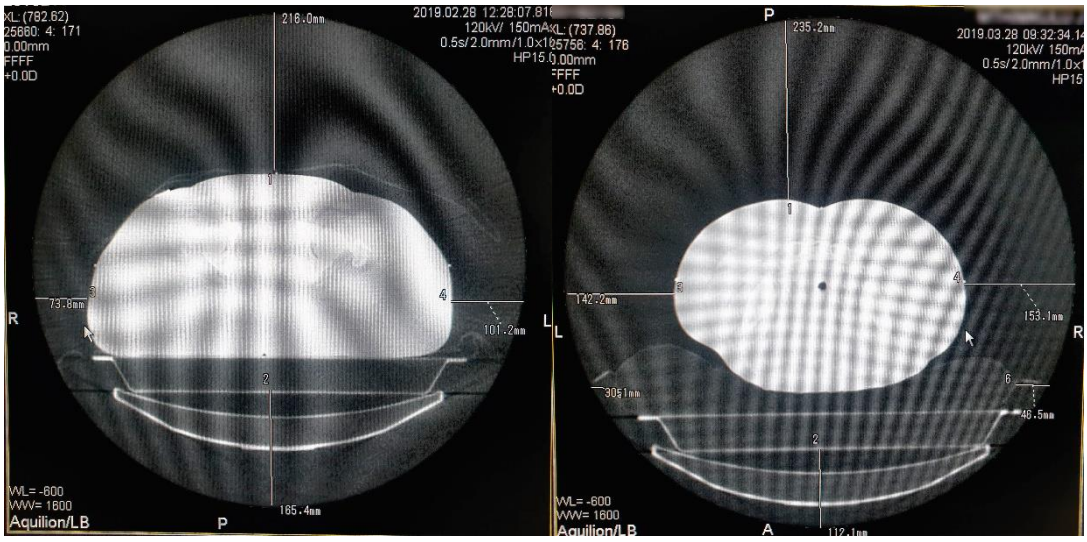

Figure 3.7: Overweight patients scanned with an XL FOV (on the right the patient is in a vac-bag).

The following section discusses the results as indicated in this section.

3.4. Discussion

This research was conducted to establish the CT dose delivered from pelvic CT localisation scans at the oncology department. CT dose is determined by various settings on the CT console. The CT settings that influence the CT dose are examined. The effective dose as calculated from these settings is determined as well as the SSDE. The effect of the patient's BMI on the CT dose is observed. The dose received through a rescan is explored as well as the FOV utilised during this specific research. Finally, the methods that may be used to decrease dose is determined.

3.4.1. CT Settings that Influence Dose

In research conducted by Karim *et al.* (2016) the authors examined radiation dose to different areas of the patient. Their research involved 23 patients who received pelvic CT examinations and 94 patients who underwent abdominal CT examinations. A total of 376 patients' CT scans were examined, these were mainly for diagnostic purposes (Karim *et al.*, 2016). The premise of the research by Karim *et al.* (2016) research was also utilised in this specific research project in order to establish how dose is calculated for a CT scan as well as CT and patient parameters that should be examined (see section: 1.4). The differences between the manner in which the CT scans were conducted during their research and the current research are examined. All patients in the current research were scanned with 120 kV, and with the exception of one patient (350 mA) all patients had 300 mA. The patient scanned at 350 mA was modified by the oncology radiographer at the time of the CT scan. This particular patient had the highest measured BMI of the participating patients and the second largest effective diameter. In Karim *et al.* (2016) the kV used by the different hospitals ranged from 110 kV, 120 kV and 130 kV. Qurashi *et al.* (2017) did research into optimising the CT abdominal protocol for obese patients. Their research noted that when using 120 kV the mean doses were statistically higher than when employing doses that were 100 kV (Qurashi *et al.*, 2017). Karim *et al.* (2016) in their research found that for the pelvic and abdominal examination, the slice thickness was mainly 5 mm with one hospital utilising 3 mm for some of their scans. At the oncology department the slice thickness is often set to 2 mm, which as stated by (Bridge & Tipper, 2011) (see section: 1.2.2) is common in oncological settings but does increase the CT dose. This increase is noted as the reconstructed slice thickness decreases, as there is an increase in image noise, which is due to the decrease in the number of photons (Raman *et al.*, 2013). If the radiation dose is increased, then constant noise levels within the smaller slice thickness can be maintained (Raman *et al.*, 2013). Therefore, the smaller slice thickness used for the pelvic CT scans may have an influence on the CT dose that is received by the patients at the department of oncology, Free State. As well as the consistent 120 kV, Qurashi *et al.* (2017) determined that 100 kV could be utilised for overweight patients. Thus, in the current research the dose could be reduced by using 100 kV for patients, especially underweight patients. To implement the change of kV, the CT technician would have to adjust the CT console settings. After which the medical physicists would need to determine the $CTDI_{vol}$ for the new kV setting.

When establishing DRLs, the $CTDI_{vol}$ and DLP are most often quoted in relation to dose (see section: 2.1.4). During the current research, patients were scanned with 300 mA, which showed a consistent $CTDI_{vol}$ of 100.2 mGy for the L, LL and XL FOV. The DLP for these patients was between 910.9 mGy.cm and 1400.8 mGy.cm, with a median value of 1077.8 mGy.cm. The single patient who was scanned with 350 mA had a $CTDI_{vol}$ of 138.7 mGy and the DLP was 1943.8 mGy.cm, indicating that the use of the higher mA increased the CT dose. The $CTDI_{vol}$ is independent of patient characteristics aside from the radiation delivered per unit length of the patient (Karim *et al.*, 2016). In the research of Karim *et al.* (2016) the mean $CTDI_{vol}$ for the abdomen varied between 7.0 mGy ±1.8 mGy to 15.1 mGy ±7.5 mGy at the different hospitals. The DLP for the abdomen varied between 263.6 mGy.cm ±104.5 mGy.cm to 720.5 mGy.cm ±428.4 mGy.cm. For the pelvis the $CTDI_{vol}$ varied between 15.7 mGy ±3.4 mGy to 18.4 mGy ±6.3 mGy. The DLP was between 519.2 mGy.cm ±190.6 mGy.cm to 539.2 mGy.cm ±134.8 mGy.cm. This is significantly lower than the current research $CTDI_{vol}$ of 100.2 mGy and DLP with a median of 1077.8 mGy.cm. The reason for the increase may be attributed to the smaller slice thickness as well as the increased scan length. The mAs also varied between the research studies. Karim *et al.* (2016) demonstrated mAs that varied between 80 to 244.0 (±92.9). In the current research the mAs varied between a low of 5920 to a maximum of 8560 for the 300 mA scans, and the 350 mA caused a result of 11860 mAs. In further research by Karim *et al*. (2017) they examined the radiation risk to patients who received CT scans for the kidney, ureter and bladder (KUB). In this research 130 kV was used and the $CTDI_{vol}$ had a mean of 11.0 ±3.5 mGy and ranged from 5.8 mGy to 15.5 mGy (Karim *et al.*, 2017). Automatic exposure control was used, which adapts the mAs according to patient habitus and body thickness (Karim *et al.*, 2017). The DLP varied between 300.8 mGy.cm to 692.9 mGy.cm with a mean of 431.5 mGy.cm and a SD of ±60.7 mGy.cm (Karim *et al.*, 2017). At the oncology department automatic exposure control is not presently utilised. The DLP had a mean value of 1090.4 mGy.cm and ranged between 910.8 mGy.cm to 1943.8 mGy.cm, which is much higher than in the research results from the Karim *et al.* (2017) research. The scan data influences the CT dose that is delivered. A range between 5.8 mGy to 15.5 mGy with a mean value of 11 mGy ±3.5 mGy was measured for the $CTDI_{vol}$ in the Karim *et al.* (2017) research. The tube current was influenced by the automatic mAs, which varies with patient body habitus and thickness.

The CT settings influence the CT dose. An examination of the dose based on the effective dose for both the pelvis and abdomen will be discussed hereafter followed by a determination of the SSDE.

3.4.2. Effective Dose

In this specific research the pelvic effective dose had a median dose of 16.5 mSv, with the minimum measured at 13.9 mSv and the maximum at 29.7 mSv for all patients. In the Karim *et al.* (2016) research the pelvic effective dose ranged from 4.3 mSv to 8.9 mSv at one hospital and between 2 mSv to 8.9 mSv at another. However, this researcher's effective dose for the pelvis measures much higher when compared to the Karim *et al.* (2016) finding. This may be due to the increased scan length needed for the CT localisation scan. This specific research determined that the median effective dose for the abdomen was 13.9 mSv with the minimum measured at 11.8 mSv and the maximum of 25.1 mSv. In the research conducted by Karim *et al*. (2016), the abdomen ranged from 4.8 mSv to 37.7 mSv, 2.6 mSv to 7.4 mSv and 1.2 mSv to 12.1 mSv at the various hospitals. For the KUB CT scan, as researched by Karim *et al.* (2017) the effective dose calculated to a range of 4.2 mSv to 10.1 mSv with a mean of 6.6 mSv ±2.3 mSv. Smith-Bindman *et al.*, (2009) conducted research on the radiation dose for common CT scans consisting of 1119 patients scanned at four different institutions. Their research focused on the CT effective dose for common examinations and the lifetime cancer risk that is associated with these CT scans. The lowest median effective dose for an abdomen and pelvis CT scan without contrast was 15 mSv (IQR 10-20 mSv) calculated from results of 120 patients. This is equivalent to the patient receiving 220 chest radiographs (Smith-Bindman *et al.*, 2009). This measurement is closer to the effective dose calculated for this specific research. Furthermore, a routine CT of the abdomen and pelvis that included contrast presented a median of 16 mSv (IQR 11-20 mSv) with 117 patients (Smith-Bindman *et al.*, 2009). Their research further showed that an effective dose of 31 mSv (IQR 21-43 mSv) was measured for multiphase abdominal and pelvic CT scan seen with 110 patients, which is equivalent to 442 chest radiographs. It was determined that from the different sites that were scanned the abdomen and pelvis had the highest variable and the higher effective doses (Smith-Bindman *et al.*, 2009). This variation was seen both in and between institutions. The research further investigated the lifetime attributable risk (LAR) of cancer. For a multiphase abdominal and pelvis CT scan the LAR was calculated at 4 patients per 1000 (Smith-Bindman *et al.*, 2009). The risk of cancer increases as age decreases, also gender plays a role. Female patients have a higher risk when compared to their

male counterparts (Smith-Bindman *et al.*, 2009). The increased risk of females is without a clearly understood biological basis, however females are at an increased risk of lung, thyroid as well as ovarian, uterine and breast cancer (Kalra *et al.*, 2015). A 20-year-old woman, based on the highest effective dose, who received a multiphase abdomen and pelvis CT scan would have a one in eighty associated risk of developing cancer (Smith-Bindman *et al.*, 2009). From Figure 3.2 it was determined that in the current research only 1% of patients fell into the 20-year age category. While most patients were in their fifties and sixties, 18% of patients were in their thirties.

The DLP was utilised for the calculation of the effective dose. The DLP determined by Karim *et al.* (2016) had a mean value at the different hospitals of 720.5 mGy.cm, 263.6 mGy.cm and 445.5 mGy.cm for the abdomen and 519.3 mGy.cm and 539.2 mGy.cm for the pelvis. In comparison the mean value for all patients was 1090.4 mGy.cm. The increase in the scan length accounts for the increase in effective dose. The SSDE is measured in mGy, and then in this study converted to cGy, whilst the effective dose is measured in mSv. These two dose methods can be compared numerically due to the type of radiation used in CT (Lyra *et al.*, 2019). As quoted by Lyra *et al.* (2019) "*The dose equivalent (mSv) is equal to the product of the absorbed dose (mGy) and the radiation quality factor Q; since Q equals 1 for radiations used in CT (and in diagnostic radiology in general), absorbed dose in mGy and dose equivalent in mSv are numerically equal and are many times used interchangeably*". Thus, the effective dose can be converted into mGy and then further into cGy.

In research often only effective dose is determined, however the AAPM report 204 of 2011, suggested that size of the patient influences dose and thus stated that the SSDE be determined to estimate dose received by the patient from the CT scan

3.4.3. SSDE

The measurement for the effective dose is based on scan length for the patient's CT scan (DLP). The SSDE is based on the patient's effective diameter. The SSDE in this research ranged from 85.2 mGy to 191.3 mGy which converts to 8.5 cGy and 19.1 cGy, with a median value of 14.3 cGy. The SSDE differs for the different BMI categories. The median value is lowest for the overweight BMI category at 12.3 cGy, the normal BMI category has a median of 14.8 cGy and underweight BMI category is 17.1 cGy. This indicates that the size of the patient influences dose when comparing it to the effective dose.

The DLP median value for the underweight BMI category is 1059.3 mGy.cm, the normal BMI category has a median value of 1077.8 mGy.cm and the overweight BMI category is 1096.4 mGy.cm, which is inverse of the SSDE. Thus, determining dose with the use of effective dose when compared to determining the dose by the diameter of the patient demonstrates the effect of size on the dose estimate. The patients of smaller body habitus therefore receive a higher dose compared to the larger body habitus patients. The increased dose is due to the higher *f* factor as stated previously (refer to 3.3.3).

Figure 3.3 (refer to 3.3.3.) demonstrates the effective dose as the BMI increases, since the effective dose is dependent on the DLP there is no true relation to the BMI. However, the SSDE does determine dose based on patient size. Thus, in Figure 3.4 the effect of patient size on dose is illustrated, with the dose increasing as the patient BMI decreases.

3.4.4. BMI

A determination of the effect the BMI has on the CT dose will now be examined. As stated previously, the 131 patients were divided into three BMI categories, namely underweight, normal and overweight. The median value for the effective dose of both the pelvis and abdomen increases with an increase in BMI category. The underweight BMI abdomen has a median value of 16.2 mSv, the normal BMI 16.5 mSv and the overweight BMI 16.8 mSv. The pelvis effective dose median is 13.7 mSv for the underweight, 13.9 mSv for the normal BMI and 14.1 for the overweight BMI patient category. The effective dose is often used to quantify radiation risk. Research has shown that long term survivors of Nagasaki and Hiroshima atomic bombs, have an increased risk of cancer, if they received an effective radiation dose from 10 mSv – 100 mSv (Smith-Bindman *et al.*, 2009). A single scan can produce the same amount of exposure and the patient may receive multiple CTs over time (Smith-Bindman *et al.*, 2009).

3.4.5. Rescan Dose

The rescan dose that occurs is often the same as the scan needed to plan the radiation therapy. In terms of dose this can have a significant impact. Thus, the rescan dose is examined to determine the cumulative dose that is received by the patient. When only a zero slice is scanned the resultant SSDE was 2.4 cGy, 11.6 cGy and 13.4 cGy dose. In the research one patient was scanned four times. After the initial scan it was

determined that the patient's bowels were too full. The second scan proceeded after the patient's bowels had preparation to clear them. The third scan was for a full bladder (a technique used to move the small bowel away from the area of interest to reduce dose to the small bowel) and the fourth scan was the consequence of further bowel preparation. Each CT scan resulted in a 12.8 cGy dose estimate to the patient; the resultant dose is a total of 51.2 cGy. The effective dose was 17 mSv for the abdomen and 14 mSv for the pelvis, thus for the four scans the total effective dose was 68 mSv for the abdomen and 56 mSv for the pelvis. This increases the patient's likelihood of developing a secondary cancer.

3.4.6. Selected FOV

The FOV most frequently utilised in the current research is the XL, followed by the LL and lastly the L. All three these FOV result in the same $CTDI_{vol}$ of 100.2 as determined by the phantom dose study in this research (refer to 2.3). Habibzadeh *et al.* (2012) determined that miscentring of 1.7 cm increased patients' surface dose by 17.6%. In their research, Habibzadeh *et al.* (2012) examined the effect of miscentring for both phantom and patient studies. The researchers concluded that miscentring increased the surface dose delivered to a patient (Habibzadeh *et al.*, 2012). They also determined that slim patients in comparison to obese patients were more often miscentred. In the current research the patient is centred in the CT based on the anatomy of the patient. The zero slice is the centre of the planned isocentre for the patient's treatment. As stated, the entire patient contour must be visible in the CT scanned image. In Figure 3.5 an underweight BMI category's patient is seen in the L FOV; the patient appears to be in the centre of the scanned FOV. In Figure 3.6 a normal weight BMI category patient is seen; the L and LL FOV are demonstrated. The LL FOV shows the entire table top, which is necessary for IMRT patient scans. In both images the patient appears to be centred in the FOV. The overweight BMI category patient is seen in Figure 3.7; the XL FOV was used. The patient is again in the centre of the FOV. The image on the right demonstrates the vacbag that must appear in the FOV for IMRT planning. Table 3.17 illustrates that the majority of the patients are in the centre of the FOV for all three BMI categories (Overweight = 78%, normal weight = 84% and underweight = 80 %). Habibzadeh *et al.* (2012) determined that obese patients had a mean value of 0.6 cm below the centre of the scan, while slim patients had a mean value of 2.7 cm. The current research did not use such small margins to determine if the patient was in the centre, also the methodology differed from that of Habibzadeh *et al.* (2012). In their research Habibzadeh *et al.* (2012) used the AP and Lat scout views

to determine if the patient was centred correctly, the lateral scout view determined the miscentred image. Further research at the oncology department would need to be conducted to determine if the dose differed as indicated in the research of Habibzadeh *et al.* (2012).

3.4.7. Methods to Modify Dose

Research by Israel *et al.* (2010) during which 91 patients were scanned, examined the effect that patient size had on radiation exposure when using automatic exposure control for chest, thoracic and pelvic CT examinations. Their research determined that as a function of patient weight the $CTDI_{vol}$ increased. The average was 25.9 mGy and ranged between 4.9 mGy to 71.7 mGy (Israel *et al.*, 2010). The CTD_{Ivol} values were approximately 11 mGy, 22 mGy and 33 mGy respectively when the patients' weight was 60 kg, 80 kg and 100 kg respectively (Israel *et al.*, 2010). Automatic exposure control is not currently used at the oncology department.

3.5. Conclusion

The CT dose to patients who received CT localisation for pelvic radiation was determined in the research. The SSDE was the measurement used to determine dose based on patient size. The patients were divided into BMI categories, overweight, normal and underweight. From the BMI categorisation it was determined that the SSDE increased as the patients' BMI decreased.

The rescan dose was also examined. The rescan dose increases the risk of a patient developing a secondary cancer later in life. This risk is increased as the patient's age decreases. Therefore, younger patients and especially paediatric patients should be scanned with the ALARA principles in mind.

The second and third chapter have determined CT dose for pelvic localisation based on phantoms and then on patient dose. The chapter which follows, will determine image quality as determined by phantom CT scans.

References

American Association of Physicists in Medicine. 2011. Size-Specific Dose Estimates (SSDE) in Paediatric and Adult Body CT Examinations. *AAPM Report No. 204*. Report of AAPM Task Group 204, developed in collaboration with the International Commission on Radiation Units and Measurements (ICRU) and the Image Gently Campaign of the Alliance for Radiation Safety in Paediatric Imaging. Date of Access: 25 November 2017. <https://www.aapm.org/pubs/reports/RPT_204.pdf>

Bowers, A. 2008. *Medical Statistics from Scratch: An Introduction for Health Professionals*. 2nd edition. John Wiley & sons Limited: New Jersey.

Bridge, P. and Tipper, D.J. 2011. *CT Anatomy for Radiotherapy*. M&K Publishing: Cumbria.

Brazier, Y. 2017. *How Useful is the Body Mass Index (BMI)?* Medical News Today. Date last visited 28 August 2020. <https://www.medicalnewstoday.com/articles/255712>

Code of Federal Regulations: 2017. *Title 21: Food and Drugs, Chapter 1-Food and Drug Administration Department of Health and Human Services. Subchapter: Radiological Health. Part 1020- Performance Standards for Ionizing Radiation Emitting Products*. (Volume 8). Date of Access: 24 November 2017. <https://www.accessdata.fda.gov/scripts/cdrh/cfdocs/cfcfr/CFRSearch.cfm?FR=1020.33>

De Vos, A.S., Strydom, H., Fouché, C.B. and Delport, C.S.L. 2011. *Research at Grass Roots: for the Social Sciences and Human Service Professions*. 4th edition. Van Schaik Publishers: Pretoria.

Habibzadeh, M.A., Ay, M.R., Kamali Asl, A.R., Ghadiri, H. and Zaidi, H. 2012. Impact of miscentering on patient dose and image noise in x-ray CT imaging: phantom and clinical studies. *Physica Medica*. (28) 191-9.

Halperin, EC, Wazer, D.E., Perez, C.A. and Brady, L.W. 2013. *Perez and Brady's Principles and Practice of Radiation Oncology*. 5th edition. Lippincott Williams & Wilkins: Philadelphia.

Israel, G.M., Cicchiello, L., Brink, J. and Huda, W. 2010. Patient Size and Radiation Exposure in Thoracic, Pelvic and Abdominal CT Examinations Performed with Automatic Exposure Control. *American Journal of Roentgenology*. 195 (1342- 1346).

Kaasalainen, T., Palmu, K., Reijonen, V. and Kortesniemi, M. 2014. Effect of Patient Centering on Patient Dose and Image Noise in Chest CT. *American Journal of Roentgenology*. 203: 123-130.

Kalara, M.K., Sodickson, A.D..and Mayo-Smith, W.W. 2015. CT Radiation: Key Concepts for Gentle and Wise Use. *Radiographics*. 35: 1706-1721.

Kalender, W.A. 2014. Dose in X-Ray Computed Tomography. *Physics in Medicine and Biology*. 59 (R129-R150.).

Karim, M.K.A., Hashim, S., Bakar, K.A., Bradley, D.A., Ang, W.C., Bahrudin, N.A. and Mhareb, M.H.A. 2017: Estimation of radiation cancer risk in CT-KUB. *Radiation Physics and Chemistry*. 137 (130-134).

Karim, M.K.A.; Hashim, S.; Bradley, D.A., Bakar, K.A., Haron, M.R. and Kayun, Z. 2016. Radiation doses from computed tomography practice in Johor Bahru Malaysia. *Radiation Physics and Chemistry*. 121 (69-74).

Kumar, R. 2011. *Research Methodology: A Step-by-Step Guide for Beginners*. 3rd Edition. SAGE Publications Ltd: London.

Lyra, M., Rouchota, M., Michalitsi, M., Boultadaki, A., Letsas, B., Floros, I., Andreou, M., Synefia, S., Valassi, A., Argyrou, M. and Sotiropoulos, M. 2019. Effective dose and size-specific dose estimate (SSDE) of the torso: In low dose MDCT protocol in multiple myeloma. *Radiology and Diagnostic Imaging Journal.* Volume 3 (1-6).

Masuda, T., Funama, Y., Kiguchi, M., Imada, N., Oku, T., Sato, T. and Awai, K. 2016. Radiation Dose based on CNR index with low-tube voltage scan for paediatric CT scan: experimental study using anthropomorphic phantoms. *Springer Plus*. 5: 2064.

McCollough, C.H., Leng, S., Yu, L., Cody, D.D., Boone, J.M. and McNitt-Gray, M.F. 2011. CT Dose Index and Patient Dose: They Are Not The Same Thing. *Radiology*. Volume 259: (311-316).

Petrie, A. and Sabin, C. 2000. *Medical Statistics at a Glance*. Blackwell Science LTD: France.

Qurashi, A., Rainford, L., Ajlan, A., Khashoggi, K., Ashkar, L., Al-Raddadi, M., Al-Ghamdi, M., Al-Thobaiti, M. and Foley, S. 2017. Optimal Abdominal CT Protocol for Obese Patients. *Radiography*.1-12.

Raman, S.P., Mahadeveppa, M., Blasko, R.V., and Fishman, E.K. 2013. CT Scan Parameters and Radiation Dose: Practical Advice for Radiologists. *Journal of American College of Radiology*. 10: 840-846.

Sanderud, A., England, A., Hogg, P., Fossa, K., Svensson, S.F. and Johansen, S.; 2016. Radiation Dose Differences between Thoracic Radiotherapy Planning CT and Thoracic Diagnostic CT Scans. *Radiography*. (22) 107-111.

Schawkat, K., Fischer, R.M., Heverhagen, J.T. and Christe, A. 2017. The Impact of Integrated Circuit Detector Technology in Routine MDCT: Improved Image Quality Compared to Conventional Detector Design for Constant SSDE. *Hellenic Journal of Radiology*. 2 (1): 23 – 29.

Smith-Bindman, R., Lipson, J., Marcus, R., Kim, K.P., Mahesh, M., Gould, R., Berrington de Gonzalez, A. and Miglioretti, D.L. 2009. Radiation Dose Associated with Common Computed Tomography Examinations and the Associated Lifetime Attributable Risk of Cancer. *Archives of Internal Medicine.* 169 (22): 2078 – 2086.

World Health Organisation (WHO). 2020. *Body Mass Index (BMI).* Date of Access: 28 August 2020. <https://www.euro.who.int/en/health-topics/disease-prevention/nutrition/a-healthy-lifestyle/body-mass-index-bmi >

Chapter 4

Computed Tomography Image Quality Derived from Water Phantom Scans in an Oncology Environment

4.1. Introduction

As indicated in the previous chapters, the researcher determined the CT dose in terms of phantom (Chapter 2) and patient (Chapter 3). This led to the achievement of the first and second objective of the research. In addition to the CT dose, the CT image quality is of utmost importance. Therefore, the third objective, is to verify through the use of water phantoms if the field of view (FOV) modifies the image quality for the phantoms of different sizes. As a result, this chapter examines the effect of the different FOV and kV settings on the image quality of water phantoms of different sizes.

A water filled phantom can be used to gain information on the quality of the scanners imaging capabilities (International Atomic Energy Agency (IAEA), 2012). Other facts gleaned from the water phantom are information on the CT number, image noise and uniformity, as well as visualisation of any image artefacts (IAEA, 2012). In addition, the effect of the FOV and kV settings and their influence on the image quality can be determined. The following quality assurance checks were performed to determine the image quality of the phantoms: (i) the CT number accuracy, (ii) image noise, (iii) the field uniformity of the CT image, as well as examining the effect of the (iv) FOV on the image quality.

4.1.1. Phantoms and CT Images in Radiation Therapy Planning

In radiotherapy treatment planning an essential step is to calculate the correct distribution of dose within the treatment volume (Skryzński *et al.*, 2010). The heterogeneity of the patient's body influences the dose distribution in the treatment planning. The characterisation data for each patient is calculated by the CT images obtained (Skryzński *et al.*, 2010). The fundamental role of the CT images in radiotherapy treatment planning, is to provide the information as to how the patient's tissue attenuates the radiation in the form of CT numbers expressed in Hounsfield units (HU) (Skryzński *et al.*, 2010). The HU may differ between CT scanners as the HU is dependent on the quality of the x-ray beam (Skryzński *et al.*, 2010). When a single CT scanner is utilised, the CT numbers may differ for the same tissue type due to kV

setting and beam filtration. Thus, if the CT settings are modified to use 80 kV instead of 130 kV, this may result in as much as a 2% difference in the treatment planning systems dose calculations, if the relationship used for the HU remains constant (Skryzński *et al.*, 2010). A more precise calculation can be made using phantoms that contain tissue equivalent materials (i.e., materials of which the composition is similar to the atomic composition of human tissue). The data obtained when scanning these phantoms at a CT with the different kV settings can be introduced into the radiotherapy treatment planning system to ensure that more precise treatment dose calculations are obtained (Skryzński *et al.*, 2010). The dimension of a phantom and the location of the phantom on or off axis affects the HU observed for a given material. Different positioning of the tissue-equivalent material in the phantom can lead to a difference of up to 80 HU (Skryzński *et al.*, 2010). The difference in beam quality caused by the different settings and the different depths in the phantom may attribute to the difference in HU (Skryzński *et al.*, 2010).

Research performed by Karmazyn *et al.* (2013), examined the effect of different kV (tube voltage) and the resultant CT noise level for different sized phantoms. The researchers used four cylindrical water phantoms of varying diameters, that is 10 cm, 20 cm, 25 cm and 30 cm to simulate the body sizes of an infant, a child (10 years old, weighing 30 kg), an adolescent (15 years of age, weighing 50 kg) and an adult (weighing 80 kg) (Karmazyn *et al.*, 2013). The image noise was measured using the standard deviation (SD) of the CT attenuation number in HU, which was measured in the centre and in the peripheral twelve o'clock position by a region of interest (ROI). The ROI was 5% of the phantom size as a fixed ROI for the smaller phantoms would have included more peripheral area (Karmazyn *et al.*, 2013).

Choi *et al.* (2018) conducted research into the optimisation of the dose and image quality for paediatric abdominal CT scans. They used self-produced phantoms of various diameters to simulate paediatric abdominal CT scans. The dose to a paediatric patient is approximately 2 to 3 times higher, as their organs have a greater sensitivity to radiation compared to adult patients, when performing an abdominal CT scans for diagnosis of pancreatic and rectal cancers (Choi *et al.*, 2018). An increase in image noise with a decrease in CT dose leads to a reduction in the image quality produced (Choi *et al.*, 2018). Their research sought to optimise dose and image quality for paediatric abdominal CT scans. They used phantoms with a diameter of 12 cm, 16 cm, 20 cm and 24 cm; these were dose measuring phantoms, into which they injected an iodine solution to determine the image contrast (Choi *et al.*, 2018).

Researchers Mansour *et al.* (2016) scanned the American College of Radiology (ACR) phantom to evaluate the CT image quality and increase it. The ACR phantom consists of four independent parts used to determine image quality (Mansour *et al.*, 2016). One of the parts contains rods for assessing the CT number for water, polyethylene, acrylic, bone and air (Mansour *et al.*, 2016). Other CT image quality tests that can be performed with the phantom include the CT number, image noise and CT image uniformity as well as others beyond the scope of this current research.

In Iran researchers assessed the CT number, image noise and field uniformity of water in CT scanners in the Urima metropolis (Goldoost *et al.*, 2018). The research was conducted in two centres using a Siemens 6 slice scanner and a Philips 64 slice scanner (Goldoost *et al.*, 2018). The researchers utilised the CT water phantoms provided by the machine manufacturers and scanned at 110 kV and 120 kV, respectively with 100 mAs and 350 mAs. (Goldoost *et al.*, 2018).

The aforementioned research demonstrated that the use of water phantoms and water phantoms with inserts can be scanned with different kV settings to determine the effect on the image quality. The image quality in oncology is an essential part of the patient's treatment when utilising the radiotherapy treatment planning system. Quality assurance CT checks performed with the use of water phantoms in a radiation therapy department determine the CT image quality capabilities.

4.1.2. CT Image Quality Assurance Checks

There are three CT image quality assurance (QA) checks namely, (i) CT number, (ii) image noise and (iii) field uniformity, which are routinely performed by the medical physicists as per criteria set out by the IAEA (2012). The checks are performed on a water phantom of 30 cm in diameter, and by placing an ROI (region of interest) in the centre of the field. Four other ROIs of the same size as the central ROI, are placed on the periphery of the water phantom (IAEA, 2012). The tolerances for these checks are presented in Table 4.1, as used by the oncology department. These tolerances are based on the Canadian Association of Provincial Cancer Agencies (CAPCA) QA checks and are comparable with the IAEA tolerances.

Table 4.1: Tolerance used for quality assurance CT checks.

QA Checks Performed	Tolerance of CT Number
CT number accuracy of water	± 5 HU
Image noise	± 10 HU
Field uniformity of water	± 10 HU

A detailed description of the QA checks will now follow.

4.1.2.1. CT Number Accuracy

The CT number accuracy check is internationally performed by using a ROI that is placed in the centre of the water phantom. The ROI measures the mean CT number of water and other materials (Njiki *et al.* 2018). Phantoms with different inserts of known densities are measured for CT number accuracy checks (Njiki *et al.*, 2018). Examples of the inserts that may be found are teflon, acrylic, bone, polystyrene, air and polyethylene. These phantoms contain distilled water (Njiki *et al.*, 2018). The tolerance limit for CT number is set at ± 5 HU (Njiki *et al.*, 2018). The HU for water should be close to 0. The CT number is checked in the central ROI to ensure that the phantoms are within tolerance.

4.1.2.2. Image Noise

Image noise in a CT scanner image is the variation of the HU in a uniform material, such as water. Image noise is important, since there is usually a difference between normal and pathological tissue in the attenuation coefficient (AAPM, 1977). Image noise is determined by the standard deviation (SD). Both the central and peripheral regions of the scan should be checked for image noise (AAPM, 1977). To determine image noise the ROI is placed in the centre of the field, with four additional ROIs in the periphery, at 0º, 90º, 180º and 270º (Roa *et al.*, 2015). The image noise is quantified by measuring the SD in the ROI (IAEA, 2012). The tolerance for the image noise is set at ±10 HU. The SD indicates the image noise and, the lower the SD, the lower the noise level. All five ROIs are examined to determine if the noise level is within tolerance.

4.1.2.3. Field Uniformity

The uniformity of an image is determined by the field uniformity test. This test is to determine in a homogenous material, the consistency of the CT numbers (Njiki, *et al.*, 2018). The ROIs' placement is the same as for the image noise scan, which is the ROI

in the centre and the four peripheral ROIs. The field uniformity tolerance limit is set at ±10 HU (Njiki *et al.*, 2018). The field uniformity is measured by the central ROI and the difference in value found at the periphery. The closer the peripheral ROI is to the HU in the centre, the more uniform is the field. A pronounced variation of CT number and image noise is measured if the phantom is not centred in the isocentre of the CT (IAEA, 2012). With radiation therapy planning, the CT scanner is used for quantitative assessment of CT values, therefore the uniformity of the CT number is particularly of great importance (IAEA, 2012).

4.1.2.4. Field of View Parameter

The FOV was discussed in Chapter 2 and 3 (refer to: 2.1.3 and 3.1.3, respectively). The FOV in radiation therapy is an important aspect. The magnitude of the selected FOV determines the size of the pixel (Bellon *et al.*, 2014). The pixel is x and y dimension of a 3D voxel. The slice thickness, which influences the voxel in an image affects the setup of both the patient as well as the treatment planning. This is due to the dependence of the tumour delineation on the slice thickness of the CT image (Bellon *et al.*, 2014). Research has demonstrated that reducing slice thickness from 3 mm to 1.5 mm improved precision of head localisation with a factor of two for frameless radiosurgery (Bellon *et al.*, 2014). In the research of Bellon *et al.* (2014) they did a retrospective reconstruction of the slice thickness and FOV to determine the effect these elements have on tumour delineation for stereotactic radiosurgery. The results of the research determined that the clinical interpretation of the gross tumour volume (GTV) is influenced by the image parameters, which were selected at the time of CT acquisition (Bellon *et al.*, 2014). They determined that the slice thickness had a greater influence than the FOV modification. However, both the slice thickness and FOV contribute towards uncertainties in tumour delineation (Bellon *et al.*, 2014).

Thus, it was essential to perform the afore mentioned CT image QA checks to ensure that the image quality was acceptable for the different FOV and kV settings and that the results were within tolerance as stipulated by the departmental protocol (Table 4.1). These methods used to determine CT image quality in a phantom are explicated in the following section.

4.2. Methodology

The researcher scanned water-phantoms of varying sizes (small, medium, large and extra-large) as well as a medium sized water phantom with inserts to determine the effect of different FOV and kV settings on the image quality. The scans were performed once-off. Each water phantom (as described in the aforementioned paragraph) was scanned with a different FOV and kV setting, selected on the CT scanner. The resultant images were evaluated for image quality using the QA checks. These checks were the (i) CT number accuracy, the (ii) image noise and the (iii) field uniformity. The tolerances for these checks are demonstrated in Table 4.1.

In the measurement section of the CT console a ROI circle diameter was chosen. There were five ROIs placed for measurement of the image quality. The ROI indicates the HU mean value across the volume of the circle as well as the SD. The ROIs were 2 cm in diameter. The first ROI was placed in the centre of the water phantom. The second ROI was placed posterior, the third and fourth on the right and left side of the phantom respectively, with the fifth ROI anterior. Each water phantom was scanned, using different FOV and kV combinations as allowed by the CT scanner. The central ROI's mean value was used for the CT number accuracy. The image noise (SD measurement) was also determined by the central ROI. The field uniformity was determined by the deviance of the peripheral ROIs from the central ROI (IAEA, 2012).

The majority of the QA measurements taken by the medical physicist are based on a medium water phantom. For image quality usage Toshiba included with their CT scanner a medium water phantom with different inserts. This phantom is known as the PX78-01377 phantom. This medium water phantom with inserts (TOS phantom) was scanned to assess the image quality, in relation to the FOV and kV setting used. The TOS phantom has varying inserts, which can be compared to the HU given. Table 4.2 demonstrates the different inserts and their corresponding HU.

Table 4.2: TOS phantom insert tissue type and associated HU.

Insert Type	HU
Polypropylene	-100
Nylon	100
Acrylic	125
Delrin ®	340
Air	-990
Water (background)	0

Courtesy of Kayugawa *et al.* (2015).

The position of the different insert types of the TOS phantom is illustrated in Figure 4.1.

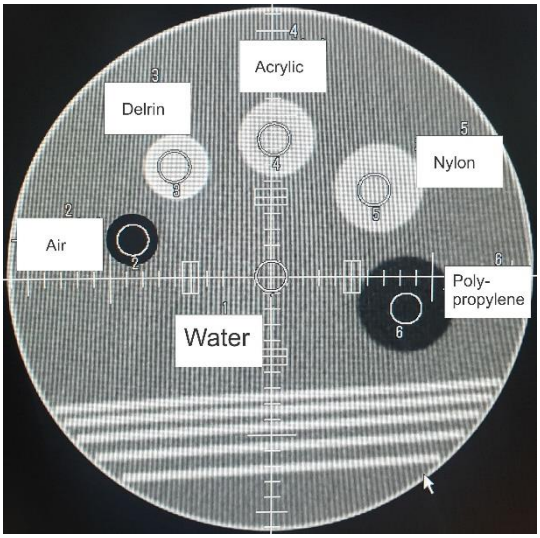

Figure 4.1: Position of TOS phantom inserts.

The ROI for each insert type was placed in the centre of the insert material. The ROI was placed in the centre of the TOS phantom for the measurement of the water, as determined by the scales tool.

4.2.1. Research Tools

Listed as follows are the research tools that were used during the research process. Note that the research tools 1 and 2 were described in Chapter 2 (refer to: 2.2.1).

1. A TSX-201A (Toshiba Aquilion © Large Bore (LB)) CT scanner, as described in Chapter 2 (refer to: 2.2.1-1).
2. The pelvic examination setting was chosen on the CT console and used for the research (refer to: 2.2.1-2).

- The FOVs used were the extra-large (XL), large-large (LL), large (L) and medium (M) for the 135 kV and 120 kV respectively.
  The small (S) FOV was used with the 80 kV.
- The kV settings used for the research were the 135 kV, 120 kV and 80 kV.

3. Water phantoms of various sizes (small, medium, large and extra-large) were utilised. These phantoms were scanned with different FOVs and kV settings.
4. The TOS phantom, which consists of different types of inserts, was scanned with different FOV and kV settings.
5. Quality assurance checks to determine if the CT number, image uniformity and image noise measure in tolerance. Tolerances are illustrated in Table 4.1.
6. The medium water phantom with inserts TOS phantom's insert information for comparison to the CT scans, showing the different types and their appropriate HU as indicted in Table 4.2.

4.2.2. Research Process

The research process used to determine the image quality produced with water phantoms with the use of different FOV and kV settings for the QA checks are illustrated in Figure 4.2.

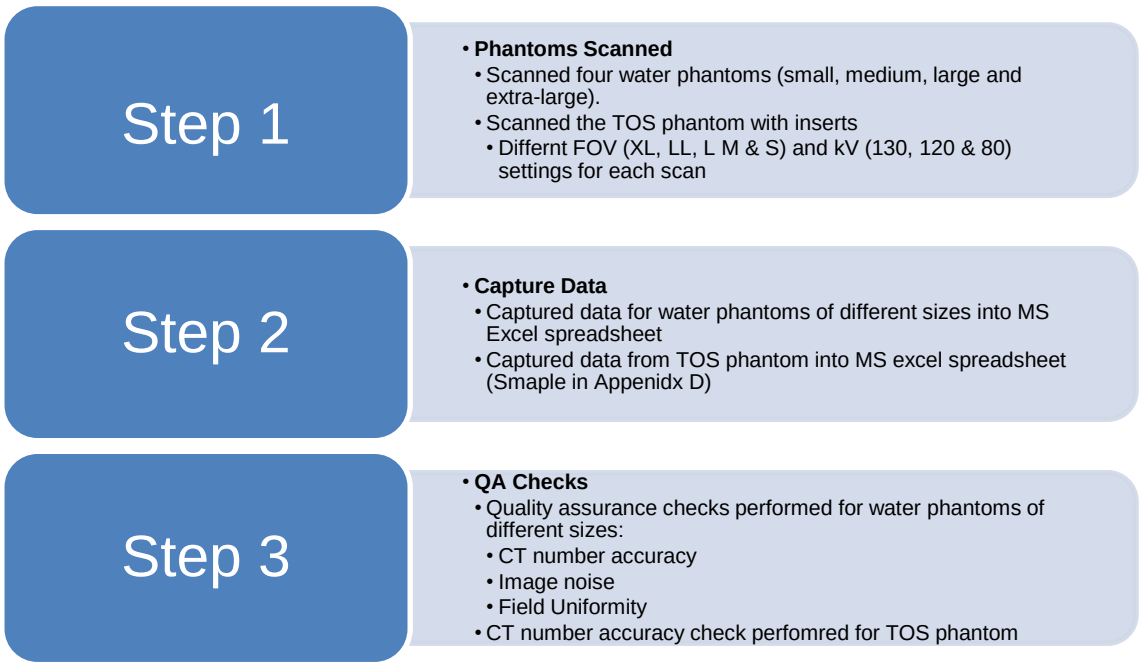

Figure 4.2: The research process to determine image quality utilising water phantoms at different FOV and kV settings.

4.2.2.1. Step 1 –Phantoms Scanned

The set-up procedure for the four water phantoms was replicated as described in Chapter 2 (refer to 2.2.2.1). The TOS phantom set-up procedure simulated the previously mentioned set-up. The water and TOS phantoms were scanned using different FOV and kV settings, for each scan. The collection of the CT data will follow in the next section.

4.2.2.2. Step 2 - Data Capture

The following section explains how the data was collected for each water phantom of different size as well as the TOS phantom.

Water Phantoms of Different Size

The four water phantoms of varying sizes namely, the small, medium, large and extra-large, were scanned. The small water phantom is generally used for head and neck radiation checks. The phantom measures 25 cm in diameter with a neck section of 18 cm in diameter. Only the 25 cm diameter part of the phantom data was examined. The medium phantom has a diameter of 30 cm. The large water phantom is 40 cm in diameter. The extra-large water phantom is 50 cm in diameter.

After the water phantoms were scanned, the researcher assessed each scan. Five ROIs were used and their HU's mean and SD were determined. The ROIs were 2 cm in diameter. For consistent placement of the ROI the scale tool was used (see Figure 4.3). The placement was as follows, the first ROI was placed in the centre, the second and third placed left and right of the phantom, the fourth anterior and the fifth ROI was placed posterior.

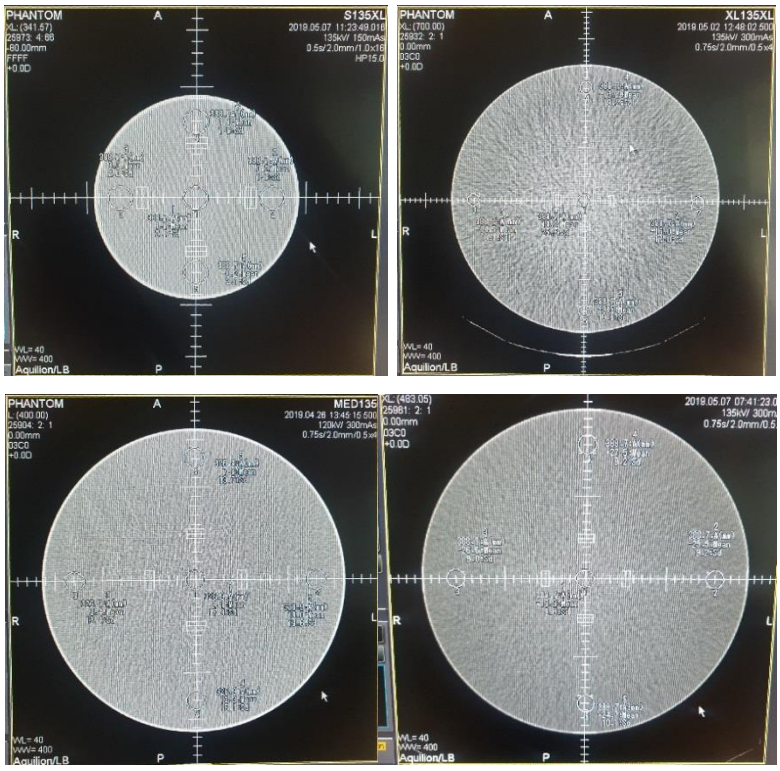

Figure 4. 3: The CT scale as used to determine ROI placement for the water phantoms of various sizes (i.e. small, medium, large and extra-large).

Each water phantom was scanned using the different FOV and kV settings as allowed by the CT scanner. Figure 4.3 demonstrates the placement of the ROI with the use of the CT scales for the small, medium, large and X-large phantoms. For each different FOV and kV setting the scales remained consistent to ensure that the data collected was from the same area on the water phantoms.

The data for the water phantoms were collected by the researcher. The data were captured for the water phantoms of different size on a MS Excel spreadsheet, an example of which is demonstrated in Table 4.3. A photograph was taken of each image for verification purposes.

Table 4.3: Data collected for water phantoms for image quality analysis.

Water Phantom Scans				HU						SD						SNR
No:	*Phantom Name*	*FOV*	*kV*	*Mid*	*L*	*R*	*Ant*	*Post*	HU Mean	*Mid*	*L*	*R*	*Ant*	*Post*	SD Mean	Calculation

The N0 is the number of the scan. The phantom name is the size of the phantom, therefore small, medium, large or extra-large. The chosen FOV and kV used for the creation of the scan are indicated. The HU and SD are measured by the ROIs. The Mid is the middle ROI, the L = left ROI, R = Right ROI, Ant is the anterior ROI and Post the posterior ROI. The readings of each are captured, ensuring the data comes from the ROI indicated (i.e. the middle of the phantom, left or right of the phantom or posterior or anterior).

The QA checks utilised the data that were captured on the MS Excel spreadsheet and determined if these checks were in tolerance.

TOS Phantom

The TOS phantom was also scanned with different FOV and kV settings. Figure 4.1. demonstrates the ROI placements in each tissue type and the central ROI indicating the water. The TOS phantom data was entered onto the MS Excel spreadsheet as illustrated in Table 4.4.

Table 4.4: Data collected for TOS phantom data.

no:	FOV	kV	Type	SD	HU

The No: is the number of the scanned image. The FOV and kV are read from the scanner information. Type is the insert type that was measured, either polypropylene, Nylon, Acrylic, Delrin, air or water. The SD and HU for each tissue type were measured.

Each scan for the TOS phantom was captured for each tissue type. The tissue types as indicated previously (Table 4.2) were used to determine if the CT number accuracy and image noise was in tolerance.

4.2.2.3. Step 3 -Quality Assurance Checks

This refers to the data that was captured and evaluated to ensure that it was within tolerance as stipulated in QA checks (refer to: 4.1.2).

Furthermore, the CT number accuracy test determined if the number was within 5 HU from the required HU number. QA checks were performed for water phantoms of different sizes. This was determined for each water phantom scan, including the TOS phantom's insert tissue types. The image noise was evaluated by the SD of each of the five positioned ROIs. The SD had to be within 10 HU for the image to have an acceptable noise level. All the water phantoms of different sizes as well as the TOS phantom were evaluated for image noise. The field uniformity was assessed only in the water phantoms of different size. By examining the HU in the periphery, ROI were within 10 HU from the central ROI HU.

4.2.3. Validity and Reliability

The water phantoms and TOS phantom scans were part of the pilot study for the research project. The researcher applied the same principles of validity and reliability as previously described in Chapter 2. Additional points are included in the following:

- Image quality was examined on a window width and window level, which is programmed into the CT. The CT has three programmed buttons available. The button that is set for soft tissue viewing was used. This button has a set value for the window width and window level (set to 400 and 40) therefore each image had the same contrast when viewed and measured.
- The researcher photographed each phantom scan image on the CT to ensure correct information was maintained. These photographs were used to verify the captured data for every phantom in the research, thereby ensuring that the captured data was as it was found on the CT on the day of the CT scan.

A detailed account of the methodology used in the research has been described in this section. The next section will present all the results from the research.

4.3. Results

The image quality from phantoms of different sizes and the TOS phantom was determined. The QA checks were performed on these phantoms to determine if they were within tolerance. These checks determined if the image quality was acceptable or not for the different FOV and kV settings. The results of the QA checks and the influence of the different FOVs and kV settings on the image quality will be reported. The accompanying compact disc contains full details (Table Annex, Chapter 4).

4.3.1. Quality Assurance Checks

The following section provides the analysed results for the three QA checks performed (refer to: 4.1.2). All four water phantoms and the TOS phantom were scanned for this section of the research. The TOS phantom was utilised for only two QA checks (CT number accuracy and image noise checks).

4.3.1.1. CT Number Accuracy

The CT number accuracy is quantified by determining if the HU in the middle of the phantom was within ±5 HU from the desired HU. The CT number accuracy test was performed on the four water phantoms of different sizes as well as the TOS phantom. The water phantoms of different sizes will be discussed first. The TOS phantom information is found at the end of the QA checks (refer to: 4.3.1.4). The water phantoms, as the name indicates, are composed of water. Therefore, the HU should be as close to 0 as possible to be in tolerance with the CT number accuracy test. Figure

4.4 demonstrates the CT number quality accuracy test results, demonstrating the different sized phantoms' middle HU for each FOV and kV setting.

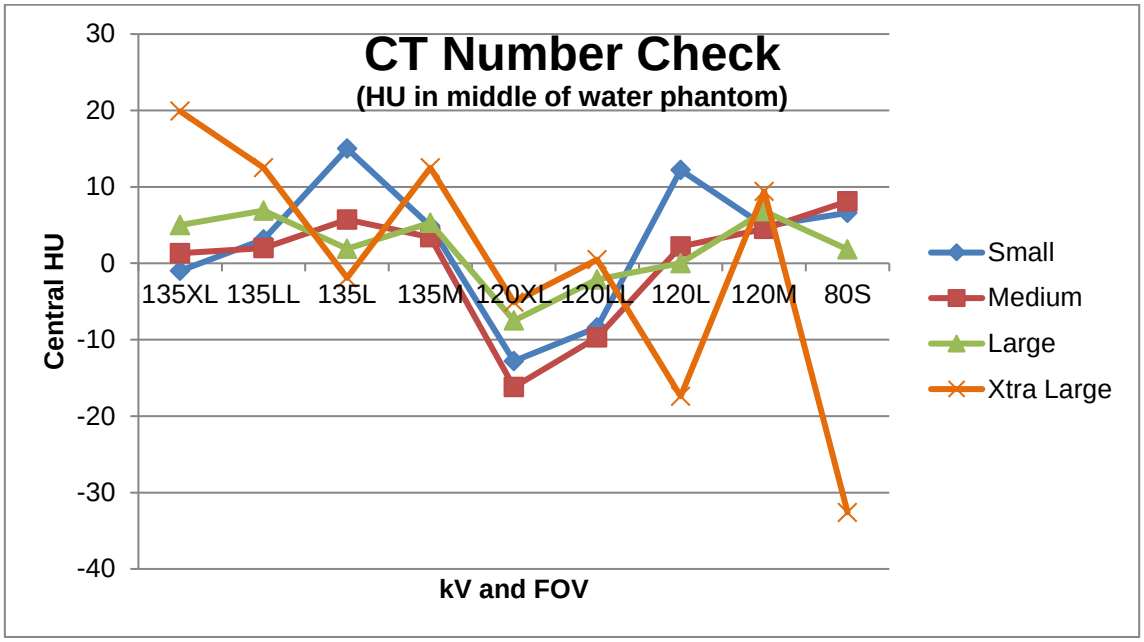

Figure 4.4: CT number accuracy test for central HU from small, medium, large and extra-large water phantoms with different FOV and kV settings.

The fluctuation of the CT number accuracy check from zero HU can be observed in Figure 4.4. The CT number accuracy check for the small water phantom for the 135 kV was within tolerance for all FOV's, with the exception of the L FOV. However, for the 120 kV, only the M FOV was within tolerance. The CT number accuracy results for the medium water phantom was the same as determined for the small water phantom, with the exception of the L FOV with 120 kV, which also measured within tolerance. The CT number accuracy check for the large water phantom revealed that the 135 kV with XL and L FOV were within tolerance. The results for the 120 kV with LL and L FOV were also within tolerance. The CT number accuracy check results for the extra-large phantom showed large variations in the HU (between 1.3 to 24.2) with the exception of the 135 kV with the L and 120 kV LL being within tolerance.

4.3.1.2. Image Noise

In order to determine the image noise, the SD was used. The SD as stated in literature (refer to: 4.1.2.2.) has to measure within ±10 HU. The image noise QA check was performed on the small, medium, large and extra-large water phantoms in conjunction with the TOS phantom (view results in 4.3.1.4). The image noise QA check for the water phantoms was conducted on the middle ROIs as well as the peripheral ROIs.

The results for the peripheral ROIs were in line with the middle ROIs. Figure 4.5 demonstrates the SD for each water phantom of different size with the various FOV and kV combinations, using the measurements from the middle ROI.

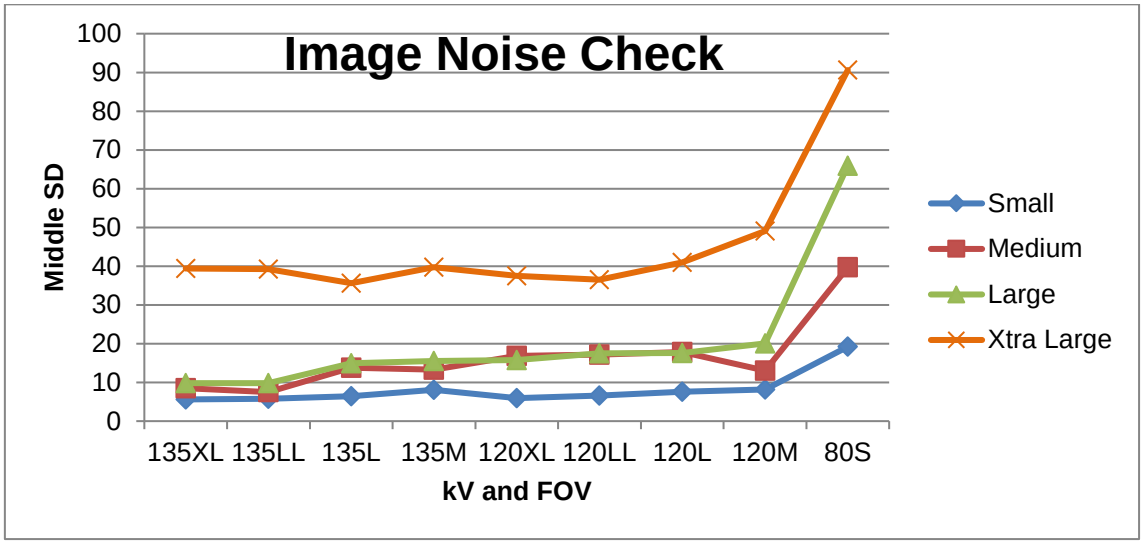

Figure 4.5: Image noise quality assurance test for the small, medium, large and extra-large water phantoms showing the middle SD, using different kV and FOV settings.

The image noise QA check for the small water phantom was within tolerance for all the FOVs and kV settings, with the exception of the S FOV with 80, which was out of tolerance. The image noise check for the medium water phantom was within tolerance for only the XL and LL FOV with a 135 kV setting. The results of the large water phantom followed the same trend. The image noise QA check for the extra-large water phantom was out of tolerance (varied between 28.3 SD and 95 SD) for all image noise checks.

4.3.1.3. Uniformity

The last QA check conducted by the researcher was for image uniformity. For the uniformity to be in tolerance, the peripheral ROIs had to be within ±10 HU from the middle ROI. The small, medium, large and extra-large water phantoms were scanned to assess their uniformity. Table 4.5 demonstrates the results for the different water phantoms' FOV and kV settings. The ROIs positions for the uniformity check, as described in the methodology section, are indicated in Table 4.5 as L, R, Ant and Post. The green highlighted area in Table 4.5 demonstrates that the HU is within tolerance from the middle HU (HU Mid).

Table 4.5: Quality assurance test of uniformity for the small, medium, large and extra-large water phantoms at different kV and FOV settings.

Uniformity Test													
Phantom	**kV**	**HU Mid**	***L***	***R***	***Ant***	***Post***	**kV**	**Phantom**	**HU Mid**	***L***	***R***	***Ant***	***Post***
Small	135XL	**-1**	-5.1	-5	-4.2	-5.5	135XL	***Large***	**5**	-4.2	-3.5	-5.9	-6
Small	135LL	**3.1**	0.6	1.1	1	0.2	135LL	***Large***	6.9	-1.1	-1.8	-1.6	-0.1
Small	135L	15	19.4	19.1	18.1	22.3	135L	***Large***	**1.9**	3.1	2.7	-0.3	11.9
Small	135M	**4.9**	1.6	1.3	0.3	5.6	135M	***Large***	5.3	4.5	4.9	3.2	13.5
Small	120XL	-12.8	-13	-12.2	-12.2	-12.7	120XL	***Large***	-7.5	-14.3	-14.2	-13.7	-12.9
Small	120LL	-8.4	-8.4	-7.4	-7.4	-7.7	120LL	***Large***	**-2.1**	-7.6	-7.7	-6.2	-8.9
Small	120L	12.2	17.8	18.1	16.9	19.8	120L	***Large***	**0**	4.7	2.9	0.7	11.8
Small	120M	**4.9**	0.7	0.8	-1	3.7	120M	***Large***	6.8	8	5.2	3.7	11.2
Small	80S	6.6	7.7	7.6	4.1	7.9	80S	***Large***	**1.8**	17.3	24.1	8.5	20.3
Phantom	**kV**	**HU Mid**	***L***	***R***	***Ant***	***Post***	**kV**	**Phantom**	**HU Mid**	***L***	***R***	***Ant***	***Post***
Medium	135XL	**1.3**	-6.5	-6.3	-5.1	-5.4	135XL	***Extra Large***	19.9	12.6	16.2	9	10.7
Medium	135LL	**2**	-1.8	-1.9	-1.9	-2.4	135LL	***Extra Large***	12.5	18.4	14.6	11.5	13.1
Medium	135L	5.7	10.7	10.1	8.7	13.9	135L	***Extra Large***	**-1.9**	0.6	0.7	-4.9	12.6
Medium	135M	**3.4**	3.1	2.2	0.1	10.5	135M	***Extra Large***	12.5	6.6	13.9	11.8	25.4
Medium	120XL	-16.2	-14.1	-14.7	-15.5	-15.1	120XL	***Extra Large***	-5.1	7.9	7.2	-1.9	-1.8
Medium	120LL	-9.7	-8.8	-9.2	-9.5	-10.2	120LL	***Extra Large***	**0.5**	11.8	7.1	1.4	5.6
Medium	120L	**2.2**	9.7	9.6	6.6	13.7	120L	***Extra Large***	-17.4	6.4	4.3	-3.9	20.9
Medium	120M	**4.5**	1.3	2.7	-1.4	12	120M	***Extra Large***	9.4	8.8	11	10.1	34.4
Medium	80S	8.1	9.5	14.2	13.2	15.4	80S	***Extra Large***	-32.6	43.6	36.5	34	39.5

Phantom= Name of phantom (which is the phantom size. kV= The chosen kV and FOV used to create the CT scan. HU mid= Is the HU measurement for the middle ROI. Other ROI placements are: L=Left, R=Right, Ant=Anterior, Post=Posterior.

The image uniformity check was within tolerance for all imaging variations (FOV and kV settings) for the small water phantom. The uniformity check for the medium water phantom was within tolerance for all, with the exception of the 120 kV with the L FOV. The uniformity check for the large water phantom was within tolerance for the LL, L and M FOV with the 135 kV. The XL, L and M FOV with the 120 kV was also within tolerance. However, the image uniformity check determined that the extra-large water phantom was only within tolerance for the LL FOV with the 135 kV.

4.3.1.4. TOS Water Phantom and the Quality Assurance Checks

The TOS water phantom contains the following inserts: air, Delrin, acrylic, nylon and polypropylene. The appropriate HU for each tissue type is found in Table 4.2 (refer to: 4.2). The TOS phantom consists of water in the non-insert areas. The HU for water was determined in the centre of the phantom. By employing the CT number accuracy check, the HU is within tolerance if found to be ±5 HU for the appropriate HU, as stated by Njiki *et al.*, (2018) (refer to: 4.1.2.1.). Figure 4.6 demonstrates the different tissue types and the variation that occurred with the various FOV and kV settings.

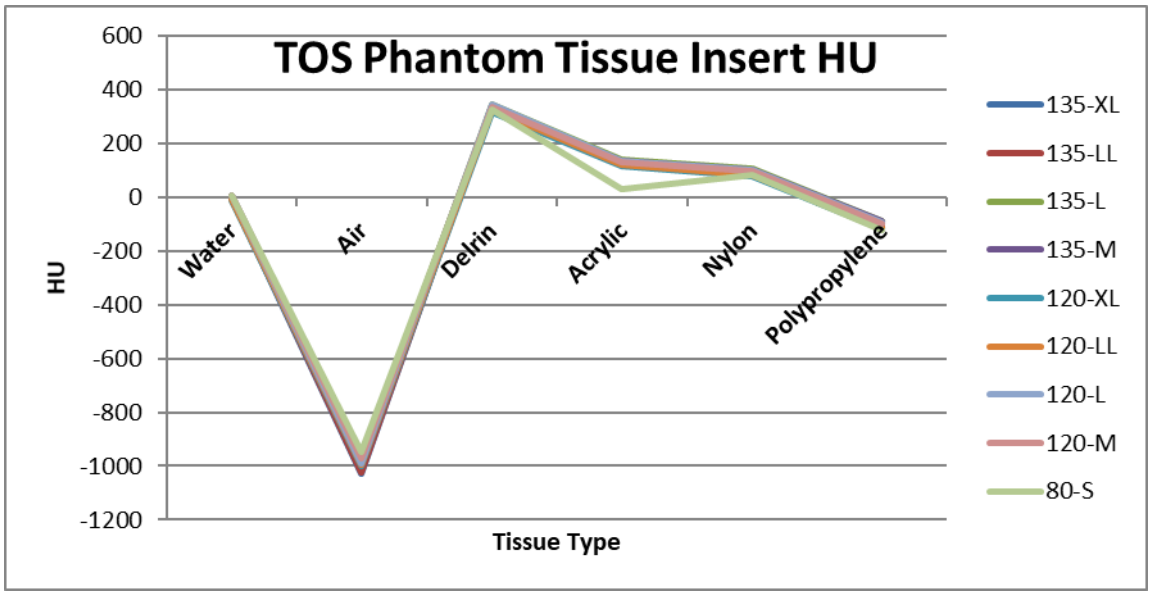

Figure 4.6: TOS phantom insert types HU with different FOV and kV settings.

From Figure 4.6 it can be determined that the S FOV with 80 kV had the greatest effect on the acrylic and air CT numbers. The acrylic insert had an average of 120 HU while the S FOV with 80 kV measured 32 HU, which is a difference of 88 HU. The air inset type had an average of -991 HU while the S FOV and 80 kV measured -949 HU; a difference of 38 HU was calculated. These are the most significant differences between the average and measured HU for the different insert types, with the different FOV and

kV settings. Note attached compact disc contains the full results as per Table TA.4.3 to Table TA.4.8.

A more detailed examination of the insert types using both the CT number accuracy check as well as the image noise check is expounded upon in the following section.

CT Number and Image Noise for FOV and kV

The *water tissue type* should have a measured HU value of close to 0 with a tolerance of ±5 HU for acceptability. From Table 4.6 it can be gleaned that the 135 kV XL, and LL, L and M FOV were all within tolerance as well as the 120 kV L FOV for the CT number accuracy check. The image noise, which should have a SD of ±10 HU, was within tolerance for the 135 kV, XL and LL FOV.

The *air tissue type* should have a measured HU value close to -990 HU. The CT number accuracy check was within tolerance for the 135 kV L FOV as well as for the 120 kV, XL, LL and L FOV. The image noise test was only within tolerance for the 135 kV XL FOV test, as reflected in Table 4.6.

The *Delrin tissue type* should measure close to 340 HU value. Table 4.6 indicates this tissue type and determines that the CT number accuracy check measures within tolerance for the 135 kV XL, LL and M FOV, 120 kV L and M FOV scans. The image noise check measures within tolerance for only the 135 kV XL FOV scan.

The *acrylic tissue type* which is within tolerance with a CT number of close to 125 HU, is illustrated in Table 4.6. The 120 kV LL and M FOV meets the requirements for the CT number accuracy check (as seen in Table 4.6). The CT image noise check is only met by the 135 kV LL FOV.

The *Nylon tissue type* should have a measured CT number close to 100 HU. The 135 kV XL, LL and M FOV all fulfilled the CT number requirements for tolerance (as illustrated in Table 4.6), as does the 120 kV L and M FOV CT scans. The image noise is within tolerance for the 135 kV XL and LL FOV scans.

The *polypropylene tissue type* CT number should measure close to -110 HU value. Using this as a reference, the 120 kV M FOV met the requirements. The image noise tolerance is met by the 135 kV XL FOV, as can be determined from Table 4.6.

Table 4.6: TOS water phantom tissue type in-tolerance quality assurance tests.

	Water	Air	Delrin	Acrylic	Nylon	Polypropylene
CT tolerance test	**In Tolerance**	**In Tolerance**	**In Tolerance**	**In Tolerance**	**In Tolerance**	**In Tolerance**
CT Number	135 XL, LL, L, M	135 L	135 XL, LL, M		135 XL, LL, , M	
	120 L	120 XL LL L	120 L M	120 LL M	120 L,M	120 M
Image Noise	135 XL LL	135 XL	135 XL	135 LL	135 XL, LL	135 XL

135= 135 kV, 120= 120 kV, XL=Extra-large FOV, LL=Large large FOV, L=Large FOV, M=Medium FOV.

4.3.1.5. Summary of Quality Assurance Tests

A summary of the small, medium, large and extra-large water phantoms is demonstrated in Table 4.7, indicating which of the QA checks were found in tolerance. The table indicates, for each sized phantom, which FOV and kV setting combination, was found to be within or out of tolerance for each QA check.

.

Table 4.7: Summary of quality assurance tests for small, medium, large and extra-large water phantom.

	Small Phantom		Medium Phantom		Large Phantom		Extra- Large Phantom	
CT tolerance test	**In Tolerance**	**Out of Tolerance**	**In Tolerance**	**Out of Tolerance**	**In Tolerance**	**Out of Tolerance**	**In Tolerance**	**Out of Tolerance**
CT Number	135 XL, LL, M	135 L	135 XL, LL, M	135 L	135 XL, L	135 LL, M	135 L	135 XL, LL, M
	120 M	120 XL, LL, L	120 L, M	120 XL, LL	120 LL, L	120 XL, M	120 LL	120 XL, L, M
		80 s		80 s		80 s		80 S
Image Noise	135 XL, LL, L, M		135 XL, LL	135 L, M	135 XL, LL	135 L, M	NONE	135 XL, LL, L, M
	120 XL, LL, L, M			120 XL, LL, L, M		120 XL, LL, L, M		120 XL, LL, L, M
		80 S		80 S		80 S		80 S
Uniformity	135 XL, LL, L ,M		135 XL, LL, L M		135 LL, L M	135 XL	135 LL	135 XL, L, M
	120 XL, LL, L, M		120 XL, LL, M	120 L	120 XL, LL, M	120 L		120 XL, LL, L (complete fail), M
	80 S		80 S			80 S		80 S (complete fail)

135= 135 kV, 120= 120 kV, 80= 80 kV, XL= Extra-large FOV, LL= Large large FOV, L= Large FOV, M= Medium FOV, S= Small FOV.

A summary of the QA checks is illustrated in Table 4.7. The table denotes the CT number accuracy, the image noise and the field uniformity QA checks. The QA data were modified to determine the number of QA checks that were within tolerance in terms of water phantom size.

The water phantoms, as indicated in Chapter 2, represent the effective diameter of a patient. Thus, the image quality as determined by the QA checks indicate how the image quality is affected by a patient's size. By examining Table 4.7, it can be determined that each phantom was scanned with135 kV XL, LL, L and M FOV. Thus, four tolerance checks for the CT number, four tolerance checks for the image noise and four tolerance checks for the image uniformity, therefore 12 QA checks were performed in total. The same was true for the 120 kV. The 80 kV only had one CT number tolerance check, one image noise tolerance check and one image uniformity tolerance check; therefore, only three checks were performed. In Table 4.8 a summary of the water phantoms of different sizes and the number of checks deemed within tolerance, with the total number of checks performed, is illustrated.

Table 4.8: Summary of the small, medium, large and extra-large phantoms with the number of tolerances found per check for the 135 kV, 120 kV and 80 kV.

Phantom Size	kV	# Within Tolerance	Total Number of Checks
Small	135	11	12
	120	9	12
	80	1	3
Medium	135	9	12
	120	5	12
	80	1	3
Large	135	7	12
	120	5	12
	80	0	3
Extra-Large	135	2	12
	120	1	12
	80	0	3

From Table 4.8 it can be gleaned that the image quality checks met the highest rate of compliance for the 135 kV, followed by the 120 kV setting. The 80 kV setting has the lowest rate of compliance. The small phantom had the highest rate of compliance for the QA checks that were within tolerance, being 77.8% (21 checks out of 27 checks in tolerance). This determined that the small phantom had the most acceptable image quality. The medium phantom was within tolerance for 55.6% (15 checks out of 27 checks in tolerance). The large phantom was only within tolerance for 44.4% (12 checks out of 27 checks) of the QA checks, while the extra-large phantom was within tolerance for only 11% (3 checks out of 27 checks) of the QA checks.

The QA checks that were performed demonstrated that the small water phantom was within tolerance for the CT number, image noise and uniformity for the 135 kV XL, LL and M FOV scans as well as for the 120 kV M FOV. The medium phantom was within tolerance for the CT number, image noise and uniformity for the 135 kV XL and LL FOV scans. The large phantom, 135 kV LL FOV scan was the only scan to be within tolerance of more than one CT QA check, this being the noise and uniformity check. The extra-large phantom was within tolerance for only one of the QA checks, which was the 135 kV L FOV. The 120 kV LL FOV also had only one QA check within tolerance, the CT number. The 120 kV XL FOV and 120 kV L FOV did not measure within tolerance for any of the quality control checks. The 135 kV produced an improved image quality for all scans. The 120 kV demonstrates a few of the checks within tolerance, while the 80 kV was out of tolerance for most checks as well as for all the large and extra-large phantom scans. The 80 kV was only in tolerance for uniformity of the small and medium phantom. All phantoms were out of tolerance for the CT number and image noise. This indicates that the 80 kV is unable to penetrate the phantoms, the implementation and examination of 100 kV would be recommended.

The TOS phantom as previously stated is a medium sized phantom (30 cm in diameter). The results indicated that the 135 kV was within tolerance for most of the CT scans, with the exception of acrylic, in terms of CT number. The 135 kV was also within tolerance for image noise. The FOV that proved most within tolerance was the XL for the 135 kV and the L for the 120 kV. Although the 120 kV was only within tolerance for the CT number, the 135 kV was within tolerance for the CT number and image noise checks. The medium water phantom and the 135 kV XL FOV was within tolerance for all three QA checks. The 120 L had only the CT number check within tolerance for the medium phantom.

4.3.2. Influence of FOV and kV Settings on Image Quality

The FOV is the only modification that is made by the oncology radiographer when performing the CT scans for radiation therapy planning purposes, at the oncology department. Therefore, it is important to establish the effect of the FOV on the image quality for the phantoms of different sizes.

4.3.2.1. Small FOV

Each phantom was scanned with the different FOV and kV settings. Figure 4.7 illustrates a section of the different water phantoms from small to extra-large with S

FOV and 80 kV setting. The graininess of the extra-large phantom was visible and improved as the water phantoms decreased in size (Figure 4.7). The uniformity QA check was within tolerance for the small and medium phantom with this S FOV and 80 kV setting, all other water phantoms QA checks were out of tolerance for the S FOV settings.

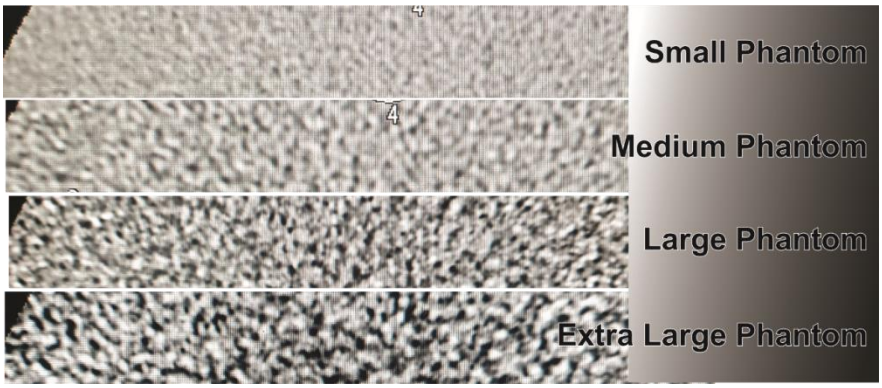

Figure 4.7: S FOV showing a section of the small, medium, large and extra-large water phantoms.

The S FOV with 80 kV, measured within tolerance for two out of the twelve QA checks. This resulted in a within tolerance rate of 16.7 % for the QA tolerance checks with all the water phantom sizes.

4.3.2.2. Medium FOV

The M FOV for the different sized water phantoms with the 135 kV and 120 kV settings are demonstrated in Figure 4.8. The small phantom was within tolerance for the M FOV with both the 135 kV and 120 kV settings, and with all three QA checks performed (CT number, image noise and uniformity).

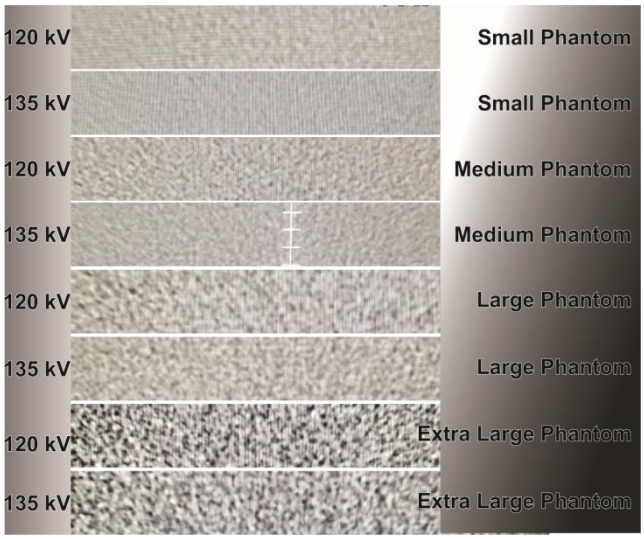

Figure 4.8: Medium FOV water phantoms.

The QA checks for the medium FOV were within tolerance for 50 % of the checks (twelve checks out of twenty-four checks) for the 135 kV and 120 kV for all size of water phantoms. The M FOV with 120 kV and 135 kV were within tolerance for the CT number image noise and uniformity for the small phantom. Both were also in tolerance for the CT number and uniformity for the medium phantom. Lastly, both 135 kV and 120 kV were within tolerance for the uniformity for the large phantom. No checks were within tolerance for the extra-large phantom with a M FOV.

4.3.2.3. Large FOV

Figure 4.9 illustrates the images produced by the L FOV. It was determined that 50% of the checks (six out of twelve) of the scans with L FOV, 135 kV were within tolerance. The image noise was found within tolerance for the small phantom, as was the uniformity for both the 120 kV and 135 kV settings. The medium phantom's uniformity was within tolerance for 135 kV. The large phantom was within tolerance for both the CT number and the uniformity checks, using the 135 kV setting. The extra-large phantom was within tolerance for the CT number, for the 135 kV. Only 33.3% (four checks out of twelve checks) were within tolerance for the 120 kV QA checks, with the image noise and uniformity passing also for the small phantom. The medium and large water phantoms were found within tolerance for the CT number.

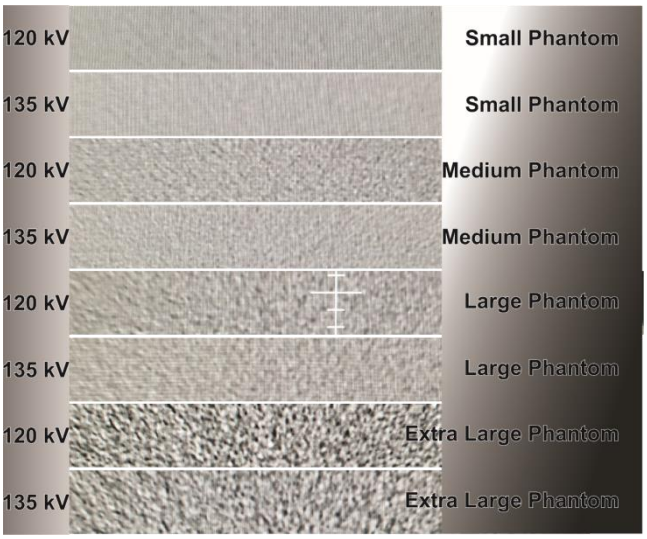

Figure 4.9: Large FOV water phantoms.

The L FOV CT number proved to be acceptable for both the 135 kV large and extra-large phantom and for the 120 kV, medium phantom scans. The small phantom was within tolerance for the image noise and uniformity for both 120 kV and 135 kV respectively. The medium and large water phantoms were within tolerance for only the uniformity QA check. A slight shift was seen with the CT number tolerances for the smaller phantoms, with the large phantoms starting to measure within tolerance for the L FOV where previously it was out of tolerance.

4.3.2.4. Large-Large FOV

The LL FOV setting results are illustrated in Figure 4.10 for the small, medium, large and extra-large water phantoms. The 135 kV setting had a 75% within tolerance QA check outcome (nine out of twelve checks). The CT number was found to be within tolerance for both the small and medium phantoms. The image noise was within tolerance for all phantoms, with the exception of the extra-large water phantom. All four (small, medium, large and extra-large) water phantoms were within tolerance for the uniformity QA check (this was the only time that the extra-large phantom was within tolerance with the uniformity QA check). The 120 kV was only within tolerance for the CT number of the large and extra-large phantoms. The small phantom was the only phantom within tolerance for the image noise with the 120 kV. The uniformity QA check was within tolerance for the small, medium and large water phantoms.

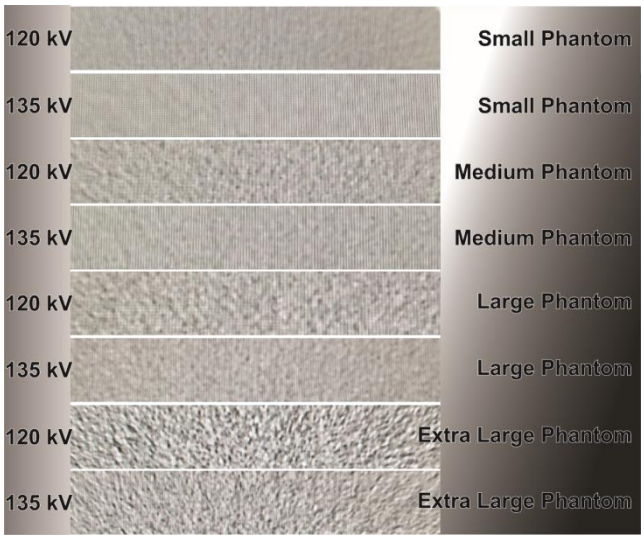

Figure 4.10: Large large FOV water phantoms.

The LL FOV proved to be acceptable for the small, medium and large phantoms, with the CT number within tolerance for the 120 kV setting. The 135 kV; uniformity check was within tolerance for the extra-large water phantom (the only time these checks were within tolerance for the respective kV settings). The large water phantom had more QA checks within tolerance with the CT scan QA check results.

4.3.2.5. Extra-Large FOV

Lastly, the XL FOV for all the phantom scans is illustrated in Figure 4.11. For the 135 kV, the CT number, image noise and uniformity were all within tolerance for the small and medium phantoms. The large phantom was only out of tolerance with the uniformity check. The extra-large phantom was not within tolerance for any QA checks with the 135 kV setting. With the 120 kV setting, only 33.3% (four out of twelve checks) of the QA checks were within tolerance for the XL FOV. These QA checks were the image noise and uniformity for the small phantom. The medium and large phantoms were within tolerance for the uniformity QA checks.

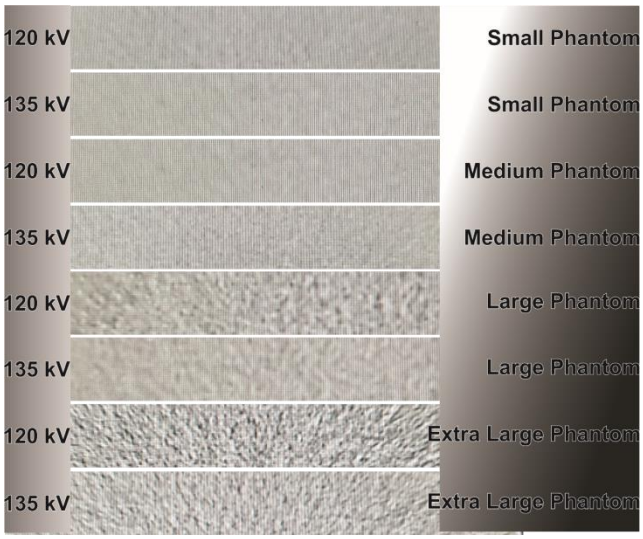

Figure 4.11: Extra-large FOV water phantoms.

The small phantom was within tolerance for most of the QA checks using both the 120 kV and 135 kV settings respectively. The medium phantom was within tolerance for all the QA checks with the 135 kV setting and the large phantom was within tolerance for two of the three checks with the 135 kV.

4.4. Discussion

This objective of this specific section of the research study was to investigate the effect of different FOV and kV settings on the image quality of water phantoms of different sizes in an oncology environment. In addition, other aspects of determining image quality were also examined. These being three QA checks, which are the CT number accuracy, image noise and field uniformity checks. Utilising these results, the image quality was determined, first in terms of phantom size, followed by the influence the FOV and kV settings had on each phantom of different size.

In the research conducted by Karmazyn *et al.* (2013) the authors used four cylindrical water equivalent phantoms to evaluate the effect of kV on image noise for different sized phantoms, which they equated to patients of different ages. Therefore, in this current research the small water phantom represents a person with an effective diameter of 25 cm, which when applying Karmazyn *et al.* (2013) as a guideline, indicates a small adult or an adolescent. The medium phantom can be seen to represent an average adult, with a diameter of 30 cm. The largest effective diameter that can be calculated with the conversion factor created by the AAPM (2011) is 45 cm. The large water phantom represents a larger person with an effective diameter of 40

cm, therefore overweight. The extra-large phantom at 50 cm in diameter represents a very obese patient. The TOS phantom has the same diameter as the medium water phantom.

4.4.1. CT number

The CT number accuracy check for the water phantoms of different sizes determined that the higher the kV, the higher the rate of tolerance that was found. In this specific research the 80 kV, which can only be scanned with a S FOV, no phantom was within tolerance for this QA check (Table 4.7). This aligns with the TOS phantom data (Table 4.6), which also shows no insert type was in tolerance for the CT number check when the S FOV and 80 kV was utilised.

The 120 kV setting resulted in the medium and large water phantoms each having two FOVs that were within tolerance for the CT number water check, while both the small and extra-large phantoms had only one FOV that was within tolerance (Table 4.7). The TOS phantom data in Table 4.6 demonstrated that, with the 120 kV setting, at least one FOV was within tolerance for each insert type. Amongst all the inserts used the air insert was mostly within tolerance with the XL, LL and L FOV, followed by Delrin, nylon (L and M FOV) and acrylic (LL and M FOV).

The best CT number accuracy was obtained by the 135 kV setting. The extra-large water phantom was the only phantom, with only one FOV, that was within tolerance (Table 4.7). The large phantom had two FOVs within tolerance and the medium and small phantoms both had three FOVs within tolerance.

The afore mentioned demonstrated that, as the kV increased, the image quality, in terms of CT number increased as well. Njiki *et al.* (2018) reported that the CT number for the different CT scanners differed for some insert types. A different trend was noted with the TOS phantom 130 kV setting. The water insert type was within tolerance for all four FOVs (XL, LL, L and M), the Delrin and nylon inserts were within tolerance for all, with the exception of the L FOV. Finally, the acrylic and polypropylene inserts were out of tolerance in all FOVs with the 130 kV setting. This variation in the TOS phantom is corroborated by research conducted by Mansour *et al.* (2016), in which they determined that the CT number test for the different materials was within tolerance with the exception of the bone insert of which the value was out of tolerance. Additional corroboration of this finding is the research of Njiki *et al.* (2018), which states that the CT numbers were accurate for most inserts with the exception of Delrin, polystyrene,

Teflon, bone 20% and bone 50%. The researchers then verified the CT linearity in order to establish the constancy of contrast scale over the range of CT numbers (Njiki *et al.*, 2018). This specific research did not check the CT linearity from the results as it was not part of the study objectives. However, the CT linearity has been determined and is checked annually, for the CT scanner by the medical physicist at the oncology department.

A variation of HU for different kV settings and scanners has been researched by Cropp, *et al.* (2013) during which they scanned an ACR phantom on different makes of CT scanners to determine their CT numbers. The researchers determined that the CT number increased with kVp for polyethylene and acrylic, while decreasing for bone equivalent CT numbers (Cropp *et al.*, 2013). They concluded that a significant difference occurred between scanners from different manufactures for water and air in terms of CT numbers and stated that manufacture specific and kVp tolerance ranges must be determined for CT numbers to improve the effectiveness of QA tests (Cropp *et al.,* 2013). In the research at hand the CT numbers for the TOS phantom values were as those stated by the researchers Kayugawa *et al.* (2015). They scanned the TOS phantom with 120 kV and different mAs (Kayugawa *et al.*, 2015). In a published article by McCollough *et al.* (2004) the authors indicated that for the ACR phantom, the following CT number reference should be used: for air between -1005 HU to -970 HU; for acrylic +110 HU to +130 HU; polypropylene -107 HU to -87 HU and bone +850 HU to +970 HU. These results indicated that a slight variation of CT numbers could be determined for different phantom and CT combinations. Kodlulovich *et al.* (2008), stated that the CT numbers for air and water are two fixed points in the CT value scale and thus, for every CT scanner these points are set for each kV and x-ray filtration available for the scanner. This demonstrates that the air and water are the most important inserts in determining if the CT numbers are within tolerance for the CT number tests and as demonstrated earlier, slight variations can be found. The researchers Goldoost *et al.* (2018) stated that in radiotherapy, the CT number uniformity is of great importance as the CT number is used for quantitative assessment.

4.4.2. Image Noise

Image noise in terms of CT, is in a uniform medium the fluctuation of the CT number around its average value (Goldoost *et al.*, 2018). In this specific research the image noise was out of tolerance for all 80 kV scans for all phantoms of different size, including the TOS phantom. The 120 kV image noise check was only within tolerance

for the small water phantom. All the other phantoms were out of tolerance for this QA check, including the TOS phantom. The 135 kV was within tolerance for all phantoms with the LL FOV, for the L and M FOV for the large, medium and small water phantom.

The small water phantom was within tolerance for all image noise checks for the 135 kV. The TOS phantom was within tolerance for the 135 kV XL FOV for all, except the acrylic insert types. For the LL FOV the water, acrylic and nylon was within tolerance for the image noise check. This aligns with the statement by Choi *et al.* (2018) that in terms of image noise, there is a decrease in value as the tube voltage increases. In their research, which was conducted with all the phantom diameters, they found that the 140 kV was approximately two times lower than for 80 kV in terms of mean noise values. The researchers explained that the reason for the decrease with increased kV was that the penetrating force increased and the scatter rays decreased as the ray permeated through the tissue. Thus, the noise level decreased (Choi *et al.*, 2018). If the kV remained constant but the mA was increased, the noise levels decreased due to an increase in the number of x-rays detected (Choi *et al.*, 2018). At the oncology department the mA is not usually modified for a CT scan, however this option could be explored in order to improve image quality with a decreased kV for improved image quality and decrease in CT dose. Karmazyn *et al.* (2013) scanned four water equivalent phantoms of different sizes. The results of their research indicated that, with an increase in the phantom's diameter or when the kV is decreased, there was an increase in the image noise (Karmazyn *et al.*, 2013). Figure 4.5 of this specific research demonstrates the same effect. The extra-large water phantom had an increase in image noise for all FOV and kV combinations. The small water phantom had the lowest image noise for the same FOV and kV combination. The lowest kV of 80 demonstrates the highest noise levels for all the phantoms of different sizes.

4.4.3. Uniformity

The uniformity QA check for the water phantoms of different sizes was within tolerance for the small and medium water phantoms only. The small water phantom was in tolerance for all FOVs. The uniformity of the ACR phantom in the research of Mansour *et al.* (2016) was deemed acceptable as all five ROIs were within 5 HU from each other. The ACR phantom used in the research of Mansour *et al.* (2016) measured 20 cm in diameter, which is close to the 25 cm diameter of the small water phantom used, in the current research. Furthermore, in the current research the 120 kV was within tolerance for the XL, LL and M FOV for the small, medium and large water phantom. For the medium water phantom the L FOV was the only one out of tolerance. The

uniformity results of Karmazyn *et al.* (2013) indicated that the central to peripheral ratio increased, regardless of kV with larger diameters. However, there was no difference for the 25 cm and 30 cm diameter phantoms at 120 kV when comparing the central to peripheral noise ratio in their research. These results correlate well with that of the current research.

However, when the phantom diameter was increased from 10 cm to 30 cm in the research study by Karmazyn *et al.* (2013), the mean relative noise level between the central and periphery increased by 7% and 37%, respectively. In the current research the extra-large phantom, which has a diameter of 50 cm, was out of tolerance for the 80 kV in all dimensions (Table 4.5). The large water phantom was also out of tolerance for the 80 kV for the left, right and posterior dimension, only being within tolerance for the anterior. The 120 kV L FOV for the extra-large phantom was also out of tolerance in all dimensions; the large phantom had the posterior out of tolerance for the 120 kV L FOV as well as the medium water phantom. The posterior ROI for the extra-large phantom was out of tolerance for five of the FOV and kV combinations (Table 4.5). Four of the left HU were out of tolerance for uniformity for the extra-large water phantom and one for the large water phantom. The lack of uniformity in the extra-large phantom could be due to it not being centred correctly or due to the bowtie filter not being correct for the size of the phantom. The posterior ROI is the most often out of tolerance for all directions of uniformity.

In a research study conducted by Goldoost *et al*. (2018) it was found that both scanners passed the CT number and the image uniformity QA check as the results were within acceptable limits. Goldoost *et al.* (2018) stated that the reconstruction algorithm, which calculates the CT number, was working correctly if the CT number test and uniformity were within tolerance. In terms of the current research the water phantoms displayed the highest compliance with both QA checks with the 135 kV, especially the small and medium water phantom. The large and extra-large water phantoms have a lower outcome.

4.4.4. Image Quality Determined by Phantom Size

Examining phantom size in relation to image quality derived during CT scans has demonstrated that the small water phantom had the highest rate of compliance to all the QA checks (Table 4.4). The compliance decreased as the phantom size increased. Therefore, if phantom size is correlated to patient size, the small and average adult

patients will produce an improved image quality, while patients with a large effective diameter, that is overweight patients, for both the 120 kV and 135 kV settings will have a decrease in image quality. The 80 kV setting produced low results in terms of tolerance as stated previously.

In the effort to determine which kV should be used it was observed that the 135 kV, had a 60% within tolerance rate across the different phantom sizes. The 120 kV had a 42% in tolerance rate and 80 kV a 16% in CT QA checks. Linking to Chapter 2, the dose measured was significantly lower for the 120 kV than for the 135 kV CT scans. Karmazyn *et al.* (2013) stated that an increase in noise level was exponential to the increase in phantom size and the decrease of tube current (kV). In the current research a similar trend was noted as the image noise increased as the phantom size increased.

The FOV is currently the only modification made by the radiation therapist on the CT for the pelvic localisation scans at the oncology department. Miyata *et al.*; (2020) stated that higher spatial resolution and clearer images are often associated with S FOV. In the current research, the S FOV had a 17% (two out of twelve checks) within tolerance rate for all the water phantoms of different sizes. The large water phantom also had a grainy appearance (refer to Figure 4.7). However, in the current research the 80 kV can only be scanned with a S FOV setting. The M FOV had a 50% (twelve out of twenty-four checks) within tolerance rate for the 135 kV and 120 kV and the small water phantom had 100% compliance with the three QA checks. The medium water phantom was compliant for CT number and uniformity however, it was out of tolerance for the 135 kV and 120 kV image noise QA check. The large water phantom was only within tolerance with the uniformity of the image. Miyata *et al.* (2020) stated that the S FOV increased noise and the image quality deteriorated. In the current research the L FOV had a 42% (ten out of twenty-four checks) overall compliance for both the 135 kV and 120 kV for the water phantoms of different sizes. The large phantom was within tolerance for the CT number and uniformity with the 135 kV and the CT number for the 120 kV, indicating a large FOV is more acceptable for a large patient. The LL FOV attained a 63% (fifteen out of twenty-four) compliance to the QA checks for both 120 kV and 135 kV. Lastly, the XL FOV attained a compliance of 50% (twelve out of twenty-four checks), indicating that, in this specific study, the LL FOV produced the highest image quality for all the phantoms of different sizes.

From these results it can be concluded that small water phantom, which measures 25 cm in diameter, and thus represents an adolescent, as stated by Karmazyn *et al.* (2013), result in a higher rate of tolerance for the QA checks. Therefore, a valid

deduction to be made is that in adolescent patients, a more improved image quality is obtained, compared to that which is found with patients of increased size. In addition, as patients increase in size, their image quality declines. The 135 kV had an improved image quality for the TOS phantom in comparison to the 120 kV. Patients should therefore be scanned with either 120 kV or 135 kV, as shown by both the water phantoms of different sizes and the TOS phantom.

Image quality is a very important aspect of radiation oncology in terms of delineation for treatment planning. The more photons that reach the detector, which inadvertently implies a higher dose, the more the electronic noise becomes insignificant. However, at low doses the image quality degrades and electronic noise becomes dominant (Schawkat *et al.*; 2017). Obese patients can also affect the image quality by increasing electronic noise, which in turn could then constrain the ability to reduce patient dose (Schawkat *et al.*, 2017). From the phantoms scanned it was noted that the large and extra-large water phantoms produced had a very low rate of QA checks within tolerance rate, therefore a decline in image quality is noted. A means of improving image quality, while reducing dose measured, is the application of different CT techniques. One such technique is the use of iterative reconstruction algorithms, which while producing the CT image can help to reduce the electronic noise that occurs. This method produces higher resolution scans and enables lower radiation dose (Boas & Fleischmann, 2012). Further research into improving image quality while reducing radiation dose should be investigated.

4.4.5. Limitations of the Research

- The limitation of available phantoms in an oncology department, Free State, due to resource constraints.

4.4.6. Recommendations

- It is recommended that the image quality for the CT scans for pelvic localisation be further explored with modification to CT settings (FOV and kV) to determine an acceptable balance between CT dose and image quality.
- A protocol based on the image quality necessary for IMRT planning purposes to be established to ensure the most suitable image quality and dose is provided.
- A standard operating procedure should be developed for the radiation therapist to utilise during pelvic CT localisation scans. This should contain appropriate

FOV and kV selections based on the requirements for patients of different sizes whilst maintaining optimal image quality.

4.5. Conclusion

The water phantoms of different sizes were scanned at different FOV and kV combinations to determine the effect it had on the image quality of the CT scans. The small and medium water phantoms produced the highest number of QA checks being within tolerance. The extra-large phantom produced only three QA checks out of twenty-four possible checks, which were deemed within tolerance, indicating a lower quality image. Therefore, the researcher concluded that as patient dimensions increase the image quality decreases.

The highest image quality was found when the 135 kV setting was utilised, for the water phantoms of different sizes as well as for the TOS phantom. However, from the previous chapter it was determined that based on dose, the 120 kV should be used rather than the 135 kV (refer to: 2.4.). In the cases where superior image quality was necessary for radiation planning purposes, the results indicated that 135 kV should be utilised as the image quality is improved. This should however be examined further to determine if the improved image quality justifies the increase in radiation dose or if indeed the image quality can be optimised with the 120 kV setting.

The results from the effect of the different FOV on the image quality indicate that the S FOV produced very few within tolerance QA checks and considering the limiting imaging view as determined in Chapter 2, it should be excluded from being used for pelvic CT localisation scans. The use of the M FOV proved to be advantageous in the use of CT dose (Chapter 2) and for image quality in terms of children or small adults. The L FOV had an improvement in the QA tolerance checks for the large phantom and one check (135 kV) for the extra-large water phantom. The LL FOV was acceptable for the small, medium and large water phantoms as well as being in tolerance for the CT number and uniformity for the extra-large water phantom. The XL FOV was acceptable for the small, medium and large phantoms. Therefore, the small and medium water phantoms can be scanned with almost any FOV, while the large water phantom was best scanned with a L, LL or XL FOV. The extra-large phantom produced generally very few within tolerant results.

This research has identified which FOV and kV settings are needed to improve image quality when performing CT localisation scans for patients of different sizes. The QA

checks performed were within tolerance range, which rendered this outcome viable for implementation.

In Chapter 5 the image quality based on the CT scans for pelvic CT localisation of patients scanned at the oncology department will be discussed.

References

American Association of Physicists in Medicine. 1977. *Phantoms For Performance Evaluation and Quality Assurance of CT Scanners*. AAPM Report 1.

American Association of Physicists in Medicine. 2011. Size-Specific Dose Estimates (SSDE) in Paediatric and Adult Body CT Examinations. *AAPM Report No. 204*. Report of AAPM Task Group 204, developed in collaboration with the International Commission on Radiation Units and Measurements (ICRU) and the Image Gently Campaign of the Alliance for Radiation Safety in Paediatric Imaging. Date of Access: 25 November 2017. <https://www.aapm.org/pubs/reports/RPT_204.pdf>

Bellon, M.R., Siddiqui, M.S., Ryu, S. and Chetty, I.J. 2014. The Effect of Longitudinal CT Resolution and Pixel Size (FOV) on Target Delineation and Treatment Planning in Stereotactic Radiosurgery. *Journal of Radiosurgery and SBRT (Stereotactic Body Radiation Therapy)*. Vol 3: 149-163.

Boas, F.E. and Fleischmann, D. 2012. CT Artifacts: Causes and Reduction Techniques. *Imaging in Medicine Journal* (4: 229-240).

Choi, H.R., Kim, R.E., Heo, C.W., Kim, C.W., Yoo, M.S. and Lee, Y. 2018. Optimization of Dose and Image Quality Using Self-produced Phantoms of Various Diameters in paediatric abdominal CT scan. *International Journal for Light and Electron Optics.* 168: 54-60.

Cropp, RJ., Seslija, P., Tso, D. and Thakur, Y. 2013. Scanner and kVp dependence of measured CT numbers in ACR CT phantom. *Journal of Applied Clinical Medical Physics*. Vol 14 No 6.

Goldoost, G., Ebrahimpoor, M., Behrouzkia, Z.., Aghdam, R.Z. and Refahi, S. 2018. Assessment of Water CT number, Field Uniformity and Noise in Diagnostic Computed Tomography Scanners in Urmia Metropolis, Iran. *International Journal of Advanced Biotechnology and Research*. 9(1): 165-170.

International Atomic Energy Agency (IAEA). 2012. *Quality Assurance Program for Computed Tomography: Diagnostic and Therapy Application.* IAEA Human Health Series No 19. IAEA. Date of Access: 4 May 2020. https://www-pub.iaea.org/MTCD/Publications/PDF/Pub1557_web.pdf

Karmazyn, B., Liang, Y., Klahr, P. and Jennings, S.G. 2013. Effect of Tube Voltage on CT Noise Levels in Different Phantom Sizes. *American Journal of Roentgenology*. 200: 1001-1005.

Kayugawa, A., Noto, Y., Taga, T., Fukaya, T., Tasaki, K., Fujioka, T., Ohkubo, M., Niigata, J.P. and Minatoku, J.P. 2015. Characterization of the model-based iterative reconstruction algorithm: Confirmation of coexistence of dose reduction and spatial resolution improvement. *Congress ECR 2015*.

Kodlulovich, S., Jakubiak, R.R., Miquelin,C.A. and Oliveira, L. 2008. Initial Results of the Quality Control in 11 Computed Tomography Scanners at Curitiba. International Congress of the International Radiation Protection Association (IRPA): Strengthening Radiation Protection Worldwide; Buenos Aires (Argentina); 19-24 Oct 2008. Date of Access: 20 September 2020 <https://inis.iaea.org/collection/NCLCollectionStore/_Public/41/006/41006618.pdf >

Mansour, Z., Mokhtar, A., Sarhan, A., Ahmed, M.T. and El-Diasty, T. 2016. Quality Control of CT Images Using American College of Radiology (ACR) Phantom. *The Egyptian Journal of Radiology and Nuclear Medicine*. 47: 1665-1671.

McCollough, C.H., Bruesewitz, M.R., McNitt-Gray, M.F., Bush, K., Ruckdeschel, T., Payne, J.T., Brink, J.A. and Zeman, R.K. 2004. The Phantom Portion of the American College of Radiology ACR Computed Tomography (CT) Accreditation Program: Practical Tips, Artifact Examples and Pitfalls to Avoid. *Medical Physics*. Sept 31 (9): 2423-42.

Miyata, T., Yangawa, M., Hata, A., Hondai, O., Yoshida, Y., Kikuchi N., Tusbamoto, M., Tsukagoshi S., Uranishi, A. and Tomiyama, N. 2020. Influence of field of view size on image quality: ultra-high-resolution CT vs. conventional high-resolution CT. *European Radiology*. 30: 3324-3333.

Njiki, C.D., Manyol, J.E.M.N., Yigbedeck, Y.E., Abou'ou, D.W., Yimele, B.C. and Sabouang, J.F. 2018. Assessment of Image Quality Parameters for Computed Tomography in the City of Yaounde. *Open Journal of Radiology*. (8: 37 – 44).

Roa, A.M.A., Anderson, H.K. and Martinsen, A.C.T. 2015. CT Image Quality Over Time: Comparison of Image Quality for Six Different CT Scanners over a Six-year Period. *Journal of Applied Clinical Medical Physics.*2014. (16 (2): 340 – 365).

Schawkat, K., Fischer, R.M., Heverhagen, J.T. and Christe, A. 2017. The Impact of Intergrated Circuit Detector Technology in Routine MDCT: Improved Image Quality Compared to Conventional Detector Design for Constant SSDE. *Hellenic Journal of Radiology*. 2 (1): 23 – 29.

Skryzński, W., Zielińska-Dabroska, S., Wachowicz, M., Ślusarczyk-Kacprzyki, W., Kukołowicza, P.F. and Bulski, W. 2010. Computed Tomography as a Source of Electron Density Information for Radiation Treatment Planning. *Strahlentherapie und Onkologie* 186: 327-33.

Chapter 5

Image Quality Derived from Patient Computed Tomography Localisation Scans

5.1. Introduction

The research that was elucidated in Chapter 4 focussed on the image quality derived from water phantoms of different sizes and the effect of different FOV and kV settings. The following chapter is centred on the third objective of the research, which entails a study of the image quality by determining the contrast-to-noise ratio (CNR) of the CT images. The CNR determines the difference in contrast between two structures in a CT scan. In addition to the CNR, the image noise in terms of standard deviation of the CT number (SD) and signal-to-noise ratio (SNR) will be scrutinised.

In order to determine the image quality for the patients receiving pelvic CT localisation scans, the following concepts will be revisited (i) Body Mass Index (BMI), (ii) CT number (HU) and (iii) image noise. An additional concept that necessities investigation is (iii) image contrast.

5.1.1. CT and Imaging in Radiation Therapy

Clinical studies have demonstrated that the introduction of CT in radiation therapy treatment planning has a 30% to 80% benefit due to the increased target accuracy when compared to conventional simulation methods. The overall five-year survival rate of patients has increased by an estimated 3.5%, with small treatment volumes having the greatest impact (Barrett *et al.*, 2009).

The goal in radiation therapy is to ensure that a high dose is received by the tumour volume while ensuring the normal surrounding tissue receives the lowest dose possible (Chen *et al.*, 2017). Therefore, optimal image quality is essential for accurate delineation of the tumour volume (Chen *et al.*, 2017). In addition, the time required to delineate structures can be reduced by improved image quality (Chen *et al.*, 2017). The accuracy of delineating is related to both the image contrast and the level of noise in the CT image (Chen *et al.*, 2017). Furthermore, Chen *et al.* (2017) discovered a 10% reduction in the time taken to delineate the prostate, bladder and rectum contours. However, since a three to five times increase in CT dose was found with the improved image quality, this has to be weighed up against the risks associated with the additional dose to the patient - especially for paediatric patients (Chen *et al.*, 2017). With the

advent of intensity modulated radiation therapy (IMRT) in 1995, the demand for improved image quality with radiation therapy has increased. Due to the necessity for accurate delineation of the target volume and surrounding organs that are at risk, it is essential to avoid marginal tumour recurrence (Sanderud *et al.*, 2016). Image quality may therefore justify a higher dose when using radiation therapy for specialised planning techniques (Chen *et al.*, 2017).

The CT images are obtained by the attenuation coefficient determined by the different tissue types that are crossed. A level of grey is given to each pixel that makes up the final image. These levels correspond to the attenuation coefficients and are attributed by means of the Hounsfield scale (Greffer *et al.*; 2013). The CT image allows - with the use of calibration curves – for conversion of the CT number or Hounsfield Unit (HU) to relative electron densities, which provides the image with density data for radiation dose (Barret *et al.*, 2009). On a CT display each voxel is allocated a HU that ranges from -1000 to 1000 (Halperin *et al.*, 2013). A megavolt beam's main course of tissue interaction is Compton scatter. Compton scatter can be defined as the predominant interaction with soft tissue from x-ray and gamma-ray photons (Bushberg *et al.*, 2002). Compton scatter is directly proportional to electron density (Barret *et al.*, 2009). Thus, when it comes to inhomogeneous tissue such as lung tissue, the CT provides ideal density for dose correction (Barret *et al.*, 2009). As there is an intimate relationship between electron density and CT number, a more accurate volumetric target and normal anatomy can be provided during treatment planning (Sanderud *et al.*, 2016).

For tissue composition, visual assessment is less accurate than the analysis of the HU (Halperin *et al.*, 2013). Image quality in radiation is therefore not always a visual assessment. However, an assessment of the HU and the relationship of one HU to another can clarify image quality.

An increase in image noise degrades the image quality and the visibility of the edge of organs for delineation. The contrast–to-noise ratio (CNR) is defined as the ratio of the contrast, between two regions of interest (ROI). Thus, the difference of the mean CT numbers and the average of standard deviation of CT numbers in the ROIs (Chen *et al.*, 2017). An increase in image dose increases CNR, which in turn improves the ability to distinguish between boundaries of lower contrast objects (Chen *et al.*, 2017). The visual inspection of a CT image is seen as the contrast between two organs. Therefore, the lower the image's contrast, the more difficult it is to visualise the organ edge for delineation. The edge of the organs is more visible with a sharp change in contrast (Chen *et al.*, 2017). Image contrast in radiography is the difference in the grey scale of

the image, between different anatomical structures in the image (Bushberg *et al.*, 2002). Contrast resolution is in essence the ability to see low contrast objects. As the noise level decreases, the contrast in the image is more easily visualised. Thus, the ability to observe low contrast objects is related to the noise in the image (Bushberg *et al.*, 2002).

In the previous chapter, the phantom image quality was discussed and the concept of the CT number as well as the image noise were explored. Following hereafter is a further examination of these topics in relation to the patient CT scans and the concept of image contrast.

5.1.2. BMI

The BMI was discussed in depth in Chapter 3 (refer to: 3.1.4). Obesity is a growing concern in western society (Forbrig *et al*., 2019). BMI is a common diagnostic tool that is applied to characterise the obese population and is an indirect measurement of body fat (Qurashi *et al.*, 2017). However, BMI cannot characterise the distribution of body fat and it is also unable to distinguish between lean mass and fat mass (Qurashi *et al.*, 2017). Imaging an obese patient can be challenging, an 80 cm gantry diameter helps as does a higher tube voltage and a large FOV. The image quality in terms of image noise increases as body size increases (Karmazyn *et al*., 2013). Researchers Pauchard *et al.* (2017), state that, in comparison to slim patients, the more obese patients' small interstitial fat planes allow for an improved delineation of visceral organs and muscles. The BMI is calculated using equation 3.1 (refer to: 3.1.4) and the BMI index table (refer to: Table 3.1)

5.1.3. CT Number

The CT number also known as the Hounsfield Unit (HU), as described in Chapter 4 (refer to: 4.1.2.1.) is used in radiation treatment planning to establish the relationship between the relative electron density and the HU in order to compute the dose distribution (IAEA, 2012). The HU for the bladder, prostate and rectum was obtained from the scans in research conducted by Chen *et al.* (2017). On a CT display each voxel is allocated a HU that ranges from -1000 to 1000 (Halperin *et al.*, 2013). For tissue composition visual assessment has proven to be less accurate than the analysis of the HU (Halperin *et al.*, 2013).

5.1.4. Image Noise

The concept of image noise was first introduced in Chapter 4 (refer to: 4.1.2.2.). The production of x-rays and their interaction with matter produce image noise. In a uniform material this can be shown by examining at pixel level in terms of the CT number, which fluctuates around a mean value (IAEA: 2012). Noise, in terms of a CT image can also be defined as the standard deviation (SD) of the HU within a ROI (IAEA, 2012). In order to objectively determine the image quality, researchers Pauchard *et al.* (2017) measured the HU and SD of the psoas muscle. The objective image noise was determined by the SD.

By measuring the ability to distinguish between two organs in the body is a method with which to measure the image quality. An increase in image noise degrades the image and the visibility of the edge. Therefore, the lower the image contrast, the harder it is to visualise the edge for delineation. The edge of the organs are more visible with a sharp change in the contrast (Chen *et al.*, 2017). The number of photons which reach the detector determines the electronic noise. When a CT examination has a low dose, the electronic noise dominates and degrades the image quality (Schawkat *et al.*, 2017).

5.1.5. Image Contrast

Contrast in radiography is the difference in the image grey scale, between different anatomical structures (Bushberg *et al.*, 2002). Contrast resolution is in essence the ability to see low contrast objects. As the noise level decreases, the contrast in the image is more easily visualised. Thus, the ability to observe low contrast objects is related to the noise in the image (Bushberg *et al.*, 2002). An increase in image dose increases contrast-to-noise ratio (CNR), which in turn improves the ability to distinguish between boundaries of lower contrast objects (Chen *et al.*, 2017). Therefore, the image quality is assessed on the ability to delineate correctly for the planning CT.

The CNR is defined as the ratio of the contrast which, by using two regions of interest (ROI), is the difference of the mean CT numbers and the average of standard deviation of CT numbers in the ROIs (Chen *et al.*, 2017). The CNR equation is:

$$CNR = 2\frac{\left|\overline{\mu}_S - \overline{\mu}_B\right|}{\sigma_S + \sigma_B}$$

Equation 5.5: Contrast-to-noise ratio.

The equation is populated with the CT numbers for the signal ($\overline{\mu}_S$) and background ($\overline{\mu}_B$) ROIs as well as the standard deviation for the signal (σ_S) and background (σ_B) ROIs, respectively (Chen *et al.*, 2017). An additional step is to add dose to the equation, thereby deriving a dose weighted contrast-to-noise ratio dose (CNRD), which is calculated as follows:

$$CNRD = \frac{CNR}{\sqrt{D}}$$

Equation 5.6: Contrast-to-noise ratio and dose.

The equation utilises the square root of the dose (D) calculated for the patient. The maximum CNDR represents the minimum dose value for a given image quality level. Therefore, a maximum CNDR occurs when optimisation is achieved (Chen *et al.*, 2017).

Research by Qurashi *et al.* (2017) examined obese patients and their abdominal CT protocol. The researchers examined the quality of the CT image and the dose for these patients. In order to measure the image quality, the noise standard deviation (SD) and mean CT number, also known as the Hounsfield Unit (HU), in a 2 cm^2 ROI was measured on three consecutive CT slices (Qurashi *et al.*, 2017). These slices measured the inferior segment of the right hepatic lobe and the inferior vena cava, as well as the psoas muscle and peripheral subcutaneous fat (Qurashi *et al.*, 2017) as illustrated in Figure 5.1.

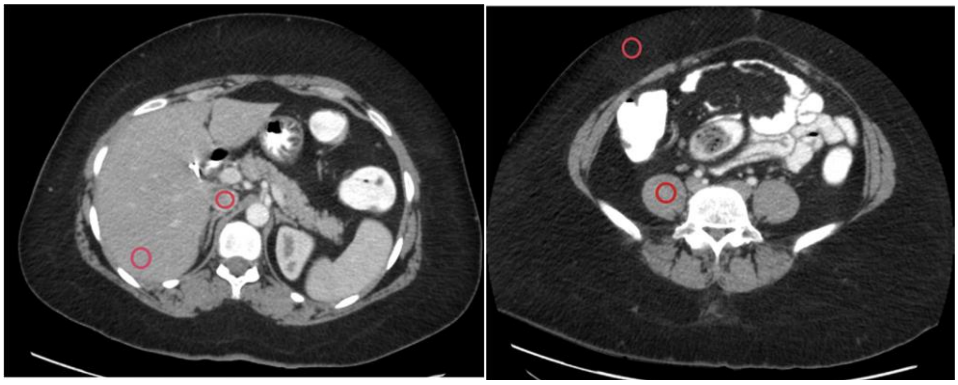

Figure 5.1: On the left is the ROI for the liver and inferior vena cava and on the right the ROI for the psoas muscle and subcutaneous fat.

Courtesy of Qurashi *et al.*, 2017.

To determine and potentially improve image quality, the CNR and signal-to-noise ratio (SNR) were calculated as relevant to muscle as well as for the liver (Qurashi *et al.*, 2017).

The equation used for SNR:

$$SNR = SD/HU$$

Equation 5.7: Signal-to-noise ratio.

CNR calculation is:

$$CNR = \frac{HU_L - HU_M}{\sqrt{SD_L^2 + SD_M^2}}$$

Equation 5.8: Contrast-to-noise Ratio.

Where HU is the average CT number for the liver and psoas muscle, HU_L is the liver and HU_M is the psoas muscle, SD is the standard deviation for liver (SD_L) and psoas muscle (SD_M), respectively.

In the research of Forbrig *et al.* (2019) the CNR for the liver and spleen was determined to be significantly higher in the lower BMI group in comparison to the higher BMI group. The researchers determined that this was due to lower image noise in the lower BMI group as a result of the superficial anatomical location of the liver and spleen (Forbrig *et al.*; 2019).

Research conducted by Bhosale *et al.* (2015) in which they examined the effect of different reconstruction algorithms on image quality in their quantitative assessment of the image quality examined the CNR, SNR and SD of the images.

5.1.6. Viewing CT Images

Images on a CT are created by the production of x-rays and the way in which the different tissue types absorb them. A higher HU number is created by the greater x-ray attenuated in denser tissues. Water HU is always set to 0, while air is set at -1000 HU (Xue *et al.*, 2012). To view the image the HU is converted to grayscale values ranging between 0 and 255, allowing different features of the image to be visualised (Xue *et al.*, 2012). To view the CT image created on a monitor, window and level controls are used

(Bushberg *et al.*, 2011). The window width and window level are called windowing (Xue *et al.*, 2012). This enables CT images to display tissue with the specified HU values of window width and level (Xue *et al.*, 2012). The window width determines the number of different HU values that will be displayed. The HUs that are of lower value are displayed as black and all HU higher than values are displayed as white (Xue *et al.*, 2012). The windows level determines the midpoint of the HU value (Bushberg *et al.*, 2011). The lower the windows level the brighter the image (Stepwards, 2020).

The following section describes the methodology used in the research study to determine the image quality derived from patient CT localisation scans.

5.2. Methodology

This prospective research methodology involved quantitative data collection of the image quality produced by the patient's CT localisation scan of the pelvis. CNR related equations were utilised to obtain image quality derived from pelvic localisation CT scans. In addition, the researcher divided the patients into three different BMI categories (underweight, normal weight and overweight) and evaluated the influence of their BMI on the image quality.

Chapter 3 contains information on the study sample (refer to: 3.2.1.), the inclusion and exclusion factors (refer to; 3.2.1.1.) pertaining to the patients participating in the current research. It also contains the ethical consideration (refer to: 3.2.3.), as the same patients' data were utilised for the image quality.

5.2.1. Research Tools

Listed below are the research tools that were used during the research process. The research tools 1 to 3 are a duplicate of those listed in Chapter 3.

1. A TSX-201A (Toshiba Aquilion © Large Bore (LB)) CT scanner, as used and discussed in Chapter 5 for the phantom studies.
2. The pelvic examination setting was chosen on the CT console and used for the research. The only variable that is was modified during the time of the patients' scans is the FOV.
3. A digital scale was used to determine the patient's weight. A height measurement was affixed to the wall to measure the patient's height. Both measurements were used to calculate the patient's BMI.

4. The CT monitor was used to examine the image quality of the images. The window width and level (refer to: 5.1.6) that was chosen was set to 400 and 40; this is a soft tissue window viewing option.
5. Equations utilised in the research were as follow:
    - BMI: The consenting patient's Body Mass Index (BMI) was calculated from their weight and height measurements measured at the time of the CT scan. The BMI determines if the patient is considered as being overweight, ideal weight or underweight as illustrated in Table 3.1. The Microsoft Excel spreadsheet was utilised to calculate the patient BMI.

      The BMI was measured using the following formula (refer to: 3.1.4):

      $$BMI = \frac{Weight}{(Height)^2}$$ (Equation 3.1)

    - The image quality for each patient's scan was determined by using the SNR and CNR for the CT images. The equation used for SNR is:

      $$SNR = SD/HU$$ (Equation 5.3)

    - CNR is calculated using the SD and HU of a specific organ, in the case of the research the HU for liver and the psoas muscle were used. The calculation formula is:

      $$CNR = \frac{HU_L - HU_M}{\sqrt{SD_L^2 + SD_M^2}}$$ (Equation 5.4)

    - CNRD is calculated using the results from the CNR and dividing it by the square root of the dose calculated for the patient. The calculation formula is:

      $$CNRD = \frac{CNR}{\sqrt{D}}$$ (Equation 5.2)

5.2.2. The Research Process

The research process to determine image quality for the patients scanned for CT localisation scans is demonstrated in Figure 5.2.

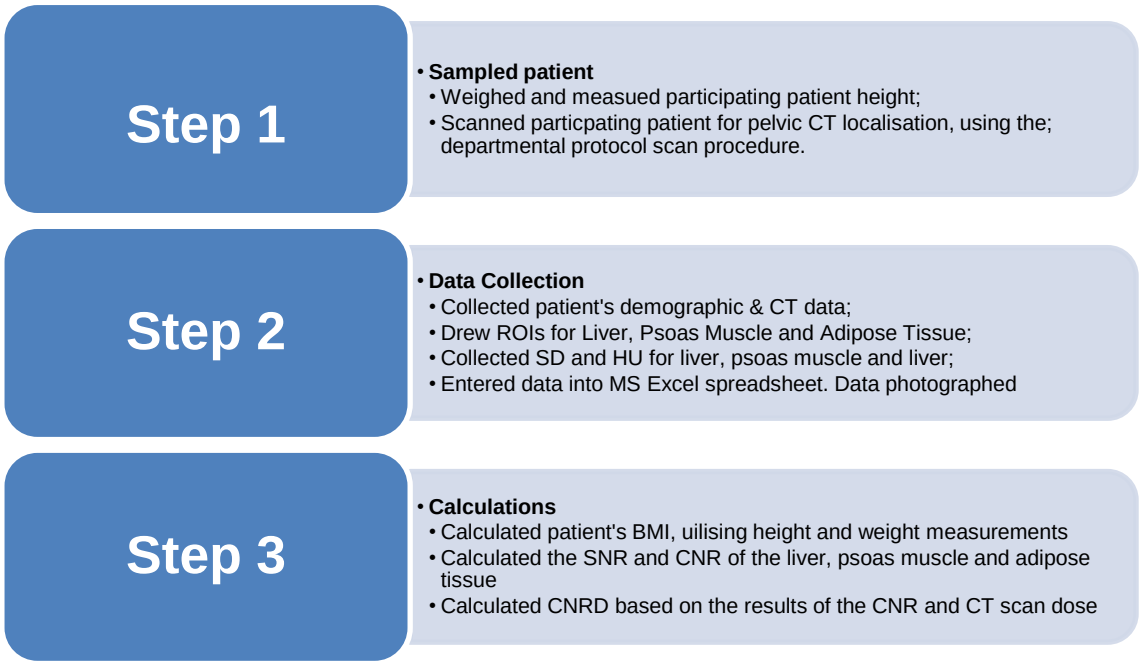

Figure 5.2: Research process image quality for patients CT scans.

5.2.2.1. Step 1: Patient Sample

In Chapter 3 the dose derived from pelvic CT localisation scans was determined. The patients who participated in the research are the same patients of which image data was examined (refer to: 3.2.2.1).

In brief, the consenting patients were weighed using a digital scale. The consenting patient's height was measured against a wall with height measurements affixed; which was setup by the researcher at the CT scanner. The patient's BMI was calculated. The patient was scanned on the Toshiba Aquilion © Large Bore CT scanner. The pelvic protocol of the oncology department was utilised in the production of the images used for the research. Therefore, the patients were scanned from T10 to below the symphysis pubis and the pelvic CT localisation scan option was selected on the CT console.

5.2.2.2. Step 2: Data Collection

The researcher examined the CT image quality on a weekly basis. The patient's demographic and scan data were a duplicate of that obtained in Chapter 3 (refer to: 3.2.2). The image quality of the consenting patients was examined from the CT localisation scan on the scanner's monitor, with the windows width and level set to soft tissue viewing (400 and 40).

The image quality data was captured onto the MS Excel spreadsheet (Table 5.1).

Table 5.1: Image quality analysis data captured for adipose, liver and psoas muscle tissue.

	Image Quality Analysis						
ID	***HU Adipose***	***HU Liver***	***HU Psoas Muscle***	***SD Adipose***	***SD Liver***	***SD Psoas Muscle***	Circle size

ID= The identifying number given to the CT scan by the researcher, this number links the data to the dose for the same patient. HU = The mean HU measured by the ROI, the HU is measured for the adipose tissue, liver tissue and psoas muscle of the patient. The SD is the mean SD measured by the ROI, the same tissue type is measured here. The circle size indicates in cm the diameter of the ROI used for the HU and SD measurements.

The CT image information was photographed and captured onto a MS Excel spreadsheet. The CT scanner that was utilised in the research was bi-monthly cleared of scan data, therefore the photographs were taken in order to verify all the data and to ensure that no incorrect data were entered. The researcher added a ROI for the adipose tissue, liver tissue and psoas muscle. The liver ROI was added to the lower lobe of the liver. The adipose and psoas muscle ROIs were placed where possible on the same CT image slice however, as patient anatomy differs, in some cases this could not be done. The researcher then scrolled the CT image to a more suitable placement for the ROI. The ROI size ranged between 1 cm and 2 cm in diameter; the size determined by the anatomy of the patient. The ROI size was indicated as demonstrated in Table 5.1. The HU and SD for the different tissue types were added to the MS Excel spreadsheet, refer to Table 5.1.

Calculations were then required to determine the SNR, CNR and the CNRD.

5.2.2.3. Step 3: Calculations

The patients were divided into BMI categories, those being underweight, normal weight and overweight. The BMI was determined in Chapter 3 (refer to: 3.2.2.3) for each patient that participated in the research.

Once the CT data were entered onto the MS Excel spreadsheet (Table 5.1)., the calculations of the SNR, CNR and CNRD were performed automatically by the MS Excel programme to be reflected on the spreadsheet. Table 5.2 demonstrates the calculations that were derived.

Table 5.2: Patient image quality calculations.

Patient Image Quality – Calculations				
CNR	***SNR Adipose***	***SNR Liver***	***SNR Psoas***	***CNRD***

CNR=The contrast-to-noise ratio between the liver and psoas muscle. The SNR= The signal to noise ratio as determined for the adipose, liver and psoas muscle. The CNRD = The CNR and dose calculation.

The calculations of the CNR, between the liver and psoas muscle and the SNR for the three different tissue types were performed automatically. Lastly the CNRD was calculated.

The ethical considerations (refer to: 3.2.3), the validity and reliability (refer to: 3.2.4) and the statistical information (refer to: 3.2.5) remained exactly as were stated in Chapter 3, due to the identical patients' data utilised for both dose and image quality determinations. The image quality data were analysed by the statistician and evaluated with the same test (Shapiro-Wilk) as described in Chapter 3 (refer to: 3.2.5).

The methodology employed to determine the image quality has been described in this section. The following section describes the resultant data obtained from the research.

5.3. Results

The image quality was determined for patients who received pelvic CT localisation scans at the oncology department. The research examined the image quality in terms of the tissue types, i.e. adipose, liver and psoas muscle. The image quality was quantified by examining the SNR, SD and CNR. The image quality was examined for each BMI category. The data pertaining to all image quality results are found in TA 5.1, presented on the accompanying CD.

5.3.1. Tissue Types

There were three tissue types that were examined by the researcher, the adipose tissue the liver tissue and the psoas muscle. The objective of this specific phase of the research was to determine the image quality by determining the contrast-to-noise ratio (CNR) of the CT images.

An examination of the HU associated with these tissue types will now be described, with a look at the different BMI patient categories and how they affect the results. Detailed results are available in Table A.5.1 on the accompanying CD, which demonstrates all the image quality data that were obtained from all the patients. The data include the measured HU for the adipose tissue, liver and psoas muscles.

Table 5.3 examines all BMI categories tissue types (adipose, liver and psoas muscles) median, IQR, minimum and maximum values.

Table 5.3: BMI categories median, IQR, minimum and maximum values for HU of various tissue types.

Variable	Median	IQR		Min	Max
		Lower Quartile	Upper Quartile		
OW HU Adipose	-124.95	-129.40	-120.40	-138.40	-107.40
OW HU Liver	45.10	39.90	48.60	17.50	55.50
OW HU Psoas Muscle	31.55	26.10	34.10	14.70	40.10
NW HU Adipose	-118.10	-124.20	-110.50	-135.00	-28.30
NW HU Liver	47.70	44.00	53.70	25.10	84.40
NW HU Psoas Muscle	31.30	27.70	36.80	14.70	66.00
UW HU Adipose	-81.20	-104.60	-41.40	-128.90	47.70
UW HU Liver	51.90	42.30	72.30	32.50	82.30
UW-HU Psoas Muscle	38.10	31.50	56.80	20.70	72.20

OW=Overweight BMI category, NW= Normal Weight BMI category, UW=Underweight BMI category. Min=Minimum and Max=Maximum. The overweight BMI patient category variable is illustrated in orange, the normal weight in green and the underweight is illustrated in yellow. The adipose is indicated by a lilac row and the psoas muscle in grey. The interquartile range (IQR) is from the lower and upper quartile.

From Table 5.3 it can be determined that the adipose tissue HU median value is lowest for the overweight BMI category patients. The highest median value was observed in the underweight BMI category patient. Using the IQR values, Figure 5.3 demonstrates the adipose tissue HU from lowest to highest value for the different BMI categories.

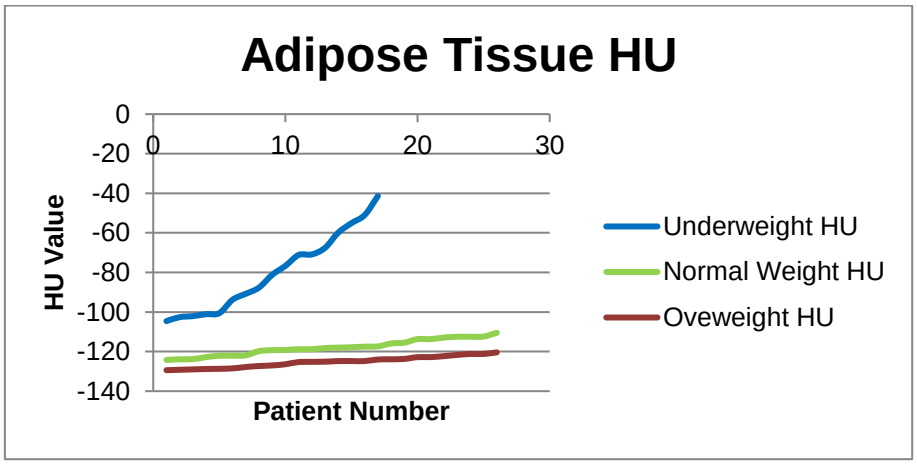

Figure 5.3: IQR Adipose tissue for different BMI categories.

The median, minimum and maximum value of the adipose tissue follow the trend of the psoas muscle (the only exception is the minimum value for the psoas muscle), which is the same for the overweight and normal BMI patient category.

The liver tissue has a median value that is lowest for the overweight BMI patient category and is highest for the underweight BMI category. However, the normal BMI patient category has a 3 HU higher maximum value in comparison to the underweight BMI category. Figure 5.4 illustrates the IQR value from lowest to highest for the liver tissue and for each BMI patient category.

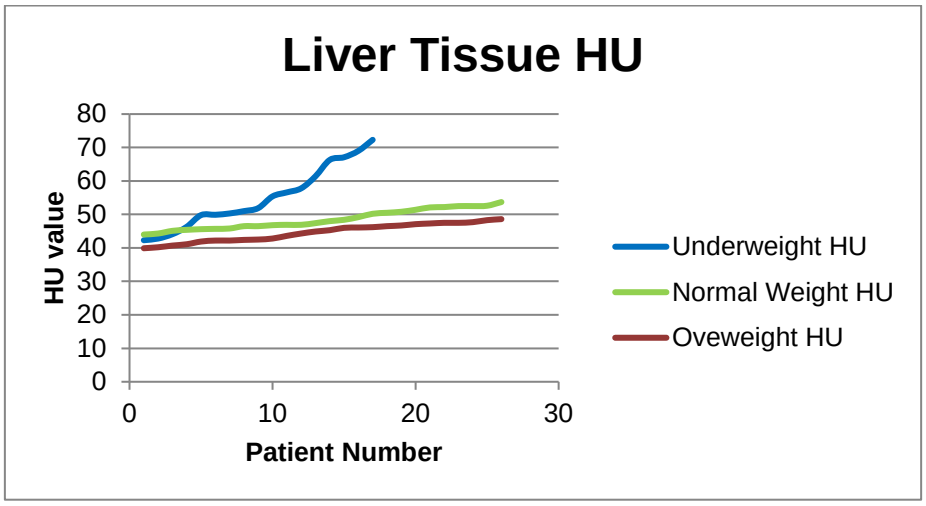

Figure 5.4: IQR liver tissue for different BMI categories.

The difference between the minimum and maximum HU values for the liver tissue and psoas muscle for the overweight, normal and underweight BMI categories were as follow: Overweight - 38 HU and 25 HU, Normal - 59 HU and 51 HU and Underweight - 50 HU and 52 HU, respectively. The IQR for the psoas muscle tissue is demonstrated in Figure 5.5 for the different BMI categories.

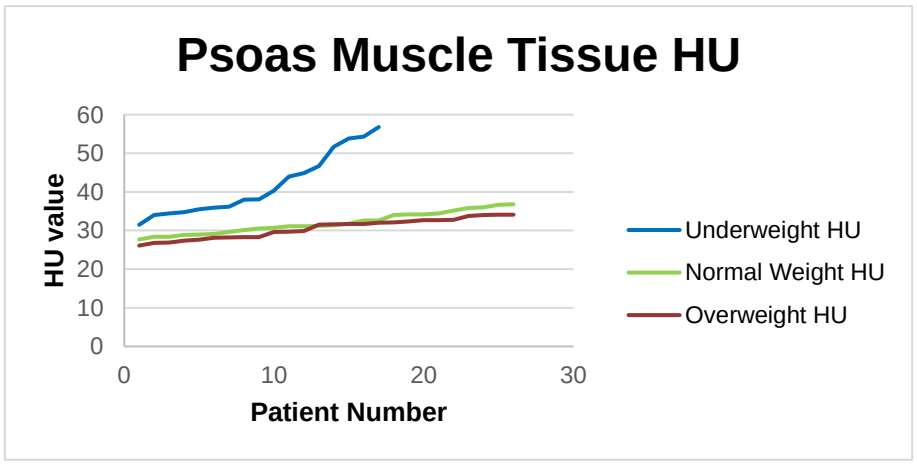

Figure 5.5: IQR psoas muscle tissue for different BMI categories.

The adipose tissue however, had a much higher difference in HU for the overweight, normal and underweight BMI categories: Overweight - 31 HU, Normal - 107 HU and

Underweight - 177 HU, respectively. The overweight BMI category thus always had the smallest difference in HU in comparison to the normal and underweight BMI categories. This trend follows through to the interquartile range (IQR). As already stated in Chapter 3 (refer to 3.4.1), the IQR discards a quarter of the data, from both ends of the distribution in the case of outliers. The IQR indicates that the difference between the upper and lower range for the overweight, normal and underweight BMI categories are 9 HU, 14 HU and 63 HU, respectively for the adipose tissue. For the liver tissue the results are 9 HU, 10 HU and 30 HU, while for the psoas muscle the results are 8 HU, 9 HU and 25 HU for the overweight, normal and underweight BMI categories, respectively.

5.3.2. Image Quality

Image quality is based on the ability to distinguish between two different tissue types, as stated in the introduction (refer to: 5.1). This is linked to the image contrast. The image quality can be determined in terms of image noise, which is indicated by the SD of the different HU for the different tissue types (refer to: 5.1.4). The SNR is the division between the signal produced and the noise produced. The CNR is the calculated contrast between the liver and psoas muscle (refer to: 5.1.5).

5.3.2.1. Image Noise

The image noise is indicated by the **SD** of the mean HU. In Table 5.4 the SD for the different BMI category patients with the three different tissue types is demonstrated.

Table 5.4: SD for the different BMI weight categories and different tissue types.

Variable	Median	Lower Quartile	Upper Quartile	Mean	Min	Max
OW-SD Adipose	10.10	7.90	12.20	10.14	5.20	16.80
OW-SD Liver	9.85	7.50	13.00	10.30	5.70	16.20
OW-SD Psoas Muscle	14.25	13.10	16.00	14.68	8.20	23.40
NW-SD Adipose	9.40	7.40	11.20	9.95	4.90	25.60
NW-SD Liver	6.20	5.30	7.70	6.86	3.20	18.50
NW-SD Psoas Muscle	10.10	7.40	12.30	10.54	4.50	25.50
UW_SD Adipose	11.00	9.10	14.20	12.13	4.90	27.30
UW-SD Liver	5.30	4.70	6.70	5.94	3.10	15.70
UW-SD Psoas Muscle	6.80	5.70	11.30	9.08	4.00	36.50

OW=Overweight BMI category, NW= Normal Weight BMI category, UW=Underweight BMI category. Min=Minimum and Max=Maximum. The overweight BMI patient category variable is represented by orange, the normal weight green and the underweight is reflected in yellow. The interquartile range is from the lower and upper quartile.

The adipose tissue SD median value is highest for the underweight patients (11.0), followed by the overweight and then the normal weight BMI category patients have the lowest SD (9.4) for the adipose tissue. The liver tissue has the lowest SD for the underweight BMI category patients in terms of median value (5.3). The highest median value is seen for the overweight patients' SD liver tissue (10). The psoas muscle tissue type is highest for the overweigh BMI category patients and lowest for the underweight BMI category patients.

The overweight BMI category patients had a SD median value for the adipose tissue, liver tissue and psoas muscle at 10, 10 and 14, respectively. The normal BMI category patients had a median value of 9, 6 and 10 for the adipose, liver and psoas muscle tissue variables. Lastly, the underweight BMI category patients had a median value of 11, 5 and 7 for the adipose, liver and psoas muscle tissue. The SD indicates the amount of noise in an image. The noise levels for all three BMI categories are relatively similar.

The **SNR** for the different BMI weight categories is illustrated in Table 5.5.

Table 5.5: SNR for the different BMI weight categories and different tissue types.

Variable	Median	Lower Quartile	Upper Quartile	Mean	Min	Max
OW-SNR Adipose	-12.30	-15.90	-10.33	-13.32	-25.56	-6.93
OW-SNR Liver	4.20	3.33	6.27	4.76	1.62	9.10
OW-SNR Psoas	2.04	1.66	2.56	2.14	0.78	4.22
NW-SNR Adipose	-12.32	-16.50	-9.95	-12.96	-27.53	-1.81
NW-SNR Liver	7.74	6.18	9.23	7.96	1.99	15.07
NW-SNR Psoas	2.99	2.25	4.96	3.88	0.82	9.30
UW-SNR Adipose	-6.45	-9.94	-3.29	-6.51	-18.41	9.73
UW-SNR Liver	10.27	8.14	12.59	10.25	3.68	17.51
UW-SNR Psoas	6.73	3.67	8.35	6.26	0.57	12.03

OW=Overweight BMI category, NW= Normal Weight BMI category, UW=Underweight BMI category. Min=Minimum and Max=Maximum. The overweight BMI patient category variable is represented in orange, the normal weight in green and the underweight in yellow. The interquartile range is from the lower and upper quartile.

The statistical data for the SNR determined that neither the overweight BMI category patients' data were skewed, nor was the psoas muscle for the normal BMI patients. The underweight BMI category patients' data were skewed. The overweight median values were as follows: for the adipose tissue - 12, liver tissue -4 and psoas muscle -2 respectively. The normal BMI category patient had the following median value: adipose - 12, liver tissue - 8 and psoas muscle – 3, respectively. The underweight BMI category patients had a median value of 7, 10 and 7 for the adipose, liver and psoas muscle, respectively. All three BMI categories indicated an improved SNR for the adipose tissue and the lowest SNR for the psoas muscle.

The **CNR** and **CNRD** for the different BMI categories are demonstrated in Table 5.6.

Table 5. 6: CNR and CNRD for all three category BMI patients.

Variable	Median	Lower Quartile	Upper Quartile	Mean	Min	Max
OW-CNR	0.78	0.57	1.14	0.84	-0.65	2.35
OW-CNRD	0.08	0.05	0.10	0.08	-0.06	0.21
NW-CNR	1.30	0.79	1.75	1.30	-0.95	3.74
NW-CNRD	0.10	0.06	0.14	0.11	-0.08	0.31
UW-CNR	1.18	0.50	1.69	1.17	-0.75	2.61
UW-CNRD	0.09	0.04	0.13	0.09	-0.06	0.20

OW=Overweight BMI category, NW= Normal Weight BMI category, UW=Underweight BMI category. Min=Minimum and Max=Maximum. The overweight BMI patient category variable is presented in orange, the normal weight in green and the underweight in yellow. The interquartile range is from the lower and upper quartile.

From Table 5.6 it can be gleaned that CNR mean values of 0.8, 1.3 and 1.2 were found for the overweight, normal and underweight BMI category patients, respectively. These results demonstrated that the normal BMI category patients had the best image quality followed by the underweight BMI patient category. Figure 5.6 illustrates the CNR for patients in relation to their BMI. As seen in Figure 5.6 a few CNR are found in the negative. The negative CNR values occur when the HU for the liver is lower than the HU for the psoas muscle. A discussion of variations of the HU is further explored in section 5.4.1.

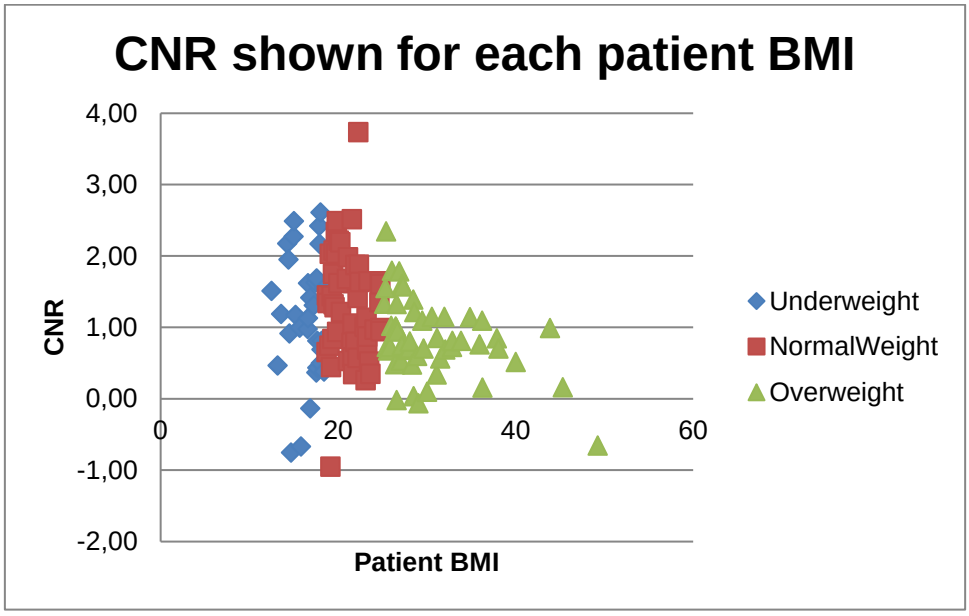

Figure 5.6: CNR per patient BMI.

The mean CNRD values were 0.08, 0.11 and 0.09 for the overweight, normal and underweight BMI categories, respectively. The maximum CNRD value was observed

for the normal BMI patient category. As stated by Chen *et al.* (2017) (refer to: 5.1.4) the maximum CNRD in terms of image quality represents the minimum dose value and occurs when optimisation is achieved. Therefore, the normal patient BMI category has the most optimal image quality.

The following section examines the image quality based on BMI patient category. The image quality will be determined based on the HU for the three tissue types as well as the image noise and contrast calculated.

5.3.2.2. Overweight patient Image quality.

The overweight BMI category patient's HU for the different tissue types is illustrated in Figure 5.7. The median HU for the different tissue types were as follows: for adipose tissue it was -125 HU, for liver it was 45.1 HU and finally for the psoas muscle it was 31.6 HU.

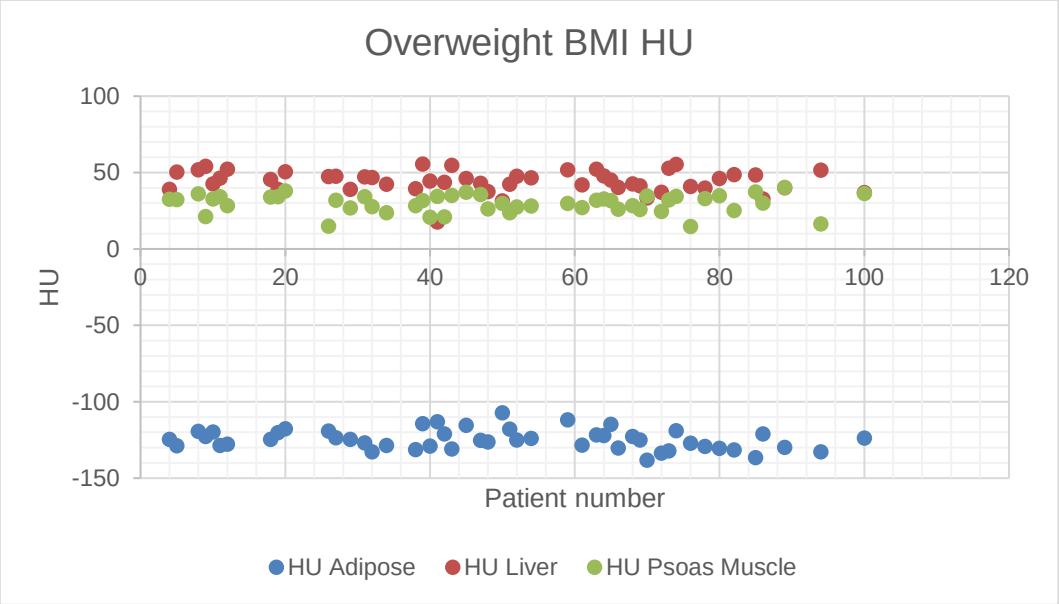

Figure 5.7: Overweight BMI HU for adipose, liver and psoas muscle.

5.3.2.2.1. Overweight BMI Adipose Tissue HU

The lowest HU was -107,4 and the highest HU was -138,4. Statistically, the adipose HU for the overweight patients demonstrated that the data had a normal distribution, with a p-value of 0.8405 in the Shapiro-Wilk test. The standard deviation for the data was 6.6. Looking at Figure 5.7, 5.1 and Figure 5.2, the HU distributions were much

smaller than for the other BMI patients, as demonstrated by the blue dots. The median HU for adipose tissue for overweight patients was -124.7 HU.

5.3.2.2.2. Overweight BMI Liver HU

The lowest HU was 17.5 and the highest HU was 55.5. Statistically the data for the liver HU for overweight patients were skewed as indicated by the Shapiro-Wilk p-value of 0.0105. The median value was 45.1 HU and the IQR was between 39.9 and 48.6. Figure 5.7 demonstrates these values. The Standard deviation was 7.1 (Table 5.4). The data collected was also lower than for the other BMI patients' values.

5.3.2.2.3. Overweight BMI Psoas Muscle HU

The overweight BMI psoas muscle HU presented a skewed data results, as demonstrated by the p-value for the Shapiro-Wilk test, which was 0.0225. The median value was 31.6 and IQR was between 26.1 and 34.1. Figure 5.7 illustrates that the data range was the smallest for the 3 BMI categories; the standard deviation was 5.9.

5.3.2.2.4. Overweight BMI – SD, SNR, CNR and CNRD

The image quality is defined by the SD and SNR in terms of image noise, while the CNR and CNRD relate to the image contrast. Both image noise and image contrast in these terms are quantitative image measurements to determine CT image quality. Figure 5.8 illustrates the overweight BMI patient category images produced from the lower and upper quartile images for the various tissue types respectively.

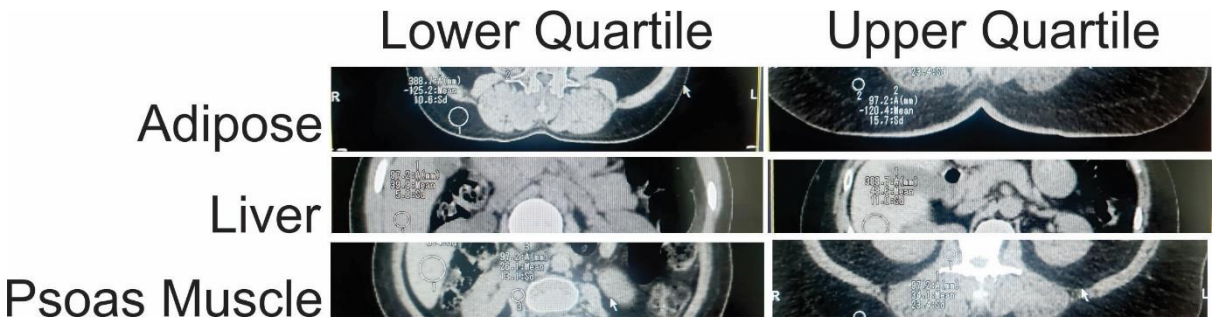

Figure 5.8: Overweight patient upper and lower quartile images for all tissue types.

Table 5.7 presents the SD, SNR and CNR and CNRD values for the overweight BMI category patients.

Table 5.7: Statistical data for overweight BMI category patient.

Variable	SD	Median	Lower Quartile	Upper Quartile	Mean	Min	Max
SD Adipose	2.73	10.10	7.90	12.20	10.14	5.20	16.80
SD Liver	3.16	9.85	7.50	13.00	10.30	5.70	16.20
SD Psoas Muscle	3.05	14.25	13.10	16.00	14.68	8.20	23.40
CNR	0.54	0.78	0.57	1.14	0.84	-0.65	2.35
SNR Adipose	4.11	-12.30	-15.90	-10.33	-13.32	-25.56	-6.93
SNR Liver	1.82	4.20	3.33	6.27	4.76	1.62	9.10
SNR Psoas	0.75	2.04	1.66	2.56	2.14	0.78	4.22
CNRD	0.05	0.08	0.05	0.10	0.08	-0.06	0.21

The **SD** demonstrates how far the values deviated from the HU tissue type that is indicated. The mean for the psoas muscle had the greatest deviation of 14.7 HU, followed by the adipose tissue at 10.1 HU and finally the liver tissue with 10.3 HU.
The **SNR** indicates the signal vs. the noise ratio. The adipose had the greatest mean SNR of 13.3, followed by the at liver 4.8 and lastly the psoas muscle at 2.1. The **CNR** for the overweight patients has a mean value of 0.8. The **CNRD** has a mean value of 0.08.

Figure 5.9 demonstrates the overweight BMI category patients with the lowest and highest SNR for the liver tissue.

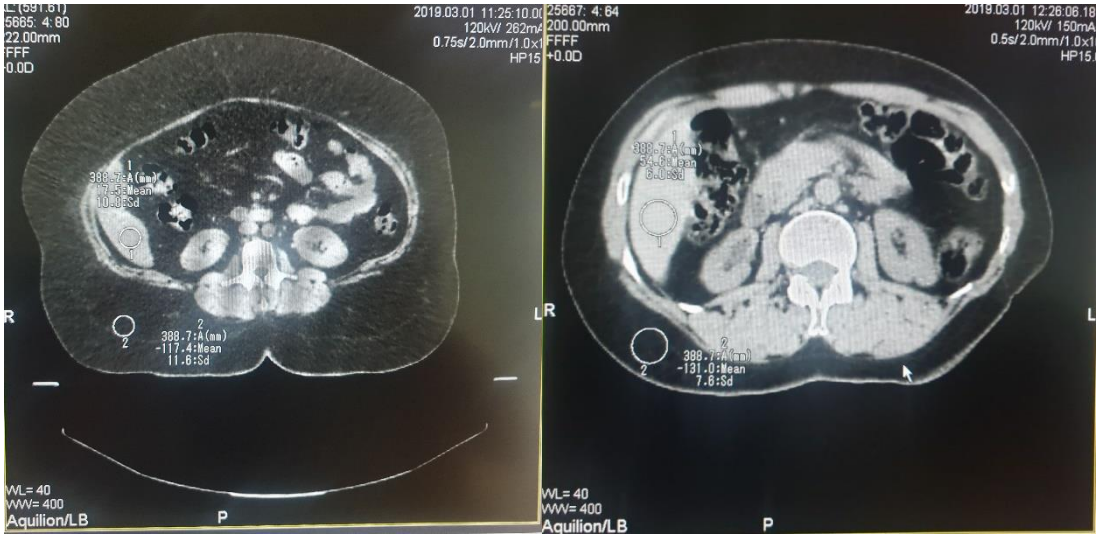

Figure 5.9: Overweight BMI category, lowest and highest SNR.

The lowest SNR value in the overweight BMI category was 1.6, which appears noisier than the highest SNR (9.1), which had a smoother appearance.

In Figure 5.10 the overweight BMI category patients with the lowest CNR of -0.7 and the highest CNR value of 2.4 is indicated.

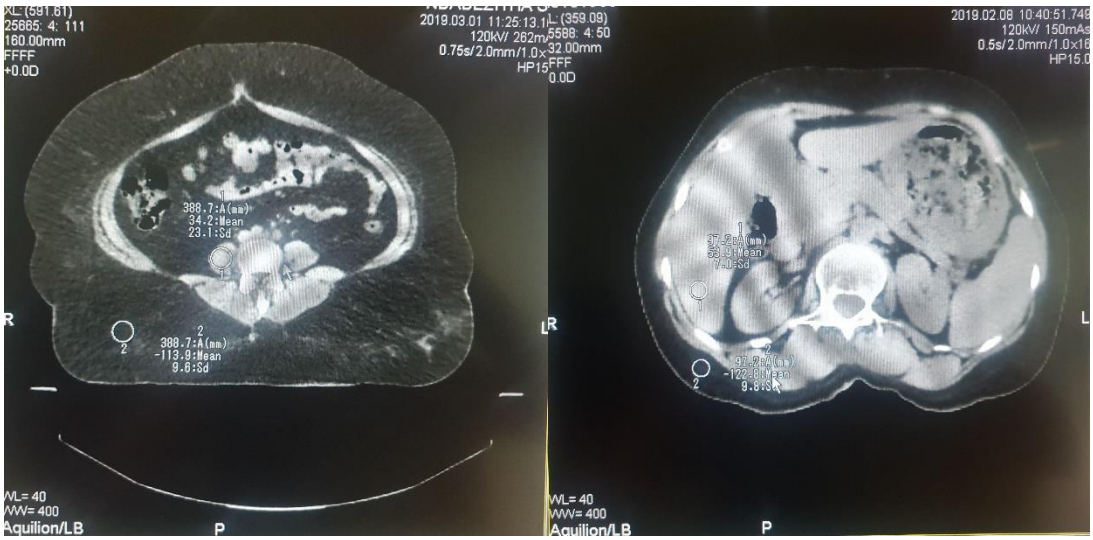

Figure 5.10: Overweight BMI category, lowest and highest CNR values.

From Figure 5.10 it can be seen that the lowest CNR image calculated has a grainer appearance, creating a nosier image, than that of the highest CNR image.

5.3.2.3. Normal Weight Patient Image Quality

The normal patient image HU is illustrated in Figure 5.11.

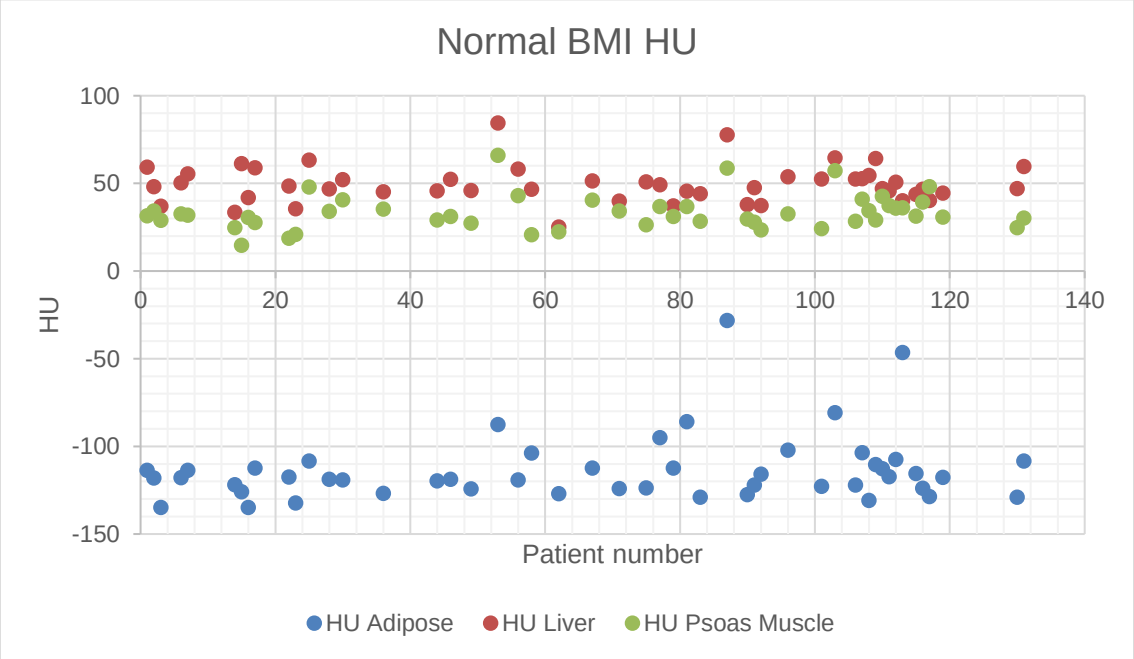

Figure 5.11: Normal BMI HU for adipose, liver and psoas muscles.

The median HU for the different tissue types was as follows, for adipose tissue -118.1 HU, for liver it was 47.7 HU and finally for the psoas muscle it was 31.3 HU. The liver and psoas muscle showed a similar HU to the overweight patient median values. The adipose differed by almost 7 HUs.

5.3.2.3.1. Normal Weight BMI Adipose Tissue HU

The normal BMI category patient adipose tissue HU had a low value of -135 HU and a high value of -28.3 HU. Statistically the data was skewed as seen by the Shapiro-Wilk test with a p-value of 0.0001. The median value was -118.1 HU and the IQR value ranged from -124.20 HU to -110.5 HU. As per Figure 5.11 the blue represents the normal BMI category adipose HU; which appears, to be slightly higher than the overweight BMI as demonstrated in Figure 5.3. Figures 5.7 and Figure 5.11 indicate that the range was greater than seen with the overweight BMI category values. The standard deviation of the data was 19.7, thus greater than that of the overweight BMI category values.

5.3.2.3.2. Normal Weight BMI Liver HU

The normal BMI category patients had a low of 25.1 HU and a high of 84.4 HU for the liver tissue. The HU liver for the normal BMI category patient data is skewed, as demonstrated by the p-value for the Shapiro-Wilk test, which was 0.0262. The median HU value was 47.7 and the IQR was between -124.2 HU and -110.5 HU. Figure 5.7 and Figure 5.11 demonstrate that the data range was slightly higher than that of the overweight BMI patients' data. The standard deviation was 10.5, which is only slightly greater than that of the overweight BMI patients' data.

5.3.2.3.3. Normal Weight BMI Psoas Muscle HU

The psoas muscle HU data for the normal weight BMI category patients were skewed with a p-value for the Shapiro-Wilk test of 0.0025. The median value was 31.1 HU and IQR was between 27.7 HU and 36.8 HU. Therefore, as seen in Figure 5.7 and Figure 5.11, the data range was just above that of the overweight BMI patients' data. The standard deviation was 9.9.

In Figure 5.12 the various tissue types for the normal weight BMI category are illustrated, using the IQR lower quartile image and upper quartile images.

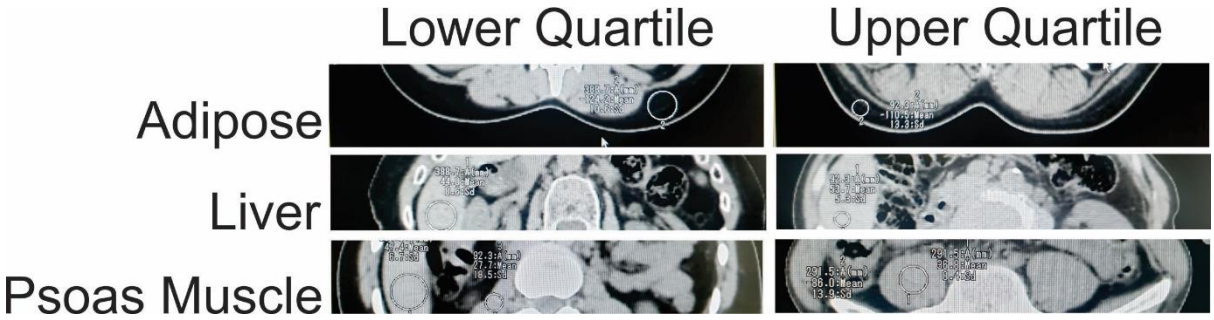

Figure 5.12: Normal weight BMI category patient HU images for all tissue types.

The normal BMI category patient data for the SD, SNR, CNR and CNRD are demonstrated in the next section.

5.3.2.3.4. Normal Weight BMI – SD, SNR, CNR and CNRD

Table 5.8 gives the SD, SNR and CNR and CNRD values for the normal weight BMI category patients.

Table 5.8: Statistical data for Normal weight patient category.

Variable	Shapiro-Wilk p Value	SD	Median	Lower Quartile	Upper Quartile	Mean	Min	Max
SD Adipose	0.0001	3.51	9.40	7.40	11.20	9.95	4.90	25.60
SD Liver	0.0001	2.47	6.20	5.30	7.70	6.86	3.20	18.50
SD Psoas Muscle	0.0003	4.39	10.10	7.40	12.30	10.54	4.50	25.50
CNR	0.2004	0.77	1.30	0.79	1.75	1.30	-0.95	3.74
SNR Adipose	0.2456	5.14	-12.32	-16.50	-9.95	-12.96	-27.53	-1.81
SNR Liver	0.1181	2.90	7.74	6.18	9.23	7.96	1.99	15.07
SNR Psoas	0.0001	2.30	2.99	2.25	4.96	3.88	0.82	9.30
CNRD	0.128	0.06	0.10	0.06	0.14	0.11	-0.08	0.31

The **SD** illustrates how the values deviated from the HU for the tissue type indicated. The mean value for the psoas muscle was the greatest at 4.4, followed by the adipose tissue at 3.5 and finally the liver tissue at 42.5. These values were much lower than found those in the overweight BMI patient category.

The **SNR** represents the signal vs. the noise ratio. The adipose tissue had the greatest mean SNR value of -13 followed by SNR value for the liver tissue of 8 and lastly the SNR value for psoas muscle of 3.9.

The **CNR** for the overweight patients had a mean value of 1.3. The **CNRD** had a mean value of 0.11. The highest CNRD value was found in the normal weight BMI category with a value of 0.3.

In Figure 5.13 the patient with the lowest CNR value of -0.9 and the highest CNR value of 3.7 CNR for the normal weight BMI category is demonstrated.

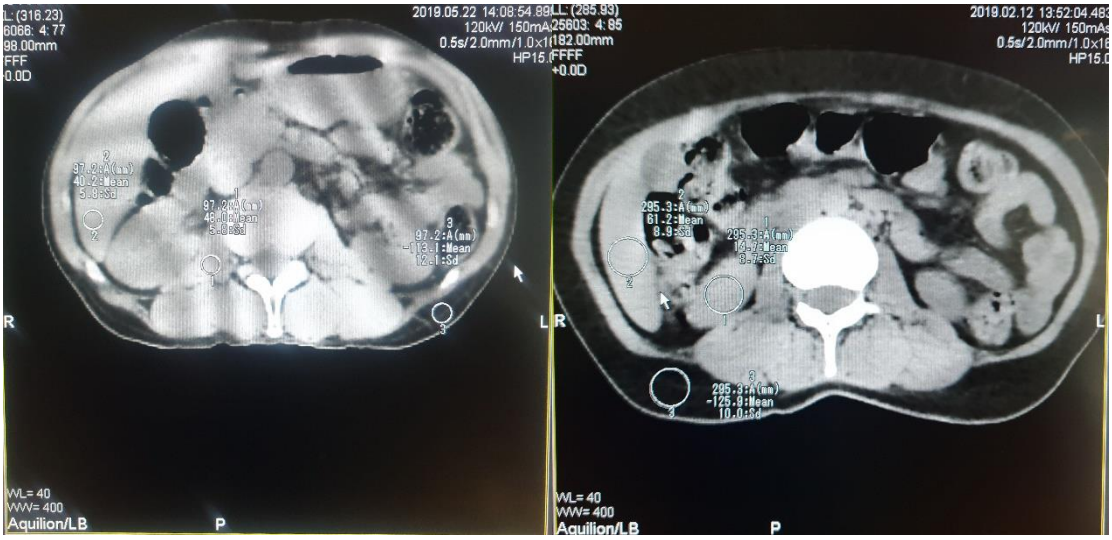

Figure 5.13: Normal weight patient category lowest and highest CNR.

In Figure 5.14 the normal BMI category patients with the lowest and highest SNR for the liver tissue is presented. The lowest SNR value was 2 and the highest SNR value was 15.1, respectively.

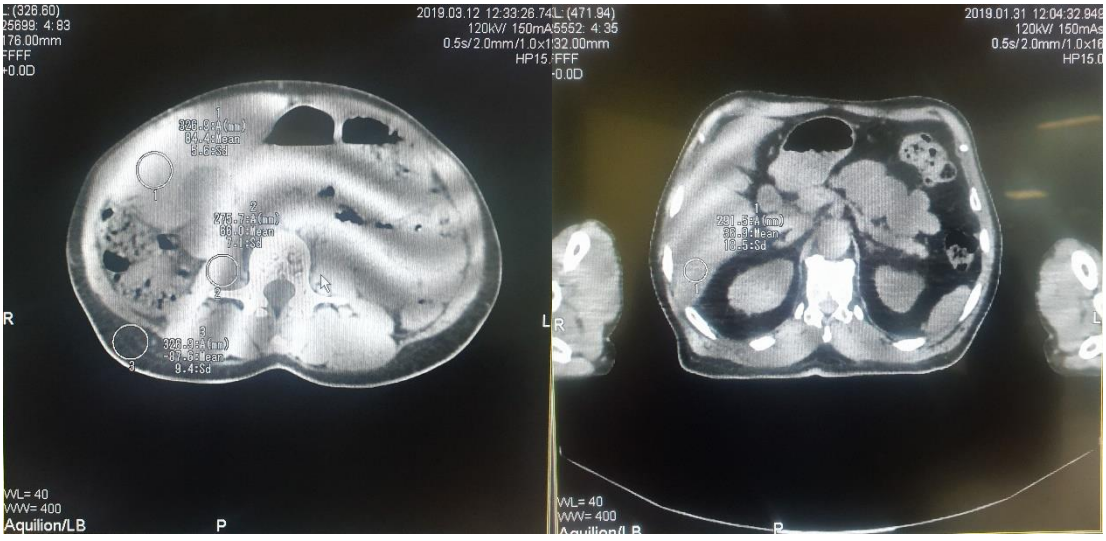

Figure 5.14: Normal weight patient category, lowest and highest SNR liver.

A view of the underweight BMI patient category image quality follows.

5.3.2.4. Underweight Patient Image Quality

The HU for the underweight patient image is illustrated in Figure 5.15.

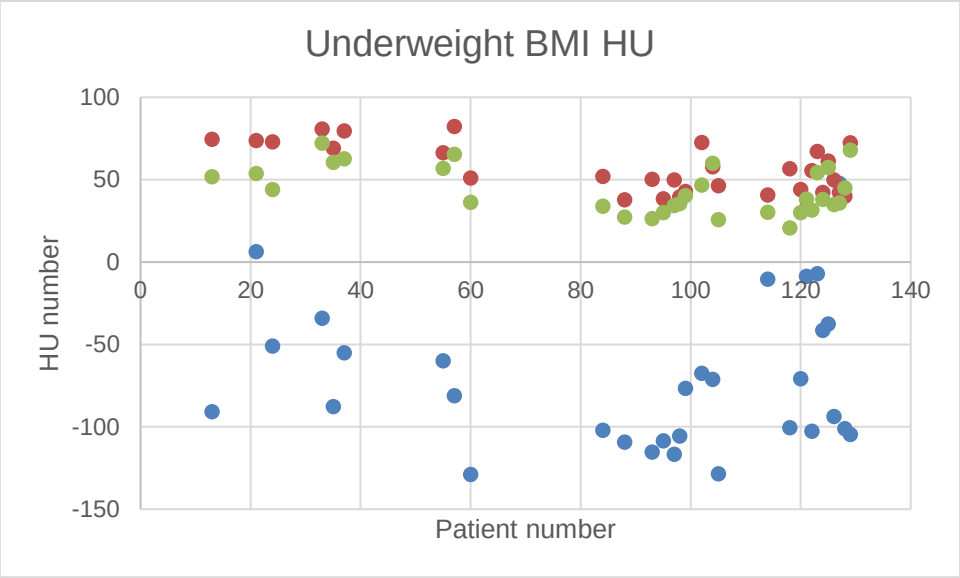

Figure 5.15: Underweight BMI HU for adipose, liver and psoas muscle.

The median HU for the different tissue types were as follows: for adipose tissue it was -81.2 HU, for liver it was 51.9 HU and finally for the psoas muscle it was 38.1 HU. The adipose tissue differed by 37 HUs from the normal weight BMI category patients' median. The liver and psoas muscle were less than 10 HUs apart.

5.3.2.4.1. Underweight BMI Adipose Tissue HU

The underweight BMI category patient adipose tissue HU ranged from a minimum of -128.9 HU and a maximum of 47.7 HU. Two patients' HUs were in the positive numbers, while the rest of the patients remained in the negative. The Shapiro-Wilk test proved the data to be skewed with a p-value of 0.264. The median HU was -81.2 and the IQR was between -104.6 and -41.4 HU for adipose tissue. Figure 5.7, Figure 5.11 and Figure 5.15 demonstrate the greater difference in HU values, with a standard deviation of 43.5.

5.3.2.4.2. Underweight BMI Liver HU

The underweight 32.5 HU was the lowest and 82.3 was the highest HU. The statistical p-value for the Shapiro-Wilk test was 0.457 and therefore the results were deemed to be skewed. The median value was 51.9 HU and the IQR was between 42.3 and 72.3.

The standard deviation was 14.9. Figure 5.7, Figure 5.11 and Figure 5.15 demonstrated that the range was greatest for the underweight BMI category patients.

5.3.2.4.3. Underweight BMI Psoas Muscle HU

The HU for the psoas muscle for the underweight patient data had a normal distribution as demonstrated by the Shapiro-Wilk p-value of 0.0895. The standard deviation was 14.2 and the mean value was 43.3. In respect of the other BMI category weight values, the median value was 38.1 HU and the IQR was between 31.5 HU and 56.8 HU. Figure 5.11 illustrates the HU data for the different tissue types to have a larger range, as can be seen by the standard deviation (14.2). The HU is also slightly higher than the previous two BMI categories' data.

5.3.2.4.4. Underweight BMI – SD, SNR, CNR and CNRD

In Figure 5.16 the underweight BMI category patient HU for all the tissue types is demonstrated by means of the IQR in the lower quartile and upper quartile CT images.

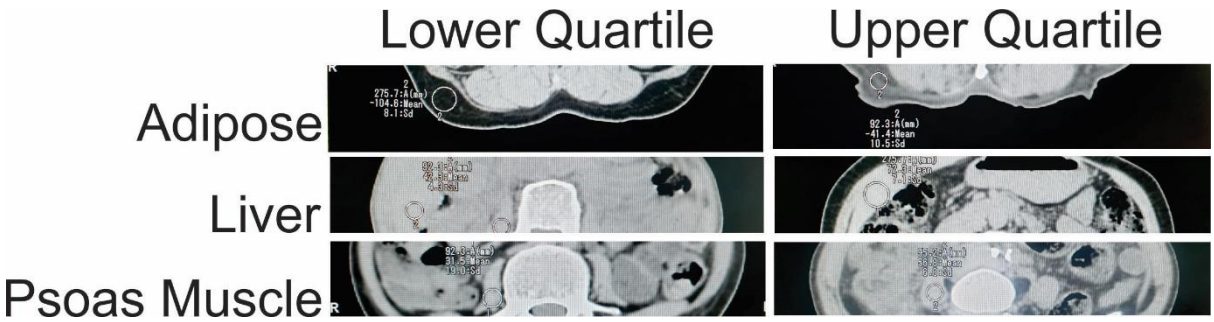

Figure 5.16: Underweight patient HU images for all tissue types.

Table 5.9 provides the SD, SNR and CNR and CNRD values for the underweight BMI category patients.

Table 5.9: Statistical data for underweight patient category.

Variable	Shapiro-Wilk p Value	SD	Median	Lower Quartile	Upper Quartile	Mean	Min	Max
SD Adipose	0.0096	4.58	11.00	9.10	14.20	12.13	4.90	27.30
SD Liver	0.0001	2.31	5.30	4.70	6.70	5.94	3.10	15.70
SD Psoas Muscle	0.0001	6.34	6.80	5.70	11.30	9.08	4.00	36.50
CNR	0.5629	0.86	1.18	0.50	1.69	1.17	-0.75	2.61
SNR Adipose	0.2722	5.51	-6.45	-9.94	-3.29	-6.51	-18.41	9.73
SNR Liver	0.9219	3.32	10.27	8.14	12.59	10.25	3.68	17.51
SNR Psoas	0.3382	3.08	6.73	3.67	8.35	6.26	0.57	12.03
CNRD	0.639	0.07	0.09	0.04	0.13	0.09	-0.06	0.20

The **SD** reveals how far the values deviate from the HU that is indicated. The mean value for the psoas muscle was the greatest at 6.3, followed by the adipose tissue at 4.6 and finally the liver tissue at 2.3. These values followed the same trend as were observed in the overweight and normal weight BMI category patients. However, the value was higher than either of the other two categories.

The **SNR** indicates the signal vs. the noise ratio. The adipose tissue had the greatest mean SNR value of -6.5, followed by the liver tissue with a value of 10.5 and finally, the psoas muscle with a value of 6.3. The greatest SNR for adipose tissue was seen in the overweight category, followed closely by the normal weight category patients. The best SNR for the liver was observed in the underweight patient category, followed by the normal weight patients' category. The SNR value was greatest for the psoas muscle in the underweight BMI category patients. The **CNR** for the overweight patients had a mean value of 1.2. The CNR was thus highest for the normal weight patient category followed by the underweight and lastly by the overweight category.

The **CNRD** has a mean value of 0.09. The CNRD followed the same order from high to low as observed for the CNR. The CNRD highest value was 0.2, while the overweight BMI category CNRD highest value was 0.21, thus a slight improvement over the underweight BMI category patients.

In Figure 5.17 the underweight BMI category patients with the lowest and highest SNR for the liver tissue is illustrated.

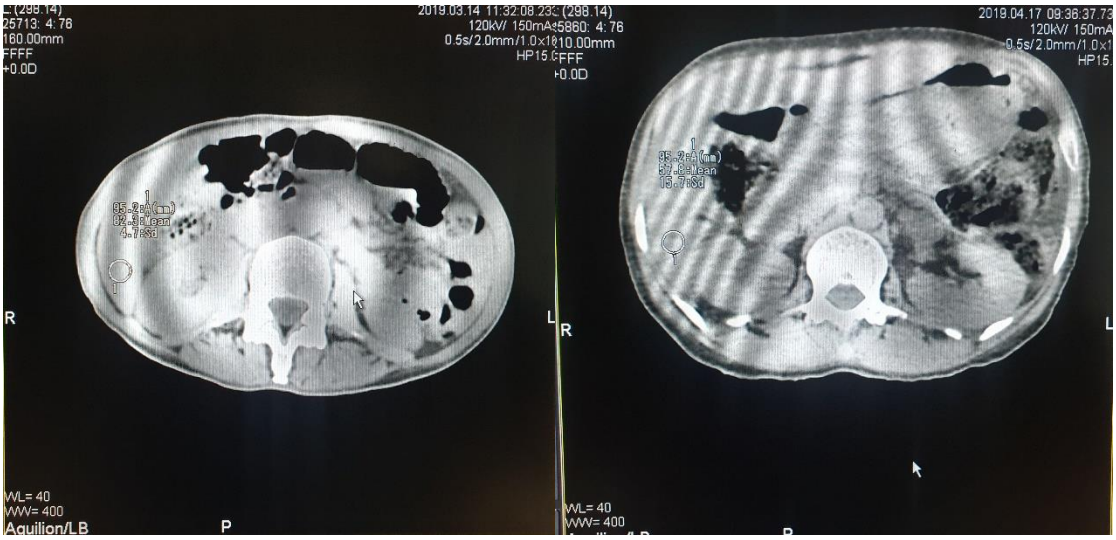

Figure 5.17: Underweight patient category, lowest and highest SNR for the liver tissue.

The lowest SNR value of 3.7 and the highest SNR value of 17.5 were observed. Both images appear to have had an almost grey appearance.

In Figure 5.18 the underweight BMI category patient with the lowest CNR value of -0.8 and the highest CNR value of 2.6 is exhibited.

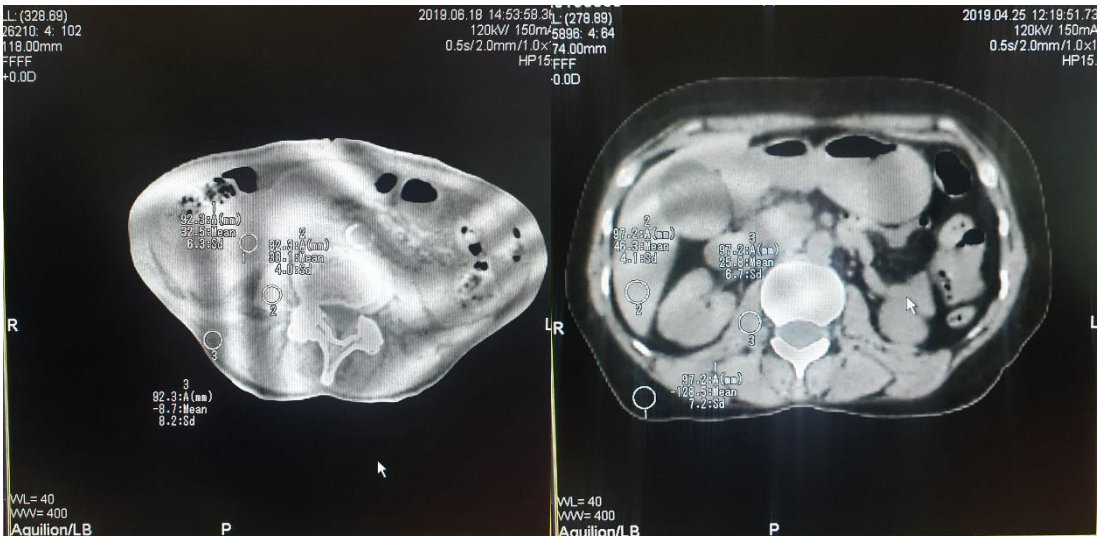

Figure 5.18: Underweight BMI category patients' lowest and highest CNR.

The lowest CNR image appeared to show less distinction between the different organs, when compared to its highest CNR counterpart.

A discussion of the results that were presented in this section, will now follow.

5.4. Discussion

This research examined the image quality of the patients' CT localisation scan by determining the CNR of the CT images. Factors that affect the image quality of the CT localisation scans of the pelvis, such as the patient's BMI, of which the research population was divided into overweight, normal weight and underweight BMI categories. Other aspects of image quality such as the HU for three tissue types (i.e. adipose tissue, liver tissue and psoas muscle) were examined as well as the SD and SNR for those tissue types. The CNRD, which is the CNR and dose, will also be discussed in this section.

5.4.1. HU and Tissue Types

The CT number, which is also known as the HU as previously stated, is used in the radiation oncology planning to determine the effect the radiation treatment will have on the tissue type it encounters. This is done by converting the HU into its relative electron density, thereby being able to compute the dose distribution (refer to 5.1.2). The medical physicists at any oncology department, with the assistance of an electron density CT phantom, perform dosimetric calculations to ensure accurate representation of the electron densities for differential dose distribution of various materials (IAEA, 2012). This, being the CT number of multiple material tests for radiation therapy use of the CT. If the electron density is inaccurate, it can ultimately lead to the incorrect treatment of an oncology patient (IAEA, 2012). The accuracy is ±20 HU, which is deemed to be within tolerance (IAEA: 2012). At the oncology department the electron density CT phantom utilised is the Gamex RMI 465, which includes a liver and adipose tissue type CT number check. The results for the Gamex RMI 465, averaged over a period of three years as -92 HU for adipose tissue and 85 HU for liver (as determined for 2017 to 2019 statistics at the oncology department). The adipose, liver and psoas muscle HU as determined by this research will now be discussed.

During this specific research, the adipose tissue, liver tissue and psoas muscle HU were measured for each patient scan. The median values were lowest for the overweight BMI patient category in terms of all three tissue types (adipose= -125 HU; liver= 45.1 HU and psoas muscle= 31.6 HU). The highest median value for the three tissue types was found in the underweight BMI patient category (adipose= -81.2 HU; liver= 51.9 HU and psoas muscle= 38.1 HU). The overweight category patients had the smallest difference between the HU for each of the tissue types. Halperin *et al.* (2013) state that the analysis of the HU is more accurate than the visual assessment of tissue.

Thus, the HU for a tissue type can be a valuable diagnostic tool for medical doctors. The median HUs for the patients in this current research are not within 20 HU from the Gamex RMI 465 phantom data, however a reason for the variation of the HU in a patient can be determined by other factors. A detailed, examination of the different tissue type HUs will be presented.

Adipose tissue can be divided into subcutaneous adipose tissue and visceral adipose tissue. In this research the subcutaneous adipose tissue was measured. Researchers Rosenquist *at al.* (2013) reported that higher BMI levels (for both genders) correlate with lower CT attenuation of both types of adipose tissue. In the current research this trend is also noted as the adipose had the lowest HU for the minimum (-138.4 HU) and maximum (-107.4 HU) and thus the median (-125 HU) values for the overweight BMI patient category. These values increased as the BMI category decreased, i.e. the normal and underweight BMI categories, as demonstrated in Figure 5.3. The overweight and normal BMI values followed a similar trend, with the normal BMI just above but almost parallel to the overweight BMI adipose HU (Figure 5.3). However, the underweight BMI data spiked as the data ranges from -104.6 to -41.4 HU. In Figure 5.16 this difference is visually noted. For the underweight BMI category, the upper quartile presented a grey contrast to the adipose tissue, but this is not observed in the normal weight BMI category (Figure 5.12) or overweight BMI category patients' (Figure 5.8) BMI quartile images. Researchers Rosenquist *et al.* (2013) state that a CT HU range of -195 to -45 is typically associated with adipose tissue. In the current research, utilising the Rosenquist *et al.*' range, five patients measured out of this HU range in the underweight BMI category. In the normal weight BMI patient category one patient was out of the range and for the overweight BMI patient category all patients where within the range. Lower HU values, demonstrated by small animal studies, are associated with higher levels of lipid content in adipose tissue (Rosenquist *et al*., 2013). These radiological findings in a small paediatric population were assessed clinically (Rosenquist *et al.*, 2013). Therefore, the patients with lower HU for the adipose tissue could have higher levels of lipid content, which could indicate the difference in results noted.

The HU for the ***liver*** can have significant impact on the health of a patient. Research conducted by Wells *et al.* (2016) on the incidental finding of non-alcoholic fatty liver disease, determined that liver attenuation that was at least 10 HUs less than that measured of the spleen or less than 40 HU of absolute liver attenuation can be used as criteria in diagnostic CT scans. For a non-contrast CT, the sensitivity ranged from 43%

to 95% and this increased to 93% when more than 33% of the liver was involved. However, in the current research study the spleen was not examined and therefore no correlation between the spleen and a fatty liver could be determined. The HU for the liver was lowest median value (45.1 HU) for the overweight BMI patient category and increased as the BMI category increased. In Figure 5.4 the trend is the same as seen for the adipose tissue. From Table 5.3 it can be determined that the lower and upper quartile for the liver HU for the overweight BMI patient category, as well as the normal weight BMI patient category, differed by no more than 10 HUs. However, the underweight BMI patient category differed (42 HU to 72 HU) by 30 HU. Research conducted by Zeb *et al.* (2012) stated that liver HU less than 40 HU have proven in studies to reliably represent more than 30% liver fat content. If this criterion is added to the current research, then for the underweight BMI category 16% (five out of thirty-one patients) have more than 30% liver fat content. The normal BMI patient category 20% (ten out of fifty patients) and 26% (thirteen out of fifty patients) for the overweight BMI patient category also have more than 30% liver fat content. Figure 5.4 illustrates the IQR for the liver, which excludes the HU below 40, for all but the overweight BMI. The graph followed a similar trend as seen for the adipose tissue (Figure 5.3), where the normal and overweight BMI patient categories are almost parallel, as demonstrated in Figure 5.4. However, the underweight BMI patient category, as stated already, had a 30 HU difference between the lower and upper quartile range. In Figure 5.16 the liver HU lower quartile (underweight BMI patient category) image appeared to have an overall grey appearance. This was not observed for the normal (Figure 5.12) or overweight (Figure 5.8) BMI patient categories.

The HU average calculation of the ***psoas muscle*** was utilised in research conducted by Lo *et al.* (2018) to predict the outcome after enterocutaneous fistula repair. The researchers determined that a low HU average calculation was a significant predictor of a poor outcome after the repair (Lo *et al.*, 2018). From their research Lo *et al.* (2018) determined that an HU less than or equal to 32.6 (this was an average taken from the left and right psoas muscle) was considered a low HU. The psoas muscle HU in the current research had a similar median value for the normal (31.3 HU) and overweight (31.6 HU) BMI patient categories. The underweight median value was slightly higher (38.1 HU). If the criterion determined by Lo *et al.* (2018) is applied in the current research, the underweight BMI patient category at 26% (eight out of thirty-one), the normal BMI patient category at 58% (twenty-nine out of fifty) and overweight BMI patient category 62% (thirty-one out of fifty) respectively, have a low psoas muscle HU. However, as the psoas muscle was only evaluated on one slice of the CT, these results

are not absolute, but indicate a method to quantify these HUs. In Figure 5.7 the overweight BMI patient category HUs are indicated. The HUs appear to not deviate too far from each other. Figure 5.11 indicates the normal BMI HU, where a slight deviation is noted and finally the underweight BMI patient category is indicated in Figure 5.15, where a clear deviation is noted, in particular for the adipose tissue. In terms of HU the overweight BMI patient category appears to have the best image quality.

The different tissue types CT numbers have been discussed. Following hereafter is an examination of the image quality calculations.

5.4.2. Image Noise

The image noise is defined as the ***SD*** of the mean attenuation values (Schawkat *et al.*, 2017). Therefore, in order to determine image noise, an assessment of the SD of the different tissue types was deemed necessary. The current research resulted in a SD that was highest (11 HU) for the underweight BMI patient category for the adipose tissue and lowest (9.4 HU) for the normal BMI patient category. The liver tissue SD was highest (9.8 HU) for the overweight BMI patient category and lowest (5.3 HU) for the underweight BMI patient category. The psoas muscle was highest (14.3 HU) for the overweight BMI patient category and lowest (6.8 HU) for the underweight BMI patient category. The overweight BMI patient category was highest for both the liver and psoas muscle tissue types. This outcome indicates that the images contained more noise, while the least noise was found for the underweight BMI patient category for the same tissue types. The underweight patients' scans contained the least volume with regard to adipose tissue, especially at the lower end of the BMI scale (due to less body fat). The SD in the research by Bhosale *et al.* (2015) for different kernels (reconstruction imaging software) measured the minimum and maximum SD for the liver ROI at 12.8 to 26.3. In the current research study, the image noise (determined by the SD) revealed an average of 11 HU for the overweight BMI patients and 8 HU for both the normal and underweight BMI patient categories for the three tissue types. Therefore, the overweight BMI patients had images that received less photons and therefore produced more image noise.

The ***SNR*** for the current study has indicated that the adipose tissue median (-12.3) was the same for the over- and normal weight BMI patient categories. The liver (10.3) and psoas muscle (6.7) SNRs median was highest for the underweight BMI patient category. This indicated that the underweight BMI patient category had the highest image quality in terms of the lowest image noise and the highest signal. Figure 5.17

demonstrates the lowest and highest SNR values observed for the underweight BMI patient category. The number of photons that reaches the detector influences the electronic noise. With high dose examinations the image noise becomes insignificant, however with lower doses the image quality degrades as the noise becomes more dominant (Schawkat *et al.*, 2017).

The SNR is also a quantifier of image noise. The overweight patients had a lower SNR in comparison to the other two BMI categories (with the exception of the adipose tissue). The lowest and highest SNR is seen in Figure 5.9. Qurashi *et al.* (2017) stated that subjective image quality is increased as patients' diameter increase when measured noise is held as a constant variable. In the research conducted by Qurashi *et al.* (2017) they determined that the SNR and CNR objective image quality were statistically similar across the different protocols they used.

5.4.3. Image Contrast

The ***CNR*** for the current study was highest (1.3) for the normal BMI patient category and lowest (0.8) for the overweight BMI category. This indicates that the normal BMI patient category reflected a higher image quality in terms of CNR. CNR is used as an ideal for image quality, as distinguishing between different tissue types or lesions depends on the balance between the image noise and the contrast of the image (Masuda *et al.*; 2016). The CNR is the main quantifier for delineation as this indicates the ability to distinguish between two organs. As the image noise decreases the CNR increases as seen by Masuda *et al.* (2016). Chen *et al.* (2017) stated that, with an increase in CT dose the CNR increases, which makes it easier to distinguish between boundaries of low contrast objects. In the current research study, the CNR measured 0.8 for the overweight BMI patient category. The lowest and highest CNR for the overweight BMI patient category can be observed in Figure 5.10. It was noted that the highest CNR has a lower volume of adipose tissue. For the normal BMI category, the CNR median value measured 1.3 and for the underweight 1.2. The Figure 5.13 demonstrates the normal weight BMI patient category's lowest and highest CNR and Figure 5.18 demonstrates the lowest and highest CNR for the underweight BMI category. For both the aforementioned BMI categories the highest CNR has an increase in adipose volume. The lowest CNR appears grey, indicating very low contrast between the structures. The normal BMI category patients' CNR was slightly higher than the underweight BMI patient category. Figure 5.6 illustrates the correlation between CNR and BMI. It should be noted that for the overweight BMI patient category (Figure 5.10), the lowest CNR image appeared to be noisier (therefore less photons

reached the detector) than its counterpart. However, the highest CNR appeared to have had less contrast visible between the different organs. Schawkat *et al.* (2017) stated that with obese patients the reduction of dose to the patient is significantly impacted by the increase in electronic noise.

The maximum ***CNDR*** represents, for a given image quality level the minimum dose value. Therefore, a maximum CNDR occurs when optimisation is achieved (Chen *et al.*, 2017). The average CNRD obtained for the current study was 0.08 for the overweight BMI patient category. For the normal weight BMI category, the CNRD was calculated at 0.11 and the underweight BMI category calculated at 0.09. Therefore, the optimal dose to image ratio for this specific research study is the normal BMI patient category. The CNRD follows the same trend as the CNR and the most optimised image quality was found with the normal BMI patient category. The least optimised is the overweight BMI patient category.

5.4.4. Limitation

- A quantitative assessment only was made of the CT images. In other research studies a subjective component was usually added whereby a number of radiologists also assessed the CT image quality.
- Only one CT slice was used per patient in order to determine the HU while in other research studies, three slices were examined and the average HU was used.

5.4.5. Recommendations

- Further research into the image quality for the patients scanned for pelvic localisation should be conducted and determine if improvements can be made. This is especially applicable to the different BMI categories.

5.5. Conclusion

The image quality produced from patient CT localisations scans from the normal BMI patient category demonstrated the highest CNR, followed by the underweight- and overweight BMI patient categories. The CNR for the overweight BMI patient category occurred as a result of the amount of scatter produced during the patients' CT scans. In addition, the highest SD for each of the tissue types examined was also from the overweight BMI patient category.

These results indicate that the current CT scanner set up at the oncology department is optimal for normal BMI patient scans in terms of image quality. However, for the overweight BMI patient category a different strategy should be examined with regard to dose and image quality. The following chapter will conclude this research.

References

Barrett, A., Dobbs, J., Morris, S. & Roques, T. 2009. *Practical Radiotherapy Planning*. 4th edition. Hodder Arnold: London.

Bhosale, P., Wagner-Bartak, N., Wei, W. Kundra, V. and Tamm, E. 2015. Comparing CNR, SNR and Image Quality of CT Images Reconstructed with Soft Kernel, Standard Kernel and Standard Kernel plus ASIR 30% Technique. *International Journal of Radiology.* 2(2) 60-65

Bushberg, J.T., Seibert, J.A., Leidholdt, E.M. and Boone, J.M. 2002. *The Essential Physics of Medical Imaging*. 2nd edition. Lippincott Willimas & Wilkins: Philadelphia.

Bushberg, J.T., Seibert, J.A., Leidholdt, E.M. and Boone, J.M. 2011. *The Essential Physics of Medical Imaging*. 3rd edition. Lippincott Willimas & Wilkins: Philadelphia.

Chen, G-P., Noid, G., Tai, A., Liu, F., Lawton, C., Erikson, B. and Li, X.A. 2017. Improving CT Quality with Optimized Image Parameters for Radiation Treatment Planning and Delivery Guidance. *Physics and Imaging in Radiation Oncology*. (4) 6-11.

Forbrig, R., Ingrish, M., Stahl, R., Winter, K.S., Reiser, M. and Trumm, C.G. 2019. Radiation dose and image quality of high-pitch emergency abdominal CT in obese patients using third generation dual-source CT (DSCT). *Scientific Reports*. 9:15877. Date of Access: 15 September 2020 <https://doi.org/10.1038/s41598-019-52454-5>

Geffer, J., Fernandez, A., Macri, F., Freitag, C., Metge, L. and Beregi, J-P. 2013. Which Dose for What Image? Iterative Reconstruction for CT Scan. *Diagnostic and Interventional Imaging* (94) 1117.

Halperin, E.C,, Wazer, D.E., Perez, C.A. and Brady, L.W. 2013. *Perez and Brady's Principles and Practice of Radiation Oncology*. 5th edition. Lippincott Williams & Wilkins: Philadelphia.

International Atomic Energy Agency (IAEA). 2012. *Quality Assurance Program for Computed Tomography: Diagnostic and Therapy Application.* IAEA Human Health Series No 19. IAEA. Date of Access: 30 January 2018 <https://www-pub.iaea.org/MTCD/Publications/PDF/Pub1557_web.pdf>.

Karmazyn, B., Liang, Y., Klahr, P. and Jennings, S.G. 2013. Effect of Tube Voltage on CT Noise Levels in Different Phantom Sizes. *American Journal of Roentgenology*. 200: 1001-1005.

Lo, W.D., Evans, D.C. and Yoo, T. 2018. CT Measured Psoas Density Predicts Outcomes After Enterocutaneous Fistula Repair. *Journal of Parenteral and Enteral Nutrition*. 42 (1): 176-185.

Masuda, T., Funama, Y., Kiguchi, M., Imada, N., Oku, T., Sato, T., and Awai, K. 2016. Radiation Dose based on CNR index with low-tube voltage scan for paediatric CT scan: experimental study using anthropomorphic phantoms. *Springer Plus*. 5: 2064.

Pauchard, B., Higashigaito, K., Lamri-Senouci, A., Knebel, J-F., Berthold, D., Verdun, F.R., Alkadhi, H. and Schmidt, S. 2017. Reduced-Dose CT: Which Type Ensures Diagnostic Image Quality in Young Oncology Patients? *Academic Radiology Journal*. 24: 1114-1124 .

Qurashi, A., Rainford, L., Ajlan, A., Khashoggi, K., Ashkar, L., Al-Raddadi, M., Al-Ghamdi, M., Al-Thobaiti, M. and Foley, S. 2017. Optimal Abdominal CT Protocol for Obese Patients. *Radiography*.1-12.

Rosenquist, K.J., Pedley, A., Massaro, J.M., Therkelsen, K.E., Murabito, J.M., Hoffman, U. and Fox, C.S. 2013. Visceral and Subcutaneous Fat Quality is Associated with Cardiometabolic Risk. *Journal of the American College of Cardiology.* 6(7): 762-771.

Sanderud, A., England, A., Hogg, P., Fossa, K., Svensson, S.F. and Johansen, S. 2016. Radiation Dose Differences between Thoracic Radiotherapy Planning CT and Thoracic Diagnostic CT Scans. *Radiography*. (22) 107-111.

Schawkat, K., Fischer, R.M., Heverhagen, J.T. and Christe, A. 2017. The Impact of Integrated Circuit Detector Technology in Routine MDCT: Improved Image Quality Compared to Conventional Detector Design for Constant SSDE. *Hellenic Journal of Radiology*. 2 (1): 23 – 29.

Stepwards. 2020. *Fundamentals Of Computed Tomography Studies: Windowing*. Date of Access: 12 October 2020. <https://www.stepwards.com/?page_id=21646#WINDOW_SETTINGS_WINDOW_WIDTH_VS_WINDOW_LEVEL>.

Wells, M.M., Li, Z., Addeman, B., McKenzie, C.A., Mujoomdar, A., Beaton, M. and Bird, J. 2016. Computed Tomography Measurement of Hepatic Steatosis: Prevalence of Hepatic Steatosis in a Canadian Population. *Canadian Journal of Gastroenterology and Hepatology.* Volume 2016. Article ID: 4930987.

Xue, Z., Antani, S., Long, R., Demner-Fushman, D. and Thoma, G.R. 2012. Window Classification of Brain CT Images in Biomedical Articles. *American Medical Informatics Association (Amia) 2012 Symposium*. Date of Access: 24 September 2020. <https://www.ncbi.nlm.nih.gov/pmc/articles/PMC3540547/pdf/amia_2012_symp_1023.pdf >.

Zeb, I., Li, D., Masir, K., Katz, R., Larijani, V-N. and Budoff, M.J. 2012. Computed Tomography Scans in the Evaluation of Fatty Liver Disease in a Population Based Study: The Multi-ethnic Study of Atherosclerosis. *Academic Radiology*. 19(7): 811-818.

Chapter 6
Conclusion

6.1. Introduction

The aim of this research was to examine the CT dose and image quality as pertaining to pelvic CT localisation scans. This research has answered the question as to the dose and image quality pertaining to pelvic CT localisation scans. It has been determined that currently 120 kV, L, LL or XL FOV settings should be utilised in the oncology department for pelvic CT localisation scans.

The first objective of the research was to utilise phantoms to determine a baseline dose, as well as glean information about the increase and decrease of CT dose based on phantom size (refer to: Chapter 2). The second objective was to determine the CT dose from pelvic localisation scans as derived from patient data (refer to: Chapter 3). The third objective was to determine the image quality pertaining to phantoms of different sizes and the influence of different FOV settings of the image quality obtained (refer to: Chapter 4). The fourth objective was to examine the image quality based on the CNR for patients scanned for pelvic localisation scans (refer to: Chapter 5). The following concludes the researcher's findings on radiation dose and the image quality of CT for pelvic localisation in an oncology environment.

6.2. Computed Tomography Dose

Mclaughlin *et al.* (2018) state that presently there is an industry drive and considerable research into maintaining image quality while reducing radiation dose during CT scanning. In order to reduce the CT dose, the current CT dose must be determined. The first and second objectives of the research were addressed, which were to establish a baseline dose by utilising of phantoms and then evaluate the CT dose received by the patient. A reflection on the rescan dose for CT localisation scans will be presented.

At the oncology department, the baseline dose measured by an anthropomorphic phantom was determined to be constant with 120 kV for either L, LL or XL FOV, the SSDE for the anthropomorphic phantom calculated to 14 cGy (refer to: 2.4.2). The first objective was achieved by determining that the best dose results were for the 120 kV, in comparison with the 135 kV (calculated to a higher dose, 19 cGy). The 80 kV, which measured the lowest dose of 8 cGy, was not acceptable as the FOV available (S FOV)

did not cover the anthropomorphic phantom entirely. The M FOV, available with the 120 kV and 135 kV, was excluded as the entire body contour of the anthropomorphic phantom was not visible throughout the scan. With the utilisation of the phantoms of different sizes, the research results indicated that, as the phantom size increased the CT dose decreased. The SSDE for the small, medium, large and extra-large phantom calculated to 15 cGy, 12 cGy, 9 cGy and 7 cGy.

The second objective was to determine the patient CT dose from the CT localisation scan of the pelvis by means of the SSDE (refer to: 3.4.3.). The patient's dose scans for the normal patient BMI category had a median SSDE value of 14.3 cGy, which was in line with the baseline dose. The median for the overweight BMI patient category was 12.3 cGy and the underweight BMI patient category was 17.1 cGy, in terms of SSDE. This indicated that, for the underweight BMI patient category and by extension the paediatric patient category, a method to decrease the CT dose should be examined. The section that follows here provides an observation of the rescan dose.

6.2.1. Rescan Dose

In this research 15% of patients underwent a rescan, of which 40% of patients received more than one rescan (refer to: 3.3.4). The accumulation of dose is a concern as the stochastic effect is thought to have a threshold effective dose of 100 mSv. This would result in one in two hundred adults being diagnosed with fatal cancer (Lumbreras *et al.*, 2019). In this current research one patient received a total of three rescans (refer to: 3.3.4), due to the need for bowel preparation twice and in addition a need for a full bladder which moves/pushes the bowels away from the area of interest. The cumulative dose of the four scans resulted in an effective dose of 57.5 mSv for the abdomen and 65.2 mSv for the pelvis. In the research of Lumbreras *et al.*, (2019) conducted over a twelve-year period, 4844 (3.1%) of the participants had an cumulative dose between 50 mSv and 100 mSv and 2298 (1.5%) participants received an effective dose in excess of 100 mSv. The effective dose in the current research calculated to just over half of the threshold dose. Another consideration is that for cancer diagnosis the patient may have received other CT examination procedures prior to the CT localisation scans.

The resultant SSDE in the current research was calculated to 51.2 cGy. In order, to provide context, for cervix cancers, the fractionised regimes of 40 Gy to 50 Gy total dose in daily 180 cGy to 200 cGy fractionations over a period of four to five weeks is utilised (The Royal College of Radiologist, 2019). The CT scan therefore produced a

quarter of a day's CT dose to all organs in the field including the organs at risk, as no shielding can be performed such, as when the radiation treatment is delivered.

Researchers O'Connor *et al.* (2016) stated that, compared with therapeutic and related scatter doses, CT localisation dose has been considered insignificant. In diagnostic radiography, radiation protection measures have been established to limit the stochastic risk of malignancy from the CT scan. One of the limiting factors for radiation therapy CT localisation scans in terms of lowering the dose is the need for high image quality for delineation of tumours. In the next section the image quality of the phantom and patient CT scans are examined.

6.3. Computed Tomography Image Quality

The image quality for CT pelvic localisation was examined as part of the third and fourth objective of this research. The image quality was examined first by phantoms of different sizes. The research then examined the image quality found for the patient scans from the CT localisation scans.

The water phantoms of different sizes were scanned to determine the effect of different FOV and kV settings with a variety of sizes, being the third objective of the research. The 135 kV had proven the highest quality but it also resulted in an increase in the dose (refer to: 2.3.1.2.). This would exclude the 135 kV for use even with a higher image quality. Another consideration as to which kV should be utilised is influenced by research conducted by Skryzński *et al.* (2010) in which they stated that the HU and electron density relationship can differ between scanners as well as different kV settings, therefore between 80 kV and 130 kV. A difference in dose calculations of as much as 2% can be found. Mitaya *et al.* (2020) stated that with smaller FOV in CT, it generally is associated with clearer images and a higher spatial resolution. In the current research the phantoms of different sizes were scanned to evaluate the image quality. The L, LL and XL FOV gave the highest image quality for the variety of phantom size (refer to: 4.3.1.5.). As stated by Mitaya *et al.* (2020), the reason for this could be, that with a reduction in the FOV the image quality deteriorates, and the image noise is increased. Based on the aforementioned, in terms of achieving the third objective, the 120 kV is the improved choice. The 80 kV with S FOV measured a 16.7% within tolerance rate. The M FOV had a 50% within tolerance rate, L FOV 42% within tolerance, the LL had a 63% within tolerance rate and the XL had a 50% within tolerance rate. In terms of the phantom size the small and medium phantoms produced

the most within tolerance scans. The extra-large phantom produced the lowest number of intolerance scans. In addition, the third objective of this research was also to determine if the FOV modified the image quality for phantoms of different sizes. The small and medium water phantoms indicated that most FOV provide a within tolerance scan. The large water phantom had the most within tolerance for the L, LL or XL FOV (refer to: 4.3.1.5.). The extra-large water phantom had very few within tolerance scan results. Therefore, it can be concluded that the scanner settings for both the image quality and dose are 120 kV, with a L, LL or XL FOV for all patients scanned in the oncology department.

The fourth objective of the research was to determine the image quality in terms of the CNR for the patients scanned for pelvic CT localisation (refer to: Chapter 5). The image quality based on patient scans determined that in terms of BMI category, the normal BMI patient category had the highest image quality (CNR median=1.3). The underweight BMI category had the second highest (CNR median=1.2) and the lowest image quality was found in the overweight BMI category (CNR median=0.8) (refer to: 5.4.3.) The overweight BMI patient category results stem from high SD, which indicates image noise. This could be due to scatter. The SD for the overweight BMI patient category median results for all three tissue types measured above 10 HU.

6.4. Overall Validity and Reliability

The validity and reliability of the research was maintained by the initial pilot study. The pilot study consisted of the phantom scans, followed by two patients in each BMI category (refer to: 3.1.4). The pilot study confirmed that the MS Excel spreadsheets contained no errors when automatic calculations were performed. This ensured the validity and reliability of the research study. The pilot study also ensured that all relevant data were captured. The validity was further ensured by photographing the valid aspects of each scan, which allowed verification of all data in order to ensure that no incorrect data were entered onto the MS Excel spreadsheet. All data were collected by the researcher only, therefore consistency, especially for the image quality was maintained, as the researcher consistently endeavoured to maintain the same ROI size and position for each patient. The researcher examined the calculations during the pilot study in order to ensure accuracy. Prior to the commencement of the research, the medical physicist in charge of the CT examined the equations used in the research.

6.5. Limitations

Limitations of the research are indicated in each phase of the research. This section offers additional limitations. A limitation was that only one anthropomorphic phantom was available. Thus, comparison of different sized anthropomorphic phantoms in terms of dose was not achievable (refer to: 2.4.6). The image quality could also not be established with the anthropomorphic phantom as no organs or tissue type was found in the anthropomorphic phantom used in the research. The image quality was established using only a quantitative method, for both the phantom and patient research. Only one CT slice was examined in the research for the image quality (refer to: 4.4.5 and 5.4.4.). The researcher gathered the data, therefore the researcher's perspective, was not objectively verified.

6.6. Future Considerations

Advancements in CT development include features such as metal artefact reduction, dual-energy imaging, automatic kilovoltage selection and iterative reconstruction, all of which may benefit radiation therapy planning CT scans (Davis *et al.*, 2017).

At the oncology department where the research was conducted there are two CT scanners; one dedicated for CT localisation and the other is utilised for brachytherapy. Therefore, when maintenance is being performed on the localisation CT, the brachytherapy CT may be utilised for CT localisation scans. The brachytherapy CT has a pre-set of 350 mA instead of the 300 mA, as found at the localisation CT. Verification of the CT dose should be undertaken with the use of phantoms to determine the effect on the dose. In the current research the resultant dose was 11.8 cGy, however the patient had the second largest effective diameter (40 cm). The median value for the overweight BMI patient category was 12.3 cGy. The patient with a higher effective diameter (40.8 cm) had a resultant dose of 8.5 cGy, but the preceding effective diameter (39.7 cm) patient had a dose of 8,8 cGy, thus, the patient scanned at 350 mA received a higher dose.

A new four-dimensional CT (4DCT) has recently (2020) been installed in the oncology department. The 4DCT is used to monitor the motion of a lesion in a patient for radiation therapy purposes, with respect to the respiration signal (Yang *et al.*, 2018). With the 4DCT data the intra-fractional motion of the lesion and organs can be observed for thoracic and abdominal regions. The 4DCT data is created by overlapping the respiratory motion of the tissue. This results in a rapid increase in CT dose to the

organs at risk (Yang *et al.*, 2018). The researchers concluded that between the patients' effective diameter and the mean organ dose to the thoracic organs there was a strong inverse correlation (Yang *et al.*, 2018). There was a 12,8-fold higher average dose with the 4DCT in comparison to the 3D CT scan (Yang *et al.*, 2018). Yang *et al.* (2018) further state that 4DCT radiation dose has a substantial increased risk for developing lung cancer, associated with the 4DCT dose and the size of smaller patients.

A recent procurement for the oncology department was two contrast infusion pumps for improved delineation of contours through the use of contrast medium with the CT scans as well as for the 4DCT scans. The Health Professions Council of South Africa (HPCSA) stated only recently (2020) that diagnostic, therapy, nuclear and ultrasound radiographers will need to obtain a Professional Board for Radiography and Clinical Technology (PBRCT) accredited postgraduate qualification in order to gain knowledge and competencies e.g. in the administration of contrast medium. These recommendations are awaiting approval from the Minister of Health (HPCSA, 2020). The contrast medium assists in improved contouring of the images and the establishment of improved treatment parameters. However, as established in research conducted by Smith-Bindman *et al.* (2009) the effective dose increased from 15 mSv to 16 mSv when contrast medium was added (refer to: 3.4.2). As the HUs are utilised in the treatment planning system, the need for a non-contrast CT examination would be preferential, thus the CT dose will be doubled when utilising contrast-based CT scans.

A recommended future procurement would be the purchase of a magnetic resonance imaging (MRI) simulation machine. From the onset CT images have inadequate soft tissue contrast and initially diagnostic MRIs were utilised for contouring purposes (Devic, 2012). MRI has superb soft-tissue definition however, diagnostic MRI has a curved cushion lined couch, whereas in radiation therapy a flatbed couch is needed for reproducible positioning at the time of treatment (Devic, 2012). The difference in patient position from a diagnostic MRI to the radiation therapy localisation scan can differ greatly (Devic, 2012). As a result, the MRI simulator was created. For pelvic examinations the benefit of the MRI simulator is that for rectal cancer the accurate contouring of the tumour is virtually impossible without the use of MRI (Devic, 2012). For other pelvic examinations such as the prostate and gynaecological tumours, the MRI simulator brings clear improvement with delineation of the tumour volumes (Devic, 2012). The only drawback with regards to MRI and CT fusion for the pelvis are the anatomical changes in the shape of the tumour and organs at risk, which occur due to

physiological fillings of the rectum and bladder (Devic, 2012). A high-quality MRI image is necessary for use in conjunction with the CT data. The voxel size of CT data for CT simulation is usually 1 mm (due to 1 mm to 2 mm slice thickness). Diagnostic CT images are usually 3 mm voxel size, which is accommodated by the diagnostic MRI (Devic, 2012). Therefore, a high image quality is a prerequisite for an MRI simulator, which will increase the acquisition time (Devic, 2012). A technique to decrease the acquisition time is to reduce the area to be imaged, usually encompassing the tumour volume (Devic, 2012).

These new and future developments at the oncology department and the findings of the current research inspire further research and modifications that could be made to the current clinical practice.

6.7. Recommendations

Recommendations for improved CT dose and image quality in the oncology department include suggestions for further research and modifications to clinical practices. The following outlines suggestion for future research, which include methods to decrease the CT dose and the establishment of DRLs.

6.7.1. Future research

The patients who receive radical treatment at the oncology department for cervix cancer also receive an internal brachytherapy treatment. To deliver this treatment a CT scan is performed to ensure correct placement of the delivery source. Research into the CT dose received per scan and the cumulative dose should be strongly considered. Establishment of the dose and image quality found with other regions of CT localisation (i.e. the head and neck as well as thorax scans) should be formally investigated. It is furthermore recommended that the dose received by paediatric patients in all anatomical regions should also be determined. An assessment of the image quality for patients of different body habitus should be made to determine if the CT scan protocol can be modified. The 4DCT dose should be established for all anatomical regions.

The CT dose for pelvic localisation scans should be decreased. Methodology currently used in research in order to decrease the CT dose is examined in the section that follows.

6.7.1.1. Methods to Reduce Computed Tomography Dose

Current methods employed to reduce CT dose include automated tube current modulation and iterative reconstruction. These have reduced CT dose levels by approximately 70% to 75% compared to a decade ago (McLaughlin, *et al.* 2018). Automatic exposure can reduce CT dose by 50% however, the resultant dose may be higher than expected for heavier patients, because in order to maintain constant image noise, the tube current is increased (Israel *et al.*, 2010). In the current research automatic exposure is not presently being utilised and the CT dose was determined to be higher for the underweight patients and decreases for overweight patients. CT dose reduction, as stated by McLaughlin *et al.* (2018), is challenged by the difference in patient size and body weight.

In research conducted by Chang *et al.* (2017) the authors evaluated the effect of the scan parameters on the radiation dose and image quality, while aiming to determine the optimal CT scanning protocols by scanning an ACR accredited phantom. The protocols that were examined were different kVp, mAs and iterative reconstruction algorithms (Chang *et al.*, 2017). They examined the CT dose in terms of the $CTDI_{vol}$ and the image quality in terms of CNR. Other imaging quality metrics examined were CT number accuracy and SNR (Chang *et al.*, 2017). Resulting from their research Chang *et al.* (2017) recommended that for adults 100 kVp and between 150 mAs to 250 mAs be utilised. In instances where low contrast resolution CT scans were required, they recommended the modification of the kVp to 120. In terms of paediatric CT scans the researchers determined that 80 kVp and 50 mAs, or increasing the mAs to 300 to be optimal, depending on what needs to be visualised (maxillary sinus and brain stem vs temporal bone). Chang *et al.* (2017) also determined that by using and iterative reconstruction (IR) a further increase of 40% for the CNR without an increase in the radiation dose delivered could be achieved.

Radiation therapy departments often have a dedicated CT for localisation purposes however, a “one-size-fits-all” approach is often followed, with minimal scan parameter variation (Davis *et al.*, 2017). In contrast though, in diagnostic departments CT scan protocols often modify parameters such as slice width, FOV, tube current, reconstruction algorithm and others (Davis *et al.*, 2017). The reluctance by radiation therapy departments is based on a concern that by modifying these parameters the HU values produced by the images will be changed, which may lead to inaccurate dosimetric information being introduced in the radiation planning system (Davis *et al.*, 2017). However, this approach may produce compromised image quality whereby

suboptimal images may be used to identify and outline key structures. A source of uncertainty in the radiation therapy process is the variability and inaccuracies in the outline process. Some of the causes of the uncertainty includes pathological variation that occurs in the patient as well as the similar densities between tissues, which make it difficult to distinguish between tissue types. Poor CT image quality can be detrimental to this process (Davis *et al.*, 2017).

In radiation therapy an adjustment to fundamental scan parameters could deliver a higher image quality and have the potential to improve accuracy at the contouring stage of planning. These parameters include reconstruction algorithms and FOV, which are more appropriate for the body region being scanned (Davis *et al.*, 2017). However, in order to utilise these techniques a good understanding is required about the variations in HU that can be tolerated for different CT imaging techniques as well as which do not adversely affect the distribution of the dose in the radiation therapy planning system (Davis *et al.*, 2017).

Further research into the effect of these modifications to the CT HU should be considered. Another technique used in diagnostic CT reduction is the use of DRLs, which will be discussed in the section that follows.

6.7.1.2. Diagnostic Reference Levels

O'Connor *et al.* (2016) state that CT localisation scans are governed by the ALARA principles (refer to: 2.1.1) as they are considered as non-therapeutic dose. These researchers stipulate that it is vital to ensure the CT dose received by the patient adheres to the ALARA principles. ICRP introduced the concept of DRL in 1996 (refer to: 2.1.4). DRLs were established to assist in radiation dose optimisation by providing an easily measured quality assurance quantity and thereby playing a leading role in radiation protection (Meyer *et al.*, 2017). In diagnostic radiography there has been determination of local DRLs (LDRLs) for an imaging practice or a hospital. Moreover, national DRLs for specific patient groups and examinations have also been determined, not to mention the regional DRLs (Meyer *et al.*, 2017). DRLs are determined by examining the third quartile of the collected reference data (local, national or regional), which is the level below which 75% of the data occurs. This indicates the adopted reference level (Meyer *et al.*, 2017). Since the establishment of DRLs, a decrease in CT dose has been initiated (O'Connor *et al.*, 2017).

The primary value of the DRL is to assist in identifying unjustifiably high radiation doses. This is done by applying the threshold above which an investigation into the CT dose is warranted (O'Connor *et al.*, 2016). The established diagnostic DRLs cannot be used for radiation therapy CT localisation plans, as different scanning volumes and image requirements prevent diagnostic DRLs from being utilised (O'Connor *et al.*, 2016). Through their research O'Connor *et al.* (2016) also established national diagnostic levels for CT localisation protocol for breast cancer in Ireland. At the conclusion of their research, they determined that significant discrepancies in breast cancer CT localisation dose were measured at the different radiation therapy centres (O'Connor *et al.*, 2016). The researchers further determined that the significant dose variation was unjustifiable, as the CT images served exactly the same clinical purpose all over (O'Connor *et al.*, 2016: 5). After their research the first national Irish radiation therapy CT DRLs were proposed for breast cancer localisation CT scans (O'Connor *et al.*, 2016).

Following the concept of DRLs for oncology as established by O'Connor *et al.* (2016) local DRLs should be established for the oncology department for both the CT and 4DCT scanners. Regional DRLs and national DRLs could also be established to determine the CT dose utilised for CT localisation scans and to increase knowledge about the CT dose delivered. With the assistance of the medical physicist and with the use of thermoluminescent dosimeter (TLD), the CT dose to organs at risk, such as the thyroid, lens of the eye or breast tissue when scanned for CT localisation can be established (with the use of phantoms).

6.7.2. Clinical Practice

In clinical practice the establishment of different protocols for patients with different BMI categories could reduce the dose and improve the image quality. The same applies for establishment of a protocol for paediatric patients. A system to decrease rescans should be put in place. One suggestion would be a thorough examination of prior CT examinations to establish if a chronic bowel issue exists and/or the position of the bowel. This could assist in determining if a CT scan prone with a full bladder may be required. It is recommended that education and training programmes be implemented for all radiation therapists and that awareness pertaining to the CT dose be created in the oncology department.

Due to widely reported overexposure from diagnostic CTs, the first legalisation to regulate CT dose came into effect on 1 July 2012 in the state of California (Zucker *et al.*, 2015). The introduction of the senate bill 1237 determined that a CT dose reporting protocol page has to be attached to any CT report. The dose reporting requires that the $CTDI_{vol}$ and DLP of the CT scan be indicated or a dose unit approved by the AAPM be used (Zucker *et al.*, 2015). Sung and Shin (2013) state that various countries and international organisations have other dose reducing programmes. These include Wallet card at Beaumount Hospital in Pennsylvania, MyChild's Medical Imaging Record at the American College of Radiology, Smart card project at the International Atomic Energy Agency (IAEA), Radiation Exposure Monitoring (REM) Integration Profile in Japan, Patient Exposure Registry (PER) in the European Union (Dose DataMed (DDM) ProjectPACS) and Radiation Passport Project in Canada. Parakh *et al.* (2016) state that in terms of dose optimisation, the vast disparity between the scientific information and clinical practice is due to a lack of dose tracking. Utilising the information on CT dose an establishment of a method to track CT dose related to oncology patients would create awareness of the CT dose and assist in optimisation of the dose.

6.8. Conclusion

The essence of the Hippocratic oath is often conceived as being "first do no harm". The citation actually belongs to Hippocratic treaties on Epidemics, which when translated states "*In illnesses one should keep two things in mind, to be useful rather than cause no harm*" (Retsas, 2019). Two categoric statements in the Hippocratic oath are cited as demanding beneficial intervention on behalf of the patient. These are "*Into whatever house I enter, I will do so for the benefit of the sick*" as well as "*I will apply the*

regiments of treatment according to my ability and judgement for the benefit of the patient and protect them from harm and injustice" (Retsas, 2019). Therefore, the focus of clinical practice should remain on being to the benefit of the patient (Retsas, 2019).

CT dose and image quality are complex topics in oncology. The necessity for a high image quality while lowering the CT dose, thus maintaining the ALARA principles, is essential. Bearing this is mind, the statement by oncologist Spyros Retsas (2019) becomes very relevant "*Can harm always be averted even with the most beneficent of intentions? Probably not, but the intention to be useful to the receiving patient, rather than cause no harm, should continue to guide medicine. Perhaps the Hippocratic oath remains possible, even in our times!"*

The present research has established the radiation dose and image quality for localisation scans in oncology. The image quality in oncology is the main indicator for a higher CT dose in comparison to diagnostic radiography. The research of Sanderud *et al.* (2016) stated that radiation therapy scans were conducted with a very low noise index in comparison to their diagnostic counterparts. The reason for this being adherence to the requirements for radiation therapy purposes.

This research established the need to determine ways in which to decrease dose to patients with a small body habitus (underweight BMI category as well as paediatric patients) as well as to improve the image quality for patients in the overweight BMI patient category. The research should always be conducted with the end goal in mind, which is to establish improved scanning capabilities for the benefit of the patient. As William J Mayo (1861-1939), founder of the Mayo Clinic in the United States of America stated: "*The best interest of the patient is the only interest to be considered*". This is supported in the research by O'Connor *et al.* (2016) who established national DRLs in Ireland for breast cancer CT protocols. These DRLs provide radiation oncology departments worldwide a basis for dose optimisation and reduction in the cumulative radiation dose to patients (O'Connor *et al.*, 2016).

The future of radiation therapy could drastically be altered through the field of artificial intelligence (AI). Research by McCollough and Leng (2020) conclude that further reduction of radiation dose with the use of AI in CT is promising. This also pertains to a reduction in the image noise optimising of image reconstruction parameters through advanced reconstruction algorithms (McCollough & Leng; 2020). The CT dose and image quality are contemporary topics and research continues to decrease the dose and improve the image quality. This research hopes to further inspire the continued

search for optimal CT parameters for the pelvic CT localisation scans in the oncology environment.

““We ourselves feel that what we are doing is just a drop in the ***ocean****. But the* ***ocean*** *would be less because of that missing drop.”*

'I ***alone cannot change the world****, but I can cast a stone across the waters to create many ripples*

Mother Teresa (1910 -1997)

References

American Association of Physicists in Medicine (AAPM). 2011. Size-Specific Dose Estimates (SSDE) in Paediatric and Adult Body CT Examinations. *AAPM Report No. 204*. Report of AAPM Task Group 204, developed in collaboration with the International Commission on Radiation Units and Measurements (ICRU) and the Image Gently Campaign of the Alliance for Radiation Safety in Paediatric Imaging. Date of Access: 25 November 2017. <https://www.aapm.org/pubs/reports/RPT_204.pdf>

American Association of Physicists in Medicine (AAPM). 1977. *Phantoms for Performance Evaluation and Quality Assurance of CT Scanners*. AAPM Report 1.

Auxier, J.A. and Dickenson, H.W. 1983. Guest editorial: concern over recent use of the ALARA philosophy. *Health Physics*. 44 (6) 595-600.

Barrett, A., Dobbs, J., Morris, S. and Roques, T. 2009. *Practical Radiotherapy Planning*. 4th edition. Hodder Arnold: London.

Bellon, M.R., Siddiqui, M.S., Ryu, S. and Chetty, I.J. 2014. The Effect of Longitudinal CT Resolution and Pixel Size (FOV) on Target Delineation and Treatment Planning in Stereotactic Radiosurgery. *Journal of Radiosurgery and SBRT (Stereotactic Body Radiation Therapy)*. Vol 3: 149-163.

Bharkhada, D., Yu, H., Dixon, R., Wei, Y., Carr, J.J., Bourland, J.D., Best, R., Hogan, R. and Wang, G. 2009. Demonstration of Dose and Scatter Reduction for Interior Computed Tomography. *Journal of Computer Assisted Tomography*. 33 (6): 967-972.

Brazier, Y. 2017. *How Useful is the Body Mass Index (BMI)?* Medical News Today. Date of Access 28 August 2020 <https://www.medicalnewstoday.com/articles/255712>.

Bhosale, P., Wagner-Bartak, N., Wei, W. Kundra, V. and Tamm, E. 2015. Comparing CNR, SNR and Image Quality of CT Images Reconstructed with Soft Kernel, Standard Kernel and Standard Kernel plus ASIR 30% Technique. *International Journal of Radiology.* 2(2) 60-65.

Bluemke, D.A. and Liu, S. 2012. *Principles and Practice of Clinical Research. 3rd edition*. Elsiveir. Chapter 41 – *Imaging in Clinical Trials* (pages 597-617).

Boas, F.E. and Fleischmann, D. 2012. CT Artifacts: Causes and Reduction Techniques. *Imaging in Medicine Journal* (4: 229-240).

Bowers, A. 2008. *Medical Statistics from Scratch: An Introduction for Health Professionals*. 2nd edition. John Wiley & sons Limited: New Jersey.

Bridge, P. and Tipper, D.J. 2011. *CT Anatomy for Radiotherapy*. M&K Publishing: Cumbria.

Bushberg, J.T., Seibert, J.A., Leidholdt, E.M. and Boone, J.M. 2002. *The Essential Physics of Medical Imaging*. 2nd edition. Lippincott Willimas & Wilkins: Philadelphia.

Bushberg, J.T., Seibert, J.A., Leidholdt, E.M. and Boone, J.M. 2011. *The Essential Physics of Medical Imaging*. 3rd edition. Lippincott Willimas & Wilkins: Philadelphia.

Chang, K-P., Hsu, T-K., Lin, W-T. and Hsu, W-L. 2017. Optimization of Dose and Image Quality in Adult and Paediatric Computed Tomography Scans. *Radiation Physics and Chemistry*. 140: 260-265.

Chen, G-P., Noid, G., Tai, A., Liu, F., Lawton, C., Erikson, B. and Li, X.A. 2017. Improving CT Quality with Optimized Image Parameters for Radiation Treatment Planning and Delivery Guidance. *Physics and Imaging in Radiation Oncology*. (4) 6-11.

Choi, H.R., Kim, R.E., Heo, C.W., Kim, C.W., Yoo M.S. and Lee, Y. 2018. Optimization of Dose and Image Quality Using Self-produced Phantoms of Various Diameters in paediatric abdominal CT scan. *International Journal for Light and Electron Optics.* 168: 54-60.

Code of Federal Regulations: 2017. *Title 21: Food and Drugs, Chapter 1-Food and Drug Administration Department of Health and Human Services. Subchapter: Radiological Health. Part 1020- Performance Standards for Ionizing Radiation Emitting Products*. (Volume 8). Date of Access: 24 November 2017. <https://www.accessdata.fda.gov/scripts/cdrh/cfdocs/cfcfr/CFRSearch.cfm?FR=1020.33>

Cropp, RJ., Seslija, P., Tso, D. and Thakur, Y. 2013. Scanner and kVp dependence of measured CT numbers in ACR CT phantom. *Journal of Applied Clinical Medical Physics*. Vol 14 No 6.

Davis, A.T., Palmer, A. L. and Nisbet, A. 2017. Can CT Scan Protocols Used for Radiotherapy Treatment Planning be Adjusted to Optimize Image Quality and Patient

Dose? A Systematic Review. *British Journal of Radiology*. 90: 20160406 Date of Access: 3 May 2020 <https://doi.org/10.1259/bjr.20160406 >.

Devic, S. 2012. MRI Simulation for Radiotherapy Treatment Planning. *Medical Physics*. 39 (11).

De Vos, A.S., Strydom, H., Fouché, C.B. and Delport, C.S.L. 2011. *Research at Grass Roots: for the Social Sciences and Human Service Professions*. 4th edition. Van Schaik Publishers: Pretoria.

European Commission. 2018. Radiation Protection: European Guidelines on Diagnostic Reference Levels for Paediatric Imaging. *Radiation Protection N° 185.*

Forbrig, R., Ingrish, M., Stahl, R., Winter, K.S., Reiser, M. and Trumm, C.G. 2019. Radiation dose and image quality of high-pitch emergency abdominal CT in obese patients using third generation dual-source CT (DSCT). *Scientific Reports*. 9:15877. Date of Access: 15 September 2020 <https://doi.org/10.1038/s41598-019-52454-5>

Geffer, J., Fernandez, A., Macri, F., Freitag, C., Metge, L. and Beregi, J-P. 2013. Which Dose for What Image? Iterative Reconstruction for CT Scan. *Diagnostic and Interventional Imaging* (94) 1117.

Goldoost, G., Ebrahimpoor, M., Behrouzkia, Z., Aghdam, R.Z. and Refahi, S. 2018. Assessment of Water CT number, Field Uniformity and Noise In Diagnostic Computed Tomography Scanners in Urmia Metropolis, Iran. *International Journal of Advanced Biotechnology and Research*. 9(1): 165-170.

Goldman, L.W. 2007. Principles of CT Radiation Dose and Image Quality. *Journal of Nuclear Medicine Technology*. Vol 35 no 4. 213-225.

Habibzadeh, M.A., Ay, M.R., Asl, A.R., Ghadiri, H. and Zaidi, H. 2012. Impact of miscentering on patient dose and image noise in x-ray CT imaging: phantom and clinical studies. *Physica Medica*. (28) 191-9.

Halperin, E.C., Perez, C.A. and Brady, L.W. 2008. *Perez and Brady's Principles and Practice of Radiation Oncology*. 5th edition. Lippincott Williams & Wilkins: Philadelphia.

Halperin, EC, Wazer, D.E., Perez, C.A. and Brady, L.W. 2013. *Perez and Brady's Principles and Practice of Radiation Oncology*. 5th edition. Lippincott Williams & Wilkins: Philadelphia.

Health Professional Council of South Africa (HPCSA). 2020. Radiography and Clinical Technology News. *Newsletter for Professional Board for Radiography and Clinical Technology.* Issue: 01/08/2020.

International Atomic Energy Agency (IAEA). 2012. *Quality Assurance Program for Computed Tomography: Diagnostic and Therapy Application.* IAEA Human Health Series No 19. IAEA. Date of Access: 30 January 2018 <https://www-pub.iaea.org/MTCD/Publications/PDF/Pub1557_web.pdf>.

International Commission on Radiological Protection (ICRP). 1990. Annuals of ICRP: ICRP Publication 60. *The 1990 Recommendation of the International Commission on Radiological Protection.* Volume 21 No.'s 1-3.

International Commission on Radiological Protection (ICRP) 2007. Annuals of the IRCP. IRCP Publication 103. *The 2007 Recommendation of the International Commission on Radiological Protection*. Volume 37. No.'s 2-4.

International Commission on Radiological Protection (ICRP). 1985. Annuals of ICRP: ICRP Publication 44. *Protection of the Patient in Radiation Therapy.* Volume 15 No 2.

International Commission on Radiological Protection (ICRP). 1990. Annuals of ICRP: ICRP Publication 60. The 1990 Recommendation of the International Commission on Radiological Protection. Volume 21 No.'s 1-3.

Israel, G.M., Cicchiello, L., Brink, J. and Huda, W. 2010. Patient Size and Radiation Exposure in Thoracic, Pelvic and Abdominal CT Examinations Performed with Automatic Exposure Control. *American Journal of Roentgenology*. 195 (1342- 1346).

Kaasalainen, T., Palmu, K., Reijonen, V. and Kortesniemi, M. 2014. Effect of Patient Centering on Patient Dose and Image Noise in Chest CT. *American Journal of Roentgenology*. 203: 123-130.

Kalender, W.A. 2014. Dose in X-Ray Computed Tomography. *Physics in Medicine and Biology*. 59 (R129-R150.).

Kalara, M.K., Sodickson, A.D. and Mayo-Smith, W.W. 2015. CT Radiation: Key Concepts for Gentle and Wise Use. *Radiographics*. 35: 1706-1721.

Kanal, K.M., Butler, P.F., Sengupta, D., Bargavan-Chatfield, M., Coombs, L.P. and Morin, R.L. 2017. U.S. Diagnostic Reference Levels and Achievable Doses for 10 Adult CT Examinations. *Radiology.* (248: 1): 120 – 133.

Karim, M.K.A., Hashim, S., Bakar, K.A., Bradley, D.A., Ang, W.C., Bahrudin, N.A. and Mhareb, M.H.A. 2017: Estimation of radiation cancer risk in CT-KUB. *Radiation Physics and Chemistry*. 137 (130-134).

Karim, M.K.A., Hashim, S., Bradley, D.A., Bakar, K.A., Haron, M.R. and Kayun, Z. 2016. Radiation doses from computed tomography practice in Johor Bahru Malaysia. *Radiation Physics and Chemistry*. 121 (69-74).

Karmazyn, B., Liang, Y., Klahr, P. and Jennings, S.G. 2013. Effect of Tube Voltage on CT Noise Levels in Different Phantom Sizes. *American Journal of Roentgenology*. 200: 1001-1005.

Kayugawa, A., Noto, Y., Taga, T., Fukaya, T., Tasaki, K., Fujioka, T., Ohkubo, M., Niigata, J.P. and Minatoku, J.P. 2015. Characterization of the model-based iterative reconstruction algorithm: Confirmation of coexistence of dose reduction and spatial resolution improvement. *Congress ECR 2015*. Poster No.: C-0946.

Kodlulovich, S., Jakubiak, R.R., Miquelin,C.A. and Oliveira, L. 2008. Initial Results of the Quality Control in 11 Computed Tomography Scanners at Curitiba. International Congress of the International Radiation Protection Association (IRPA): Strengthening Radiation Protection Worldwide; Buenos Aires (Argentina); 19-24 Oct 2008. Date of Access: 20 September 2020. <https://inis.iaea.org/collection/NCLCollectionStore/_Public/41/006/41006618.pdf>

Kumar, R. 2011. *Research Methodology: A Step-by-Step Guide for Beginners*. 3rd Edition. SAGE Publications Ltd: London.

Lo, W.D., Evans, D.C. and Yoo, T. 2018. CT Measured Psoas Density Predicts Outcomes After Enterocutaneous Fistula Repair. *Journal of Parenteral and Enteral Nutrition*. 42 (1): 176-185.

Lyra, M., Rouchota, M., Michalitsi, M., Boultadaki, A., Letsas, B., Floros, I., Andreou, M., Synefia, S., Valassi, A., Argyrou, M. and Sotiropoulos, M. 2019. Effective dose and size-specific dose estimate (SSDE) of the torso: In low dose MDCT protocol in multiple myeloma. *Radiology and Diagnostic Imaging Journal.* Volume 3 (1-6).

Lumbreras, B., Salinas, J.M. and Gonzalez-Alvarez, I. 2019. Cumulative Exposure to Ionising Radiation from Diagnostic Imaging Tests: a 12 Year Follow-up Population-Based Analysis in Spain. *BMJ Open*.

Mansour, Z., Mokhtar, A., Sarhan, A., Ahmed, M.T. and El-Diasty, T. 2016. Quality Control of CT Images Using American College of Radiology (ACR) Phantom. *The Egyptian Journal of Radiology and Nuclear Medicine*. 47: 1665-1671.

Masuda, T., Funama, Y., Kiguchi, M., Imada, N., Oku, T., Sato, T., and Awai, K. 2016. Radiation Dose based on CNR index with low-tube voltage scan for paediatric CT scan: experimental study using anthropomorphic phantoms. *Springer Plus*. 5: 2064.

McCollough, C.H. 2010. *Diagnostic Reference Levels*. American College of Radiology. Date of Access: 10 December 2017. <http://www.imagewisely.org/~/media/ImageWisely-Files/Medical-Physicist-Articles/IW-McCullough-Diagnostic-Reference-Levels.pdf>.

McCollough, C.H., Bruesewitz, M.R., McNitt-Gray, M.F., Bush, K., Ruckdeschel, T., Payne, J.T., Brink, J.A. and Zeman, R.K. 2004. The Phantom Portion of the American College of Radiology ACR Computed Tomography (CT) Accreditation Program: Practical Tips, Artifact Examples and Pitfalls to Avoid. *Medical Physics*. Sept 31 (9): 2423-42.

McCollough, C.H. and Leng, S. 2020. Use of Artificial Intelligence in Computed Tomography Dose Optimisation. *Annuals of IRCP*. Abstract. Date of Access: 20 October 2020 <https://pubmed.ncbi.nlm.nih.gov/32870019/>.

McCollough, C.H., Leng, S., Yu, L., Cody, D.D., Boone, J.M. and McNitt-Gray, M.F. 2011. CT Dose Index and Patient Dose: They Are Not The Same Thing. *Radiology*. Volume 259: (311-316).

McCollough, C.H., Primak, A.N., Braun, N., Kofler, J., Yu, L and Christner, J. 2009. Strategies for Reducing Radiation Dose in CT. *Radiologic Clinics of North America*. Volume 47: (27-40).

McLaughlin, P.D., Chawke, L., Twomey, M., Murphy, K.P., O'Neil, S.B., McWilliams, S.R., James, K., Kavanagh, R.G., Sullivan, C., Chan, F.E., Moore, N., O'Connor, O.J., Eustace, J.A., Maher, M.M. 2018. Body Composition Determinants of Radiation Dose During Abdominopelvic CT. *Insights into Imaging*. 9: 9-16.

Meyer, S., Groenewald, W.A. and Pitcher, R.D. 2017. Diagnostic Reference Levels in Low- and Middle-Income Countries: Early "ALARAm" Bells? *Acta Radiologica*. 58 (4) 442-448.

Miller, D.L. and Schauer, D. 2015. The ALARA principles in Medical Imaging. AAPM Newsletter. Vol 40 No 1.

Miyata, T., Yangawa, M., Hata, A., Hondai, O., Yoshida, Y., Kikuchi N., Tusbamoto, M., Tsukagoshi S., Uranishi, A. and Tomiyama, N. 2020. Influence of field of view size on image quality: ultra-high-resolution CT vs. conventional high-resolution CT. *European Radiology*. 30: 3324-3333.

Munjal, R.K., Negi, P.S., Babu, A.G., Sinha, S.N., Anand, A.K. and Kataria, T. 2006. Impact of 6MV photon Beam Attenuation by Carbon Fiber Couch and Immobilization Devices in IMRT Planning and Dose Delivery. *Journal of Medical Physics.* 31: (2) (67-71).

Njiki, C.D., Manyol, J.E.M.N., Yigbedeck, Y.E., Abou'ou, D.W., Yimele, B.C. and Sabouang, J.F. 2018. Assessment of Image Quality Parameters for Computed Tomography in the City of Yaounde. *Open Journal of Radiology*. (8: 37 – 44).

O'Connor, S., Mc Ardle, O. and Mullaney, L. 2016. Establishment of National Diagnostic Reference Levels for Breast Cancer CT Protocols in Radiation Therapy. *British Journal of Radiology*.

Parakh, A., Kortesniemi, M. and Schindera, S.T. 2016. CT Radiation Dose Management: A Comprehensive Optimization Process for Improving Patient Safety. *Radiology*. Vol 280: No 3.

Pereira, G. C., Traughber, M. and Muzic Jr, R.F. 2014. The Role of Imaging in Radiation Therapy Planning: Past, Present, and Future. *BioMed Research International*. Volume 2014. Date of Access: 22 November 2017 <https://www.hindawi.com/journals/bmri/2014/231090/>.

Petrie, A. and Sabin, C. 2000. *Medical Statistics at a Glance*. Blackwell Science LTD: France.

Philips. 2016. *The Importance of Patient Centereing on CT Radiation Dose Optimization*. Online. Date of Access: 2 February 2018 <http://incenter.medical.philips.com/doclib/enc/13037837/The_Importance_of_Patient_Centering_on_CT_radiation_dose_optimization.pdf%3Ffunc%3Ddoc.Fetch%26nodeid%3D13037837>.

Pauchard, B., Higashigaito, K., Lamri-Senouci, A., Knebel, J-F., Berthold, D., Verdun, F.R., Alkadhi, H. and Schmidt, S. 2017. Reduced-Dose CT: Which Type Ensures Diagnostic Image Quality in Young Oncology Patients? *Academic Radiology Journal*.

Qurashi, A., Rainford, L., Ajlan, A., Khashoggi, K., Ashkar, L., Al-Raddadi, M., Al-Ghamdi, M., Al-Thobaiti, M. and Foley, S. 2017. Optimal Abdominal CT Protocol for Obese Patients. *Radiography*.1-12.

Raman, S.P., Mahadeveppa, M., Blasko, R.V., and Fishman, E.K. 2013. CT Scan Parameters and Radiation Dose: Practical Advice for Radiologists. *Journal of American College of Radiology*.

Retsas, S. 2019. Rapid Response to: First do no Harm: the Impossible oath? *British Medical Journal.* 366: l4734 Date of Access: 4 November 2020. <https://www.bmj.com/content/366/bmj.l4734/rr-2>.

Roa, A.M.A., Anderson, H.K. and Martinsen, A.C.T. 2015. CT Image Quality Over Time: Comparison of Image Quality for Six Different CT Scanners over a Six-year Period. *Journal of Applied Clinical Medical Physics.*2014. (16 (2): 340 – 365).

Rosenquist, K.J., Pedley, A., Massaro, J.M., Therkelsen, K.E., Murabito, J.M., Hoffman, U. and Fox, C.S. 2013. Visceral and Subcutaneous Fat Quality is Associated with Cardiometabolic Risk. *Journal of the American College of Cardiology.* 6(7): 762-771.

Sanderud, A., England, A., Hogg, P., Fossa, K., Svensson, S.F. and Johansen, S. 2016. Radiation Dose Differences between Thoracic Radiotherapy Planning CT and Thoracic Diagnostic CT Scans. *Radiography*. (22) 107-111.

Schawkat, K., Fischer, R.M., Heverhagen, J.T. and Christe, A. 2017. The Impact of Integrated Circuit Detector Technology in Routine MDCT: Improved Image Quality Compared to Conventional Detector Design for Constant SSDE. *Hellenic Journal of Radiology*. 2 (1): 23 – 29.

Shope, T.B., Gagne, R.M. and Johnson, G.C. 1981. A method for describing the doses delivered by transmission x-ray computed tomography. *Medical Physics.* 8(4):488–495.

Smith-Bindman, R., Lipson, J., Marcus, R., Kim, K.P., Mahesh, M., Gould, R., Berrington de Gonzalez, A. and Miglioretti, D.L. 2009. Radiation Dose Associated with Common Computed Tomography Examinations and the Associated Lifetime Attributable Risk of Cancer. *Archives of Internal Medicine.* 169 (22): 2078 – 2086.

Stepwards. 2020. *Fundamentals Of Computed Tomography Studies: Windowing*. Date of Access: 12 October 2020. <https://www.stepwards.com/?page_id=21646#WINDOW_SETTINGS_WINDOW_WIDTH_VS_WINDOW_LEVEL>.

Skryzński, W., Zielińska-Dabroska, S., Wachowicz, M., Ślusarczyk-Kacprzyki, W., Kukołowicza, P.F. and Bulski, W. 2010. Computed Tomography as a Source of Electron Density Information for Radiation Treatment Planning. *Strahlentherapie und Onkologie* 186: 327-33.

Sulieman, A., Mahmoud, M.Z., Serhan, O., Alonazi, B., Alkhorayef, M., Alzimami, K. and Bradley, D. 2018. CT Examination Effective Doses in Saudi Arabia. *Applied Radiation and Isotopes*. 141: 261-265.

Sung, D.W. and Shin, K.E. 2013. Reducing Radiation Dose in Diagnostic Radiology. Journal of Korean Medical Science. 28: 495-496.

The Royal College of Radiologist. 2019. *Radiotherapy Dose Fractionation*. 3rd edition. Date of Access: 28 November 2020 <https://www.rcr.ac.uk/publication/radiotherapy-dose-fractionation-third-edition>.

Toshiba Medical Systems Corporation. 2004. Operation Manual for Whole-Body x-ray CT scanner.

Wells, M.M., Li, Z., Addeman, B., McKenzie, C.A., Mujoomdar, A., Beaton, M. and Bird, J. 2016. Computed Tomography Measurement of Hepatic Steatosis: Prevalence of

Hepatic Steatosis in a Canadian Population. *Canadian Journal of Gastroenterology and Hepatology.* Volume 2016. Article ID: 4930987.

Winslow, J.F., Hyer, D.E., Fisher, R.F., Tien, C.J. and Hintenlang, D.E. 2009. Construction of Anthropomorphic Phantoms for use in Dosimetry Studies. *Journal of Applied Clinical Medical Physics*. 10 (3): 195 – 203.

World Health Organisation (WHO). 2020. *Body Mass Index (BMI).* Date of Access: 28 August 2020. <https://www.euro.who.int/en/health-topics/disease-prevention/nutrition/a-healthy-lifestyle/body-mass-index-bmi >.

Wu, R.Y., Williamson, T.D., Sahoo, N., Nguyen, T., Ikner, S.M., Liu, A.Y., Wisdom, P.G., Lii MF., Hunter, R.A., Alvarez, P.E., Gunn, G.B., Frank, S.J., Hojo, Y., Zhu, X.R. and Gillin, M.T. 2020. Evaluation of the high definition field of view option of a large-bore computed tomography scanner for radiation therapy simulation. *Physics and Imagining in Radiation Oncology.* 13 (44-49).

Xue, Z., Antani, S., Long, R., Demner-Fushman, D. and Thoma, G.R. 2012. Window Classification of Brain CT Images in Biomedical Articles. *American Medical Informatics Association (Amia) 2012 Symposium*. Date of Access: 24 September 2020. <https://www.ncbi.nlm.nih.gov/pmc/articles/PMC3540547/pdf/amia_2012_symp_1023.pdf >.

Yang, C., Liu, R., Ming, X., Liu, N., Guan, Y. and Feng, Y. 2018. Thoracic Organ Doses and Cancer Risk from Low Pitch Helical 4-Dimensional Computed Tomography Scans. *BioMed Research International*. Volume 2018, Article ID 8927290, 6 pages. Date of Access: 7 October 2020. <https://doi.org/10.1155/2018/8927290>.

Zacharias, C., Alessio, A.M., Otto, R.K., Lyer, R.S., Philips, G.S., Swanson, J.O. and Thapa M.T. 2013. Paediatric CT Strategies to Lower Radiation Dose. *American Journal of Roentgenology.* 200: 950-956.

Zeb, I., Li, D., Masir, K., Katz, R., Larijani, V-N. and Budoff, M.J. 2012. Computed Tomography Scans in the Evaluation of Fatty Liver Disease in a Population Based Study: The Multi-ethnic Study of Atherosclerosis. *Academic Radiology*. 19(7): 811-818.

Zucker, E.J., Larson, D.B., Newman, B. and Barth, R.A. 2015. Radiologist Compliance with California CT Dose Reporting Requirements: A Single-Center Review of Pediatric Chest CT. *American Journal of Roentgenology.* 204: 810-816.

Appendix A

Conversion Factors

Table A.1: Table of conversion factors based on 32 cm PMMA phantom for $CTDI_{vol}$. for SSDE.

Table 1A			Table 1B			Table 1C			Table 1D	
Lat+AP	ED	*f*	Lateral	ED	*f*	AP	ED	*f*	ED	*f*
16.00	7.70	2.79	8.00	9.20	2.65	8.00	8.80	2.69	8.00	2.76
18.00	8.70	2.69	9.00	9.70	2.60	9.00	10.20	2.55	9.00	2.66
20.00	9.70	2.59	10.00	10.20	2.55	10.00	11.60	2.42	10.00	2.57
22.00	10.70	2.50	11.00	10.70	2.5	11.00	13.00	2.30	11.00	2.47
24.00	11.70	2.41	12.00	11.30	2.45	12.00	14.40	2.18	12.00	2.38
26.00	12.70	2.32	13.00	11.80	2.40	13.00	15.70	2.08	13.00	2.30
28.00	13.70	2.24	14.00	12.40	2.35	14.00	17.00	1.98	14.00	2.22
30.00	14.70	2.16	15.00	13.10	2.29	15.00	18.30	1.89	15.00	2.14
32.00	15.70	2.08	16.00	13.70	2.24	16.00	19.60	1.81	16.00	2.06
34.00	16.70	2.01	17.00	14.30	2.19	17.00	20.80	1.73	17.00	1.98
36.00	17.70	1.94	18.00	15.00	2.13	18.00	22.00	1.65	18.00	1.91
38.00	18.60	1.87	19.00	15.70	2.08	19.00	23.20	1.58	19.00	1.84
40.00	19.60	1.80	20.00	16.40	2.03	20.00	24.30	1.52	20.00	1.78
42.00	20.60	1.74	21.00	17.20	1.97	21.00	25.50	1.45	21.00	1.71
44.00	21.60	1.67	22.00	17.90	1.92	22.00	26.60	1.40	22.00	1.65
46.00	22.60	1.62	23.00	18.70	1.86	23.00	27.60	1.34	23.00	1.59
48.00	23.60	1.56	24.00	19.50	1.81	24.00	28.70	1.29	24.00	1.53
50.00	24.60	1.50	25.00	20.30	1.76	25.00	29.70	1.25	25.00	1.48
52.00	25.60	1.45	26.00	21.10	1.70	26.00	30.70	1.20	26.00	1.43
54.00	26.60	1.40	27.00	22.00	1.65	27.00	31.60	1.16	27.00	1.37
56.00	27.60	1.35	28.00	22.90	1.60	28.00	32.60	1.12	28.00	1.32
58.00	28.60	1.30	29.00	23.80	1.55	29.00	33.50	1.08	29.00	1.28
60.00	29.60	1.25	30.00	24.70	1.50	30.00	34.40	1.05	30.00	1.23
62.00	30.50	1.21	31.00	25.60	1.45	31.00	35.20	1.02	31.00	1.19
64.00	31.50	1.16	32.00	26.60	1.40	32.00	36.00	0.99	32.00	1.14
66.00	32.50	1.12	33.00	27.60	1.35	33.00	36.80	0.96	33.00	1.10
68.00	33.50	1.08	34.00	28.60	1.30	34.00	37.60	0.93	34.00	1.06
70.00	34.50	1.04	35.00	29.60	1.25	35.00	38.40	0.91	35.00	1.02
72.00	35.50	1.01	36.00	30.60	1.20	36.00	39.10	0.88	36.00	0.99
74.00	36.50	0.97	37.00	31.70	1.16	37.00	39.80	0.86	37.00	0.95
76.00	37.50	0.94	38.00	32.70	1.11	38.00	40.40	0.84	38.00	0.92
78.00	38.50	0.90	39.00	33.80	1.07	39.00	41.10	0.82	39.00	0.88
80.00	39.50	0.87	40.00	34.90	1.03	40.00	41.70	0.80	40.00	0.85
82.00	40.50	0.84	41.00	36.10	0.98	41.00	42.30	0.78	41.00	0.82
84.00	41.50	0.81	42.00	37.20	0.94	42.00	42.80	0.77	42.00	0.79
86.00	42.40	0.78	43.00	38.40	0.90	43.00	43.40	0.75	43.00	0.76
88.00	43.40	0.75	44.00	39.60	0.87	44.00	43.90	0.74	44.00	0.74
90.00	44.40	0.72	45.00	40.80	0.83	45.00	44.40	0.73	45.00	0.71

ED= Effective Dose, *f* = the conversion factor. Lat= Lateral dimension; AP=Anterior posterior dimension. Table 1A; is used when Lat + AP dimensions are calculated then use that conversion factor. Table 1B is used if only the lateral dimension is used, Table 1C, is used with only the AP dimension. Table 1D is used when the effective diameter is calculated with both the AP and Lat dimensions. Table 1D was used in the current research.

Modified from AAPM (2011: 10 – 11)

Table A.2: Conversion factors from DLP to effective dose as a function of voltage, region and age (ICRP Publication 103).

Phantom	Tube Voltage (kV)	Abdomen	Pelvis
Adult	80	0.0151	0.0128
	100	0.0151	0.0127
	120	0.0153	0.0129
	140	0.0155	0.0131
	Mean	0.0153	0.0129
10 Year Old	80	0.0256	0.0226
	100	0.0247	0.0218
	120	0.0246	0.0216
	140	0.0246	0.0216
	Mean	0.0249	0.0219
5 Year Old	80	0.376	0.0315
	100	0.0355	0.0298
	120	0.0349	0.0294
	140	0.0349	0.0291
	Mean	0.0357	0.03
1 Year Old	80	0.0571	0.0481
	100	0.053	0.0445
	120	0.0514	0.0431
	140	0.0506	0.0425
	Mean	0.053	0.0446
Newborn	80	0.0935	0.0776
	100	0.0838	0.0699
	120	0.0804	0.0672
	140	0.0786	0.0655
	Mean	0.0841	0.0701

Appendix B

Patient Consent Forms and Information Leaflet

English Consent Form

Consent Form

Dear Sir/Madam

You are going to have a special x-ray scan called a computed tomography or CT scan. This scan is to help the doctor to plan your cancer treatment.

I, Vanessa Verreynne am doing my Master's Degree in Radiography and want to calculate the dose you received during the CT scan. The title of my study is "*Radiation dose and image quality from pelvic localisation computed tomography in oncology*." You may contact me (Vanessa Verreynne) any time if you have any questions about the research. The number is 083 661 6170.

You may contact the Secretariat of the Health Sciences Research Ethics Committee, UFS at telephone number (051) 4017794/5 if you have questions about your rights as a research subject.

We are all exposed to radiation from natural sources every day. A small dose is given with each x-ray exam. The CT dose given is controlled and the machine is checked daily to ensure the correct delivery of the dose.

The aim of the research is to calculate this dose for statistical analysis to see the dose delivery to patients of different sizes. In order to do this, I need your consent to look at your CT information as well as to measure your height and weight. All information will remain confidential. No changes will be made to your treatment if you agree or not to take part in the research. No compensation will be given to you for taking part in the research. The participation in this research is voluntary and you may withdraw from the research at any time.

By signing below, you are stating that the research has been verbally described to you including the information above. You are also stating that you voluntarily decide to take part in the research and understand your involvement.

Patient's Name in print: _____

Patient Signature: _____ Date: _____

Translator Signature: _____ Date: _____

Witness Signature: _____ Date: _____

Thank you

Information Leaflet

Study Title: "*Radiation dose and image quality from pelvic localisation computed tomography in oncology*

Dear Sir/Madam

I, Vanessa Verreynne am doing my masters in radiography and want to determine the dose received by you during your CT scan.

You are going to have a special x-ray scan called a CT scan or computed tomography. This scan is to help the doctor to plan your oncology treatment.

We are all exposed to radiation from natural sources every day. A small dose is given with each x-ray exam. The CT dose given is controlled and the machine is checked daily to ensure the correct delivery of the dose.

Research is the process used to answer a question. The research is to calculate this dose for statistical analysis to see how patients of different sizes are affected in dose delivery. In order to do this, I need your consent to look at your CT information as well as to measure your height and weight. There will be 150 patients included in the research study. The study will include any patient who comes to the Free State department of Oncology for pelvic radiation.

There is no risk in being involved in the study. The benefit of being in the study is that you will help to ensure that the dose and image quality is optimal for all patients who receive pelvic radiation in the department.

Your participation in the study is voluntary, and no changes or loss of treatment will occur if you refuse to take part in the study. You may choose to withdraw from the study at any time.

All information will remain confidential. No changes will be made to your treatment if you agree or not to take part in the research. No compensation will be given to you for taking part in the research.

Should you need further information you are welcome to contact the researcher. Vanessa Verreynne at cell: 083 661 6170.

To report complaints or problems you can contact the Health Sciences Research Ethics Committee UFS Secretariat at the telephone number (051) 4017794/5.

Afrikaans Consent Form

Toestemmingsbrief

Geagte Mnr / Mev / Me

U gaan ‘n spesiale x-straal skandering kry wat ‘n RT skandering of “rekenaar tomagrafie” genoem word. Hierdie skandering gaan die doktor help met die beplanning van jou onkologie bestraling.

Ek Vanessa Verreynne is besig met my Meesters Graad in Radiografie, en ek wil die dosis wat u gaan ontvang gedurende jou RT skandering bereken. Die titel van my studie is “*Radiation dose and image quality from pelvic localisation computed tomography in oncology”.* U kan my (Vanessa Verreynne) enige tyd kontak, indien u vrae oor die navorsing het. Die nommer is 083 661 6170.

U kan die Sekretariaat van die Gesondheidswetenskappe Navorsingsetiekkomitee, UV by telefoonnommer (051) 4017794/5 kontak indien u enige vrae het oor u regte as ‘n proefpersoon.

Elke person word daagliks blootgestel aan bestraling van natuutlike bronne. ‘n Klein dosis word gegee vir elke Xstraal ondersoek. Hierdie RT dosis word gekontroleer en die X-straal masjien word daagliks ge-toets om seker te maak dat die regte dosis gegee word.

Hierdie navorsing word gedoen om die dosis te bereken vir statistiese analise om te sien hoe pasiente van verskillende grootte geaffekteer word deur die dosis toedienning. Om hierdie navorsing te doen het ek u toestemming nodig om my toe te laat om na jou CT inligting te kyk en ook jou gewig en lengte te meet. Alle inligting sal konfidensiëel gehou word. Daar sal geen verskil wees aan u behandeling indien u deel neem aan die studie of aldan nie. Geen betaling sal aan u gegee word as u deelneem aan die navorsing nie. U deelname aan hierdie navorsing is vrywillig, en u sal nie gepenaliseer word of enige voordele verbeur as u weier om deel te neem of besluit om deelname te staak nie.

As u hier onder teken sê U dat die navorsing met jou verbaal bespreuk is, insluitend die bogenoemde inligting. U sê dat u vrywilliglik besluit het om deel te neem in die navorsing en begryp u betrokkenheid in die studie.

Pasient se Naam: _____

Pasient se Handtekening: _____ Datum: _____

Vertaler se Handtekening: _____ Datum: _____

Getuie se Handtekening: _____ Datum: _____

Baie Dankie vir u samewerking.

Inligtings Pamflet

Studietitel: *Radiation dose and image quality from pelvic localisation computed tomography in oncology*

Geagte Mnr / Mev / Me

Ek Vanessa Verreynne is besig met my Meesters Graad in Radiografie, en ek wil die dosis wat u gaan ontvang gedurende jou CT skandering bereken.

U gaan n spesiale x-straal skandering kry wat n RT skandering of “Rekenaar Tomagrafie” genoem word. Hierdie skandering gaan die doktor help met die beplanning van jou onkologie bestraling.

‘n Klein dosis word gegee vir elke Xstraal ondersoek. Hierdie CT dosis word gekontroleer en die X-straal masjien word daagliks ge-toets om seker te maak dat die regte dosis gegee word.

Navorsing is slegs die proses waardeur die antwoord op ‘n vraagstuk verkry word . Hierdie navorsing word gedoen om die dosis te bereken vir statistiese analise om te sien hoe pasiente van verskillende grootte geaffekteer word deur die dosis toedienning. Om hierdie navorsing te doen het ek u toestemming nodig om my toe te laat om na jou CT inligting te kyk en ook jou gewig en lengte te meet. Daar sal 150 pasiente deelneem aan die navorsing. Hierdie getal sal gemaak word van enige pasient wat vir onkologie beken radiotherapie kom.

Daar sal geen risiko, verbonde wees om deel te neem aan die studie nie. Die voordeel om deel te neem aan die studie is dat ons sal seker maak dat die dosis en beelding kwaliteit, optimaal is vir beken radiotherapie in die departement.

U deelname aan hierdie navorsing is vrywillig, en u sal nie gepenaliseer of enige voordele verbeur as u weier om deel te neem of besluit om deelname te staak nie.

Alle inligting sal konfidensiëel gehou word. Daar sal geen verskil wees aan u behandeling indien u deel neem aan die studie of aldan nie. Geen betaling sal aan u gegee word as u deelneem aan die navorsing nie.

Vir verdere inligting kan u navorser Vanessa Verreynne kontact by Sel: 083 661 6170.

Vir raportering van klagtes of probleme kan u Gesondheidswetenskappe Navorsingsetiekkomitee Sekretariaat kontact by telefoon nommer (051) 4017794/5.

SeSotho Consent Form

Foromo Ya Tumellano

Monghadi / Mofumahadi ya hlomphehang

O tlo nkuwa x-ray e kgethehileng e bitswang CT-Scan sena setlo thusa ngaka ho hlophisa kalafo ya hao.

Nna Vanessa Verreynne ke ithutela dithuto tse phahameng tsa di Masters ho lekala la Radiography mme ke batla ho sheba dose eo o e fumaneng nakong ya hao ya CT-Scan. Sehloho sa patlisiso yaka ke "*Radiation dose and image quality from pelvic localisation computed tomography in oncology.* O ka letsetsa Nna (Vanessa Verreynne) nako efeng kapa e feng ha ona le dipotso mabapi le patlisiso ena, nomoro ke 083 661 6170.

O ka letsetsa Mongodi wa Health Sciences Research Ethics Committee, Universiting ya Foreistata nomorong tsena (051) 401 7794/5. Ha ona le dipotso ka ditokelo tsa hao jwalo ka mongka karolo patlisisong ena.

Kaofela re fumana mahlasedi/ radiation ho tswa ho dintho tsa tlhaho ka letsatsi le leng le le leng. Dose e nyane e a fanwa ka hlahlobo enngwe le enngwe. CT dose e fanwang e ya laolwa le motjhini o a lekolwa letsatsi le leng le le leng ho netefatsa hore dose e fanwang e nepahetse.

Patlisiso ena ke ho shebisisa dose ena ya statistical analysis ho bona hore bakudi ba fetanang ka boima ba mmele ba ameha jwang ke phano ya dose. Hore hona ho kgonahale, ke hloka tumello ya hao hore Ke shebe ditokomane tseo CT e fanang ka tsona tsa dose le ho lekanya bolelele le boima ba hao. Ditokomane kaofela etlaba tsa lekunutu. Ha hona diphetoho tse tla etswa kalafong ya hao ha o dumela kapa o sa dumele ho nka karolo dipatlisisong tsena. Ha hona tefo ha o nka karolo dipatlisisong tsena. Ke boithapo honka karolo patlisisong ena, jwale oka itokolla neng kapa neng ha o batla.

Ho itlama mona tlase, ho bolela hore o hlaloseditswe ka molomo ka patlisiso. Ho kenyelletsa le tlhalosetso e hodimo. O bolela hore o kgetha ho ithaopa honka karolo patlisisong mme o utliwisisa honka karolo.

Lebitso la mokudi: _____

Signature ya Mokudi: _____ La Kgwedi _____

Signature ya Paki: _____ La Kgwedi _____

Ke a leboha

Tsebiso Bukana

Sehloho sa patlisiso ya ka ke: “*Radiation dose and image quality from pelvic localisation computed tomography in oncology*

Monghadi / Mofumahadi ya hlomphehang

Nna Vanessa Verreynne ke ithutela dithuto tse phahameng tsa di Masters ho lekala la Radiography mme ke batla ho sheba dose eo o e fumaneng nakong ya hao ya CT-Scan.

O tlo nkuwa x-ray e kgethehileng e bitswang CT-Scan sena setlo thusa ngaka ho hlophisa kalafo ya hao.

Kaofela re fumana mahlasedi/ radiation ho tswa ho dintho tsa tlhaho ka letsatsi le leng le le leng. Dose e nyane e a fanwa ka hlahlobo enngwe le enngwe. CT dose e fanwang e ya laolwa le motjihini o a lekolwa letsatsi le leng le le leng ho netefatsa hore dose e fanwang e nepahetse.

Patlisiso ke tsela e sebediswang ho araba dipotso. Patlisiso ena ke ho shebisisa dose ena ya statistical analysis ho bona hore bakudi ba fetanang ka boima ba mmele ba ameha jwang ke phano ya dose. Hore hona ho kgonahale, ke hloka tumello ya hao hore Ke shebe ditokomane tseo CT e fanang ka tsona tsa dose le ho lekanya bolelele le boima ba hao. Ditokomane kaofela etlaba tsa lekunutu. Ha hona diphetoho tse tla etswa kalafong ya hao ha o dumela kapa o sa dumele ho nka karolo dipatlisisong tsena. Ha hona tefo ha o nka karolo dipatlisisong tsena. Hotlaba le batho ba 150 bankang karolo patlisisong. Patlisiso e kenyeletsa bakudi batswang lefapheng la tsa bophelo foreistata la Oncology for pelvic radiation.

Ha hona kotsi honka karolo patlisisong. Molemo wa honka karolo ke ho Netefatsa hore bakudi ba fumana dose le boleng ba di x-ray bo Nepahetseng.

Honka karolo ha hao ke boithaopo, ha hona fetolwa letho kalafong ya hao ha o hana ho nka karolo patlisisong. Oka itokolla patlisisong nako enngwe le enngwe.

Dinomoro tsa mohala tsa motha ya etsang patlisiso Vanessa Verreynne 083 661 6170. Bakeng sa dintlha tse ikgethileng.

Dinomoro tsa Health Sciences Research Ethics Committee UFS Secretariat (051) 401 7794/5 ho tlaleha ditletlebo kapa mathata

Appendix C
CT Scan Form

Table A.3: CT scan form.

Patient Scan Information - please highlight gender and if repeat scan						
Patient RT	**Height**	**Weight**	**Gender**	**Diagnosis / reason for scan**	**Repeat Scan**	**Reason for Rescan:**
			M / F		Yes / No	
			M / F		Yes / No	
			M / F		Yes / No	
			M / F		Yes / No	
			M / F		Yes / No	
			M / F		Yes / No	
			M / F		Yes / No	
			M / F		Yes / No	
			M / F		Yes / No	
			M / F		Yes / No	
			M / F		Yes / No	
			M / F		Yes / No	
			M / F		Yes / No	
			M / F		Yes / No	
			M / F		Yes / No	
			M / F		Yes / No	
			M / F		Yes / No	
			M / F		Yes / No	
			M / F		Yes / No	
			M / F		Yes / No	
			M / F		Yes / No	
			M / F		Yes / No	
			M / F		Yes / No	
			M / F		Yes / No	
			M / F		Yes / No	
			M / F		Yes / No	
			M / F		Yes / No	
			M / F		Yes / No	
			M / F		Yes / No	
			M / F		Yes / No	
			M / F		Yes / No	
			M / F		Yes / No	
			M / F		Yes / No	
			M / F		Yes / No	
			M / F		Yes / No	
			M / F		Yes / No	

Appendix D
CT Data Capture

Table A.4 Anamorphic phantom scan Microsoft excel sheet.

Scan No.			CT information										Calculations		
	AP	*Lat*	*kV*	*mA*	*FOV*	*mAs*	*Scan Time*	*Total Number of Images*	*Scan Start*	*Scan End*	*$CTDI_{vol}$*	*DLP*	*Effective Diameter*	*SSDE*	*Effective Dose*

Table A.5: Water phantom scan data.

Water Phantom Scans					
Phantom Diameter	*FOV*	*kV*	*SD*	*HU*	*SNR Calculation*

Table A.6 Patient information.

Patient Information								
Patient RT	*Gender*	*Age*	*Diagnosis*	*Weight (Kg)*	*Height (m)*	*3D/IMRT*	*AP (cm)*	*Lat (cm)*

Table A.7: Patient CT information.

CT information									
kV	*mA*	*FOV*	*mAs*	*Scan Time*	*Total Number of Images*	*Scan Start*	*Scan End*	*$CTDI_{vol}$*	*DLP*

Table A.8: Calculations for patients.

Calculations				
Effective Diameter	*SSDE*	*BMI*	*Effective Dose -pelvis*	*Effective Dose - abdomen*

Table A.9: Scout view, with example of data.

	Scout View				Info from CT					
		Field of View			Measurement				Observation	
ID	Patient RT	Patient in relation to	Size Lat Dimension	Size Ant Post direction	LLat	RLat	Ant	Post	Comment Scout View:	Scan Start Position
		Centre of FOV	Too wide	Appropriate						
		Left of FOV	To narrow	To narrow						
		Right of FOV	Appropriate	Too wide						

Table A.10: Image quality analysis.

Image Quality Analysis						
RTNumber	*HU Adipose*	*HU Liver*	*HU Psoas Muscle*	*SD Adipose*	*SD Liver*	*SD Psoas Muscle*

Table A.11: Image calculations.

Image Calculations						
RT Number	*HU Adipose Check*	*HU Liver Check*	*CNR*	*SNR Liver*	*SNR Psoas*	*CNRD*

Appendix E
Ethical Approval

health
Department of Health
FREE STATE PROVINCE

22 October 2018

Ms. V Verreynne
Dept. of Radiography
CUT

Dear Ms. V Verreynne

Subject: Radiation dose and image quality from pelvic localisation computed tomography in oncology.

- Please ensure that you read the whole document, Permission is hereby granted for the above – mentioned research on the following conditions:
- Participation in the study must be voluntary
- A written consent by each participant must be obtained.
- Serious Adverse events to be reported to the Free State department of health and/ or termination of the study
- Ascertain that your data collection exercise neither interferes with the day to day running of Unversitas Hospital nor the performance of duties by the respondents or health care workers.
- Confidentiality of information will be ensured and please do not obtain information regarding the identity of the participants.
- **Research results and a complete report should be made available to the Free State Department of Health on completion of the study (a hard copy plus a soft copy).**
- Progress report must be presented not later than one year after approval of the project to the Ethics Committee of the University of Free State and to Free State Department of Health.
- Any amendments, extension or other modifications to the protocol or investigators must be submitted to the Ethics Committee of the Free State and to Free State Department of Health.
- **Conditions stated in your Ethical Approval letter should be adhered to and a final copy of the Ethics Clearance Certificate should be submitted to** sebeelats@fshealth.gov.za or lithekom@fsheatlh.gov.za **before you commence with the study**
- No financial liability will be placed on the Free State Department of Health
- Please discuss your study with the institution manager/CEOs on commencement for logistical arrangements
- Department of Health to be fully indemnified from any harm that participants and staff experiences in the study
- Researchers will be required to enter in to a formal agreement with the Free State department of health regulating and formalizing the research relationship (document will follow)
- You are required to present your study findings/results at the Free State Provincial health research day

Trust you find the above in order.
Kind Regards

Dr D Motau
HEAD: HEALTH
Date: 01/11/2018

Head : Health
PO Box 227, Bloemfotein, 9300
4th Floor, Executive Suite, Bophelo House, cnr Maitland and, Harvey Road, Bloemfotein
Tel: (051) 408 1646 Fax: (051) 408 1556 e-mail:khusemj@fshealth.gov.za@fshealth.gov.za/chikobvup@fshealth.gov.za
www.fs.gov.za

UNIVERSITY OF THE FREE STATE
UNIVERSITEIT VAN DIE VRYSTAAT
YUNIVESITHI YA FREISTATA

UFS·UV
HEALTH SCIENCES
GESONDHEIDSWETENSKAPPE

Health Sciences Research Ethics Committee

19-Nov-2018

Dear **Vanessa Verreynne**

Ethics Clearance: **Radiation dose and image quality from pelvic localisation computed tomography in oncology.**

Principal Investigator: **Vanessa Verreynne**

Department: **Radiography - CUT**

APPLICATION APPROVED

Please ensure that you read the whole document

With reference to your application for ethical clearance with the Faculty of Health Sciences, I am pleased to inform you on behalf of the Health Sciences Research Ethics Committee that you have been granted ethical clearance for your project.

Your ethical clearance number, to be used in all correspondence is:**UFS-HSD2018/1159/2711**

The ethical clearance number is valid for research conducted for one year from issuance. Should you require more time to complete this research, please apply for an extension.

We request that any changes that may take place during the course of your research project be submitted to the HSREC for approval to ensure we are kept up to date with your progress and any ethical implications that may arise. This includes any serious adverse events and/or termination of the study.

A progress report should be submitted within one year of approval, and annually for long term studies. A final report should be submitted at the completion of the study.

The HSREC functions in compliance with, but not limited to, the following documents and guidelines: The SA National Health Act. No. 61 of 2003; Ethics in Health Research: Principles, Structures and Processes (2015); SA GCP(2006); Declaration of Helsinki; The Belmont Report; The US Office of Human Research Protections 45 CFR 461 (for non-exempt research with human participants conducted or supported by the US Department of Health and Human Services- (HHS), 21 CFR 50, 21 CFR 56; CIOMS; ICH-GCP-E6 Sections 1-4; The International Conference on Harmonization and Technical Requirements for Registration of Pharmaceuticals for Human Use (ICH Tripartite), Guidelines of the SA Medicines Control Council as well as Laws and Regulations with regard to the Control of Medicines, Constitution of the HSREC of the Faculty of Health Sciences.

For any questions or concerns, please feel free to contact HSREC Administration: 051-4017794/5 or email EthicsFHS@ufs.ac.za.

Thank you for submitting this proposal for ethical clearance and we wish you every success with your research.

Yours Sincerely

Dr. SM Le Grange
Chair : Health Sciences Research Ethics Committee

Health Sciences Research Ethics Committee
Office of the Dean: Health Sciences
T: +27 (0)51 401 7795/7794 | E: ethicsfhs@ufs.ac.za
IRB 00006240; REC 230408-011; IORG0005187; FWA00012784
Block D, Dean's Division, Room D104 | P.O. Box/Posbus 339 (Internal Post Box G40) | Bloemfontein 9300 | South Africa
www.ufs.ac.za

Department of Oncology

Universitas Annex

Roth Avenue

9300

DR A SHERRIFF

HOD

RE: Consent to conduct research in the Department of Oncology

Dear Prof Sherriff

I, Vanessa Verreynne, am currently doing my Master's Degree in radiography (therapy) at the Central University of Technology, Free State. As part of my degree I am conducting a research project about the radiation dose received by patients during their CT localisation scans.

With your permission I would like to conduct my research in your department. My research proposal is entitled "*Radiation dose and image quality from computed tomography pelvic localisation in oncology*". I propose to determine the dose received by the patients during their pelvic CT localisation scan for radiation planning. I will also evaluate the image quality for those CT scans.

The study will be conducted over a period of months in 2019. The research will examine adult patients who receive CT localisation for pelvic radiation. Initially phantom will be scanned. These are available at the department. The scans for the phantoms will be scanned after hours and will not affect the workflow of the department. No patient will be included in the research without prior consent from the patient. As a requirement of the research the patients will be weighed and their height noted, to determine the patients BMI. No additional CT dose will be delivered to the patient as a result of the research. The capturing of the CT data will occur after hours and will in no way affect the working hours of the department. The results of the study will be made available to you upon completion of the research.

With thanks, please contact me with any enquires into the research you may have.

V Verreynne

_____

V. Verreynne

(Cell: 083 661 6170, Email: verreynne@yahoo.com)

_____

Prof. A Sherriff

14.8.18

Date